GDANSK UNIVERSITY OF TECHNOLOGY
FACULTY OF OCEAN ENGINEERING AND SHIP TECHNOLOGY
SECTION OF TRANSPORT TECHNICAL MEANS
OF TRANSPORT COMMITEE OF POLISH ACADEMY OF SCIENCES
UTILITY FOUNDATIONS SECTION
OF MECHANICAL ENGINEERING COMMITTEE OF POLISH ACADEMY OF SCIENCE

ISSN 1231 – 3998
ISBN 83 – 900666 – 2 – 9

Journal of

POLISH CIMAC

ENERGETIC ASPECTS

Vol. 2 **No. 1**

Gdansk, 2007

Science publication of Editorial Advisory Board of POLISH CIMAC

Editorial Office:

GDANSK UNIVERSITY OF TECHNOLOGY
Faculty of Ocean Engineering and Ship Technology
Department of Ship Power Plants
G. Narutowicza 11/12 80-952 GDANSK POLAND
tel. +48 58 347 29 73, e – mail: sek4oce@pg.gda.pl

This journal is devoted to designing of diesel engines, gas turbines and ships' power transmission systems containing these engines and also machines and other appliances necessary to keep these engines in movement with special regard to their energetic and pro-ecological properties and also their durability, reliability, diagnostics and safety of their work and operation of diesel engines, gas turbines and also machines and other appliances necessary to keep these engines in movement with special regard to their energetic and pro-ecological properties, their durability, reliability, diagnostics and safety of their work, and, above all, rational (and optimal) control of the processes of their operation and specially rational service works (including control and diagnosing systems), analysing of properties and treatment of liquid fuels and lubricating oils, etc.

All papers have been reviewed

ISSN 1231 – 3998

ISBN 83 – 900666 – 2 – 9

Printed in Poland

CONTENTS

CONTENTS

AFFECT OF PHENOMENON OF PISTON SEALING RINGS VIBRATIONS ON TIGHTNESS OF PRC UNIT

Karol Franciszek Abramek

Szczecin University of Technology
st. Piastów 19, 70-310 Szczecin, Poland
tel.: +48 91 4494811, fax.: +48 91 4494820
e-mail: karol.abramek@ps.pl

Abstract

In this elaboration there is showed the affect of the phenomenon of piston rings vibrations on the tightness of the piston-piston rings-cylinder liner system (PRC). There has been executed an attempt to determine the mathematical model of the phenomenon of piston rings vibrations in the radial plane and a preliminary method for a model towards the cylinder axis that affect on the blow-by to the crankcase of the piston combustion engine.

Keywords: *blow-by, ring, piston ring oscillation, cylinder*

1. Introduction

Keeping the appropriate mating among the piston, piston rings and the cylinder liner bearing surface in a wide range of temperatures and the pressure alterations causes the load losses from the working space. The load losses in the form of the blow-by to the crankshaft of the piston combustion engine by leakages of the piston-piston rings-cylinder liner (PRC) cause a reduction of the engine output. Escalation of the cylinder leakage causes a considerable reduction of the engine working parameters. It is caused by the affect of the clearance among the PRC system elements and conditions of forming of the oil film among the piston rings and the cylinder liner bearing surface. As the research for providing the tightness of the entire PRC system showed, any kinds of the piston rings movements have the affect on the tightness of this system.

The phenomenon of the piston sealing rings vibrations is, in a certain extent of the engine rotational speed, the direct reason for the excessive blow-by. For example, the extreme of maximum of the blow-by takes place at the rotational speed about 1800rpm for the SW-680 engine. In the Fig. 1 there is shown the diagram of alterations of the blow-by for the 359 engine. There are two local extremes of the blow-by for this engine. The first takes place at the speed of 1500rpm approximately and the second at the speed of 2100rpm.

The piston ring makes various kinds of movements in the piston ring groove. Despite these movements, the piston ring has to adhere to the cylinder liner to provide the tightness. As the piston extorts the movement of piston rings towards the cylinder axis and radial movements of the piston rings, the piston ring has to have a possibility to move in various directions to provide the tightness.

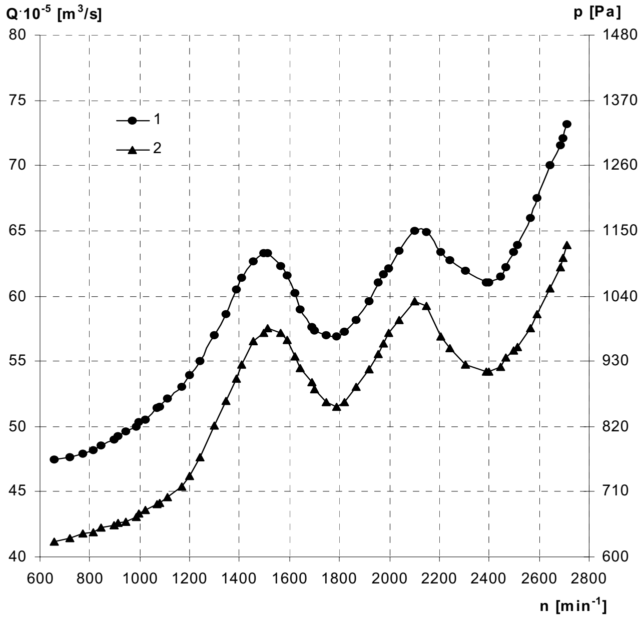

Fig 1. The characteristic of the blow-by in the function of the rotational speed of the 359 engine loaded to maximum, 1- the blow-by intensity, 2-stowing of gases in the crankcase [1]

2. Formulating a problem

According to A. Iskra, Professor, there are the most possible the vibrations with the amplitude towards the radial direction of the cylinder [4]. It can be assumed, that there are the small amplitudes of vibrations in the radial direction that result from the small harmonic amplitudes that extort vibrations, and a strong damping that causes moving of the piston ring in this direction.

However these vibrations do not cause such loss of tightness by the piston rings as the vibrations towards the cylinder axis. The piston sealing ring, detaching from the upper and lower edges of the piston ring groove, causes such a loss of the tightness as the PRC system would operate without the piston ring. This phenomenon leads to out-of-proportion escalation of the blow-by intensity to the engine crankcase. These vibrations are extorted by the reciprocating movement of the piston. The amplitude of vibrations can only be in the range of the piston groove size and is very strongly damped because of increased unit pressures in the areas of the piston-ring joint.

3. The model description

In general, the piston rings vibrations were considered in two causes: the radial vibrations and the axial vibrations (towards the cylinder axis). The radial movements of the piston ring are caused by change of the cylinder liner shape, on which the piston ring moves, with change of the oil film thickness and variable pressure force resulting from the blow-by and the pressure alterations in the cylinder working space. According to A. Iskra, Professor, in the case of the piston ring radial vibrations, the potential energy is bound almost entirely in the piston ring deflections. The radial deflections cause the longitudinal stresses, the value of which alters in a linear way.

The equation of the piston ring vibrations can be received from the condition of balance of the forces, as the non-trivial solution of the homogenous equation [4, 5]:

$$\frac{\partial^2}{\partial x^2}\left[E(x)J(x)\frac{\partial^2 y(x,t)}{\partial x^2}\right]+\rho(x)A(x)\frac{\partial^2 y(x,t)}{\partial t^2}=p(x,t) \tag{1}$$

where:

x	-	the coordinate of situating of the intersection considered,
y(x,t)	-	the deflection of the intersection form the neutral state at the t moment,
E(x)	-	the Young's modulus,
J(x)	-	the axial moment of inertia of the intersection,
ρ(x)	-	the mass density of the piston ring material,
A(x)	-	the piston ring cross-sectional area,
P(x,t)	-	the external force that extorts vibrations.

Finally, after conversions in accordance with the literature [4, 5], the piston ring movement is described with the dependency:

$$y_n(x)=F_n\left[U\left(z_n\frac{x}{l}\right)-\frac{U(z_n)}{V(z_n)}V\left(z_n\frac{x}{l}\right)\right] \tag{2}$$

where:

U, V - Krylov functions

Concerning the quoted theoretical basis of the vibration that cause deflections in the radial direction, they can be adapted for the real piston ring, what was confirmed in the literature [4].

The vibrations in the axial direction shall be considered separately for each working cycle of the engine, with the forces acting on the piston rings taken into consideration. However the biggest losses of the load are present during the working cycle of the engine. Therefore the initial stage of the research will refer to determination of possibilities of the piston rings vibrations in this cycle.

The author proposes to use the Rayleigh method of reduction of the vibrating system with parameters split to the energy-equipollent equivalent system with one degree of freedom. A relatively high accuracy can be achieved at calculations of the first natural frequency. Vibrations of the continuous system approximated with one degree of freedom is described by the function with variables separated:

$$u(P,t) = T(t)U(P) \tag{3}$$

where u(P,t) is the function that describes displacements of the point P at the moment t, $P\in\Omega$, and Ω is the area of the technical system considered. A point of reduction that moves identically as the equipollent system, it means T(t), shall be chosen in this method. The point of reduction shall be chosen there, where the vibrations of the system are the most intensive, or there, where the concentrated mass is situated. This is the best to assume, for the considered case of the ring, the point situated 180^{o} from the piston-ring joint. The substitute mass m_z is determined from the formula:

$$m_z = \int_{\Omega}\rho(P)U^2(P)dv_{\Omega}+\sum_{k=1}^{m}m_k U^2(P_k) \tag{4}$$

where ρ(P) is the mass density and m_k is the concentrated mass connected with the system in the P_k point.

Because the piston rings have a tendency to rotate in the piston ring grooves, in the expression defining the kinetic energy there must be the appropriate term that corresponds to the energy of rotation of the masses connected with the system. Comparing the potential energy of the continuous system, which energy is the form of squares of displacements and deformations for the linear system, with the potential energy of the substitute system, we can receive the formula that defines the substitute stiffness. From the equality of the work of external forces in the continual system on the virtual displacements:

$$\delta L = \int_{\Omega} f(P,t)\delta u(P,t)dv_{\Omega} + \sum_{k=1}^{m} F_k(t)\delta u(P_k,t) \tag{5}$$

and the work of the substitute force $P_z(t)$ on the corresponding displacement $\delta T(t)$:

$$(\delta L)_z = P_z(t)\delta T(t) \tag{6}$$

that takes the following equality into consideration:

$$\delta u(P,t) = U(P)\delta T(t) \tag{7}$$

the formula that defines the external force results:

$$P_z(t) = \int_{\Omega} f(P,t)U(P)dv_p + \sum_{k=1}^{m} F_k(t)U(P_k) \tag{8}$$

where: the f(P, t) is the density of the split force, the $F_k(t)$ is the concentrated force that acts on the system in the P_k point.

In Figure 2 is presented the equivalent system of vibrations.

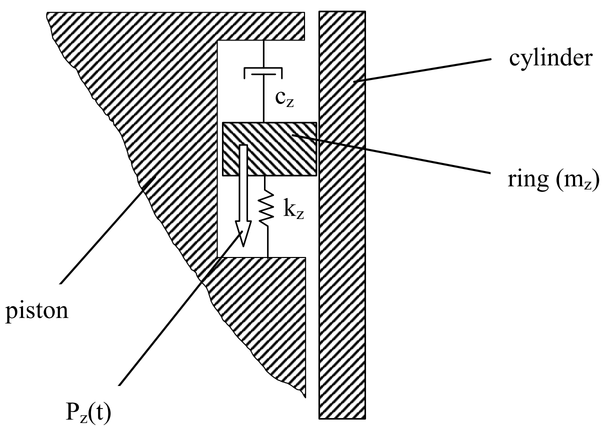

Fig. 2. Diagram of the equivalent system of vibrations (c_z – damping constant, k_z – substitute rigidity)

Comparing the energy lost by the continual system and by the substitute system we can calculate the damping constant c_z caused by the friction and presence of the oil and carbon deposits and lakes on the cylinder liner surface. The author realises that it is necessary to determine the concrete form of the formula that depends on the accepted rheological model. The curve that is the eigenfunction of the similar system can be used as the example. The assumption of the form of vibrations is equivalent with imposing of constraints on it.

4. Conclusions

Because, in accordance with the author's assumptions, the vibrations shall be considered separately for each working cycle of the engine, therefore it is necessary to collect, as much as possible, the data concerning changes of the pressure course in the cylinder, and thanks to it, alterations of the piston ring pressure to the lower edge of the piston ring groove and alterations in the thickness of the oil film, alterations of the speeds and accelerations and thanks to it, the piston ring inertia. Determination of the resultant of the force variable in time that acts on the ring, can lead to determine of the concrete equation of vibrations that describes the displacement of the piston ring towards the cylinder liner axis.

When determining the model of packing ring vibrations towards the cylinder axis according to Rayleigh's method, the external force extorting vibrations $P_z(t)$ should be set. This force is a resultant force from: in-time non-uniform piston ring inertial force resulting from piston to-and-fro motion with non-uniform acceleration, non-uniform gaseous force (non-uniform pressure of gases exerting an effect on piston ring), and non-uniform friction force, depending on oil film thickness. This method does not take into account changes in the angular position of piston rings, and consequently their effect on variation in the exciting force. The vibration damping is examined as a constant of silencer c_z, although as a matter of fact it is not constant, depending on the thickness of oil film, pressure pattern of piston ring, and changes in its position (in particular in relation to the cylinder liner). Nevertheless, for simplicity of calculations, it was assumed that vibration damping is constant and invariable in time.

References

[1] Abramek, K. F., *Charakterystyka przedmuchów w funkcji prędkości obrotowej silników SB-3.1, SW-680, 359. Zeszyt naukowy nr 4: Eksploatacja Silników Spalinowych,* Wydawnictwo Katedry Eksploatacji Pojazdów Samochodowych Politechniki Szczecińskiej, Szczecin 2001.

[2] Abramek, K. F., *Wpływ warunków pracy pierścieni tłokowych na ilość gazów przedostających się do skrzyni korbowej. Zeszyt naukowy nr 1: Eksploatacja Silników Spalinowych,* Wydawnictwo Katedry Eksploatacji Pojazdów Samochodowych Politechniki Szczecińskiej, Szczecin 2000.

[3] Abramek, K. F., *Wpływ zastosowania pierścieni wg Patentu PL 170524 na wielkość przedmuchów. Zeszyty Naukowe Wyższej Szkoły Morskiej nr 66,* Dział Wydawnictw Wyższej Szkoły Morskiej, Szczecin 2002.

[4] Iskra, A., *Wpływ drgań własnych pierścienia uszczelniającego na warunki pracy zespołu tłokowo-cylindrowego,* Journal of KONES Vol. 1, No 1, Warszawa-Lublin 1994.

[5] Kaliski, S., *Mechanika techniczna drgania i fale. Tom III,* Państwowe Wydawnictwo Naukowe, Warszawa 1986

[6] Smoczyński, M., Sygniewicz, J., *Analiza wpływu obciążeń mechanicznych na kątowe położenie tłoka względem tulei cylindrowej,* Interkonmot 1998.

[7] Smoczyński, M., Sygniewicz, J., *Przemieszczenia uszczelniającego pierścienia tłokowego w rowku pierścieniowym tłoka*, Journal of KONES Vol. 2, No 1, Warszawa-Poznań 1995.

MARINE POWER PLANT POLLUTANT EMISSIONS

Andrzej Adamkiewicz

Szczecin Maritime Academy
Wały Chrobrego 1-2, 70-500 Szczecin, Poland
tel.: +48 91 4809384, fax: +48 91 4809575
e-mail: a.adamkiewicz@am.szczecin.pl

Krzysztof Kołwzan

Polski Rejestr Statków S.A.
Al. Gen. Józefa Hallera 126, 80-416 Gdańsk, Poland
tel.: +48 58 3461700, fax: 48 58 3460392
e-mail: k.kolwzan@prs.pl

Abstract

This paper presents a comparison of toxic chemical emissions comprised in exhaust flows/fluxes of marine thermal engines of different types: diesel, gas and steam turbines (including boilers). Their impact on the environment was studied taking into account the engine type and its function in the ship power system.

Keywords: *marine power plan, emission, exhaust gas, diesel engines, gas turbines, steam turbines, boilers*

1. Introduction

A ship differs in many aspects from other means of transport, such as trucks or railway [2]. In addition to transporting different types of goods or passengers, a ship must also contain accommodation and other necessary facilities for the crew. In many cases it must also be able to handle different kinds of cargo in the harbours. In order to make this possible, a ship must be capable of a high degree of selfsufficiency and of handling its own energy supply under very varying conditions. This is why ships are equipped with different types of energy suppliers. These are identified as the main engine, auxiliary engines and the boiler.

The principal sources of marine exhaust emissions are as follows:

- main engine – used for propulsion,
- auxiliary engine – used for the generation of electricity,
- boiler.

The propulsion engines installed in today's ships are of the following types:

- diesel engines
- gas turbines,
- steam turbines.

Steam for turbines is produced by burning fossil fuels. Steam powered vessels are rapidly disappearing from merchant fleets because their specific fuel consumption is approximately 300 g/kWh, which is nearly twice as much as that of a modern diesel engine.

2. Chosen Pollutant in Exhaust Gases

There is increasing interest at all levels of society into harmful emissions to the atmosphere. This section compares the emissions from the various propulsion system options [2].

The diesel engine has undergone a powerful development process resulting in a completely new generation of engines with considerably improved performance. The specific fuel consumption of a modern two-stroke diesel engine may be in the order of 160 g/kWh, as compared to 210 g/kWh for older engines. Today the largest two-stroke diesel engines have an output of over 80 MW, which should be sufficient even for future proposed high-speed container ships. Owing to the high efficiency of diesel engines, the emissions of CO_2, CO and hydrocarbons are relatively low, however, high emissions of NO_X are also characteristic of diesel engines. The same high combustion temperatures that give a high thermal efficiency in the diesel engine are also most conducive to NO_X formation. By running on low quality fuels with a low fuel consumption, large diesel engines offer enormous savings in fuel costs compared with those of alternative prime movers.

On some smaller, more specialized ships such as cruise ships, diesel-electric engines have been installed. This means that the electrical output from several diesel-electric generators, running at constant speed, have been connected to each other. The propulsion then occurs by means of large electric motors, contrary to the conventional way wherein the propeller is fitted on a shaft connected directly, or via a driving gear, to the main engine. However, diesel-electric propulsion is still uncommon today except in cruise ships and in some of the smaller passenger-car ferries. As regards emissions, diesel-electric propulsion does not lead to any significant difference compared to a conventional installation and may experience a net increase in emissions due to the lower efficiency of the total system.

Gas turbines are characterized by the combination high output/low weight. As such they are widely used in military ships and in modern fast ferries. But their fuel efficiency is low (total approx. 215 g/kWh) as compared with diesel engines (approx 160 – 180 g/kWh), which makes them uneconomic for most commercial vessel applications. However, gas turbines are recently appearing in cruise ships where they are used to augment diesel-engined gensets. Princess Cruise's new Coral Princess, for instance, uses a 30,2 MW gas turbine (General Electric LM2500+) in conjunction with two Wartsila diesel engines (Model 9L46 @ 9.45 MW and Model 8L46 @ 8.4 MW). The gas turbine is used as a low-emission power source while hoteling as well as to meet peak power demands. The two diesels meet normal cruising power requirements. They have a fuel efficiency (85% load) of 180 g/kWh, as compared with 215 g/kWh for the LM2500+ gas turbine.

Steam for steam turbines may be produced by burning fossil fuels or by means of nuclear reactors. Steam powered vessels are rapidly disappearing from merchant fleets because their specific fuel consumption is approximately 300 g/kWh, which is nearly twice as much as that of a modem diesel engine. Some steam powered ore carriers apparently still ply the Great Lakes, and a single steam powered cruise ship visits the Port of Vancouver during the summer months. However, these vessels are a small minority of the total marine vessel fleet and hence steam engines will not be addressed in the following sections.

Auxiliary engines are running almost constantly in order to take care of part of the ship's power supply. Power is needed for pumps, cranes, cooling and heating plants, lighting, etc. Some ships have generators connected to the shaft of the main engine (known as shaft generators). These substitute for the auxiliary engines, usually while cruising at sea when the main engine is running. Since most ships turn off their main engines while in port, the auxiliary engines are the dominating source of emissions during the time spent in port. The older auxiliary engines burned lighter fuel oil (e.g. marine diesel oil) so that their emissions were cleaner than those from the main engine. However, modern auxiliary diesel engines are designed to burn the same heavy bunker oil as the main engines do.

Figure 1 presents a mass balance for a modern ship's main diesel engine burning bunker oil, with
8 kg/kWh coming into the engine as fuel, air and lubricating oil and with 8 kg/kWh leaving the engine as exhaust gas. About 0.4% of the exhaust is comprised of the emissions i.e. (NO_X, SO_X, hydrocarbons and particulate), while 6.2 % of the greenhouse gas CO_2.

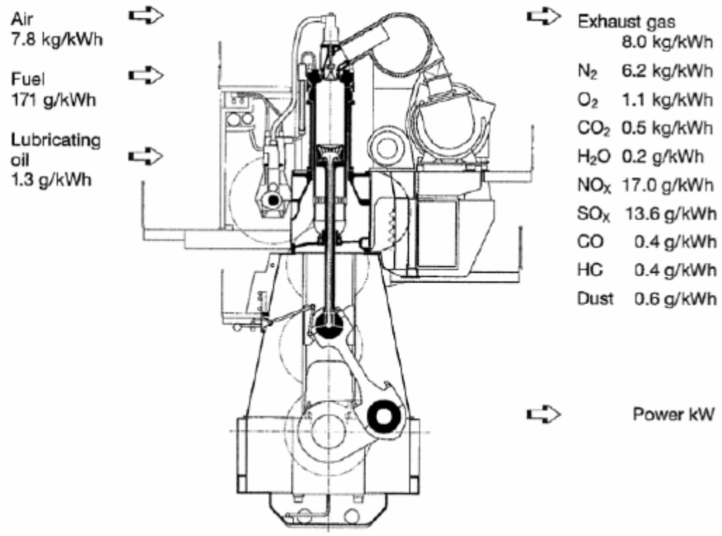

Fig. 1. Emissions from a modern diesel engine [3]

The following table 1 summarises the emissions for various types of propulsion system [2]. These figures are derived from various sources and are indicative only, since such factors as fuel composition and quality of maintenance can affect the values.

Tab. 1. Emissions from Marine Prime Movers [6]

Propulsion system	**NO_X g/kWh**	**SO_X g/kWh**	**CO_2 g/kWh**	**Particulates g/kWh**
2 Stroke Diesel Low Speed	17	12.9	0.058	0.5
4 Stroke Diesel Medium Speed	12	13.6	0.0612	0.4
Dual Fuel Diesel Electric	1.3	0.05	0.042	0.05
Dual Fuel Diesel Slow Speed	14.5	0.2	0.041	0.1
Steam Turbine	1	11.0	0.085	2.5
Gas Turbine	2.5	0	0.048	0.01

1. The figures for the 2-stroke and 4-stroke diesel engines are based on engines consuming heavy fuel oil, such as RMH 35 with a typical sulphur content of about 3.5 %.
2. The dual fuel diesel electric burn gas with a 1% pilot injection of light diesel such as DMA and the slow speed DFD is assumed to be burning gas with 1 % HFO pilot fuel.
3. The steam turbine option is based on dual fuel boilers with 50 % of the energy input coming from HFO and 50 % from boil-off gas.
4. The gas turbine is open cycle configuration and the fuel is 100 % gas, based on standard fuel combustors, even though "low NO_X" combustors are available.

2.1. Sulphur Oxides

Emissions of Sulphur Oxides (SO_X) are purely a function of the sulphur content of the fuel and the amount of fuel consumed. The figures in the table are based on typical fuel oil with 3.5 % sulphur content. The primary fuel for the DRL *(Slow Speed Diesel with Reliquefaction)* option is HFO *(Heavy Fuel Oil)*, hence the emissions level for this concept is significantly worse than the alternatives.

For the gas turbine based propulsion systems, where the primary fuel is gas, the emissions of SO_X compounds are zero in normal operations. For the short periods in service when gas is not available, i.e. for voyages to and from refit, the vessel will use light diesel fuel of DMA quality. These, compared to HFO, have a low sulphur content.

For the DFDE *(Dual Fuel Diesel Electric Engine),* the SO_X emissions are derived purely from the sulphur content of the pilot injection fuel and hence are very low compared with DRL burning HFO and steam turbine plants burning a mixture of HFO and boil-off gas (see Table 1 above).

As for DFDE, the high pressure injection DFD engine SO_X emissions are purely a function of how much pilot HFO is consumed.

The DRL option has no practical optionality for fuel choice, it cannot burn boil-off gas in the engines, therefore, considering the potential 40 year life of these vessels, this aspect represents a significant uncertainty about the long-term economics concerning the supply of the fuel for these engines. For the other alternative propulsions systems, they may operate with the primary fuel source as gas, with no sulphur content; and they also have the technical option of burning gas in port (subject to the terms of Sales and Purchase agreements). Whilst most of the effort has been about reducing the sulphur content of fuels in the first instance, alternative technical solutions, such as scrubbing of the exhaust gases to remove SO_X compounds, are considered feasible. However, there are issues relating to the treatment of the effluent scrub water and the space needed for the installation.

Whereas there is established methodology to put a value on CO_2 emissions, there is currently no equivalent for SO_X.

2.2. Nitrogen Oxides

NO_X emissions are a function of the combustion process. The key factors are the peak temperature achieved and the duration that the gases are at this peak temperature.

Slow speed diesel engines, as used in the diesel with reliquefaction option, are the worst offenders as far as emitting NO_X (see Table 1). The DFDE engine, however, is really operating as a gas engine and, as such, is inherently a low NO_X engine, particularly when compared with engines running on HFO. IMO MARPOL Annex 6 limits the NO_X emissions, based on the engine type. For slow speed diesels, the limit is 17 g/kWh and modern diesel engines will need careful maintenance to stay within these limits.

For the high pressure injection DFD *(High Pressure Gas Injection Slow Speed Diesel engine),* engine, earlier work indicated a reduction of about 15 % for the NO_X emissions compared to a conventional HFO-burning slow speed diesel engine.

For the gas turbine option, even with standard combustors, NO_X emissions are low compared to diesel engine technology. Should even lower levels be required, then technology exists in the form of dry, low-NO_X combustors (DLN) for the gas turbines. NO_X can be removed from the exhaust gas by selective catalytic reduction.

2.3. Carbon Dioxide

Carbon Dioxide (CO_2) emissions are primarily a function of the quantity of fuel burnt, but are also a function of the composition of the fuel being burnt. From this, it is clear that the efficiency of the plant has a major impact on the quantity of carbon dioxide emissions, and this is demonstrated in Table 1 above, which shows the steam turbine as the worst in this respect. The next in this respect is the DRL *(Slow Speed Diesel with Reliquefaction),* option. The open cycle gas turbine option is better than the diesel with reliquefaction option and almost as good as the dual fuel diesel. All internal combustion options are significantly better than the steam plant.

2.4. Particulate Matter

Particulate matter emissions have become a serious health concern in many countries. This applies especially to particulate matter below the size of 10 µm (PM_{10}). Diesel engines are a main source of these particulates. Diesel engines burning low quality fuel emit significantly more particulate matter than those burning clean fuels, such as gas.

The dual fuel diesel emits few particulates compared with diesel engines running on HFO. In operation, the particulate emissions for steam turbine are a function of how much HFO is burnt and peaks during "soot-blowing"' operations. However, the particles generated are considered sufficiently large (i.e. larger than PM_{10}) do not present a health hazard.

Gas turbines burning gas emit virtually no particulates. There is currently no methodology for putting a value on particulates.

3. Current Methodologies and the Best Practices in Preparing Port Emission Inventories

The weakest link in deep sea vessel emission inventories is the emission factors for Category 3 ship engines (according to EPA Marine Compression Ignition Engine Categories, Category 3 ship engine – displacement ≥ 30 liters per cylinder, use to OGV *(Ocean Going Vessels)* propulsion and with approximate Power Ratings > 3000 kW). [4]

Emission factors continue to be derived from limited data. Emission testing of OGV is an expensive and difficult undertaking; and thus, emissions data are relatively rare. In most cases, the power generated is only estimated, leading to inaccuracies in the overall emission factors.

3.1. Propulsion Engine Emission Factors

The most recent study of emission factors was done by Entec, and these factors are generally accepted as the most current set available. Entec analyzed emissions data from 142 propulsion engines and included 2 of the most recent research programs, Lloyd's Register Engineering Services in 1995 and IVL Swedish Environmental Research Institute in 2002. Entec lists individual factors for three speeds of diesel engines: SSD (*Slow-speed diesel),* MSD *(Medium-speed diesel),* HSD (H*igh-speed diesel)* and ST *(Steam turbines)* and three types of fuel RO *(Residual oil)*, MDO *(Marine diesel oil)* and MGO *(Marine gas oil)*. Starcrest used these factors in their PoLA inventory with the following assumptions:

- all main engines operate only on RO (intermediate fuel oil 380 or similar specification with average sulfur content of 2.7 percent),
- slow speed engines have maximum engine speed of less than 130 rpm,
- medium speed engines have a maximum speed of greater than 130 rpm and typically over 400 rpm,
- all turbines are steam boiler turbines.

Currently recommended emission factors are shown in Table 2.

Tab. 2. Emission Factors for OGV Engines using Residual Oil [g/kWh][4]

Engine	NO_X	CO	HC	PM_{10}	$PM_{2.5}$	SO_2
Slow-speed diesel	18.1	1.40	0.60	1.08	0.99	10.3
Medium-speed diesel	14.0	1.10	0.50	1.14	1.10	11.1
Steam turbines	2.1	0.20	0.10	1.55	0.66	16.1

3.2. Auxiliary Engine Emission Factors

As with propulsion engines, the most current set of auxiliary engine emission factors comes from ENTEC. STARCREST used these emission factors for the Port of Los Angeles inventory, and they are considered the most up to date.
There is no need for a low load adjustment factor for auxiliary engines, because they are generally operated in banks. When only low loads are needed, one or more engines are shut off, allowing the remaining engines to operate at a more efficient level.

Tab. 3. Auxiliary Engines Emission Factors for [g/kWh][4]

Engine	Fuel	NO_X	CO	HC	PM_{10}	$PM_{2.5}$	SO_2
Slow-speed diesel	RO	14.70	1.10	0.40	1.14	1.10	11.1
Medium-speed diesel	MDO	13.90	1.10	0.40	0.75	0,28	6.16
Steam turbines	MGO	13.90	1.10	0.40	0.42	0.23	2,05

3.3. Boiler Emission Factors

In addition to the auxiliary engines which are used to generate electricity onboard ships, the most OGVs also have boilers used to heat RO to prepare it to use in diesel engines and to produce hot water.
Auxiliary boiler emission factors are given in terms of fuel usage, rather than power, so a fuel consumption rate also needs to be determined. During its vessel boarding program, Starcrest gathered enough data to estimate the consumption rate to be 0.0125 tonnes of fuel per hour. Auxiliary boiler emission factors, given in kilograms of emissions per tonne of fuel used, are given in Table 3.

Tab.4. Auxiliary Boiler Fuel Emission Factors, kg/tonne Fuel Consumed [4]

Emission Factors kg/tonne Fuel Consumed	
Pollutant	kg/tonne
NO_X	12,30
CO	4,60
HC	0,38
PM_{10}	1,30
$PM_{2.5}$	1,04
SO_2	54,0

5. Conclusion

The presented comparison of NO_X content for various ship engines showed their highest concentration in diesel exhaust gas (see Table 1 and Table 2). It is valid for both the main and the auxiliary engines. A similar conclusion can be drawn for the contents of sulphur compounds. In the case of these engines well-known and extensively studied methods of reduction of emissions are applied, which allow meeting the requirements of IMO MARPOL Convention [5, 7].

Better results in this field are obtained for gas turbines, which are the cleanest sources of energy. However, exhaust gas from boilers of steam turbines are characterized by the worst results of all, with high contents of SO_2, NO_X and CO. The need to lower concentrations of these compounds in exhaust gas of boilers is caused by both the requirements of environmental protection and operational efficiency and points to new directions of further studies.

References

[1] Entec UK Limited, *Quantification of Emissions from Ships Associated with Ship Movements between Ports in the European Community*, 2002.

[2] Genesis Engineering Inc., *Technologies and other options for reducing marine vessel emissions in the Georgia basin,* 2003.

[3] Holtbecker, R., Geist, M., *Exhaust emissions reduction technology for Sulzer marine diesel engines: General aspects*, Wartsila NSD Switzerland Ltd., 1998.

[4] ICF Consulting, *Current Methodologies and Best Practices in Preparing Port Emission Inventories,* Final Report, Fairfax, Virginia, USA, 2006.

[5] Wahlström,J., Karvosenoja N., Porvari, P. Reports of Finnish Environment Institute, *Ship emissions and technical emission reduction potential in the Northern Baltic Sea*, 2006

[6] Wayne, W.S., *The options and evaluation of propulsion systems for the next generation of LNG carriers*, 23rd World Gas Conference, Amsterdam, 2006.

[7] Whitney, F., *Reducing Air Emissions from Marine Diesel Engines: Regional Recommendations, 2004.*

CHARACTERISTICS OF COUNTERCURRENT FLOW HEAT EXCHANGERS

Mariusz Adamski

Białystok Technical University
ul. Wiejska 45E, 15-351 Białystok, Poland
tel.: +48 85 746 96 33, fax +48 85 746 95 76
e-mail: adamski@pb.edu.pl

Abstract

The paper includes equations described heat exchange in countercurrent flow heat exchangers. Taking the energy balance formula as a basis and dividing the heat exchanger into sections, the thermal balances of the cooled fluid, plate and heated fluid are prepared and pertinent system of three differential equations is derived.

The ε -NTU method is used in the analysis. Exemplary temperature profiles in steady state conditions are presented in a graphic form. Transfer functions and dynamic characteristic are determined. Response on step disturbance of inlet temperature is found.

Responses on step or on sin disturbance of inlet temperature in steam condensation heat exchangers are found. The results of calculations are presented in a graphic form.

Keywords: *heat exchanger, thermal balance, temperature profile, and transfer function*

1. Introduction

A heat exchanger is a device in which energy is transferred from one fluid to another across a solid surface. Exchanger analysis and design therefore involve both convection and conduction. Radiative transfer between the exchanger and the environment can usually be neglected unless the exchanger is uninsulated and its external surfaces are very hot. Exemplary countercurrent flow heat exchangers are presented in Figures 1 and 2.

The base for elaboration of control systems is knowledge of static and dynamic characteristics of heat exchangers. Two important problems in heat exchanger analysis are: rating existing heat exchangers and sizing heat exchangers for a particular application.

Rating involves determination of the rate of heat transfer, the change in temperature of the two fluids, and the pressure drop across the heat exchanger. Sizing involves selection of a specific heat exchanger from those currently available or determining the dimensions for the design of a new heat exchanger, given the required rate of heat transfer and allowable pressure drop. The *LMTD* method can be readily used when the inlet and outlet temperatures of both the hot and cold fluids are known. When the outlet temperatures are not known, the *LMTD* can only be used in an iterative scheme. In this paper the *ε-NTU* method is used to simplify the analysis.

2. Energy Considerations

The first Law of Thermodynamics, in rate form, applied to a control volume (CV) between crosses 1 – 1 and 2 – 2, can be expressed as:

energy inflow = energy outflow + exchanged heat + accumulated energy

or $$Q_{inf} = Q_{out} + Q_{exch} + Q_{acc}\,. \tag{1}$$

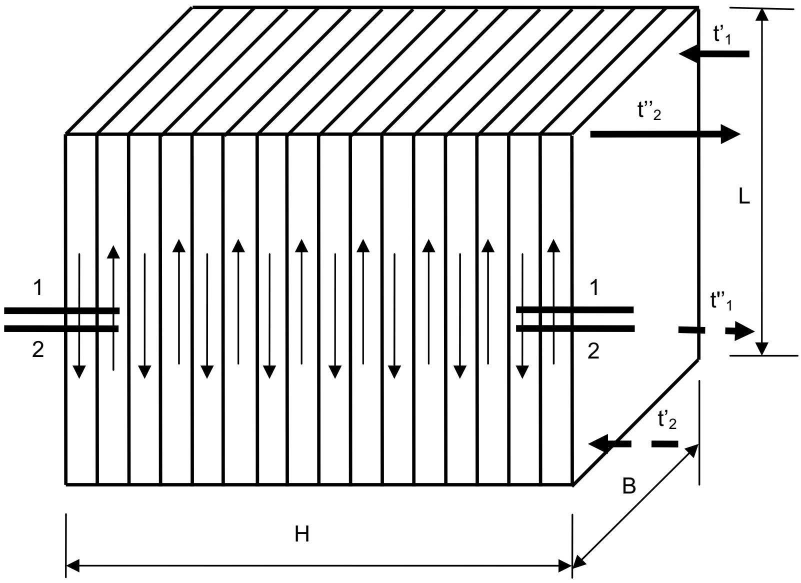

Fig. 1. Schema of plate type heat exchanger

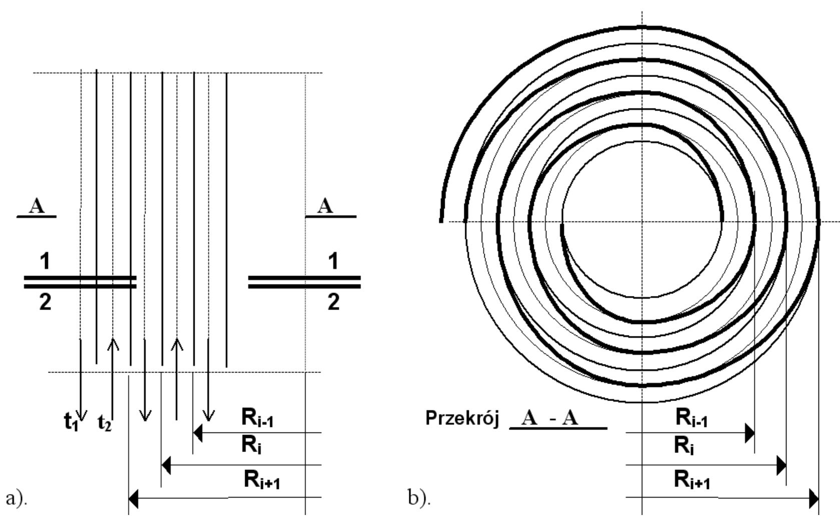

Fig. 2. Longitudinal flow heat spiral exchanger, a) longitudinal section, b) cross- section

This simplified form of the First Law assumes no work- producing processes, no energy generation inside the CV, and negligible kinetic and potential energy in the fluid streams entering and leaving the CV. In steady state operation the energy residing in the CV is constant, meaning that $Q_{acc} = 0$.

If, furthermore, the boundary of the CV is adiabatic (i.e., perfectly insulated), then $Q_{exch} = 0$.

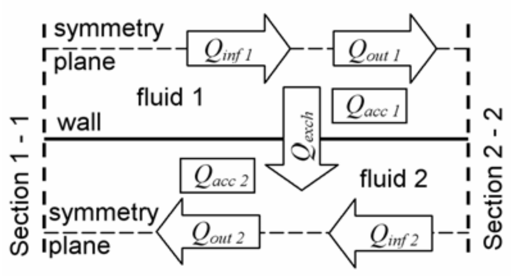

Fig. 3. Control volumes of cooled fluid (marked: fluid 1) and of heated fluid (marked: fluid 2) between sections 1-1 and 2-2 in the countercurrent flow heat exchangers

3. The thermal balances of a single stream of the cooled fluid, of plate and of the heated fluid

The following simplifying assumptions are introduced in the analysis:
- heat conductivity along the plate is disregarded,
- densities and heat capacities are constant in considered temperature range,
- overall heat transfer coefficient in constant in all points of heating surface,
- heat losses to environment are disregarded.

The ingredients of the energy balance for a single stream of the cooled fluid are as follows:

$$Q_{inf} = G'_1 c_1 \vartheta_1 dt, \tag{2}$$

$$Q_{out} = G'_1 c_1 (\vartheta_1 + \frac{\partial \vartheta_1}{\vartheta l} \partial l)\, dt, \tag{3}$$

$$Q_{exch} = \alpha_1 S_1 (\vartheta_1 - \vartheta_{sc})\, dl\, dt, \tag{4}$$

$$Q_{acc} = A_1 \rho_1 c_1 \frac{\partial \vartheta_1}{\partial t}\, dl\, dt, \tag{5}$$

By substitution equations (2 ÷ 5) into (1) we get

$$A_1 \rho_1 c_1 \frac{\partial \vartheta_1}{\partial t} dl + G'_1\, c_1 \frac{\partial \vartheta_1}{\partial l} = \alpha_1 S_1 \left(\vartheta_{sc} - \vartheta_1\right) dl\,, \tag{6}$$

thus

$$T_1 \frac{\partial \vartheta_1}{\partial t} + v_1 T_1 \frac{\partial \vartheta_1}{\partial l} = \vartheta_{sc} - \vartheta_1\,, \tag{7}$$

where:

$$T_1 = \frac{A_1 \cdot \rho_1 \cdot c_1}{\alpha_1 \cdot S_1} = \frac{D_{h1} \cdot \rho_1 \cdot c_1}{4 \cdot \alpha_1}, \quad D_{h1} = \frac{4 \cdot A_1}{S_1}, \quad G'_1 = \frac{G_1}{i} = \frac{A_1 \cdot i \cdot \rho_1 \cdot v_1}{i} = A_1 \cdot \rho \cdot v_1 = \frac{W'_1}{c_1}.$$

and

α – heat transfer coefficient [W m^{-2} K^{-1}]
A – area of duct cross – sectional [m^2]
B, L, H – width of heat exchanger, length of duct, length of exchanger, respectively [m]
c – specific heat [J kg^{-1} K^{-1}]
dl – element of length [m]
D_h – hydraulic diameter [m]

ρ – density [kg m^{-3}]
S – wetted periphery [m]
ϑ – temperature [K]
t – time [s]
T – time constant [s]
$G'c = W'$– water equivalent for one duct [W K^{-1}]
v – velocity [m.s^{-1}]
1, 2, sc – cooled, heated fluid, plate, respectively,

The thermal balance of plate takes the form:

$$Sg\rho_{sc}c_{sc}\frac{\partial \vartheta_{sc}}{\partial t}dl = \alpha_1 S(\vartheta_1 - \vartheta_{sc})dl - \alpha_2 S(\vartheta_{sc} - \vartheta_2)dl\,, \tag{8}$$

and

$$\frac{\partial \vartheta_{sc}}{\partial t} = \frac{1}{T_{1s}}(\vartheta_1 - \vartheta_{sc}) - \frac{1}{T_{2s}}(\vartheta_{sc} - \vartheta_2), \tag{9}$$

where:

g – wall thickness [m],

and

$$T_{1s} = \frac{(S \cdot g \cdot \rho_{sc}) \cdot c_{sc}}{\alpha_1 \cdot S}, \quad T_{2s} = \frac{(S \cdot g \cdot \rho_{sc}) \cdot c_{sc}}{\alpha_2 \cdot S}$$

The thermal balance of the heated fluid takes the form:

$$A_2\rho_2 c_2 \frac{\partial \vartheta_2}{\partial t}dl - G'_2 c_2 \frac{\partial \vartheta_2}{\partial l}dl = \alpha_2 S_2(\vartheta_{sc} - \vartheta_2)dl\,, \tag{10}$$

thus

$$T_2\frac{\partial \vartheta_2}{\partial t} - v_2 T_2 \frac{\partial \vartheta_2}{\partial l} = \vartheta_{sc} - \vartheta_2\,, \tag{11}$$

where:

$$T_2 = \frac{A_2 \cdot \rho_2 \cdot c_2}{\alpha_2 S_2} = \frac{D_{h2} \cdot \rho_2 \cdot c_2}{4 \cdot \alpha_2},\ D_{h2} = \frac{4 \cdot A_2}{S_2},\ G'_2 = \frac{G_2}{i+1} = \frac{A_2 \cdot i \cdot \rho_2 \cdot v_2}{i+1} = A_2 \cdot \rho_2 \cdot v_2 = \frac{W'_2}{c_2}.$$

4. Static characteristics of plate heat exchangers

If we disregard time derivatives in the balance equations (6, 8, 10), we obtain differential equations for steady state conditions:

$$W'_1\frac{\partial \vartheta_1}{\partial l} = \alpha_1 S_1(\vartheta_{sc} - \vartheta_1), \tag{12}$$

$$0 = \alpha_1(\vartheta_1 - \vartheta_{sc}) - \alpha_2(\vartheta_{sc} - \vartheta_2), \tag{13}$$

$$-W'_2\frac{\partial \vartheta_2}{\partial l} = a_2 S_2(\vartheta_{sc} - \vartheta_2), \tag{14}$$

Boundary conditions are as follows:

$$\text{for } l=0 \quad \vartheta_1 = t'_1, \tag{15}$$

$$\text{for } l=L \quad \vartheta_2 = t'_2. \tag{16}$$

where

t' – inlet temperature [K]

If we solve equations (12, 13, 14) taking into account boundary conditions (15 ÷ 16), we obtain of formulae describing temperatures for the steady state conditions:

$$\vartheta_1(l) = t'_1 - (t'_1 - t'_2)\frac{1-\exp\left((W'_1/W'_2-1)\cdot k\cdot F(l)/W'_1\right)}{1-(W'_1/W'_2)\exp\left((W'_1/W'_2-1)\cdot k\cdot F(L)/W'_1\right)}, \tag{17}$$

$$\vartheta_2(l) = t'_2 + (t'_1 - t'_2)\frac{W_1}{W_2}\frac{\exp\left((W'_1/W'_2-1)\cdot k\cdot F(l)/W'_1\right)-\exp\left((W'_1/W'_2-1)\cdot k\cdot F(L)/W'_1\right)}{1-(W'_1/W'_2)\exp\left((W'_1/W'_2-1)\cdot k\cdot F(L)/W'_1\right)}, \tag{18}$$

$$\vartheta_{sc}(l) = \frac{\alpha_1\cdot\vartheta_1(l)+\alpha_2\cdot\vartheta_2(l)}{\alpha_1+\alpha_2}, \tag{19}$$

where:

$$\frac{1}{k} = \frac{1}{\alpha_1}+\frac{1}{\alpha_2}+\frac{g}{\lambda}+R_Z,\ F(l) = 2\cdot B\cdot l,\ \frac{F(l)}{W'_1} = \frac{2\cdot B\cdot l}{A_1\cdot v_1\cdot\rho_1\cdot c_1} = \frac{4}{D_{h1}\cdot v_1\cdot\rho_1\cdot c_1}\cdot l, \tag{20}$$

and

F – heat transfer area [m^2]
k – overall heat transfer coefficient [$W\ m^{-2}\ K^{-1}$]
λ – thermal conductivity coefficient [$W\ m^{-1}\ K^{-1}$]
R_Z – additional thermal resistance of calcium precipitations [$W^{-1}\ m^2\ K$]

In balanced heat exchangers $\frac{W'_1}{W'_2}=1$. Hence from equations (17, 18) we obtain:

$$\vartheta_1(l) = t'_1 - (t'_1 - t'_2)\cdot\frac{k\cdot F(L)/W'_1}{1+k\cdot F(L)/W'_1}\cdot\frac{l}{L}, \tag{17a}$$

$$\vartheta_2(l) = t'_2 - (t'_1 - t'_2)\cdot\frac{k\cdot F(L)/W'_1}{1+k\cdot F(L)/W'_1}\cdot\left(1-\frac{l}{L}\right), \tag{18a}$$

In steam heat exchangers, $W_2 < W_1 = \infty$ and from equations (17, 18) we obtain:

$$\vartheta_1(l) = t'_1, \tag{17b}$$

$$\vartheta_2(l) = t'_2 + (t'_1 - t'_2)\cdot\left(\exp\left(\frac{k\,(F(L)-F(l))}{W_2}\right)-1\right), \tag{18b}$$

Taking into account that:

$$t''_1 = \vartheta_1(L), \tag{21}$$

$$t''_2 = \vartheta_2(0), \tag{22}$$

the outlet temperatures t''_1, t''_2 can be calculated from system of equation (17, 18), in balanced heat exchangers from equations (17a, 18a) and in steam heat exchangers from equations (17b, 18b).

5. Dynamic characteristic of plate heat exchangers. Response to disturbance of temperature

Plate heat exchanger is considered as element with two input and two output quantities:

$$\mathbf{Y_2} = \mathbf{G_{2\,x\,2}}\,\mathbf{X_2}, \tag{23}$$

$\mathbf{X_2} = \mathbf{X}\,[t'_1, t'_2]$ – input signal, two – dimensional vector
$\mathbf{Y_2} = \mathbf{Y}\,[t''_1, t''_2]$ – output signal, two – dimensional vector

$\mathbf{G}$ – transmittance matrix: $\mathbf{G} = \mathbf{G}_{2x2} = \begin{Vmatrix} G_{11} & G_{12} \\ G_{21} & G_{22} \end{Vmatrix} = \begin{Vmatrix} \dfrac{t''_1(s)}{t'_1(s)} & \dfrac{t''_1(s)}{t'_2(s)} \\ \dfrac{t''_2(s)}{t'_1(s)} & \dfrac{t''_2(s)}{t'_2(s)} \end{Vmatrix}$.

If we disregard heat accumulation in plates of exchanger (9) in the thermal balance equations (7, 9, 11), we should obtain system of two differential equations:

$$T_1\frac{\partial \vartheta_1}{\partial t} + v_1 T_1\frac{\partial \vartheta_1}{\partial l} = \vartheta_2 - \vartheta_1, \tag{24}$$

$$T_2\frac{\partial \vartheta_2}{\partial t} - v_2 T_2\frac{\partial \vartheta_2}{\partial l} = \vartheta_1 - \vartheta_2, \tag{25}$$

where T_1 and T_2 are calculated for overall heat transfer coefficient.

Let's consider small changes of temperatures from state of equilibrium:

$$\vartheta_{1,2} = \overline{\vartheta_{1,2}} + \Delta\vartheta_{1,2},$$

where $\overline{\vartheta}$ – temperature in state of equilibrium, $\Delta\vartheta = \Theta$ – change of temperature ϑ.

Let's define:

$$L^*_1 = \frac{L}{v_1 T_1},\ \ L^*_2 = \frac{L}{v_2 T_2},\ \ v^* = \frac{v_1}{v_2},\ \ t^* = \frac{v_1 \cdot t}{L},\ \ l^* = \frac{l}{L},\ \text{ i. e.: } dt^* = \frac{v_1}{L}dt,\ \ dl^* = \frac{dl}{L}.$$

Then equations (24, 25) can be written in dimensionless form [1]:

$$\frac{\partial \Theta_1}{\partial t^*} + \frac{\partial \Theta_1}{\partial l^*} = L^*_1\left(\Theta_2 - \Theta_1\right), \tag{26}$$

$$v^*\frac{\partial \Theta_2}{\partial t^*} - \frac{\partial \Theta_2}{\partial l^*} = L^*_2\left(\Theta_1 - \Theta_2\right), \tag{27}$$

We solve system of equations (26, 27) by the Laplace – transform method. Boundary conditions (15, 16) are transformed too and included into solution. Then, the transfer functions can be written as:

$$G_{11} = \frac{2q\exp(b+q)}{q-p+(p+q)\exp(2q)}, \tag{28}$$

$$G_{12} = L^*_1 \frac{1-\exp(-2q)}{p+q-(p-q)\exp(-2q)}, \tag{29}$$

$$G_{21} = L^*_2 \frac{1-\exp(-2q)}{p+q-(p-q)\exp(-2q)}, \tag{30}$$

$$G_{22} = \frac{2q\exp(-b+q)}{-p+q-(p+q)\exp(2q)}, \tag{31}$$

where:

$$b = -\left(\frac{1-r}{2}s + \frac{b_1 - b_2}{2}\right),\ p = \left(\frac{1+r}{2}s + \frac{b_1 + b_2}{2}\right),\ q = \sqrt{p^2 - b_1 b_2}\ .$$

6. Simulations example

Change of outlet temperature of cooled fluid $\Delta\vartheta''(t)$, which is response to step change of inlet temperature of heated fluid $\Delta\vartheta'(t)$ could be calculated from equation.

$$\Delta\vartheta''(t) = \frac{M(0)}{N(0)} + \sum_{k=1}^{n} \frac{M(s_k)}{s_k\, N'(s_k)} e^{s_k t}, \tag{32}$$

where $M(s_k)$ is numerator, $N(s_k)$ denominator of the taken into consideration transfer function, s_k are roots of an equation $N(s_k) = 0$ and $N'(s_k) = [dN(s)/ds]_{s=sk}$.

First summand in right part of equation (32) represents steady-state conditions, following – transient components.

The transfer functions G_{12}, G_{21} are interesting particularly. In case steam condensation heat exchangers $b_1 b_2 = 0$, hence $p = q$ and the transfer functions G_{21} takes the form:

$$G_{21} = L^*_2 \frac{1-\exp(-b_2)\exp((1+r)s)}{(1+r)s + b_2}, \tag{33}$$

Supplementary schema of heat exchanger under equation (33) with sine-response function is showed in Figure 4.

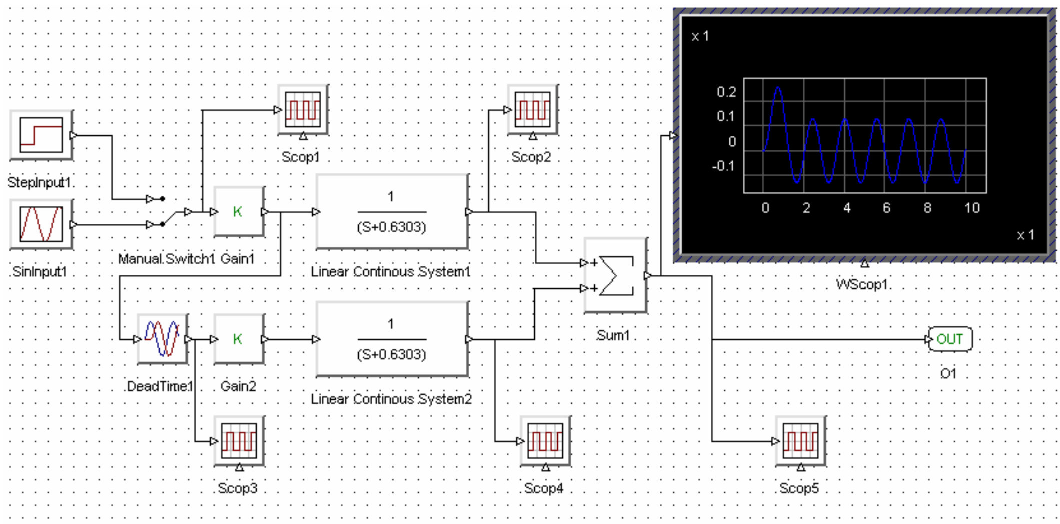

Fig. 4. Supplementary schema of heat exchanger under equation (33) with sine-response function

7. Conclusions

Values of temperatures in individual sections countercurrent flow exchangers could be computed using presented method of calculations.

Important element of this computations is determination of heat transfer coefficients α_1, α_2 and overall heat transfer coefficient k.

Better knowledge of specificities enables farther optimization heat exchangers and exchanger control systems.

This study has been made within the frame of the Project No. W/IIŚ/21/06

References

[1] Adamski, M., *Theoretical characteristics of plate heat exchangers,* VII Internationales Symposium: Wärmeaustausch und Erneuerbare Energiequellen, Polnische Akademie der Wissenschaften, Technische Universität Szczecin, Szczecin 1998, pp. 9 -16.

[2] Chmielnicki, W., Zawada, B., *Właściwości dynamiczne przepływowych wymienników ciepła,* Nowa technika w Inż. San., Ogrzewnictwo i Wentylacja Nr 14, Arkady, Warszawa 1982.

[3] Żelazny, M., *Podstawy automatyki,* PWN, Warszawa 1976.

DESIGN CONCEPT OF DIESEL-ELECTRIC POWER PLANT OF A TWO-SEGMENT PASSENGER SHIP INTENDED FOR OPERATING ON EAST-WEST INLAND WATERWAYS OF POLAND

Damian Bocheński
Jacek Rudnicki

Gdańsk University of Technology
Ul. Narutowicza 11/12, 80-952 Gdańsk, Poland
Tel.: +48 58 3472773, fax: +48 58 3472430
e-mail: daboch@pg.gda.pl , jacekrud@pg.gda.pl

Abstract

This paper presents a concept of diesel- electric power plant of a two-segment passenger ship intended for operating on inland waterways. The conceptual design was elaborated in the frame of the EUREKA InCoWaTrans E!3065 project which concerns a new generation of environment-friendly ships for inland waterways and coastal service on east-west routes of Polish waterways system.

Keywords: *inland waterways passenger ship, ship power plants, ship power systems*

1. Introduction

The EU project called *EUREKA 3065! InCoWaTrans* concerned a new generation of environment-friendly ships for inland waterways and coastal service on east-west routes of Polish waterways system. Within the frame of the project it was the task for Faculty of Ocean Engineering and Ship Technology, Gdańsk University of Technology, to elaborate a design concept of an inland waterways passenger (tourist hotel) ship intended for operating on extremely shallow and narrow inland waterways of Poland, Germany and Russia, mainly on Berlin-Kaliningrad route there and back.

The passenger ship in question (whose overall view is presented in Fig.1), is designed as a two-segment unit composed of a pusher and barge. Such system is conditioned by characteristics of the waterway on Berlin-Kaliningrad route. Along the route are located 26 locks of the dimensions which make it possible to accommodate ships not longer than 55 m and not broader than 9 m [7].

The depth of 4,8 m is assumed for the ship, which results from values of clearance under bridges located along the shipping route in question. The designed ship draught of 1,0 m is assumed with possible increasing it to 1,2 m by taking water into ship's ballast tanks. The increased draught is necessary for passing under the bridge at Łęgowo. Summing up, the main dimensions of the designed ship are as follows:

- Overall length of a single segment $L = 55{,}00\,m$
- Breadth $B = 9{,}00\,m$
- Maximum depth $H = 4{,}90\,m$
- Design draught $T = 1{,}00\,m$
- Total length of the push- train $L_C = 110{,}00\,m$

a) b)

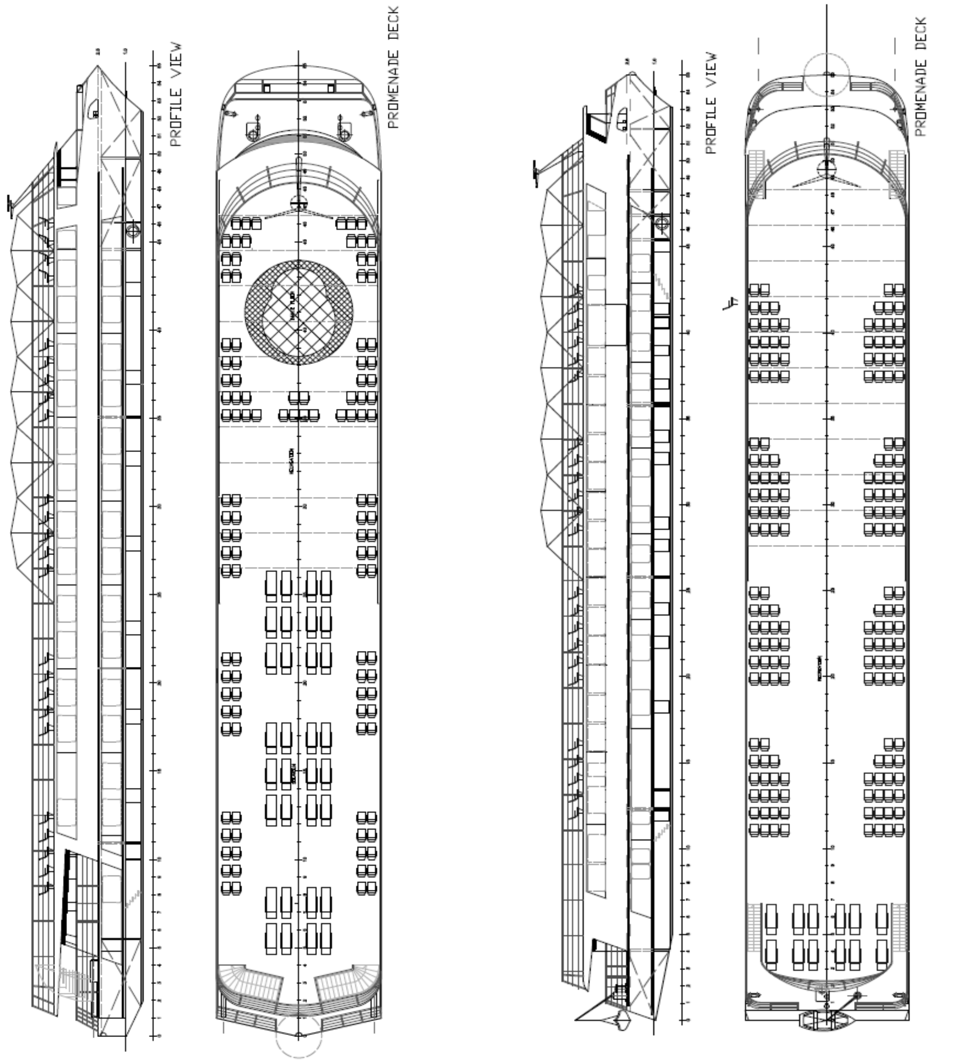

Fig.1. Overall view of the barge: (a), and of the pusher : (b)

2. Design assumptions

On the basis of comparative analyses of various propulsors it was assumed that the ship's propulsion will be consisted of two azimuthing fixed screw propellers ducted in nozzles. The propellers will be installed in the stern part of the pusher. Additionally, in the bow part of the barge will be installed an auxiliary, electrically (or hydraulically) driven propeller of about 30 kW output power. The propeller would serve as a bow thruster for the whole push-train, as well as provide - for the barge - capability to motion with the speed of about 2–3 km/h during the locking of the ship when to disconnect the train is necessary [5].

For the two assumed maximum speeds: 15 km/h in deep waters (ship delivery trials), 10 km/h in shallow and extremely shallow waters, as well as the speed of 6,5 km/h in canals, and canalized rivers, the power at the propeller cone equal to 2×150 kW, at the propeller rated speed of 600 min^{-1} [6,7], was determined. On the basis of the performed analyses [1,2,5] it was assumed that the ship in question will be equipped with a diesel-electric or diesel-hydraulic propulsion system. For electric (or hydraulic) main propulsion motors the output power of about 200 kW was determined from the analysis of service conditions of the diesel engines driving fixed screw propellers of the designed passenger ship [2].

With taking into account the assumptions concerning the equipment and mode of operation of the ship the variant consisting in the idea that the main power plant will be installed on the pusher and the auxiliary power plant - on the barge, was adopted. The main power plant is intended for delivering power for ship propulsion as well as feeding all electric energy consumers (both on the pusher and barge) in all states of the ship's operation.

The auxiliary power plant installed on the barge is first of all intended for delivering power to drive an auxiliary propeller located on the bow of the barge, as well as for feeding electric energy consumers on the barge during locking operations when the two segments must be disconnected.

Volvo Penta (and alternatively *Caterpillar*) engines were selected as main and auxiliary engines. The choice of the firms was preceded by the relevant analysis presented in [1]. Final selection of a producer of engines can be done during further design phases, after possible consulting the ship owner. In the case of the diesel-electric power plant, electric motors and frequency converters are additionally included in the main propulsion system. It was decided to apply *Cantoni* electric motors and *Danfoss* frequency converters [2,4].

In the opinion of the design team of the Department of Ship Power Plants, regardless of a ship propulsion variant, the main power plant should be composed of diesel engines of the same type, size and number. As far as the diesel-electric propulsion system is concerned the power plant will consist of three main electric generating sets driven by D9 MG *Volvo Penta* diesel engines of 239 kW rated power (216 kW output of one set). In the case of the diesel –hydraulic propulsion system also three D9 MG diesel engines will be installed, two of them to drive the hydraulic pumps of 200 kW power and additionally 50 kW electric generator, whereas one of them to drive the electric generating set of 216 kW output power.

During design process of the ship's power plant were made several decisions aimed at minimizing emission of pollutants, to the environment, resulting from power plant operation. The decisions consisted in:

- choice of diesel - electric propulsion system for the ship (or diesel-hydraulic one) that seems the most favourable for inland waterways ships from the point of view of environmental protection [9];
- choice of D9 MG *Volvo Penta* diesel engines (alternatively C9 *Caterpillar* engines) which can satisfy the strict requirements for emission of gaseous pollutants from combustion engines, contained in the so called Rhine Rules - stage II, established by the Central Commission for Shipping on the Rhine, which have to come in force in all EU countries beginning from 1 July 2007 [10];
- as to apply gas fuel was not possible – it was recommended to use distilled oil fuels of ISO-F-DMX category , as - light - as - possible;
- to apply wet exhaust gas outlet systems which are able a.o. to limit level of noise emitted from ship power plant to the environment;
- choice of an appropriate arrangement of tanks for fuel, lubricating and waste oil by separating them from side and bottom plating with the use of cofferdams;
- to store bilge water in a special tank so as to then discharge it to land-based receipt points in the time intervals precluding the tank from overflowing.

3. Main power plant on the pusher

On the pusher was provided the engine room of 8 m in length (between 4th and 12th abscissa), 8,5 m in breadth and 2,5 m in height. However it should be added that due to the applied form of the stern the ship's hull bottom in the region of the engine room has not a rectangular shape of 68 m^2 area, but a trapezoidal shape of the area of only about 50 m^2.

The main devices of the pusher's power plant will be the following:

- three D9 MG/HCM434C *Volvo – Penta* electric generating sets developing 216 kW (270 kVA) each. Each of them consists of a supercharged diesel engine assembled with an electric generator together, both fixed to a common steel foundation seated on elastic pads connected with hull structure by screw bolts. The diesel engines are of KC (keel cooling) version which makes it possible to use box coolers for fresh water cooling the engines. The engines will be equipped with a special knee duct to let exhaust gas from the engine to go together with outboard water to exhaust gas duct.
- Two main electric drive systems which can be made in two variants. The first - fitted with SEEK 315 M4C *Celma* vertical electric motors. The motors will be directly coupled with the shaft of the azimuthing propeller of "L" design (having one intersecting axis gear). The second - with SCe 315 M2 *Emit* horizontal electric motors. The motors will be connected - through a short cardan shaft – with the input shaft of the azimuthing propeller of "Z"design (having two intersecting axis gears). All the electric motors will develop 200 kW output power each. The rotational speed of motors: 1483 min^{-1}- in the first variant, and 2971 min^{-1} in the second one. The speed will be controlled by frequency changing. To this end VLT 6275 *Danfoss* frequency converters will be used.

All diesel engines of electric generating sets will be fresh-water cooled. The produced heat will be absorbed by outboard water within box coolers located in the left- and right –side Kingston valves. Each of the engines will be fitted with the high- temperature fresh-water pump, low-temperature fresh-water pump as well as the outboard-water circulating pump belonging to the wet gas exhaust system [3], all of them - driven by the engines. Expansion tanks and thermostatic valves will be also suspended on the engines.

An outboard-water pump driven by a separate electric motor will be installed to absorb heat from other devices (oil coolers of reversing-reduction gears , cooling medium condenser of air-conditioning control unit, reefer store cooler, possible cooling system of bearings etc).

Every diesel engine will be fitted with one lubricating oil circulating pump driven from the engine, double oil filter and oil cooler (cooled with high-temperature fresh water) [10]. Any purification process of lubricating oil in centrifugal separators is not taken into account.

Waste oil will be pumped from engine oil sumps to a waste oil tank by means of an oil transport pump. A fresh-oil storage tank will be also included in the system. An oil transport pump driven by a separate electric motor will be installed to transport the oil inside the ship as well as to discharge the waste oil out of the ship (possible application of hand – operated pump is also taken into account because of low flow rates and sporadic use of the pump) [3].

Every *Volvo – Penta* diesel engine will be fitted with *Bosch* combined pumping injectors, a double precise fuel-oil filter as well as fuel supply pump driven by the engine. The fuel supply pumps will suck in the fuel from the day tank placed in one of the storage tanks (or directly from the storage tanks).

As the application of the fuel oils of *ISO-F-DMX* category is assumed no centrifugal separators are provided for. An electrically-driven fuel transport pump is provided to pump fuel oil to and from the tanks. Fuel oil leaks which may occur during bunkering operations as well as those from pots under fuel devices, will be discharged to a leak oil tank and next to a separate free-standing tank or through an elastic pipe to land [3].

The wet exhaust gas outlet through ship sides is applied. Each diesel engine will have a separate duct for discharging the exhaust gas outboard. The system will be composed of an aqua-lift silencer (which serves also as a water blockade), rubber exhaust gas pipes as well as an outlet pipe connector fitted with a flap check valve. The exhaust gas outlets will be placed at least 50 mm over water line [3].

All diesel engines will be electrically started-up with the use of 24 V voltage supplied from an accumulator battery. In the pusher's power plant altogether 6 start-up batteries of 225 Ah and one 400 Ah emergency battery will be installed. They all will be acid-gel batteries chargeable from the electric network [4].

In the engine room will be also installed: the devices belonging to the water supply system on the pusher (hydrophore tank, two hydrophore pumps, hot-water circulating pump and electric heater), general-purpose outboard-water pump, auxiliary compressor, emergency drainage pump for compartments beyond the power plant, sewage discharging, bilge, ballast and fire extinguishing pumps as well as a power pack for feeding hydraulic motors on the pusher [4].

In the designed power plant of the pusher main electric generating sets, switchboards, electric motors driving azimuthing propellers as well as box coolers placed in kingston valves are the main elements to be dimensioned.

The electric generating sets will be seated on elastic pads with taking into consideration a rational route of exhaust gas ducts, location of silencers, routes of electric cables from generators, as well as structural design of foundations.

The kingston boxes are so located as to take into account that the box coolers have to be placed in them. The main which connects the kingston boxes to each other, of DN 125 diameter, will be located along 11th abscissa. Nearby will be located the outboard water pumps (ballast, fire, and general purpose pump etc) [3].

The main switchboards are placed in parallel to ship's plane of symmetry (on both side walls of the staircase leading to the main deck). The remaining auxiliary devices will be located between two electric generating sets situated port side and the transverse bulkhead at 4th abscissa and the starboard electric generating set. The devices and mechanisms are so arranged as to ensure free passage from their control and maintenance spots to emergency gangways. The main entrance to the machinery room – by the doors from the corridor that goes along the pusher on the floor level. The emergency exit - through the vertical stairs on the transverse bulkhead (at 4th abscissa) and the hatchway – up to the main deck [4].

The electric motors which drive azimuthing propellers will be located in separate compartments in the stern part of the pusher. Two variants of solving the propeller drive are possible: by using either vertical motors (of „L" design) or horizontal motors (of „Z" design). In the first case it would be necessary to shift the deck up - by about 30 cm - over the compartments of main electric motors.

The arrangement plan of the pusher's engine room is presented in Fig. 2. In Tab.1 the preliminary specification of power plant devices is given. The numbers shown in Fig. 2 correspond with those given in Tab. 1.

Tab.1. Preliminary specification of the devices of the pusher's power plant

No.	Name of device	Number of pieces	Mass [kg]	Characteristic
1	2	3	4	5
1	Main electric generating set Volvo Penta D(MG KE/HCM 434C	3	2660	N = 216 kW n = 1500 rpm
2	Main driver electric motor EMIT SCe 315M	2	1350	N = 200 kW n = 2980 rpm
3	Frequency converter DANFOSS VTL 6000	2	200	
4	Engine silencer VETUS	3		
5	Fuel – oil transport pump	1	50	Q = 2 m^3/h p = 4 bar
6	Lubricating – oil transport pump	1	20	Q = 20 dm^3/min p = 2 bar
7	Outboard water pump	1		Q = 10 m^3/h p = 2,5 bar
8	Cooling box	3		
9	Fire pump	1	400	Q = 40 m^3/h p = 6 bar
10	Ballast pump	1	180	Q = 35 m^3/h p = 2,5 bar
11	Bilge pump	1	180	Q = 35 m^3/h p = 2,5 bar
12	Auxiliary compressor	1		Q = 20 m^3/h p = 8 bar
13	Fecal matter pump	1	135	Q = 36 m^3/h p = 1,5 bar
14	Potable and sanitary water pump	2	30	Q = 2 m^3/h p = 5 bar
15	Hydrophore tank	1	400	V = 1 m^3
16	Hot – water circulating pump	1	15	Q = 1,5 m^3/h p = 2 bar
17	Water electric heater	1	150	Q = 20 kW
18	Emergency drying pump	1	180	Q = 50 m^3/h p = 2,5 bar
19	Power Pack	1	200	N = 10 kW
20	Main electric switchboard no. 1	1		
21	Main electric switchboard no. 2	1		
22	Hand operated fuel – oil pump	1	20	
23	Batteries	8	500	

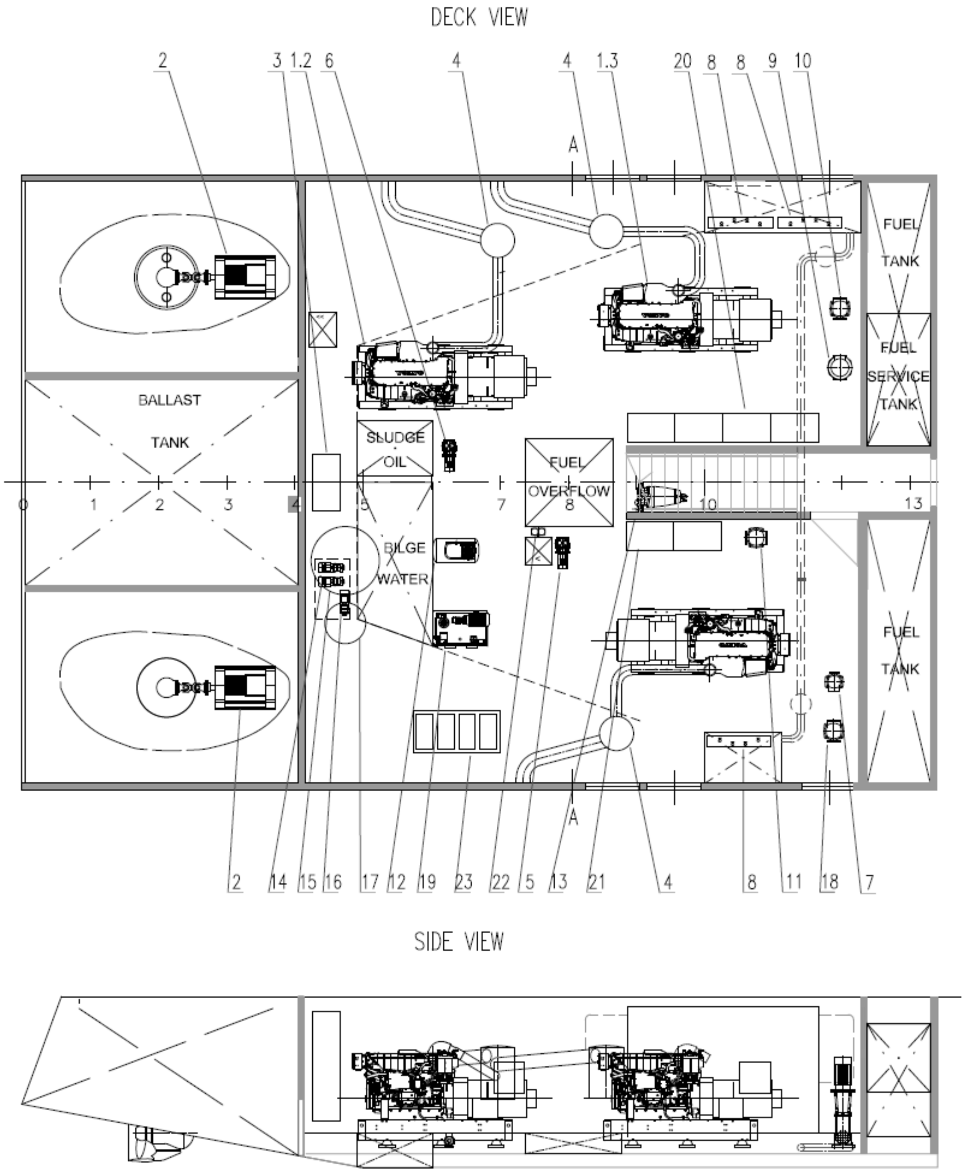

Fig.2. Arrangement plan of the devices located in the pusher's engine room

4. Auxiliary power plant located on the barge

A WCM42/5 small electric generating set of 42 kW (56 kVA) output power will be the main device installed in the barge's engine room. The auxiliary screw propeller will be located beyond the engine room, on the bow of the barge. Its electric drive will consist of Sg 180 L4 *Indukta* electric motor of 22 kW output power. Rotational speed control – by frequency changing with the use of VLT 5032 *Danfoss* frequency converter.

The diesel engine driving electric generating set is fresh-water cooled. The produced heat will be taken by outboard water in a water-water cooler. The engine will be fitted with the pumps suspended on it: fresh-water circulating, outboard water, lubricating oil and fuel supply pump. The fuel supply pump will suck-in the fuel oil from the day spare tank. The engine will be fitted with a separate pipe to discharge exhaust gas outside the ship. A dry system to exhaust gas above the promenade deck (alternatively through ship's stern) will be applied. Start-up of the engine – electric one [4].

In the barge's engine room will be also located the water supply system for the barge (containing two hydrophore tanks, two hydrophore pumps, one hot water circulating pump and electric water heater), emergency drainage pump for the compartments outside the power plant, sewage pump, ballast pump, fire pump, bilge pump as well as the power pack for feeding the hydraulic cylinders installed on the barge.

The barge's engine room will be located between the aft ballast tanks (the abscissae "0" and "5,5"). The gabarites of the engine room are the following: 5,5 m in length, 3 m in breadth, 2,5 m in height. The kingston main of DN 100 diameter, connecting the bottom kingston valve (under engine room's floor) with the side kingston valve will go along *2nd* abscissa. The electric switchboard will be fixed on the ballast tank bulkhead (port side) and in parallel the electric generating set will be placed on the other side. The remaining devices will be so arranged as to make free passage from their control and maintenance spots to emergency gangways, possible [4].

The main entrance to the machinery room– through the doors on the platform of the stairs connecting the corridor which goes on the floor level along the pusher, with the main deck. The emergency exit - through the vertical stairs and hatchway –up to the main deck.

The arrangement plan of the barge's machinery room is presented in Fig. 3. The preliminary specification of power plant devices is given in Tab. 2. The numbers shown in Fig. 3 correspond with those in Tab. 2.

Tab.2. Preliminary specification of the devices of the auxiliary power plant on *the barge*

No.	Name of device	Number of pieces	Mass [kg]	Characteristic
1	2	3	4	5
1	Auxiliary electric generating set WCM 42/5 – 60/6	1	1000	N = 42 kW n = 1500 rpm
2	Engine silencer	1		
3	Outboard – water pump	1	20	Q = 10 m^3/h p = 2,5 bar
4	Fire pump	1	300	Q = 40 m^3/h p = 6 bar
5	Ballast pump	1	180	Q = 35 m^3/h p = 2,5 bar
6	Hand operated bilge pump	1	20	Q = 7 m^3/h
7	Fecal mater pump	1	135	Q = 36 m^3/h p = 1,5 bar
8	Potable and sanitary water pump	2	30	Q = 2 m^3/h p = 5 bar
9	Hydrophore tank	1	400	V = 1 m^3
10	Hot – water circulating pump	1	15	Q = 1,5 m^3/h p = 2 bar
11	Water electric heater	1	150	Q = 20 kW
12	Emergency drying pump	1	180	Q = 50 m^3/h p = 2,5 bar
13	Power Pack	1	200	N = 10 kW
14	Main electric switchboard	1		
15	Batteries	1	120	

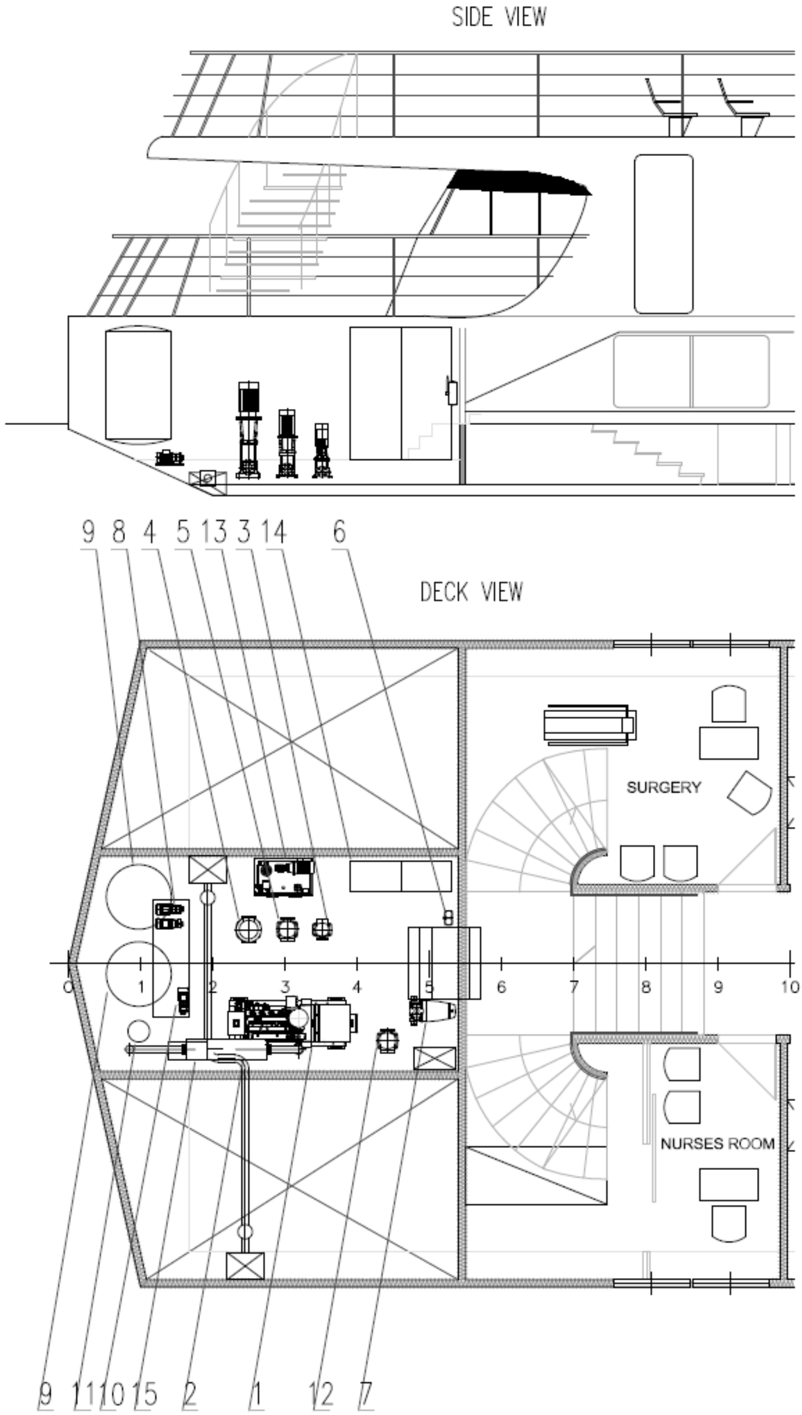

Fig. 3. Arrangement plan of the devices located in the barge's machinery room

References

[1] Bocheński, D., Kubiak, A., *Analiza i synteza warunków ruchu statku i ustalenie mocy efektywnych napędu głównego oraz propozycja rozwiązań konstrukcyjnych układu napędowego i siłowni z uwzględnieniem zapotrzebowania na energię elektryczną,* Research reports no. 94/SPB, Eureka/ 2004, Gdańsk 2004.

[2] Bocheński, D., Kubiak, A., Rudnicki, J., *Identyfikacja problemów wykonania projektu wstępnego siłowni śródlądowego statku pasażerskiego z uwzględnieniem zapotrzebowania energii do napędu głównego i odbiorników elektrycznych,* Research reports WOiO PG no. 221/SPB, Eureka/ 2005, Gdańsk 2005.

[3] Bocheński, D., Kubiak, A., Rudnicki, J., *Projekt i opis techniczny instalacji obsługujących silniki spalinowe siłowni spalinowo-elektrycznej śródlądowego statku pasażerskiego,* Research reports WOiO PG no. 241/SPB, Eureka/ 2006, Gdańsk 2006.

[4] Bocheński, D., Kubiak, A., Rudnicki, J., *Projekt siłowni spalinowo-elektrycznej śródlądowego statku pasażerskiego z napędem pędnikami azymutalnymi,* Research reports WOiO PG no. 242/SPB, Eureka/ 2006, Gdańsk 2006.

[5] Dymarski, Cz. Rolbiecki, R., *Opracowanie założeń i ogólnej koncepcji układu napędu i sterowania członu pchanego zestawu statku śródlądowego,* Research reports WOiO PG no. 196/SPB, Eureka/ 2005, Gdańsk 2004.

[6] Michalski, J., *Wstępne wyznaczenie głównych parametrów projektowych statku – prognozy oporowe kadłuba,* Research reports WOiO PG no. 96/SPB, Eureka/ 2004, Gdańsk 2004.

[7] Michalski, J., *Model matematyczny doboru optymalnych parametrów układu napędowego statków śródlądowych – aproksymacja eksperymentalnych charakterystyk oporowych kadłuba,* Research reports WOiO PG no. 182/SPB, Eureka/ 2005, Gdańsk 2005.

[8] Rosochowicz, K., *Ramowe założenia projektowe dla członowego śródlądowego statku pasażerskiego,* Projekt *Eureka INCOWATRANS E13065*, Gdańsk 2003.

[9] Wieszczeczyński, T., *Technical aspects of environmental protection concerning a small inland waterways passenger ship* (in Polish*),* Seminar on "Environmental protection in ship building and operating on inland and coastal waterways", Bydgoszcz, 21 June 2006.

[10] *Decree of Ministry of Economy and Labour, issued on 19-08-2005, on the detail requirements for combustion engines concerning limitation of emission of gaseous contamination and solid particles from the engines* (in Polish), Dz. U. (Bulletin of Legal Acts) no. 2005.202.1681.

OPERATIONAL LOADS OF POWER SYSTEMS OF BUCKET DREDGERS IN MAIN SERVICE STATES

Damian Bocheński

Gdańsk University of Technology
Ul. Narutowicza 11/12, 80-952 Gdańsk, Poland
Tel. +48 58 3472773, fax: +48 58 3472430
e-mail: daboch@pg.gda.pl

Abstract

This paper presents results of investigations of six bucket dredgers in service. The operational investigations consisted in measuring the parameters which characterize working conditions of power systems of the dredgers: operational loads of main engines as well as loads of electric generators which cover power demand from the side of auxiliary consumers.

Keywords*: bucket dredgers, power plants, ship power systems*

1. Introduction

Service states of bucket dredger significantly differ from those of a typical cargo ship. The main service state is that defined as "dredging operations". The state is consisted of the following periods: digging connected with loosening and hoisting the loosened soil onto the dredger, possible transporting the winning to land by using dredging pump, as well as dredger manoeuvring over excavation site. From the point of view of power problems of the dredger the main state is that in which at least one main technological consumer operates, hence also the main engine (to drive main technological consumers). During breaks in dredging only the auxiliary engine operates.

The second service state, analogous to that on cargo ships, is "free -floating". In the service state, manoeuvring or weathering periods can happen, depending on navigational situation. The state is characterized by a greater power demand than that for „dredging operations", hence the power system of self- propelled bucket dredgers consists of two main engines; one of them operates during dredging and both during free-floating. The free-floating state takes place only on self-propelled dredgers. Most bucket dredgers are not fitted with self-propulsion system [5]. For them the „ towing" state is equivalent to that of "free-floating", however from the point of view of energy consumption the state is identical with breaks in dredging work.

The bucket dredger power system consisted of main engine(-s) and auxiliary engines, has the task to cover power demand from the side of main consumers (bucket chain, side winches , possible main drive propellers and dredging pump) and a group of auxiliary consumers. Generally the main engines operate to cover demand of main consumers, however in the basic service states they ensure energy also for driving auxiliary consumers (all or only a selected number of them).

The character of power system operational loads is best illustrated by the loads of main engines and electric generators for ship general purposes (covering power demand from the side of the group of auxiliary consumers).

In this paper are presented characteristics of real loads of main engines in both above mentioned service states of bucket dredgers as well as loads of electric generators intended for ship general purposes. The generators - depending on a design solution of a given dredger – are driven either by auxiliary engines or both auxiliary and main engines.

2. Characteristics of power systems of the investigated bucket dredgers

The operational investigations were performed on five dredgers operating in the south Baltic Sea in the years 2000-2003 and 2005-2006 [3, 4] (during 732 measurement hours in total). The obtained results were supplemented by the data taken from the publication [7], they concern the sixth dredger, *Ivan Bachalov*. The main technical particulars of the dredgers on which the investigations in question were carried out, are presented in Tab. 1. The dredgers *Ivan Bachalov* and *Kategats* are of the same design.

The bucket dredger power systems appear in three basic types. The basic one is that in which main engine (-s) drives, during dredging, all main consumers as well as auxiliary ones, whereas auxiliary engine (-s) ensures drive for auxiliary consumers only during breaks in dredging operations [5]. Such system is installed on five investigated dredgers (Fig.1 and 2). Only the power system of the dredger *Małż II* (Fig.3) belongs to another type which is characterized by that its main engine (-s) drives main consumers and a selected, small number of auxiliary ones, whereas auxiliary engine (-s) ensures drive for the remaining, greater number of auxiliary consumers, in all service states [5]. The dredgers *Rozgwiazda* , *Inż. T. Wenda* and *Małż II* are not self-propelled, the dredger *Małż II* is additionally fitted with a silting-up system, hence the second main engine for driving the dredging pump is installed. The dredgers *Usedom, Ivan Bachalov* and *Kategats* are fitted with self-propulsion system, their power plants are consisted of two main engines.

Tab.1. Main particulars of bucket dredgers on which operational investigations were performed

Dredger	Main dimensions			$\sum N_{DE}^{nom}$	N_{ME}^{nom}	$\sum N_{AC}^{nom}$	Crew
	L_C	B	T				
	m	m	m	kW	kW	kW	persons
Małż II	33,1	8,8	1,80	630	205 [1)] 272 [2)]	136,5	8
Rozgwiazda	46,0	12,1	2,90	728	660 [1)]	310,4	10
Inż.T. Wenda	45,9	12.1	2,90	776	660 [1)]	315,5	10
Usedom	80,4	14,8	3,85	1926	970 [1)] 970+735 [3)]	1510	32
Kategats	79,9	14,4	3,75	1925	970 970+735 [3)]	1560	32

$\sum N_{DE}^{nom}$ - total rated output power of diesel engines,

N_{ME}^{nom} - rated output power of main engines,

$\sum N_{AC}^{nom}$ - total rated output power of auxiliary consumers;

1) – output power of main engine driving main technological consumers and possible auxiliary consumers,
2) – output power of main engine driving dredge pump,
3) – output power of main engines under operation during free-floating.

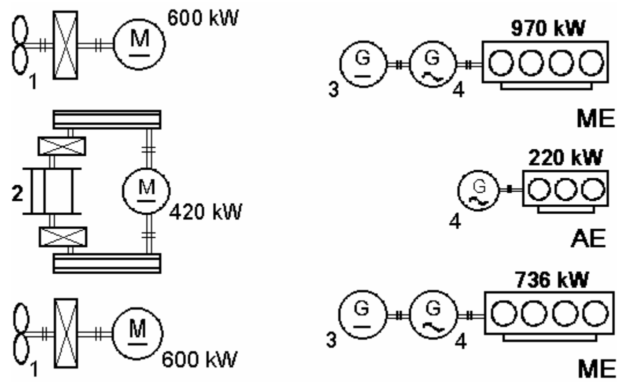

Fig. 1. Schematic diagram of the power system of the dredger „Kategats”: 1 –main screw propeller; 2 – upper tumbler driving bucket chain; 3 – main electric generator; 4 – electric generator for ship general purposes; ME – main engine; AE – auxiliary engine

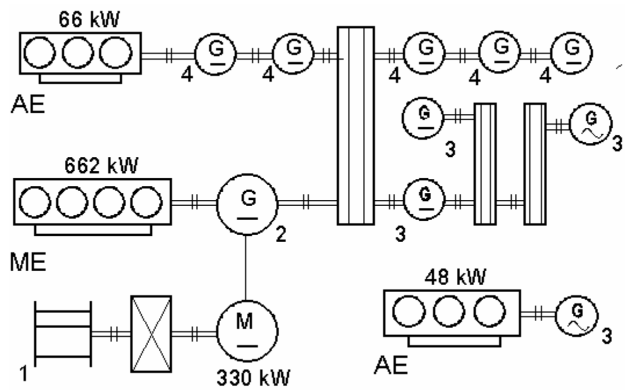

Fig. 2. Schematic diagram of the power system of the dredger„Inż. T. Wenda”: 1 –upper tumbler driving bucket chain; 2 – main electric generator; 3- electric generator for ship general purposes; 4 – electric generator of side winch; ME – main engine; AE – auxiliary engine

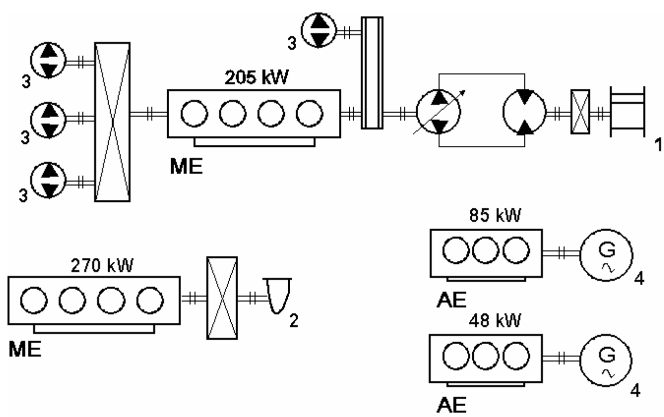

Fig. 3. Schematic diagram of the power system of the dredger „Małż II”: 1 – upper tumbler driving bucket chain; 3 – main electric generator;. 2 – dredge pump; 3 – hydraulic pump for driving side and auxiliary winches; 4 – electric generator for ship general purposes; ME – main engine; AE – auxiliary engine

3. Operational loads of main engines

Long-lasting investigations of operational loads of main and auxiliary engines are of a statistical character. Data used in such investigations are instantaneous values of engine loads recorded in assumed time intervals.

Measuring process of loads of main engines was carried out indirectly by measuring loads of electric generators driven by a given main engine. The measurements were performed by means of specially designed measuring systems. Their description and characteristics are presented a.o. in [1, 2]. For the reason of high variability of loads of the main power consumer, i.e. bucket chain, the measurements of engine loads were taken every second. The loads of electric generators were determined by measuring voltage and current values at generator terminals (in most cases it was direct current machines). Next the loading of the main engine driving a given electric generator was calculated on the basis of the known generator efficiency characteristics. In the case where several electric generators were driven by one main engine the loads were summed up.

The values of main engine loads obtained this way were taken for determining the following parameters of load characteristics distributions:

N_{ME}^{av} - average load of main engine, kW;

$\overline{N}_{ME}^{av} = \dfrac{N_{ME}^{av}}{N_{ME}^{nom}}$ - average relative load of main engine, -;

σ_{ME} - standard deviation of main engine load distribution, kW;

$v_{ME} = \dfrac{\sigma_{ME}}{N_{ME}^{av}}$ - coefficient of variance of main engine load distribution, -.

The characteristics of main engine load distributions for the investigated dredgers are given in Tab.2. The main engine load distributions are presented in Fig. 4 and 5.

Tab.2. The characteristics of main engine load distributions of six bucket dredgers in dredging and free-floating states

Name of dredger	Dredging state Medium and light soils				Free-floating state			
	N_{ME}^{av}	$\overline{N}_{ME}^{av}$	σ_{ME}	v_{ME}	N_{ME}^{av}	$\overline{N}_{ME}^{av}$	σ_{ME}	v_{ME}
	kW	-	kW	-	kW	-	kW	-
Inż. T. Wenda	170,4	0,258	45,1	0,265	-	-	-	-
Rozgwiazda	154,1	0,233	48,8	0,314	-	-	-	-
Małż II	50,2	0,245	17,9	0,357	-	-	-	-
Usedom	383,9	0,396	71,6	0,187	-	-	-	-
Kategats	401,5	0,414	86,9	0,216	793,1	0,465	309,3	0,390
Ivan Bachalov	421,3	0,434	107,7	0,256	920,7	0,540	283,8	0,307
average		0,331		0,266		0,503		0,349

The performed calculations of the parameters of main engine load distributions during dredging showed that the average relative loads of particular dredgers were contained in the range from 0,233 to 0,434 with the average value of 0,331, and the coefficient of distribution variance - in the range from 0,187 to 0,357 with the average value of 0,266. It should be mentioned that the maximum loads of main engines were contained in the range from 0,532 to 0,714. It may speak for some power margin during operations carried out in hard soils or – more probably – for highly over-dimensioned main engines.

For the free-floating state, values of the average main engine load are significantly higher than those during dredging when also greater numbers of engines operate. The relative loads were contained within the range of 0,465–0,54 with the average value of 0,503. Higher are also coefficients of variance – their average value amounts to 0,349. The so great value of coefficient of variance results from the character of free-floating state of bucket dredgers, which is characterized by short passages from port to dredging site and back, and a large number of manoeuvres.

Additionally, were performed investigations to check if it is possible to consider the relative load distribution of main engines normal one.

To confirm possible approximation of the empirical distributions of relative loads of main engines by means of normal distribution, were carried out the investigations in which the total distribution was analyzed of relative loads of engines of all investigated dredgers, normalized within the interval [0–1]. The engines' loads for the free-floating state were grouped in the left-sided, open quantifying intervals of width resulting from the splitting of rated power of main engines into 10 intervals. In the case of carrying dredging work the loads were grouped into 8 quantifying intervals as then the main engines operated under much smaller loads as compared with their rated output power values. The software *Statistica* was used for assessing the normality of variable distributions and preparing the normal distribution diagrams. The values of the variable in question have been drawn on the diagram of their dispersion respective to the expected values, under assumption that the distribution is normal. If the observed values comply with normal distribution then they have to run approximately along a straight line.

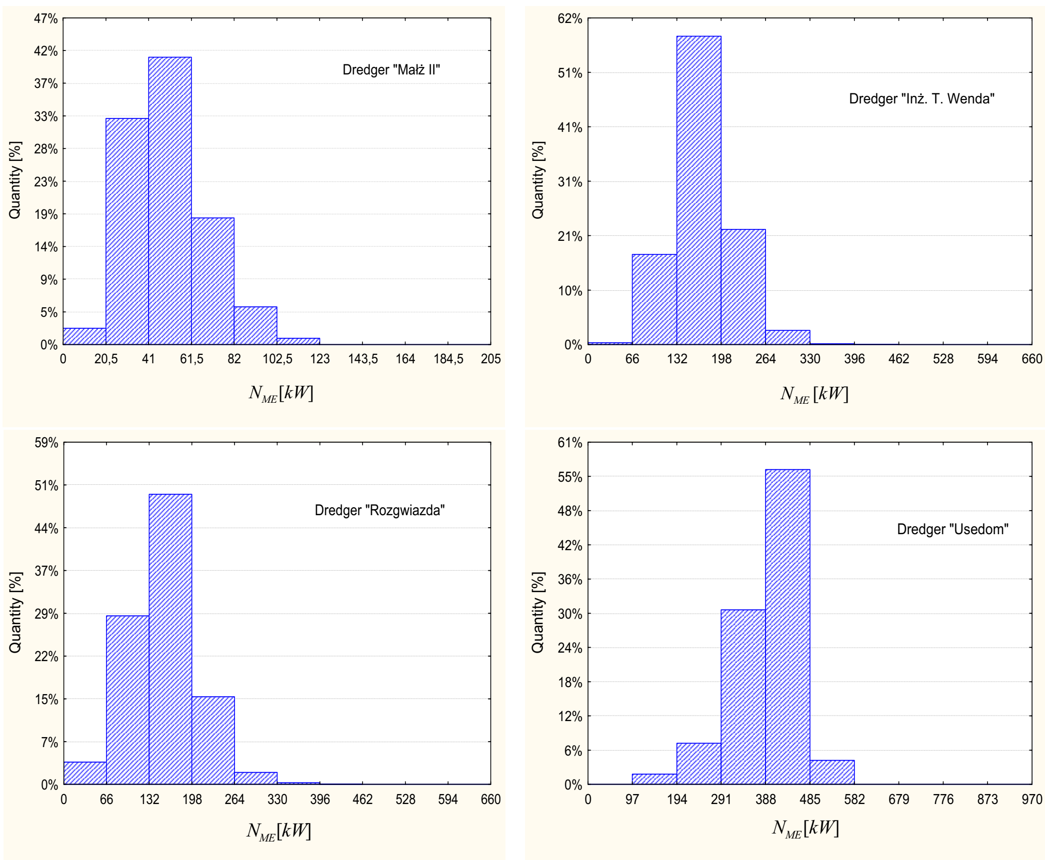

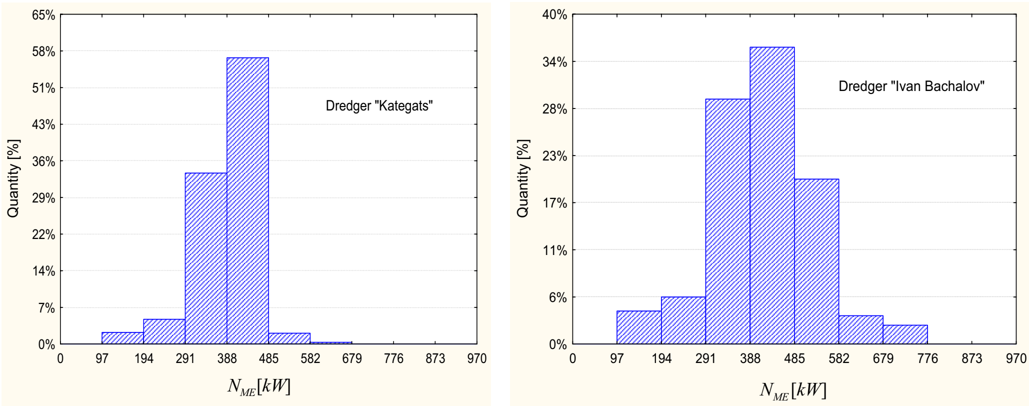

Rys. 4. Load distributions of main engines of bucket dredgers in dredging state

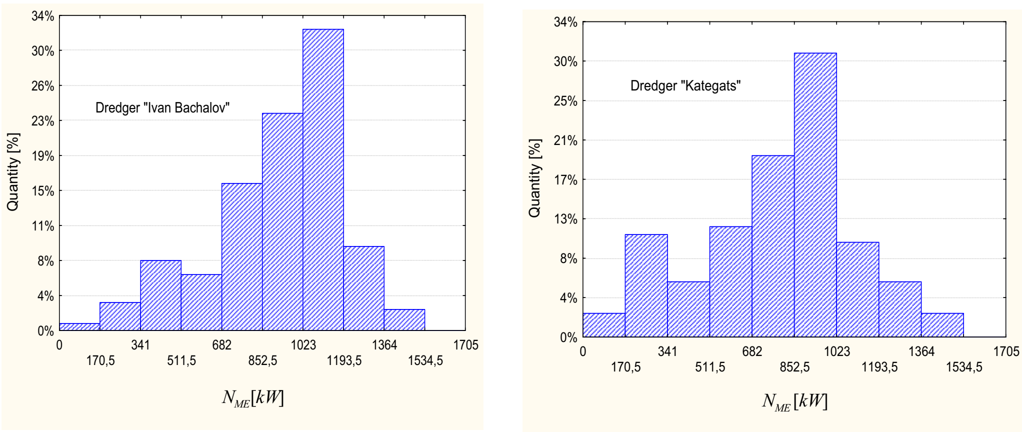

Rys. 5. Load distributions of main engines of bucket dredgers in free-floating state

The minimum sample size, m, under assumption of normal or nearly normal load distribution, was determined from the relation [6]:

$$m \geq \left(\frac{t_{\alpha} \times \overline{\sigma}}{d} \right)^2 \tag{1}$$

where:

t_{α} - critical value of the test for the confidence coefficient $(1-\alpha)$ and $(m_0 - 1)$ degrees of freedom,
$\overline{\sigma}$ - relative value of standard deviation calculated from the sample of m_0 size,
d - assumed estimation error of average value.

By taking $\overline{\sigma}$=0,07–0,12 and t_{α}=1,96 at α=0,05 and m_0> 1000 - on the basis of preliminary investigations - and assuming d=0,01, the minimum sample size m=188–554 was obtained. For all the investigated dredgers the sample sizes significantly exceeded the determined minimum one (95000 – 155000).

In Fig. 6a and 7a are presented the total load distributions of main engines of the investigated dredgers as well as the normal distribution probability density curves for both service states, whereas in Fig. 6b and 7b - the normality diagrams of the tested distributions. Their runs, especially that regarding dredging work, indicate that the distribution can be considered normal.

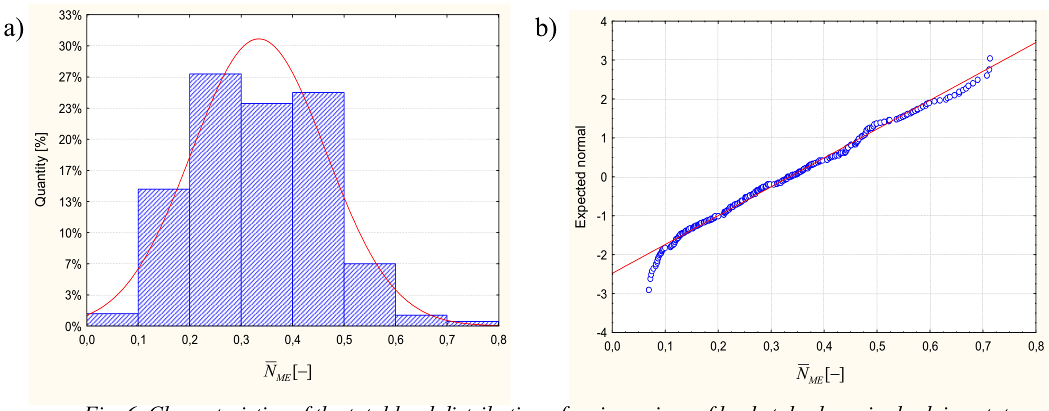

Fig. 6. Characteristics of the total load distribution of main engines of bucket dredgers in dredging state

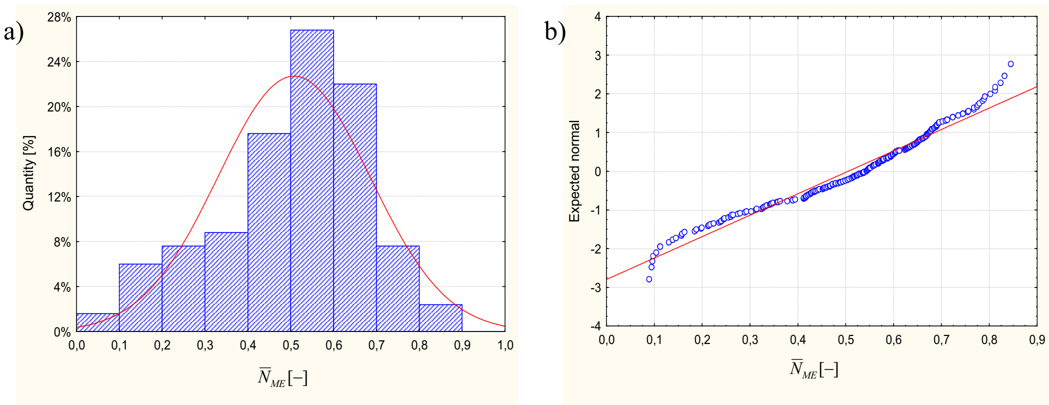

Fig. 7. Characteristics of the total load distribution of main engines of bucket dredgers in free- floating state

4. Operational loads of electric generators for ship general purposes

Load characteristics investigations of electric generators for ship general purposes were performed for two basic service states of bucket dredgers : dredging and free-floating, as well as – additionally – for the state of breaks in dredging (e.g. fuel bunkering, transporting the anchors , waiting for a dump barge) and towing.

On the dredger *Małż II* the ship general purposes electric generators were driven by auxiliary engines. On the dredgers *Rozgwiazda, Inż. T. Wenda, Kategats, Usedom and Ivan Bachalov* such electric generators were driven by main and auxiliary engines. The auxiliary engines operate only during breaks in dredging, during stays in ports, and towing.

Tab. 3, 4 and 5 contain calculated values of the parameters $(N_{EG}^{av}, \sigma_{EG}, \nu_{EG})$ of load distributions of electric generators for ship general purposes, values of the index $N_{EG}^{av} / \sum N_{AC}^{nom}$ for three service states of the dredgers, as well as the load ranges determined by values of the coefficient of the relative load range of electric generators foe ship general purposes β_{EG} :

$$(\beta_{EG})_1 = \frac{N_{EG}^{av} - N_{EG}^{\min}}{\sigma_{EG}} \quad ; \quad (\beta_{EG})_2 = \frac{N_{EG}^{\max} - N_{EG}^{av}}{\sigma_{EG}} \qquad (2)$$

The example load distributions of electric generators for ship general purposes during dredging work of four investigated dredgers are shown in Fig. 8. As in the case of main engines, the loads were grouped into 10 quantifying intervals covering the range $N_{EG}^{\min} - N_{EG}^{\max}$.

The determined average values of variance coefficients for the ship general purposes electric generators amount to: $v_{EG}^{av} = 0{,}241$ - for dredging state, $v_{EG}^{av} = 0{,}192$ - for free-floating state, as well as $v_{EG}^{av} = 0{,}175$ for breaks in dredging, for port staying and towing. And, the average values of relative variability range coefficients amount to $(\beta_{EG})_1 = 2{,}085$ and $(\beta_{EG})_2 = 3{,}508$ - for dredging state, $(\beta_{EG})_1 = 2{,}173$ and $(\beta_{EG})_2 = 2{,}896$ - for free-floating state, $(\beta_{EG})_1 = 1{,}949$ and $(\beta_{EG})_2 = 2{,}098$ - for the state of breaks in dredging, for port staying and towing.

Tab.3.Parameters of operational load distributions of ship general purposes electric generators of bucket dredgers in dredging state

Dredger	Parameters of load distribution of electric generator			Minimum load		Maximum load		$\frac{N_{EG}^{av}}{\sum N_{AC}^{nom}}$
	N_{EG}^{av}	σ_{EG}	v_{EG}	$N_{EG}^{\min}$	$(\beta_{EG})_1$	$N_{EG}^{\max}$	$(\beta_{EG})_2$	
	kW	kW	-	kW	-	kW	-	-
Małż II	19,38	3,51	0,181	10,8	2,442	25,6	1,772	0,142
Inż. T. Wenda	38,61	12,40	0,321	18,7	1,605	96,7	4,687	0,124
Rozgwiazda	34,95	12,11	0,346	17,1	1,475	88,2	4,401	0,113
Usedom	164,97	28,19	0,171	92,0	2,589	261,0	3,407	0,109
Kategats	169,33	31,20	0,184	97,1	2,318	291,2	3,899	0,108
Ivan Bachalov	187,86	45,10	0,240	94,0	2,081	318,0	2,885	0,121
average			0,241		2,085		3,508	0,119

Tab.4. Parameters of operational load distributions of ship general purposes electric generators of bucket dredgers in free-floating state

Dredger	Parameters of load distribution of electric generator			Minimum load		Maximum load		$\frac{N_{EG}^{av}}{\sum N_{AC}^{nom}}$
	N_{EG}^{av}	σ_{EG}	v_{EG}	$N_{EG}^{\min}$	$(\beta_{EG})_1$	$N_{EG}^{\max}$	$(\beta_{EG})_2$	
	kW	kW	-	kW	-	kW	-	-
Ivan Bachalov	136,58	26,11	0,191	81,4	2,113	211,7	2,877	0,088
Kategats	130,76	25,32	0,194	74,2	2,233	204,6	2,916	0,084
average			0,192		2,173		2,896	0,086

Tab.5. Parameters of operational load distributions of ship general purposes electric generators of bucket dredgers in the service state of breaks in dredging, of staying and towing

Dredger	Parameters of load distribution of electric generator			Minimum load		Maximum load		$\frac{N_{EG}^{av}}{\sum N_{AC}^{nom}}$
	N_{EG}^{av}	σ_{EG}	v_{EG}	$N_{EG}^{\min}$	$(\beta_{EG})_1$	$N_{EG}^{\max}$	$(\beta_{EG})_2$	
	kW	kW	-	kW	-	kW	-	-
Małż II	11,50	1,81	0,157	8,1	1,880	15,2	2,046	0,084
Inż. T. Wenda	18,12	3,53	0,195	10,7	2,103	24,2	1,722	0,057
Rozgwiazda	16,31	2,39	0,146	10,5	2,431	21,3	2,097	0,052
Usedom	82,33	16,96	0,206	56,1	1,547	121,9	2,334	0,054
Kategats	101,87	17,16	0,168	71,2	1,787	141,2	2,292	0,065
average			0,175		1,949		2,098	0,062

$\sum N_{AC}^{nom}$ - total rated power of electric motors of all auxiliary consumers installed onboard

A characteristic feature of bucket dredgers is the great value of the coefficient $(\beta_{EG})_2$ for the state of dredging. It results from a large number of auxiliary technological consumers for which short-lasting cyclic work is characteristic. An example is the dredger *Małż II,* majority of such consumers of which is driven by the main engine which operates within diesel engine – hydraulic systems (Fig. 3), hence the coefficient $(\beta_{EG})_2 = 1{,}772$ shows the lower value.

The $N_{EG}^{av} / \sum N_{AC}^{nom}$ index values are contained within the range of 0,108 – 0,142 - for the state of dredging, 0,084 – 0,088 - for the state of free-floating, and 0,052 – 0,084 - for the state of breaks in dredging, of staying and towing.

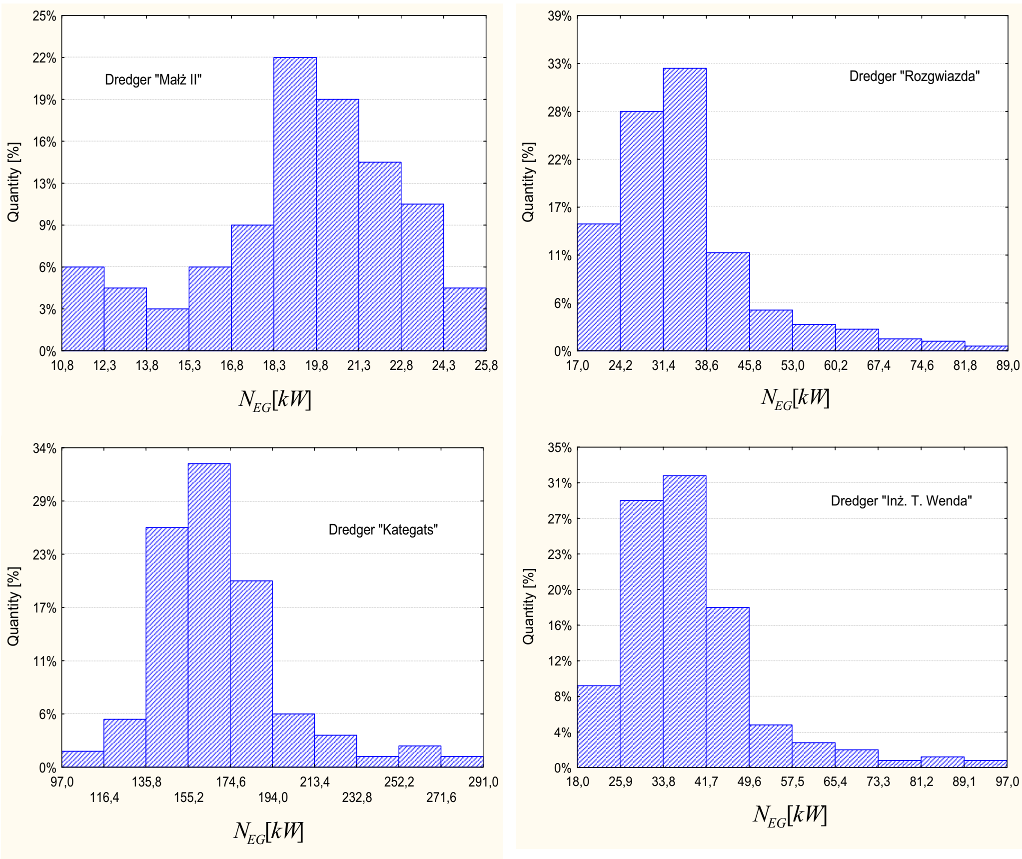

Fig.8. Example load distributions of ship general purposes electric generators of *bucket dredgers during dredging work*

As the case of main engines, the load distributions of ship general purposes electric generators should be, in compliance with the Lapunov theorem [6], close to normal distribution. The relation (1) was used to determine the minimum sample size for the assumed normal or nearly normal load distribution. The obtained minimum sample size (for the average value $\overline{\sigma}_{EG} = 0{,}09$) amounts to $m = 311$. In all the cases the sample size greatly exceeded the determined minimum sample size. The total distribution of loads of all electric generators, normalized in the interval (0, 1), was subjected to investigations – Fig. 9. The conformity shown in Fig. 9b and 9d , confirms that it is possible to assume the load distributions of ship general purposes electric generators of bucket dredgers during dredging and free-floating, to be normal ones.

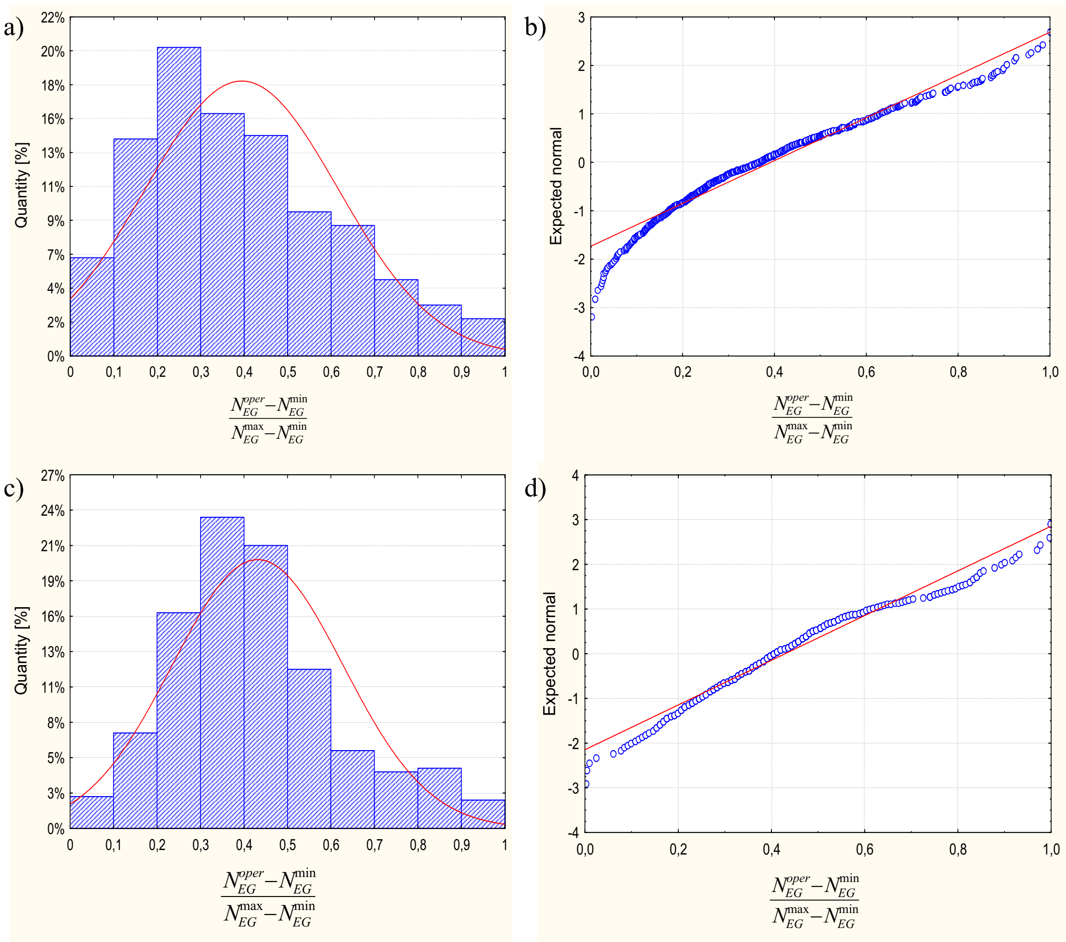

Fig. 9. Characteristics of distributions of total relative loads of ship general purposes electric generators of bucket dredgers during dredging (a,b) and free-floating (c,d)

5. Summary

The performed investigations justify offering the following remarks and conclusions:

1. The values of $\overline{N}_{ME}^{av}$ and ν_{ME} , obtained from measurements, can be used for determining recommended operational loads for main engines to be selected.

   For the state of dredging in medium and light soils $\overline{N}_{ME}^{av} = 0{,}46 - 0{,}48$ was determined under assumption that the maximum loads of main engines are contained within the range of $(0{,}85 - 0{,}9)N_{ME}^{nom}$. For the state of free-floating $\overline{N}_{ME}^{av} = 0{,}46 - 0{,}54$ was determined;
2. The indices $N_{EG}^{av} / \sum N_{AC}^{nom}$ as well as the coefficients ν_{EG}^{av} may be used for the predicting of load distributions of ship general purposes electric generators;
3. The load distributions of main engines and ship general purposes electric generators of bucket dredgers in two basic service states: dredging and free-floating, may be deemed normal ones.
4. The state of dredging should be taken as that for which the power system of non-self-propelled bucket dredgers should be designed; in the case of self-propelled dredgers also the state of free-floating should be taken into account.

5. The achieved results may be useful for solving design problems of power plants of bucket dredgers as well as for standardizing fuel consumption.

References

[1] Bocheński, D., Balcerski, A., Kubiak, A., *Identification of parameters of the systems and data collecting method techniques on dredgers and silting vessels* (in Polish), Research reports no. 28/2000/PB, Faculty of Ocean Engineering and Ship Technology, Gdansk University of Technology, Gdansk 2000.

[2] Bocheński, D., Kubiak, A., Jurczyk, L., *Measurements of the parameters characterizing operation of technological systems of dredgers* (in Polish), Proc. of the 22nd Symposium on Ship Power Plants *SymSO2001,* Szczecin 2001.

[3] Bocheński, D. (Supervisor) *et al.*, *Identification investigations of energy consumption and parameters of wining and transporting the winning on selected dredgers and silting vessels* (in Polish), Final report of KBN research project no. 9T12C01718, Research reports no. 8/2002/PB, Faculty of Ocean Engineering and Ship Technology, Gdansk University of Technology, Gdansk 2002.

[4] Bocheński, D., *Operational load* a*nalysis of main power consumers on bucket dredgers* (in Polish), Scientific Bulletins of Polish Naval Academy, no. 162. 24th Symposium on Ship Power Plants *SymSO2005,* Gdynia 2005.

[5] Bocheński, D., *Analysis of design solutions and relations which determine parameters of power systems on bucket dredgers,* Selected problems of designing and operating of ship power plants (in Polish), 27th Symposium on Ship Power Plants *SymSO2006,* Szczecin 2006.

[6] Bobrowski, D., *Probability theory for technical applications* (in Polish), ScientificTechnical Publishing House (WNT), Warszawa 1986.

[7] N.N., *Kompleksyjne technologiczieskie issledowanija sudov popolnienija instrukcyja po effjektiwnoj eksploatacji ziemsnarjada „Ivan Bachalov"* (in Russian) GDK 627.76.001.5. Rostow upon Don 1985.

PROBLEMS WITH UTYLISE OF GLICEROL FRACTION – WASTE PRODUCTS OF FAME PRODUCTION

prof. Jan Borgoń
col. Wojciech Dzięgielewski, Ph.D
Tomasz Gołębiowski, Ph.D

Air Force Institute of Technology, Warsaw
ul. Księcia Bolesława 6, 01-494 Warszawa, skr. poczt. 96

1. Introduction

One of the most popular biocomponents today for fossil fuels, except from bioethanol used widely for gasoline, is fatty acid methyl ester (FAME). It can be added to diesel fuel used in compression-ignition engines. Different blends are possible – from 5%(V/V), blends 10% up to 30%(V/V) and finally pure FAME used as fuel. FAME production is based on estrification of fats, i.e. rape seeds oil estrification with methanol (no free fatty acids). Equation 1 presents reaction of estrification (glycerol trioleinic as an example) [1].

$$
\begin{array}{lcll}
H_2C\ COO(CH_2)_7CH{=}CH(CH_2)_7CH_3 & & & CH_3\text{-}OH \\
\quad | & 3\ CH_3OH & & | \\
HC\ COO(CH_2)_7CH{=}CH(CH_2)_7CH_3 & \xrightarrow{\hspace{2em}} & 3\ CH_3(CH_3)_7CH{=}CH(CH_2)COOCH_3\ + & CH_2\text{-}OH \\
\quad | & \text{base} & & \\
H_2C\ COO(CH_2)_7CH{=}CH(CH_2)_7CH_3 & & & CH_3\text{-}OH \\
\textit{glycerol trioleinic} \quad + & \textit{methanol} \rightarrow & \textit{oleinic acid methyl ester} & +\ \textit{glycerol}
\end{array}
\qquad \textbf{(1)}
$$

This reaction by-product is glycerine fraction. In practice it is not a pure chemical compound, but widely and not correctly called glycerine, but fraction, that includes, depending on a type and efficiency od estrification equipment, from 40 to 90% of glycerine. Raw fraction is practically a waste, but after appropriate treatment may be widely used, i.e:

- in pharmaceutical and cosmetics industry;
- as a thickener in fodder for animals;
- as a component of fertilizers;
- as a component to be burned for heating purposes;
- as a component for greases and lubricants production.

2. Glycerine fraction characteristics

A few years ago, before installations for FAME production appeared in Poland, it was stated, that „glycerine" was to be sold, and income could improve economics, so production and use of so called „biodiesel" would be profitable. The reality proved something completely different. Glycerine fraction from estrification process includes many components, that as contaminants, make it completely usless for any purpose. It can not be used as fertilizer or fodder component (because of toxicity of methanol and metals), and it can not be burned (metallic compounds generated during burning process create hard ash compounds that can cause burners damages).

Depending on construction of installation for FAME production, its complexity and equipment used, technological process is different, so final product's and wastes' purity is also different. It is obvious, that ester's purity and its quality is the most important matter here, but glycerine fraction's purity and quality is also important for future use of it. Purification is a costs generating process. Building of processing module – treating glycerine fraction – is profitable for medium and big installations for FAME production. What are the most important differences between „wastes" from industrial and „home-grown" production? In the first option it is possible to receive product being recognized practically as technical glycerine. It is a clear, pale liquid highly processed. Its properties are stabilized, so for future use less complicated and less expensive treatment is required. In the second option mentioned above we receive brown, cloudy liquid, with high content of metal salts form catalyst and toxic methanol. Low level of processing and diversity (quality and composition strictly depending on raw material used for batch production). Those problems are more serious in case of use during estrification fats different than rape seeds oil, ie. vegetable oils, fried oils, animal fats. For appropriate preparation then high processing is required, that not always guaranties high quality of glycerine received finally. The only one advantage of such raw material is its proce – 35-40% lower, but finally it may not compensate for costs of processing ond purification. Additional cost generating agnt here are logistic problems connected with receiving small portions of fraction from different suppliers.
Below differences in glycerine fraction's parameters received in professional agrorefinery (with yearly FAME production over 60.000 tons) and „home-grown" installation (Table 1).

Table 1. Comparison of properties for farmaceutical glicerne and glycerine fractions

Properties	Farmaceutical glycerine	Glycerine fraction (big installation)	Glycerine fraction („home-grown" installation)
Glycerine content	99,7 %(m/m)	80 – 90 %(m/m)	35 – 40 %(m/m)
Colour	Clear, colourless	Yellow to light brown, clear	Opaque, cloudy
Sulfate ash content	max 0,01 %(m/m)	1,5 – 5 %(m/m)	
Water content	max 0,3 %(m/m)	a few %	to several a dozen or so %
Methanol content	not include	max a few %	even to 20 %
Metals content (total)	several dozen ppm	to a few % (as salts and soaps)	
Esters and its derivatives content	not include	to about 5 %	to several a dozen or so %
Others content	not include	to a few %	to several a dozen or so %

3. Glycerol formal

One of available processes for glycerine fraction treatment is its processing for substances, that can be added to engine fuels as additives improving selected parameters. It is possible after glycerine processing to glicerol formal. Below two typical chemical reactions are presented, that describe the process of glycerol formal obtaining [2]:

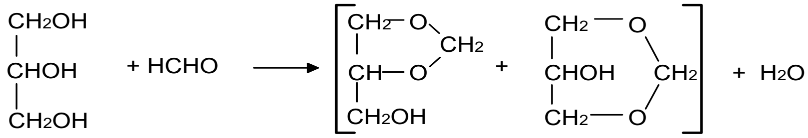 2

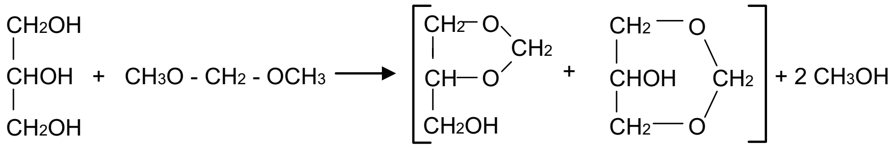 3

It was assumed, that chemical compound obtained in this way can be used as a compound for diesel fuels used in compression-ignition engines (regardless of their application: cars, machines, agregates, marine).Such product was obtained in Institute of Heavy Organic synthesis “Blachownia” in Kędzierzyn-Koźle, and testing of product was carried out in the Air Force Institute of Technology as a part of european research project Eureka [3].
Initial assumption was, that for base fuel (diesel fuel), 5%(V/V) of methylal will be added. During blending first problems appeared with its homogenosity. After intensive gomogenisation the blend was stable for a short time. But basic testing was done, according to methodology typical for diese fuels.
Testing results are presented in Table 2.

Table 2. Results of basic physical properties testing for diesel fuel blend with 5% of glycerol forma

No.	Physical property	Diesel fuel	Diesel fuel + 5% glycerol formal
1	Density, 15C	0,8242	0,8277
2	Kinematic viscosity, 40C	2,120	2,112
3	Distillation To 250C is distilled To 350C is distilled 95% (V/V) distilled to	 59,8 98,7 300,7	 60,5 98,7 299,8
4	Lubricity, HFRR	401	171
5	Flash point, C	85,0	81,0
6	Cetane index, calculated	52,0	29,9
7	Insolubles content	4,62	fuel disolve filter
8	Oxidation resistance	5,99	fuel disolve filter
9	Carbon residue, %(m/m)	0,02	0,02
10	Ash content, %(m/m)	0,001	0,001
11	Corrosive reaction on Cu	st. 1	st. 1

During testing it was observed, that glycerol formal concentration is to high. The result of it was cetane index value decrease. It is supposed, that fuel’s self-ignition properties were worsened. This thesis requires engine testing, but these were skipped because of other factors. 5%(V/V) blend could not be filtered through paper filters, that suggests, that during normal application of that fuel in engines paper filters could be damaged. Flash point temperature was decreased, but in

acceptable limits. Positive aspects of glycerol formal must be also underlined. Its lubricity improving properties are very good. Scar diameters during HFRR (High Frequency Reciprotating Rig) test was three times smaller than required by appropriate standard. This is a very interesting result, but not equivalent to all disadvantages mentioned above.
Because of results described above methylals application, that should improve fuel's thermal stability, low temperature properties, lubricity and viscosity, was not abandoned. The aim of testing but modified. Glycerol formal application as an additive for diesel fuels will be evaluated. Such testing was stared in December 2006, so the results could not be presented here.

4. Conclusions

- With development of industry dealing with fuels from estrification of vegetable and animals fats essential problem of glycerine fraction application appeared.
- It seems, that glycerine derivatives should be used as fuels additive (because of positive effect in fossil and vegetable fuels).
- Glycerine derivatives application in petroleum industry could improve economical and technological effect.
- First stage of research project was not successful, but testing results show the need for continuation of research – after program modifications.

Literature

[1] Rosiak, D., Kolczyński, J., Dzięgielewski, W., Walisiewicz–Niedbalska, W., Struś, M., *Problemy technologiczne produkcji estrów metylowych oleju rzepakowego – Odnawialne źródła energii u progu XXI wieku*, Warszawa 2001.
[2] Trybuła, S., Terelak, S., *Formal gliceryny jako komponent paliwowy*, ICSO 2006.
[3] Gołębiowski, T., Dzięgielewski, W., *Zastosowanie formalu gliceryny jako komponentu do paliw samochodowych*, ISCO 2006.

THE EXPERIMENTAL ANALYSIS OF NON-THERMAL PLASMA REACTOR USE FOR MARINE DIESEL EXHAUST

Tadeusz Borkowski, Jarosław Myśków, Marcin Hołub*, Stanisław Kalisiak*
Siegfried Müller, Rolf-Jürgen Zahn****

Maritime University
ul. Wały Chrobrego 1/2, 70-500 Szczecin, Poland
tel.: +48 91 4809419, fax: +48 91 4809585
e-mail: tborkowski@am.szczecin.pl, jmyskow@am.szczecin.pl
*Technical University**
ul. Sikorskiego 37, 70-313 Szczecin, Poland
tel.: +48 91 4494129, fax: +48 91 4494561
e-mail: mholub@ps.pl, kal@ps.pl
*Institute of Low Temperature Plasma Physics***
Friedrich-Ludwig-Jahn-Str. 19,D-17489 Greiswald, Germany
tel.: +493834554448, fax: +49 3834554301
e-mail: mueller@inp-greiswald.de, zahn@inp-greiswald.de

Abstract

The control of NO_x (NO and NO_2) emissions from marine engines remains a challenge. In recent years, there have been a number of reports show that plasma device combined with a catalyst can reduce as high as 90% of NO_x in simulated diesel exhaust gas. In the case of real diesel exhaust, the beneficial role of a plasma treatment is now thought to be the oxidation of NO to NO_2, and the formation of partially oxidized hydrocarbons that are more active for the catalytic reduction of NO_2. This paper briefly describes research efforts aimed non-thermal plasma reactor development for ships use, and primary focused on NO oxidation conditions, functionally fitted to the engine mode of operation.

Keywords: *marine diesel engine, exhaust emission gas treatment, low temperature plasma reactor*

1. Introduction

There is no doubt that the contribution from ships to global gas emissions will increase, international shipping sharing about 7% of the total sulphur and 11% nitrogen discharge. The marine diesel engine is the prime mover for vast majority of merchant vessels and dominating as drives for electricity production on ships. Diesel manufacturers and researchers have been investigating a variety of techniques in the aim of reducing diesel emissions as far as reasonably practicable. These techniques have been divided into three areas of study: pre-treatment, primary (internal) and secondary (after-treatment) methods. All these systems have different extent of success in reducing engine emissions however, their effectiveness may not be adaptable for a given ship design. Each of these categories however, are a trade-off with improving NO_x emissions and other emissions such as: hydrocarbons, particle matters and CO. The NO_x reduction technologies called as after-treatment or secondary methods are fitted externally to the engine and are applied directly to the combustion gases. One promising approach to reducing NO_X and particulates from diesel exhaust is to use a combination of plasma with catalyst.

The presently accepted model is that, a non-thermal plasma in the presence of water, oxygen and hydrocarbon will efficiently convert NO to NO_2, while only partially oxidizing the hydrocarbons present in exhaust. Some catalysts will reduce NO_2 (but not necessarily NO) in the presence of excess oxygen, if some hydrocarbon are present. In recent years selective catalytic reduction (SCR) has been promoted as a suitable after-treatment technology for the marine use. SCR is commercially available and it has been built-in to a number of vessels. The SCR process uses urea, which is water soluble and non-toxic, mixed into a solution and then injected into the exhaust stream. It reacts with the NO_x over a catalyst bed. Comparison made between the potential benefits of the non-thermal plasma and SCR systems for marine use[1]. A full scale SCR system that offers high NO_x removal (~90%), has significant disadvantages especially in the need to carry large amounts of urea solution. The non-thermal plasma at atmospheric pressure systems has been developed for incinerator flue gas clean-up. Currently, this technology is undergoing further development for diesel engine exhausts.

2. Application of NTP to marine diesel exhaust after-treatment

In conventional application of plasma to the treatment systems of power plant flue gas, the plasma reactor is used to oxidize NO_x to nitric acid [2]. A combination of non-thermal plasma (NTP) with catalysts can be referred to plasma assisted catalysts technology. The NO_x in engine exhausts – close to exhaust receiver, is composed primarily of NO. Consequently, present after-treatment schemes have focused on the reduction of NO. Recent developments in catalytic control of NO_x are revealing the significance of NO_2 as an intermediary stage for achieving higher NO_x removal efficiencies [3] [4]. This implies that the conversion of NO to NO_2 is an important intermediate step in the final reduction of NO_x to N_2 Oxidation is the dominant process for exhausts, containing NO in mixtures of N_2, O_2 and H_2O, particularly when O_2 concentration is 5% or higher. There are two removal possibilities of NO pathways from exhaust gas:

1. oxidation $$O + NO \leftrightarrow NO_2, \tag{1}$$
$$OH + NO_2 \leftrightarrow HNO_3, \tag{2}$$

2. reduction $$N + NO \leftrightarrow N_2 + O, \tag{3}$$

Reaction rate coefficients for these and other main processes are listed in table 1.

Tab.1. Basic reactions and rate coefficients of NO_x

Reaction	Rate coefficient	Reference
$NO + O + N_2 \rightarrow NO_2 + N_2$	$9{,}1\cdot10^{-28}T^{-1.6}$	[5]
$NO_2 + OH + M \rightarrow HNO_3 + M$	$2{,}2\cdot10^{-30}(T/300)^{-2.9}$	[5]
$N + NO \rightarrow N_2 + O$	$3{,}1\cdot10^{-11}$	[6]
$N + OH \rightarrow NO + H$	$3{,}8\cdot10^{-11}\exp(85/T)$	[5]
$N + O_2 \rightarrow NO + O$	$4{,}4\cdot10^{-12}\exp(-3220/T)$	[5]
$NO + O_3 \rightarrow NO_2 + O_2$	$2{,}0\cdot10^{-12}\exp(-1400/T)$	[7]

As mentioned before, in diesel engine exhaust gases, NO_x consists mainly of NO. A significant attempt to improve the NO removal at lower temperatures (modern marine diesel engines; 180-250°C) is to combine a non-thermal plasma process with the catalyst. In this kind of joint process, the main role of the non-thermal plasma is to convert NO into NO_2. It was found that the rate of NO oxidation to NO_2 by the non-thermal plasma significantly decreases with the increase in reaction temperature [2].

The alternative method capable of oxidizing NO to NO_2 is to use ozone, which can be efficiently produced by dielectric barrier discharge (DBD), externally. When ozone is mixed with the exhaust gas, NO can be easily oxidized to NO_2 without producing any by-products. Then, the oxidation of NO by mixed ozone and exhaust is efficient, and the reduction of NO_2 back to NO does not occur. Anyhow, more attractive and preferred pathway over oxidation, for marine diesel engine would be reduction (eq. 3), since the end products N_2 and O could be exhausted to the ambient atmosphere. The simulated NO removal possibility in DBD plasma reactor presented in [3]. During the current pulse, the primary radicals N, OH, O and H are produced by electro-impact dissociation feed gas. Primarily they are produced by the following reactions:

$$e+N_2 \rightarrow N + N + e, \qquad k = 9\cdot10^{-10}\ [cm^3\,s^{-1}] \tag{4}$$

$$e+H_2O \rightarrow H + OH + e, \qquad k = 6\cdot10^{-11}\ [cm^3\,s^{-1}] \tag{5}$$

$$e+O_2 \rightarrow O + O + e, \qquad k = 1\cdot10^{-9}\ [cm^3\,s^{-1}] \tag{6}$$

$$\rightarrow O + O(^1D) + e, \qquad k = 3\cdot10^{-9}\ [cm^3\,s^{-1}] \tag{7}$$

O atoms created during the current pulse are basically produced in their ground state – $O(^4S)$ and in the first excited state $O(^1D)$, latter with water, produce OH radicals:

$$O(^1D) + H_2O \rightarrow OH + OH, \tag{8}$$

Due to the likelihood that restricted species will be produced in NO plasma removal process after the NO is depleted, the DBD power level should be adjusted to current NO concentrations, and prevent O_3 formation and NO as well.

The non-thermal plasma module for marine use requires: robust design, low voltage, minimum maintenance, process with easily scaleable efficiency, as the rate of NO_x emission varies with engine load and other conditions. The efficiencies required for cleaning devices are also quite tough. This efficiency must be realized without generating significant amounts of other unwanted species. Dielectric barrier discharges plasma reactors (DBD) are compact – efficient plasma sources, commonly used as ozonizers and are attractive due to their ability to operate in a stable mode at low pressures, with high average power compared to corona-beam reactors. The oxidation from NO to NO_2 without decreasing NO_x concentration (minimum reaction byproducts) and with least power consumption is the key for the optimum reactor design.

3. Engine test bed operation and apparatus setup description

Exhaust emission plasma assisted after-treatment module is fitted on a exhaust outlet path of the marine test bed engine, with specification engine given in Table 2. Engine could be operated at steady speed and load conditions, over a range of power settings. The mode of operation is determined using the relevant for ship propulsion engines ISO test cycles [9]. In proposed solution the non-thermal plasma reactor is inserted between the engine turbocharger outlet and catalyst.

Tab. 2. Test-bed engine specification

Engine		Nominal rate	
Designation	Maker, type	Power [kW]	Speed [revs/min]
Small ship propulsion Generator sets	SULZER 6AL20/24	397	720

Figure 1 presents an outline of a laboratory plasma-catalyst system that includes non-thermal plasma (DBD) reactor, for fractional exhaust gas stream examination. The part scale plasma reactor models have been designed and were being manufactured [10]. The design of the exhaust system is suitable for the full scale concept, where it takes the place along with silencer. The approach will enable other fits, to be more suitable accommodate modules, by altering their number and length. Based on the concept that utilises a number of modules and it will minimise development risk, before going in to full scale.

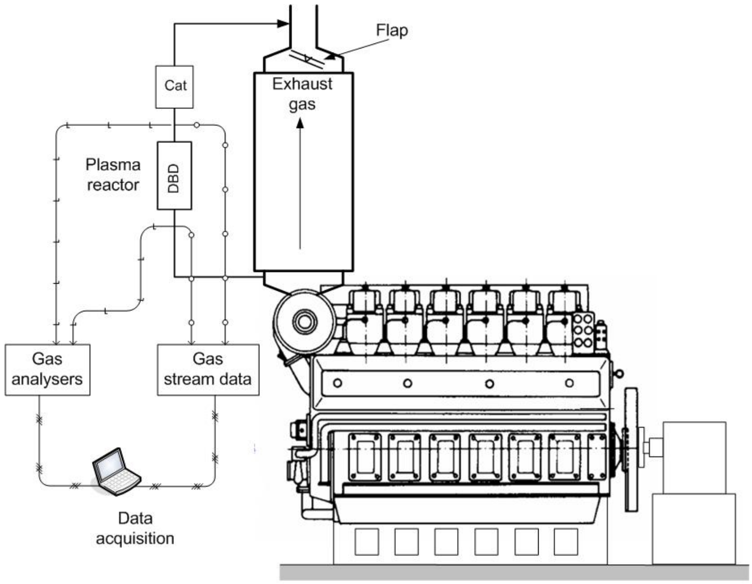

Fig. 1. Non-thermal (DBD) plasma reactor „by-pass" arrangement

Subsequently the comprehensive series of trials were performed to assess the exhaust flow properties through the main exhaust channel and plasma reactor by-pass pipe, within the engine operation effective load and consequent emission profiles achieved. Emission measurements were carried out on engine at steady-state operation. All engine performances were continuously, together with exhaust gas components concentration recorded by means of measurement assemble presented in figure 2. During the engine trials the exhaust gas flows from the engine exhaust receiver after turbocharger, via a by-pass line and main duct – exhaust gas silencer. Proportional amount of gas stream is controlled through restriction flap. The sampling unit consists two probes situated below and above the plasma reactor. Sampling gas is distributed to all analysers. The upper end of the sampling probes – a sintered ceramic filter, the probe itself, sample line, transfer pump and distribution box, are heated by means of separate temperature controlled units. Exhaust emission is subsequently recorded at intervals over a measurement period of 15 minutes on every engine load. For each of the test levels, engine performance data are recorded in as much detail as test bed equipment. In addition to the exhaust emission, some essential operating engines data are measured to asses, the respective engine operating conditions – in accordance to ISO-3046 standard. Amongst other variables, this included: effective load, speed, and fuel consumption, exhaust temperature, performance of the turbo-blowers, together with the ambient conditions prevailing at the time of the measurement The performance measurement procedure of marine engines on test beds, performed in accordance to Annex VI of Marpol 73/78 convention - with the specification given in the IMO NO_x Technical Code and ISO-8178 standard. All tests were covered by test-cycles procedure D-2 and E-2, which include generator and pitch propeller drive. To reduce emissions variability due to fuel variables, all tests performed with the selected marine distillate fuel DMX in accordance to ISO-8217 standard.

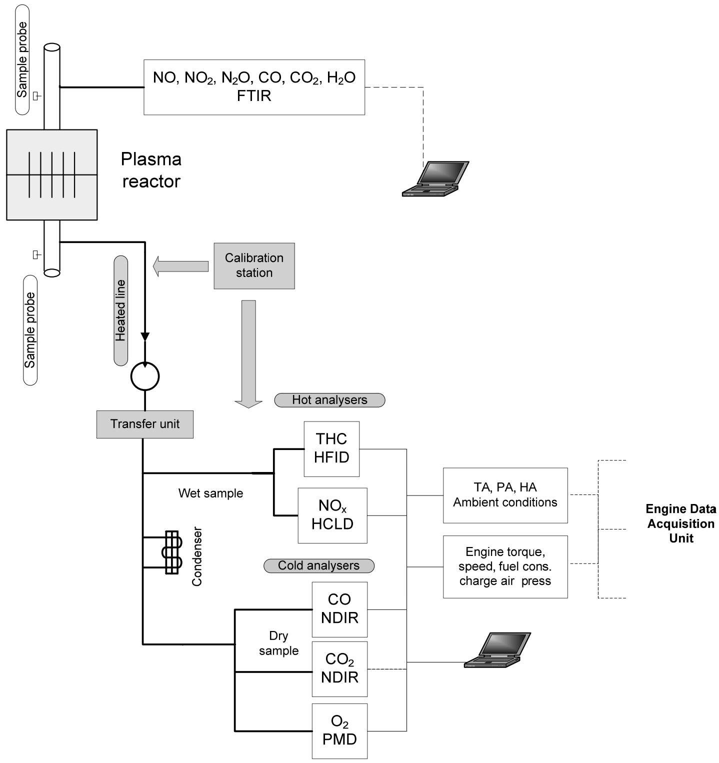

Fig. 2. Measurement equipment setup

4. Results and discussion

The NO_x reaction activities were measured in a one-stage non-thermal plasma reactor system. An marine engine functional exhaust gas was used in the plasma reactors tests. The total exhaust gas flow rate was corresponding to an engine effective load. Effectively, the exhaust flow through the plasma reactor path can be controlled by restriction flap, mounted upstream the main silencer. Equivalent reactor proportional part gas stream parameters are presented in figure 3. The total exhaust gas amount and attribute components during the engine tests presented in table 3. Typically, the reactor was heated up to reach stable temperature, adequately with exhaust gas condition without turning on the plasma. Upon reaching the exhaust gas pressure and temperature level, and as soon as the NO_x levels stabilized, the plasma was turned on at a typical power stage. Throughout the measurements, the engine outlet NO_x levels (NO and NO_2) were monitored with simultaneous NO, NO_2, N_2O measurement, allowing to estimate the quantities of unconverted NO_2. During the tests, the reaction temperature was raised usually approximately 30 K. At each temperature, sufficient time was allowed to reach steady state (or near steady state) to assure that the NO_x loss was not due to storage effects. Set of thermocouples were used to provide reference state of the plasma processor temperature. The processor temperature can not adjusted as is dependent to engine exhaust gas temperature and during test raised from room temperature up to 350°C. This has been used to investigate the operating temperature of the process. The chemistry inside the plasma reactor is complex. It is concluded that the two most important processes initiated by the plasma are the partial conversion of NO into NO_2, and the partial oxidation of unburned hydrocarbons in the exhaust gas. In fact, modeling of the gas-phase chemistry indicates that these two chemical processes are closely linked [3].

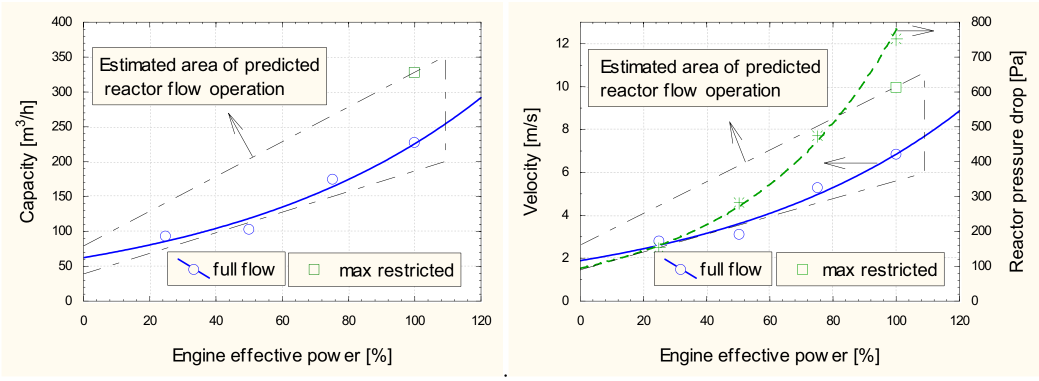

Fig. 3. Exhaust gas flow through the plasma reactor within the engine load range and

Tab. 3. Total engine exhaust gas flow and components contribution

Operation mode	D2	1	2	3	4
Engine power	[kW]	400	300	200	100
Engine speed	[rpm]	720	720	720	720
Exhaust flow	kg/h	2 690	2 229	1 675	1 040
NO_x	kg/h	5,62	4,48	2,95	1,49
CO	kg/h	0,25	0,17	0,12	0,08
CO_2	kg/h	273	210	144	76
O_2	kg/h	299	267	216	150
HC	kg/h	0,42	0,34	0,26	0,14
SO_2	kg/h	1,41	1,08	0,74	0,39

The experimental measurements demonstrate particularly significant oxidation process. In the present paper, all the results were presented in terms of constant specific energy density supplied to plasma reactor. In this application the plasma is used to oxidize NO to NO_2. Oxidation is the dominant process for exhausts containing dilute concentrations of NO. The kinetic energy of the electrons is deposited primarily into the major gas components, N_2 and O_2. The most useful deposition of energy is associated with the production of N and O radicals through electron-impact dissociation. Diesel engine exhausts contain little gaseous hydrocarbon, and under some load transient conditions a significant amount of liquid-phase hydrocarbons VOC (volatile organic fraction) in the particulates. The hydrocarbons promote the oxidation of NO to NO_2, but not the reduction of NO to N_2. The oxidation of NO to NO_2 is strongly coupled with the hydrocarbon oxidation chemistry. The plasma operation process results with the exhaust gas is shown in the Figure 4. When the electrical power to the plasma reactor is turned off and gas is passed through the reactor, the NO and NO_2 outlet concentration basically correlates to total NO_x level recorded at the reactor inlet. When the electrical power to the plasma reactor is turned on, the NO is oxidized to NO_2. The oxidation at this temperature and gas flow conditions is quite effective (idle engine load). Presumably the presence of liquid-phase hydrocarbons and propane could improve the efficiency of NO oxidation. The plasma process does not repeatedly guarantee the efficient oxidation of NO to NO_2. In the exhausts containing both O_2 and H_2O, plasma produces not only O radicals but also OH radicals, only O radical can be effective in oxidizing NO to NO_2. However, the OH radical can further oxidize NO_2 to nitric acid. This acid formation is not a desired part of the plasma process and the presence of the hydrocarbon prevents the formation of an acid products and increases the efficiency for NO to NO_2 oxidation.

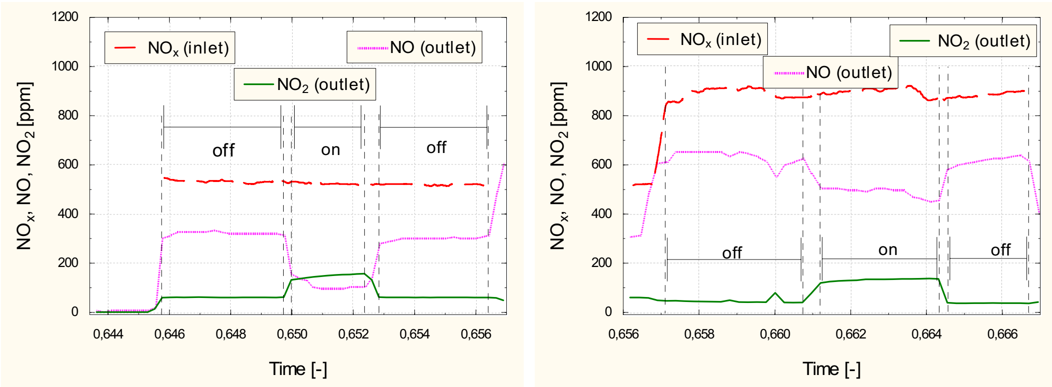

Fig. 4. Plasma reactor NO_x concentration record under two ascending engine loads

Figure 4 (second diagram) shows effect of rising exhaust flow and gas temperature on NO oxidation efficiency under engine part load condition. With higher gas flow and temperature, at given reactor energy density NO oxidation decreases. The decrease in NO oxidation efficiency could be recognized with the following reasons: the rate coefficient of oxidation reaction decreases with gas temperature increase, thus reducing the efficiency of NO conversion to NO_2, hydrocarbons influence was weakened with temperature rise and reduction of ozone which plays an significant function in NO oxidation. Figure 5 shows the exhaust gas composition regarding mass flow nitrogen oxides allocation, caused by plasma stroke. For a given electric field, the ratio of reacted NO and NO_2 – resulted was higher under engine part load than idle.

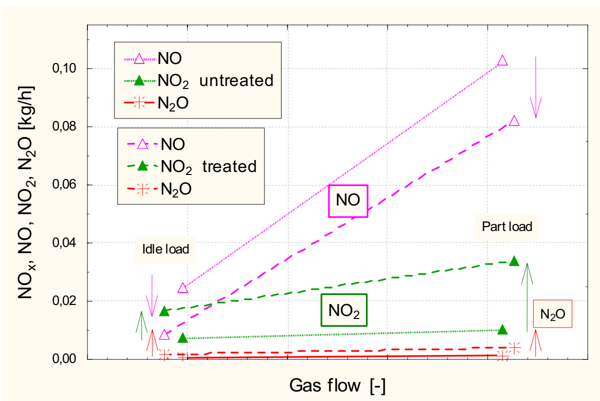

Fig. 5. Nitrogen oxides flow trends in plasma reactor operation under two ascending engine loads

5. Conclusions

Experimental studies involving a plasma reactor operation with sensible exhaust gas from marine engine performed. The primary aim of the experiment involved basic NO oxidation trends under engine characteristic mode of operation. For a given reactor energy level density, the plasma-associated process exhibits NO oxidation characteristics different for two exhaust gas states and flows – figure 6. The idle engine load reveal higher NO conversion efficiency – close to 50 %, while part load of the engine decreased final efficiency to 26%. The NO oxidation process obtained under different load conditions is characterized by: exhaust gas flow where capacity increased twice, elevated temperature and gas components share.

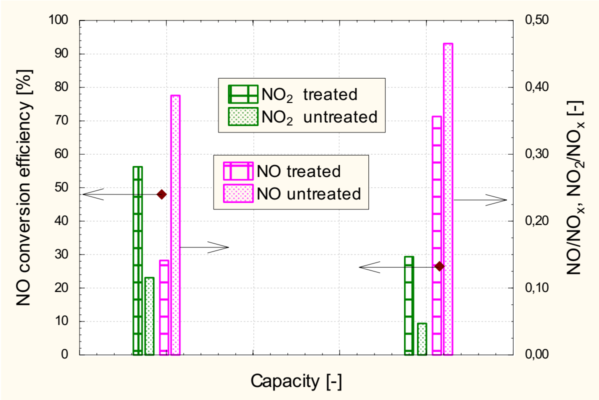

Fig.6. Plasma NO_x reaction – oxidation efficiency process under two ascending engine loads

Following the evaluation stage a programme is now underway to design, build and test a part scale reactor model to develop 1/10 th range of the exhaust gas flow. It will give the possibility to increase experimental engine effective load up to nominal level. The plasma-associated technique, exhibiting a high NO oxidation level, can be a viable alternative after treatment system.

References

[1] Hughes D. E., McAdams R., *Non-thermal plasma for marine diesel*, International Council on Combustion Engines CIMAC Congress 2004, 7-11 June, Kyoto (Japan) 2004, Paper No. 231, p. 15.

[2] Penetrante B., Schultheis S. E., *Non-Thermal Plasma Techniques for Pollution Control: Part B - Electron Beam and Electrical Discharge Processing*, Springer-Verlag, Berlin Heidelberg New York, 1993.

[3] Gentile A. C., Kuschner M. J., *Reaction chemistry and optimization of plasma remediation of N_xO_y from gas streams*, Journal Appl. Phys. 78(3) 1 August 1995.

[4] Penetrante B.M., Vogtlin G.E., Merritt B.T., Brusasco R.M., *Plasma Technology for Tail Pipe Reduction of NO_x in Diesel Exhaust*, South Coast Air Quality Management District,Symposium on Air Pollution Health Impacts, Recent Findings, Implications, Dieselization and Policy Initiatives, Diamond Car, CA November 20-21, 1997.

[5] Atkinson R., Baluch D.L., Cox R. A., Hampson R.F., Kerr J.A., Kuschner J., Troe J., Journal of Phys. *Chemical Reference Data*, 18 881, 1989.

[6] Person J. C., Ham D.O., Radiat. Phys. Chem. 31, 1, 1998.

[7] jorth J., Notholt J., Restelli G., Int. J. Chem. Kin. 24, 51, 1992.

[8] Mok Y. S., *Application of dielectric barrier discharge to selective catalytic reduction of nitrogen oxide,* Journal Chem. Eng., Japan 37, 1337, 2004.

[9] International Maritime Organisation, *Draft technical code on emission of nitrogen oxides from marine diesel engines*, 1997.

[10] Kalisiak S., Paterkowski W., *The semiconductor corona generator for cleaning gas pollution*, 4th International Conference on Unconvencional Electromechanical and Electrical Systems (UEES) St. Petersburg, Russia, June 21-24 1999.

[11] Shelef M., *Selective Catalytic Reduction of NOx with N-Free Reductants*, Chemical Reviews 95, 1995.

THE NO_X EMISSION PREDICTION IN DIESEL EXHAUST FOR LARGE BORE MARINE ENGINES

Tadeusz Borkowski

Maritime University
ul. Wały Chrobrego 1/2, 70-500 Szczecin, Poland
tel.: +48 91 4809419, fax: +48 91 4809585
e-mail: tborkowski@am.szczecin.pl

Abstract

The general IMO procedure was adopted with the main aim to achieve compliant engine performance with current environmental legislation. The paper investigates possibility of multi-zone diesel combustion model use to estimate NO_x emission. The model calculation results are compared with the experimental data obtained for marine diesel engine - Sulzer A20/24. An experimental study is conducted to investigate the use of phenomenological multi-zone model to predict NO_x emission, based on marine diesel engine operation parameters. The predicted and experimental results comparison shows reasonable agreement only within high engine loads, while serious discrepancies were found in low range operating effective power.

Keywords: *marine diesel engine, exhaust emission, combustion modeling, performance*

1. Introduction

The ever more stringent exhaust emission standards have prompted the development of marine engines systems and associated controls in order to reduce the nitric oxide. While NO_X sensors exist, that provide robust continuous measurements in diesel engines at reasonable price, the present work focuses on indirect approach. Combustion pressure is analyzed for specific quantitative values (indicated mean effective pressure, maximum pressure, firing pressure angle, cycle variation, etc.), level during certain events (valve closures and opening, peak rate of pressure rise, etc.), as well as data variation between cylinders and within a specific cylinder over a certain number of cycles. The final aim is a calculation of indicated power for each cylinder as well as the total engine power derived from the measured cylinder pressures. Engine cylinder pressure analysis is also used to balance and tune the engine: valve and fuel injection timing as well as fuel rate and compression. Development of engine diagnostics calls for improving the reliability of the engine. One of the methods used to meet these requirements is a convenient and real-time cylinder pressure measuring system. Much effort has been spent developing combustion models that will adequately predict engine performance and pollutant formation. Both multi-zone and multi-dimensional models are computationally all-absorbing for utilization within an engine system simulation, so a need exists for simpler, faster, and reasonably predictive models associated with zero-dimensional (time dependent) approaches. Generally, zero-dimensional (time dependent) models tend to have a highly empirical nature and thus are limited to particular combustion system designs. Phenomenological multi-zone models take into account the spatial differences in temperature and chemical compositions by dividing a cylinder into two or more zones. Each zone is treated as a well-mixed open thermodynamic system. Because the model can give local temperature and compositions, it can be used to predict exhaust emissions. Their predictive ability and accuracy greatly depend on what methods and sub-models are used. Many aspects of multi-zone models, for example the accuracy of simultaneous prediction of exhaust emissions and cylinder pressure, still need to be improved.

The aim of this paper is to adopt a phenomenological multi-zone combustion model for use in steady condition analysis. The model should be able to predict some aspects of engine performance and cylinder-averaged quantities such as NO_x emissions. However, it is impossible for the phenomenological models give the detailed in-cylinder data flow and temperature fields. Nevertheless, compared with the CFD model, the phenomenological multi-zone model provides a simple way to obtain full cycle simulation.

2. Model aspects

Engine combustion model is based on the undisturbed turbulent gas jets, also referenced as the "Cummins model", where diesel spray is treated as quasi-steady gas jet penetrating into gaseous environment of combustion air [1], [2], [3]. The concept of the model assumes that the liquid fuel injected into a combustion chamber as several jets is divided into many small zones. In large marine diesel engines chamber, the air flow is essentially quiescent. All combustion events in each zone: droplet break-up, evaporation , air–fuel mixing, ignition, premixed heat release, mixing-controlled heat release, heat transfer and formation of exhaust emissions, are calculated in order to achieve zonal temperature and compositions. The zonal property is representing by the average state of temperature, air-fuel ratio and NO_x concentration. The model contains: spray development, air entrainment and mixing, droplet evaporation, heat transfer, combustion and NO_x formation sub-models. In order to estimate rates of combustion and pollutant formation, a set of evolving discrete combustion zones is superimposed on the continuous calculated fuel-air distribution (Fig. 1).

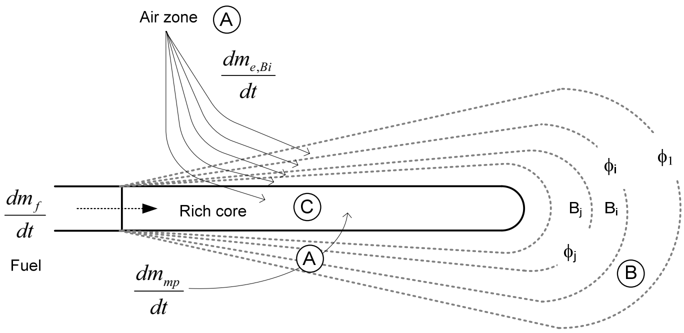

Fig. 1. The evolution of combustion zones and air entrainment

Entrainment of air into the jet is assumed to take place at each point along the jet surface at rate proportional to the velocity difference between the jet and surrounding air at that point. The considered chamber is divided into number of zones at incipient ignition, air zone corresponds to the medium into that the fuel is injected (d_{mf}/dt) – rich core and n zones B_i of combustible mixture between the lean and rich flammability limits. During the course of combustion the fuel mass in each zone B_i remains constant and the additional fuel that is diluted beyond rich flammability limit is assigned to an additional combustion zone B_j. In contrast to these constants, fuel masses in zones B_i, where air is continuously entrained ($dm_{e,Bi}$/dt) into the zones B_j and rich core. The entrainment rate into a zone is simply equal to the change of mass of this zone, because the fuel mass remains constant. The contribution of each zone to the total wall heat transfer is based on the product of zone mass and temperature:

$$\frac{dQ_{w,z}}{d\varphi} = \frac{m_z t_z}{m_A T_A + m_C T_C + \sum_{i=1}^{j} m_{Bi} T_{Bi}} \cdot \frac{dQ_{w,tot}}{d\varphi}, \qquad (1)$$

The change of composition and internal energy of each zone, caused by the mixing between the zones can be determined similarly to energy and mass balance equations for various zones. Thus, NO_x concentration caused by the mixing can be calculated from the following equations [4]:

$$\frac{d[NO]_{Ci}}{dt} = \frac{d[NO]_{Ci,A}}{dt} + \sum_{i=1}^{j} \frac{d[NO]_{Ci,B}}{dt}, \tag{2}$$

$$\frac{d[NO]_{Ci,A}}{dt} = \frac{dm_{Ci,A}}{dt} \frac{[NO]_A}{m_A}, \tag{3}$$

$$\frac{d[NO]_{Ci,B}}{dt} = \frac{dm_{Ci,B}}{dt} \frac{[NO]_{Bj}}{m_{Bj}}, \tag{4}$$

In order to enable prediction an emissions formation in terms of NO_x, the model has been equipped with the widely accepted extended Zeldovich model [1]:

$$N_2 + O = NO + N \qquad k_{1,f} = 7.6 \cdot 10^{13} exp[-38000/T] cm^3/(mol \cdot s), \tag{5}$$

$$N + O_2 = NO + O \qquad k_{2,f} = 6.4 \cdot 10^{9} exp[-3150/T] cm^3/mol \cdot s, \tag{6}$$

$$N + OH + H \qquad k_{3,f} = 4.1 \cdot 10^{13} cm^3/(mol \cdot s), \tag{7}$$

The formation rate of NO can be written as:

$$\frac{d[NO]}{dt} = k_{1,f}[N_2][O] + k_{2,f}[N][O_2] + k_{3,f}[N][OH] - k_{1,r}[NO][N] - k_{2,r}[NO][O] - k_{3,r}[NO][H], \tag{8}$$

after simplification:

$$\frac{d[NO]}{dt} = 2k_{1,f}[N_2][O] - 2k_{1,r}[NO][N], \tag{9}$$

3. Experimental details

Basically, multi-zone models should be checked against experimentally derived heat-releases profiles and recalibrated if necessary. The main objective was to predict emission, with NO_x as the primary target, of the Sulzer 6AL 20/24 engine. This engine has been used as the test engine for examination. The first step of the experiment was to establish performance parameters with greatest possible accuracy. Further, comparing the results of model calculation against the experimental based results Using test bed engine and having the specification listed in Table 1, examinations were made to predict exhaust emission. The key injection parameter needed for combustion analysis is fuel injection pressure and time of the start, when fuel first enters the cylinder. Injection pressure data and dynamic start of injection were identified as one of the key parameters that have a great impact on the qualitative and quantitative aspects of the combustion process. Hence, a strain gauge transducer measurement technique which is readily available, has been adopted to determine injection pressure data. The task includes identification of the period of fuel injection as a function of crank angle, and the measured fuel consumption.

Tab. 1. Test engine details

Engine type	Sulzer 6A20/24, non-reverse.
Number of cylinder	6
Bore/Stroke [mm]	200/240 [mm]
Rated engine speed	720 [rpm]
Output	397 [kW]
Compression ratio	14
Brake mean effective pressure	1.47 [MPa]

The combustion pressure as well as injection pressure was continuously monitored and recorded by the fast data acquisition system. It is known that the injector chamber pressure (the fuel space around the needle valve seat) varies widely during the period the injector valve is open, so the representative value is difficult to define. Accurate predictions of fuel behavior within the injection system require sophisticated hydraulic models. However, to achieve only approximate estimates of the injection rate trough the injector nozzle flow a following method was assumed. In cases when flow through nozzle is quasi steady, incompressible and one dimensional, the mass flow rate of injected fuel is given by:

$$\dot{m}_f = C_D A_n \sqrt{2\rho_f \Delta p}\,\frac{\Delta\varphi}{360n}\,, \tag{10}$$

where:

C_D - discharge coefficient,
A_n - nozzle minimum area,
ρ_f - fuel density,
Δp - pressure drop across the nozzle,
$\Delta\varphi$ - nozzle open period,
n - engine speed.

Defined heat release in functional form was chosen to match experimentally observed heat-release profile. The static injection timing, for present experiment was kept constant by engine design. The combustion pressure as well as injection pressure was recorded by the fast data acquisition system. It is known that the injector chamber pressure (the fuel space around the needle valve seat) varies widely during the period the injector valve is open, so the representative value is difficult to define. Therefore a different definition is given, it requires the use only one pressure transducer located in the fuel line near the injector and is easily used in practice. Basic fuel injection equipment characteristic and settings for nominal load presented in Table 2.

Tab. 2. Fuel oil injection equipment settings

Fuel pump setting		
Commencement stroke	[m]	0.004
Injection start	[deg]	-19.0
Effective stroke	[m]	0.006
Delivery completion	[deg]	+9.5
Injection nozzle		
Opening pressure	[MPa]	25.0
Spray angle	[deg]	159
Number of spray holes	[-]	7
Spray hole diameter	[m]	0.00026
Needle lift	[m]	0.0005

Subsequently, the trials were performed to assess the engine operation on consequent emission profiles. Emission measurements were carried out on engine at steady-state operation. All engine performances were continuously, together with exhaust gas components concentration recorded [5]. The performance measurement procedure of marine engines on test beds, performed in accordance to Annex VI of Marpol 73/78 convention - with the specification given in the IMO NO_x Technical Code and ISO standards [4]. To reduce emissions variability, all tests performed with the selected marine distillate fuel DMX [6]. Today on conventional, commercial diesel engines there are no sensors available that can be mounted directly into the combustion chamber. Therefore for this project a marine engine electronic indicator (Premet-Lemag*) was chosen.

4. Results and discussion

There are two prerequisites for being able to perform combustion experimental analysis, the fuel injection period and cylinder pressure. Both needs to be determined with great accuracy and has to be measured during the same cycle. Figure 2 illustrates the set of measured injection and cylinder pressures taken within the test cycle engine load range. Subsequent analysis of the in-cylinder pressure history, that will produce the rate of heat release profile. The pressure history displayed in Fig. 2. represents the experimental data and the simulation results obtained with the measured fuel injection input files It is shown that there is a certain discrepancy between the model and measured results. As the engine load and in-cylinder temperature decrease, the process of droplet evaporation becomes more important and is dominant.

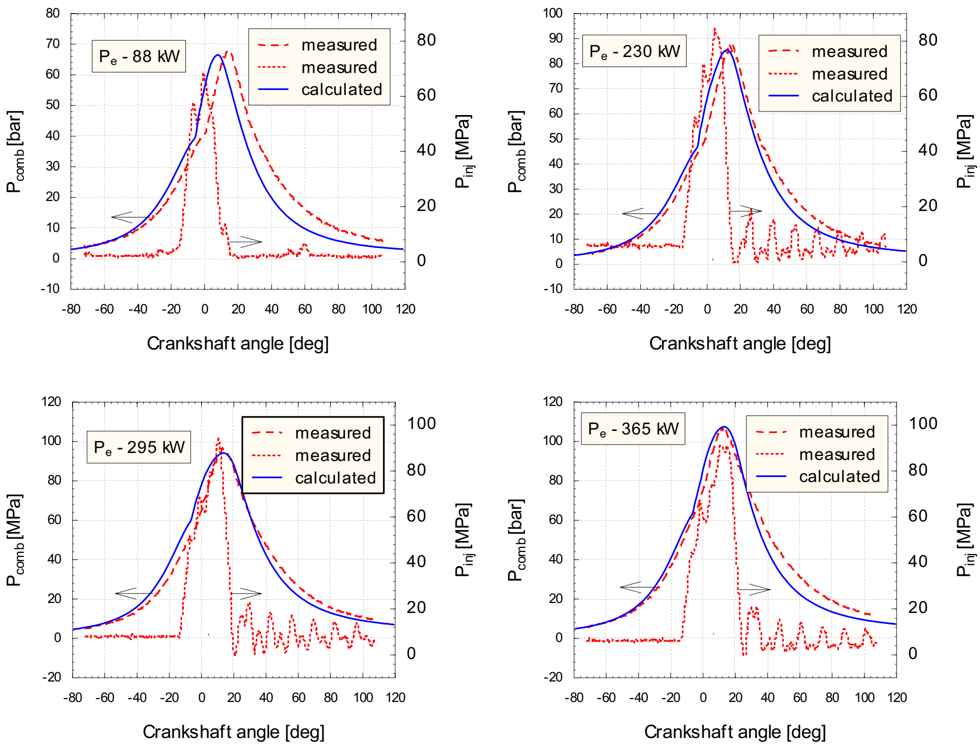

Fig. 2. Comparison of calculated and measured cylinder and injection profiles at different engine load

* Lehmann & Michels GmbH & Co. KG, Germany

Figure 3 shows rate of heat release profile comparison – model and experimental (resulted from cylinder pressure) illustrating the premixed spike during the first phase of burning and the smaller gradients during the diffusion part of burning. From the figure, it can be seen that there is only one peak in the heat release diagram for model results, while measured traces have not exhibit such occurrence. The rate of air-fuel mixing in a quiescent combustion chamber depends mainly on the fuel injection process. The key injection parameter needed for combustion studies is the actual dynamic start of injection, when fuel first enters the cylinder. During an ignition delay period, a substantial amount of combustible mixture will be formed and a significant part of the fuel will burn rapidly in the premixed mode, immediately after ignition. Once the premixed fuel is used-up, combustion becomes diffusion-controlled. If the delay is very small, depending on the conditions at the end of compression and the mixing process itself, burning is largely diffusion-controlled. The ignition delay and the rate of heat release are the key phenomena that need to be analyzed in order to characterize and quantify the burning process. Therefore, the influence of individual engine or fuel parameters can not be investigated without considering secondary influences. The fuel spray on break-up atomizes to a large number of droplets with a diameter equal to the Sauter mean diameter (SMD). The droplet heating and evaporation take place under different zone conditions according to the correlations of Hiroyasu [6]. The calculation have taken into account the formation of the liquid fuel spray and its interaction with the atomization, break-up, vaporization and combustion. In addition, the testing at low temperature in engines (low load) proved to be difficult. As already observed model results profiles – RHR, has clearly sketched first stage of combustion, that is advanced 2-4 CA degrees to the experimental traces. The largest discrepancy covers low engine load. Furthermore, it can be deduced that ignition delay of real diesel engine requires more deflected curve based on exponential equation [8].

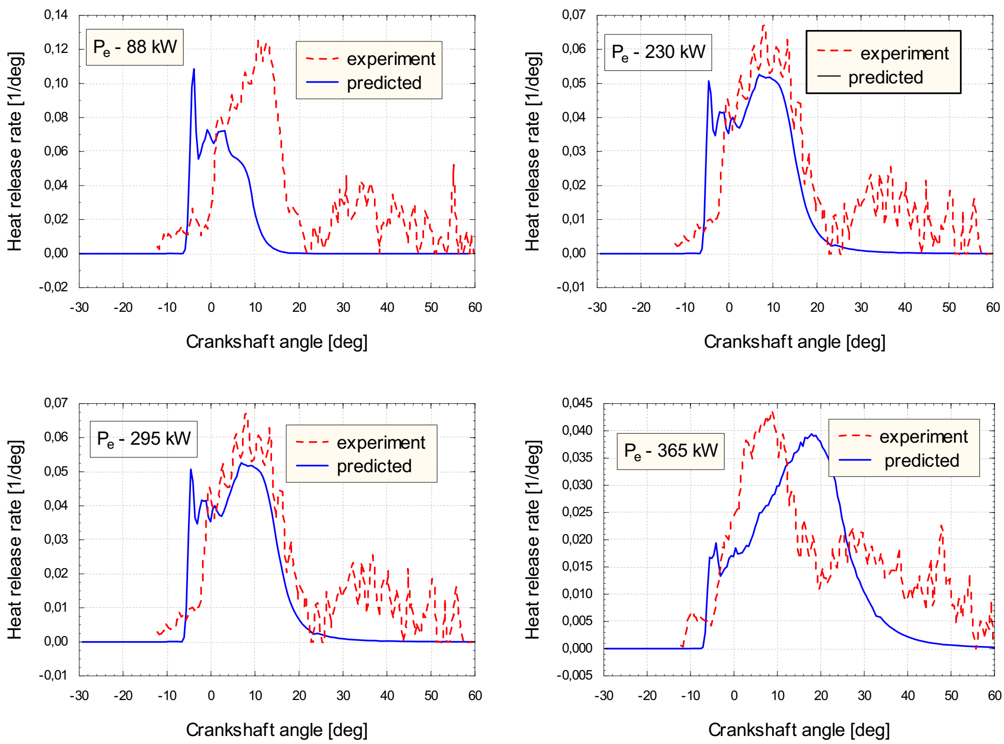

Fig. 3. Comparison of rate of heat release history comparison at different engine load

Figure 4 shows the baseline picture were NO highest densities are placed in post-flame regions - not in the highest temperature zones. That is due to slow NO formation chemistry. NO develops within hot, post-combustion gases after combustion completion, in section where flame jet had traveled. The whole flame structure is equally spread out thanks to moving fuel-air mixture along chamber surface. Temperature is at maximum value within range 20-25 CRA after TDC and it corresponds to highest NO mass fraction density. NO formation regions can be identified with fuel spray location and its dynamic actions. It should also be noted that space in central part of the cylinder exhibit lower NO mass fraction density. During the expansion the NO chemistry freezes as effect of temperature decrease and its concentration remains constant.

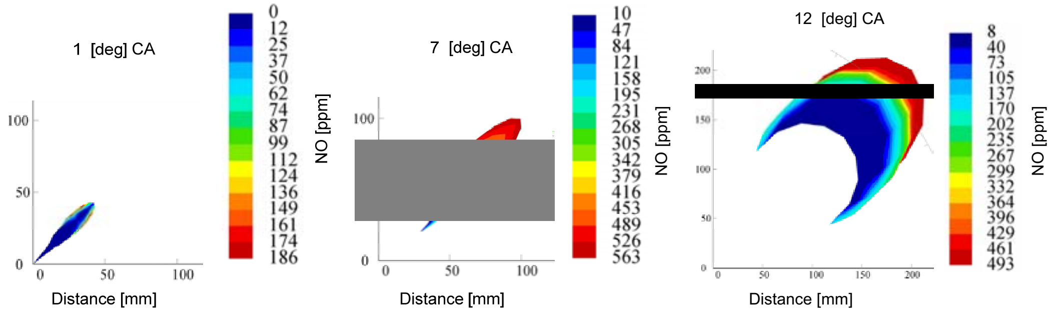

Fig.4. NO formation distribution with fuel injection spray

The spray simulation during normal operation showed droplet flow located in combustion chamber. However, a risk has arisen that some part of spray droplets can reach combustion chamber wall. Generally, the critical NO equivalence ratio formation in high-temperature and high-pressure burned gases is close to stoichiometric. The crucial time for its formation is when the burned gas temperature is at maximum, between the start of combustion and close to peak pressure occurrence. Early combustion process causes higher NO formation rate as combustion proceeds. Nearly final NO concentration is formed within the 25 CA following the start of combustion.

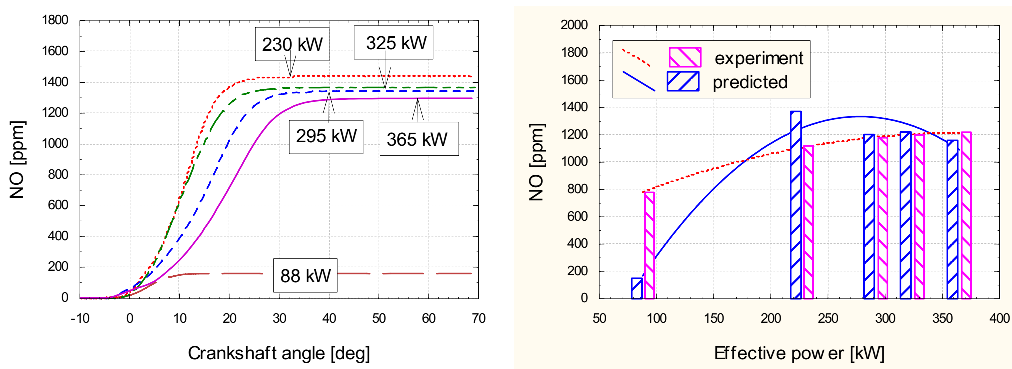

Fig. 5. Comparison of predicted (in cylinder) and measured (common outlet) NO_x emission

The investigated operating conditions expressed as the histories of NO_x concentration are displayed in Fig. 5. It can be seen that the NO_x concentrations level starts to rise after the start of combustion and continues to a maximum value. It has been shown that there are several CA delays of the start NO_x formation process, with the combustion commencing.

Later, while combustion proceeds NO_x concentration increases, up to maximum level at 10-20 CA with respect to highest cylinder pressure. However, the predicted value of NO_x emission is lower than experimental data under low part of the engine load. Coincidentally, along with the decrease of engine load, the discrepancy between the calculated and the measured cylinder pressure results becomes large.

5. Conclusions

An experimental investigation of diesel combustion contribution to NO_x emission has been tested and confronted with phenomenological multi-zone combustion model calculation results. It is found that predictive ability of the used model is partly proved – high engine load, by experiment results. There is an serious error concerning NO_x emission at low load, even if the maximum combustion pressure prediction and measurement shows reasonable agreement. Thus, model calculation influenced by ignition delay, specifically at low engine load, it needs to be modified as a further step. There is also a realistic problem to overcome – accuracy of combustion and injection pressure measurement [9]. The sub-models of spray development and air entrainment have to be improved to increase model predictive ability. Anyhow, the results are promising and shows that the phenomenological multi-zone combustion model is capable of predicting the NO_x emission.

Acknowledgements
The author would like to thank the Ricardo Software (UK) for technical support.

References

[1] Stiesch G., *Modeling engine spray and combustion processes*, Springer Verlag 2003, -282 p.
[2] Mehta P. S., Bhaskar T., *Prediction of combustion and in-cylinder emissions in a direct injection diesel engine using multi-process model*, V Symposium on Diagnostic and Modeling of Combustion in Internal Combustion Engines, COMODIA, Nagoya, July 1-4, 2001, pp. 101-107.
[3] Heywood J.B., *Internal combustion engine fundamentals*, McGraw-Hill, Inc. 1988, -930 p.
[4] Cui Y., Deng K., Wu J., *A direct injection diesel combustion model for use in transient condition analysis*, Proceedings of the Institution of Mechanical Engineers, Vol 215 part d, 2001, pp. 995-1004.
[5] ISO, 3046/1-1986 (e), 3046/iii –1979 (e), 3046/ii-1977 (e), 8178:1994 (e).
[6] ISO, *Petroleum products – fuels – specifications of marine fuels*, ISO 8217:1996(e).
[7] Kouremenos D. A., Rakopulos C. D., Yfantis E. A., Hountalas D. T., *An experimental investigation of the fuel-injection-pressure and engine-speed effects on the performance and emission characteristics of divided-chamber diesel engine*, International Journal of Energy Research, Vol.17, 1993, pp. 315-326.
[8] Pischinger F., Reuter U., Scheid E., *Self-ignition of diesel sprays and its dependence on fuel properties and injection parameters*, Journal of Engineering for Gas Turbines and Power, Vol.110/399, July 1988, pp.399-404.
[9] Timoney D. J., Desantes J. M., Hernandez L., Lyons C. M., *The development of a semi-empirical model for rapid NO_x concentration evaluation using measured in-cylinder pressure in diesel engines*, Proceedings of the Institution of Mechanical Engineers, Vol. 219 part d, 2005, p. 621-631.

ANALYSIS OF TWO DESIGN KIND OF PROPULSION FOR AN INLAND VESSEL

Czesław Dymarski

Gdańsk University of Technology
ul. G. Narutowicza 11/12, 80-952 Gdańsk, Poland
tel.: (58) 347 16 08, fax: (58) 34147 12
e-mail: cpdymars@pg.gda.pl

Abstract

This paper presents design assumptions, technical conditions and two kinds of design solution of propulsion system for an inland waterways ship. In the first version this is a combustion-electric system fitted with frequency converter and in the other - combustion-hydraulic one with hydrostatic reduction gear. There are also a preliminary comparative analysis of these systems.

Keywords: *ship propulsion systems, combustion-electric driving system, combustion-hydraulic driving system*

1. Introduction

Accede Poland to the European Union created significant increase of interest of an inland sailing especially in an east-west direction. A good example of this interest, not only our country but also European authorities, is assign some financial outlays on realization research works in European project EURECA.

One of such projects, realized mainly at Gdansk University of Technology, the Faculty of Ocean Engineering and Ship Technology, is project INCOWATRANS E!3065. The project concerns designing of passenger inland waterways ships intended for sailing on a shipping route Berlin – Torun – Kaliningrad. Acquaintance with rout of navigation is in case of inland waterways ship very essential. Construction of such ships and their propulsion systems depend on depth of the water routes, and dimensions of the existing thereon sluices, and also on different conditioning, in this also ecological.

One of the basic ship systems, which have decisive meaning for effectiveness and safety of navigation is propulsion and steering system. Several kinds of propulsion systems are applied on board modern inland waterways ships, out of which the following can be enumerated :

- conventional one fitted with a combustion engine, toothed gear and fixed or controllable pitch propeller, free or ducted in a fixed or pivot able Kort's nozzle
- combustion-electric one fitted with an electric transmission and frequency converter making it possible to steplessly control rotational speed of the propeller which may be fixed one
- combustion-hydraulic one fitted with a hydrostatic transmission and fixed propeller
- propulsion system fitted with two azimuthal propellers (rotatable thrusters) driven by combustion engines through a toothed, electric or hydrostatic transmission
- propulsion system fitted with cycloidal (Yoith- Schneider) propellers
- propulsion system fitted with water jet propellers.

Below are presented basic design assumptions and two selected design concepts of propulsion system for the mentioned ship.

2. Basic design assumption and choice of propulsion system

In this case the main external conditioning having of the principle influence on the basic projects - foundations of ship, resulted due to technical – exploitation features of the foreseen route of navigation. Some the most important of them are as follow:

- minimum depth of the water route - 1,2 m
- length of the shortest sluices - ~60 m
- minimum clearance of the bridge on the route - 3,87 m
- high ecological requirements

Taking into consideration above-mentioned conditioning worked out general concept design of the ship. Assumed that the ship would consist of two connected segments: pusher and hotel barge, which can be seen in Fig.1.

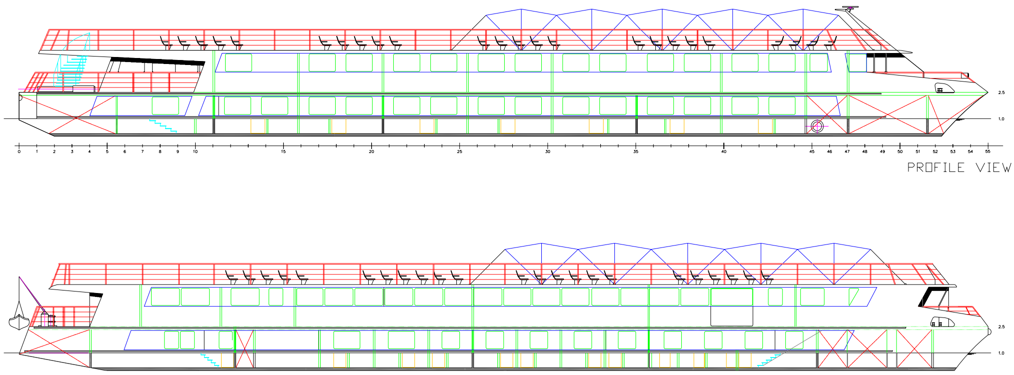

Fig. 1. View of the two segments of the designed inland ship: hotel barge – upper drawing and pusher – lower drawing

The basic technical parameters are as follow:

- overall length of the each segment L = 56 m
- overall breadth B = 9 m,
- draught T = 1 m,
- ship displacement for T = 1m $D_{1.0}$ = 440 t,
- expected velocity for T = 1m V = 14 km/h,
- required power output P = 300 kW.

The required very small draught of the ship is an important limitation in searching for a suitable propulsion system. Certainly it cannot be a propulsion system using cycloidal propellers which are located under the ship's hull. Ships driven by water jets fairly well operate in shallow waters. However such drive is unfavourable from the ecological point of view. A large water stream sucked out from under ship's bottom and thrown overboard with a great velocity destroys bottom and side structures of the waterway and biological live existing there. In this case the factor has been deemed so important that it was decided to exclude the water jet propulsion system from further considerations.

Hence only the systems fitted with screw propellers have been taken into account. As the propeller is assumed to operate in non-cavitating range, its appropriate diameter should be greater than 1 .4 m. In the case of two propellers used e.g. in Schottel rotatable thrusters the diameter of each of them might be a little smaller, equal to about 1.35 m.

Due to the small draught of the ship the above mentioned values of propeller diameter are not acceptable.

Therefore it was deemed necessary to apply a double-propeller propulsion system. This way it would be possible to decrease the diameter of the propellers to such an extent as to decrease its value to 0.83 - 0.85 m in the case of placing them in Korfs nozzles, being still large enough to transfer the assumed power. The outer diameter of the nozzles would then exceed a little the draught of l m, but if ship's hull form is suitably corected it will not be a problem. Such solution has many advantages. The double-propeller propulsion system provides higher ship's manoeuvrability and reliability. Location of the propellers inside the nozzles significantly lowers risk of catching the propeller's blade on the bottom that usually results in a failure and necessity of replacement of the propeller. Ducting the propellers also lowers unfavourable influence of screw race on the waterway bottom structure.

An additional improvement of reliability of the system and its simplification can be obtain by applying the fixed-pitch propeller. However it requires to provide the system with capability of changing magnitude and direction of rotational speed of the propeller shaft, that can be realized in the simplest way by a hydrostatic or electric transmission included in the propulsion system.

Further advantages can be achieved by replacing the fixed nozzle with pivotable one, and even better by using a rotatable thruster. This makes it possible to resign from applying the traditional rudder and in consequence to significantly decrease gabarites and weight of the device and simultaneously to improve ship's manoeuvrability.

Taking into account the above presented factors one decided to elaborate conceptual design projects of two solutions of the propulsion system fitted with rotatable thrusters, the most technically justified in the opinion of these authors, namely :

- combustion-electric one fitted with typical asynchronous squirrel-cage electric motors and frequency converters making stepless control of rotational speed of fixed propeller possible
- combustion-hydraulic one fitted with hydrostatic transmission.

3. Combustion-electric propulsion system

The elaborated combustion-electric main propulsion system of the ship is shown as a diagram in Fig.2.

Three electric generating sets were applied; each of them consisted of a four-stroke combustion engine driving a three-phase synchronous generator. The total power output of the three generating sets fully covers power demand for propelling and steering the ship. The output of the third generating set suffices to cover the assumed power demand of other consumers. So produced energy is delivered to the main switchboard. From here its main part goes to the frequency converters and next to the three-phase asynchronous electric motors driving the fixed screw propellers through the toothed intersecting-axis gear.

The ship steering functions are realized by rotating the column of rotatable thruster by an arbitrary angle around the vertical axis. To this end were used two hydraulic motors of a constant absorbing capacity, driving the column through toothed gears. The motors are fed from a constant capacity pump placed in the oil tank system, which is seen in Fig. 3. showing, in two axonometric projections, an arrangement of the main components of the presented system.

In this version of the system have been applied the electric motors in vertical position, that made it possible to obtain a modular construction of rotatable thruster, more compact and having relatively small gabarites. The drive is transmitted from the motors to the propeller shaft through the one-stage toothed gear placed inside the pod (electric podded propulsor) of rotatable thruster under water. Its reduction ratio is small because of a limited size of the pod, that makes it necessary to use a four-pole medium-speed electric motor.

A drawback of the solution is that the upper surface of the electric motor sticks out a little over the first deck of the ship (not shown in the figure). Another unfavourable feature is that the mass centre of electric motors is located high and shifted aft.

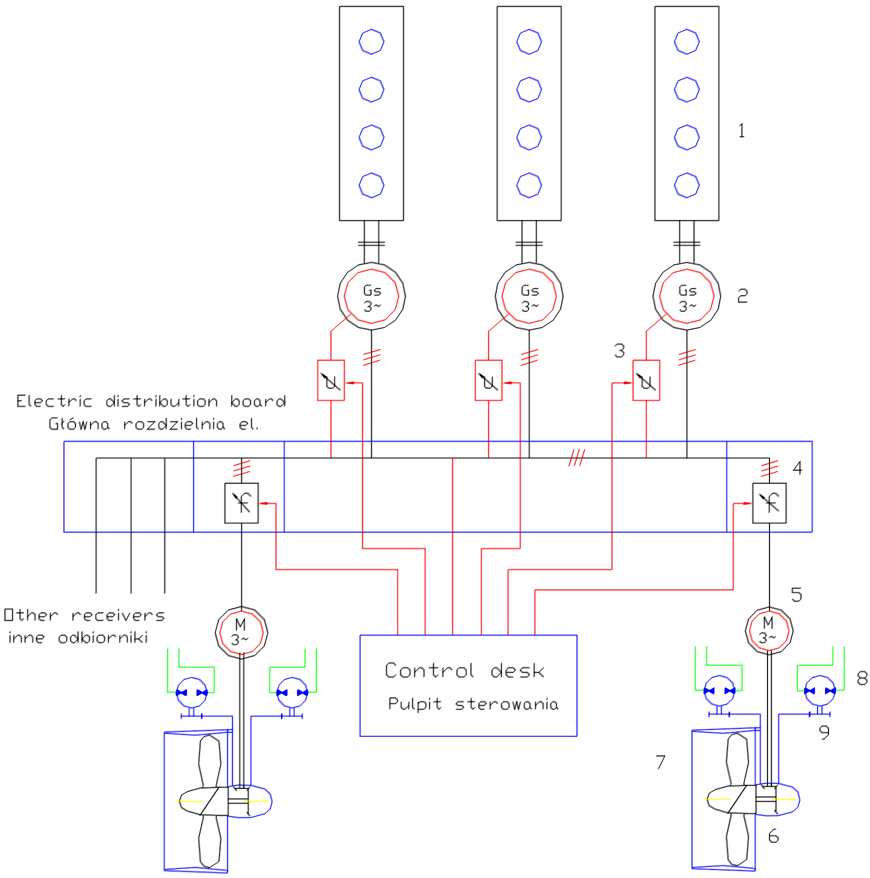

Fig. 2. Simplified schematic diagram of the combustion-electric main propulsion system of the ship. Notation: 1 – combustion engine, 2 – electric generator, auxiliary electric generating set, 3 – regulator of induce voltage of the electric generator, 4 -frequency converter, 5 - electric three-phase asynchronous cage motor, 6 – toothed intersecting-axis gear, 7 – fixed pitch propeller, 8 - hydraulic motors

a)

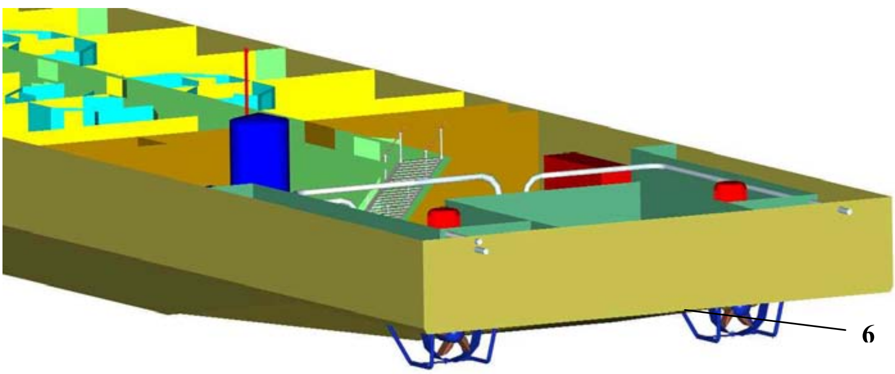

b)

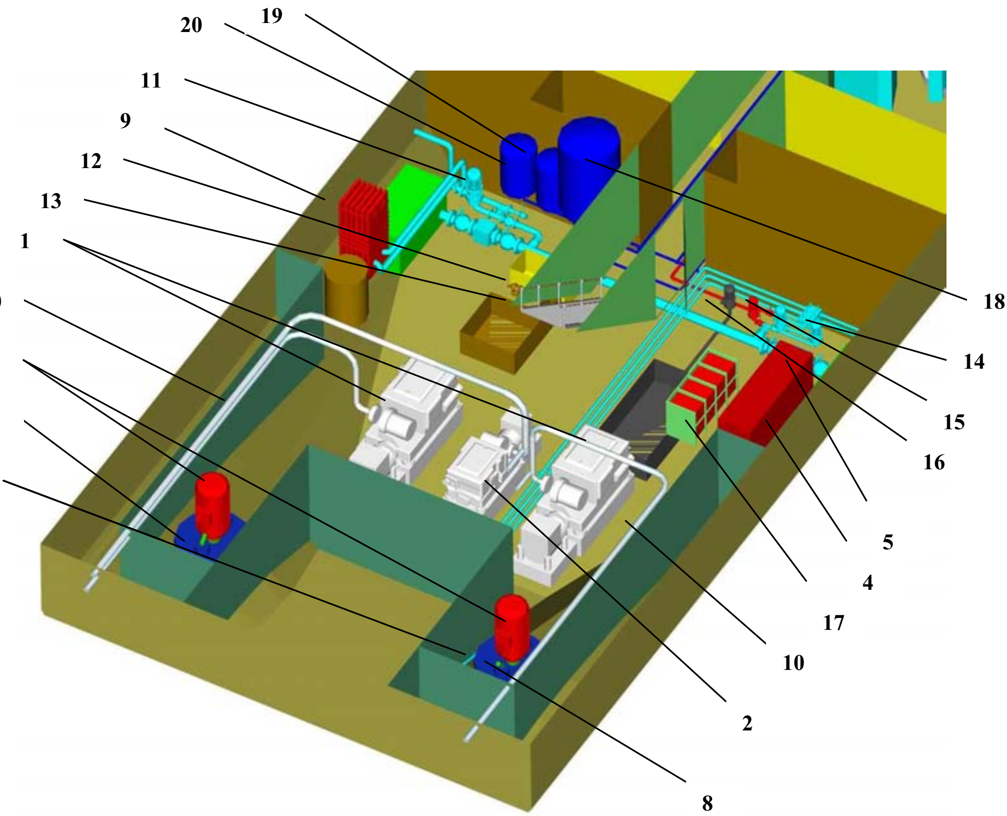

Fig.3. View of an example arrangement of the main components of the combustion-electric propulsion system. Notation : 1 - electric generating set, 2 - auxiliary electric generating set, 3 - driving the propeller, 4 -frequency converter, 5 - main switchboard, 6   rotatable thruster, 7 - hydraulic unit for supplying hydraulic motors, 8 - hydraulic motor fitted witch planetary gear to drive the mechanism rotating the column of rotatable thruster, 9 - central " outboard water - fresh water " cooler, 10-exhaust piping with silencers, 11 – outboard water pump, 12 – lubricating oil pump and tank, 13 – fuel tank and pump, 14 – ballast pump, 15 – bilge pump, 16 – fire pump, 17 – accumulator, 18 – hydrophore tank, 19 – electric water heater, 20 – water heater

4. Combustion-hydraulic propulsion system

Fig.4 shows schematic diagram of the propulsion system fitted with hydrostatic transmission.

The system is composed of two identical, mutually independent subsystems; each of them is driven by a high-speed combustion engine I. The engine, through a flexible coupling II, directly drives : an unit of two oil pumps 2 and 3, and also, through a mechanical gear III, an electric generator and a pump 4. The pomp of variable capacity 3 and the pomp of constant capacity 2 together with control unit V are the main source of energetic oil for feeding a fixed displacement hydraulic motor 11. The motor drives, through a toothed bevel gear, a fixed propeller located within a nozzle of a rotatable thruster XIV. In this case the application of a fixed propeller was justified by making it possible to steplessly control speed and direction of rotation of the hydraulic motor 11. This is realized by changing the capacity of the main pump 3 and oil pumping direction with the help of the servomechanism of the pomp.

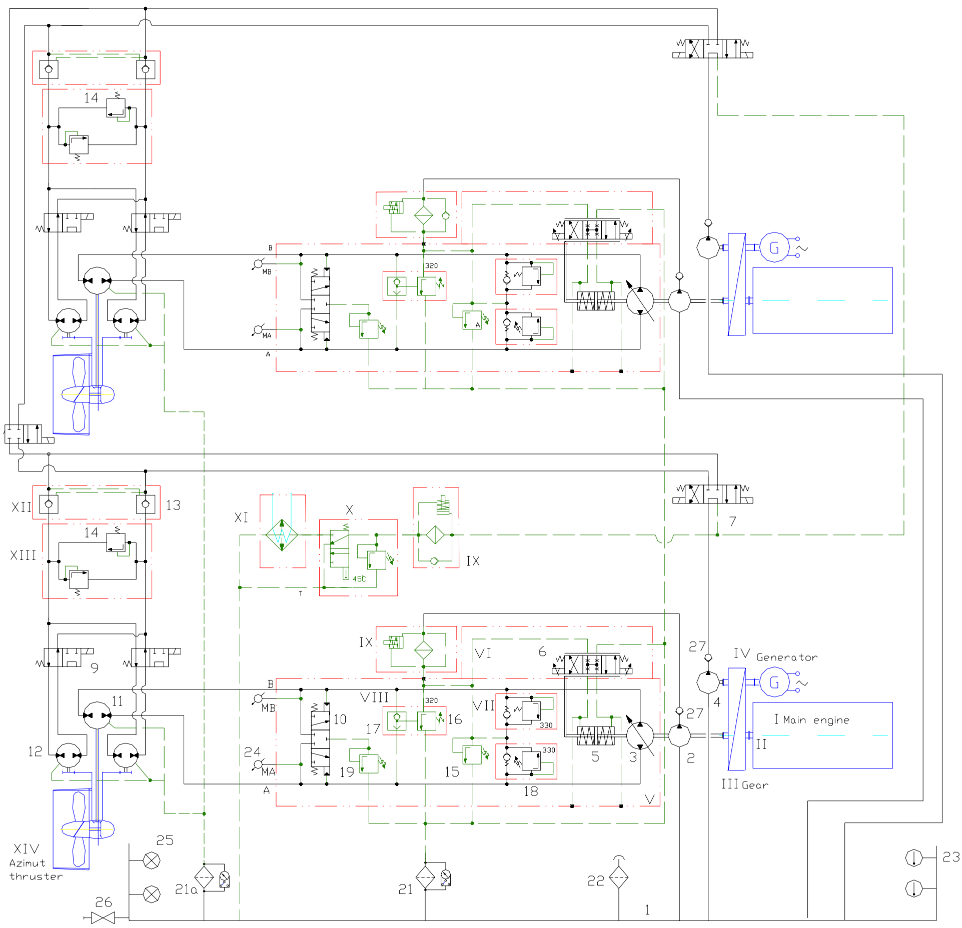

Fig. 4. Schematic diagram of the combustion-hydraulic propulsion system.

The servomechanism consist of a hydraulic cylinder 5 and a proportional valve 6 which is fed from the small pump 2 installed at the main pump 3.

The oil from the pump 2 flows through a check valves 27 to a filter in block IX and next divides into four branches:

- feeding the proportional valve 6 - block VI,
- feeding through one of two check valve a low-pressure line of the pump 3 - blocks VII,
- feeding a pressure relief valves 15,
- feeding a pilot operated relief valves 16 – block VIII,

During normal work cool and clear oil supplied from the pump 2 flows through one of two check valves in block VII into the actually low-pressure line of the main pump 3. Simultaneously from this line the same quantity of the hot oil have to be taken off. The oil flows off through a 3/3-way directional control valves 10, a pressure relief valves 19 and return filter 21 to an oil tank 1. The valve 10 is controlled by higher pressure of the both lines of the main pump 3, and always connects the low-pressure line with the pressure relief valves 19, which opening pressure value is set up a little lower than for the pressure relief valves 15.

A pressure relief valves 18 fulfill duty of safety valves and protect the both lines of the main pump 3 against excess in increasing of the oil's pressure.

As it was mentioned earlier, each propeller is driven by the hydraulic motor 11 through the reduction conical gear localized inside a pod. The hydraulic motor is placed in vertical position inside the vessel's hull directly above the azimuth thruster. A shaft of the hydraulic motor is coupled with a shaft of the conical gear.

Steering of the vessel is realized by turning of the thruster round vertical axe. A thruster's column is driven by two 2-dirctional fixed displacement hydraulic motors 12 through the reduction gear. The hydraulic motors 12 are fed by fixed displacement oil pump 4. Both lines feeding these hydraulic motors are equipped with pilot operated check valves 13 (block XI) and pressure relief valves 14 (block XII). The valves 13 protect the column with nozzle against unintentional turning caused by external hydrodynamic forces, and the pressure relief valves – against overloading mechanism in case of striking the nozzle against the bottom.

Use of two hydraulic motors and the reduction gear was dictated mainly by aim to decrease their dimensions for enable to locate all three hydraulic motors in one plane for well-chosen coronary bearing of a vertical column of the azimuth thruster. Two smaller motors make possible, as in symmetrical arrangement, to reduce the weights considerably and the same the dimensions of the toothed gear. The motors12 are fed in parallel arrangement through 4/2-way directional control valves 9, controlled electromagnetically. This enables to cut hydraulically off from feeding of any motor with simultaneous connection both hydraulic lines of the motor. In this way the thruster column can be driven by one motor only, when the second motor is working as a pump on overflow with insignificant losses of the power. It should be marked, that possible to obtainment torque would be a little less than a half of the nominal torque. However, during normal navigation on longer distances, it seems to be sufficient for control the course of the ship.

Considering, that the time of manoeuvres with turning of the azimuth thruster is relatively very short in comparison with the total time of navigation, this subsystem is used also for cleaning and a cooling oil in the reservoir 1. In periods between manoeuvres a 4/3-way directional control valve 7 is in central-position, cutting hydraulically off feeding of the motors 12 and direct the whole delivery of the pump 4 to block IX - filtration of the oil, block X - control of temperature and alternatively to block XI - cooling of the oil, and in the end to the reservoir 1. Both subsystems for drive turning mechanisms of the thrusters can be connect by means of electromagnetically controlled 4/2-way directional control valves 8. It makes possible turning both thrusters during work only by one main engine also.

Oil tank 1 is common for both main subsystems and is equipped with inlet filter 22, temperature detectors 23, sensors of oil level 25 and a manual operated shut-off valve 26, enabling draining of oil from the reservoir 1. The leakages of oil from hydraulic motors are collected in drain line and are led through a return filter 21 to the oil tank 1.

An arrangement of the main components of the system is presented in axonometric projection in Fig. 5. There are seen an electric switchboard an electric generating set which was applied to satisfy electric energy demand of other consumers.

The system was provided with one oil tank and central "outboard water - fresh water" cooler (12) that made it possible to reduce space of the ship power plant as well as a number of its auxiliary devices.

5. Comparative analysis of the systems

Final choice of the most favourable system is not an easy task as it must take into account a broad range of various factors including first of all: manoeuvrability, reliability, initial and operational costs, as well as area and space occupied by the system, its mass, location of its centre of gravity etc.

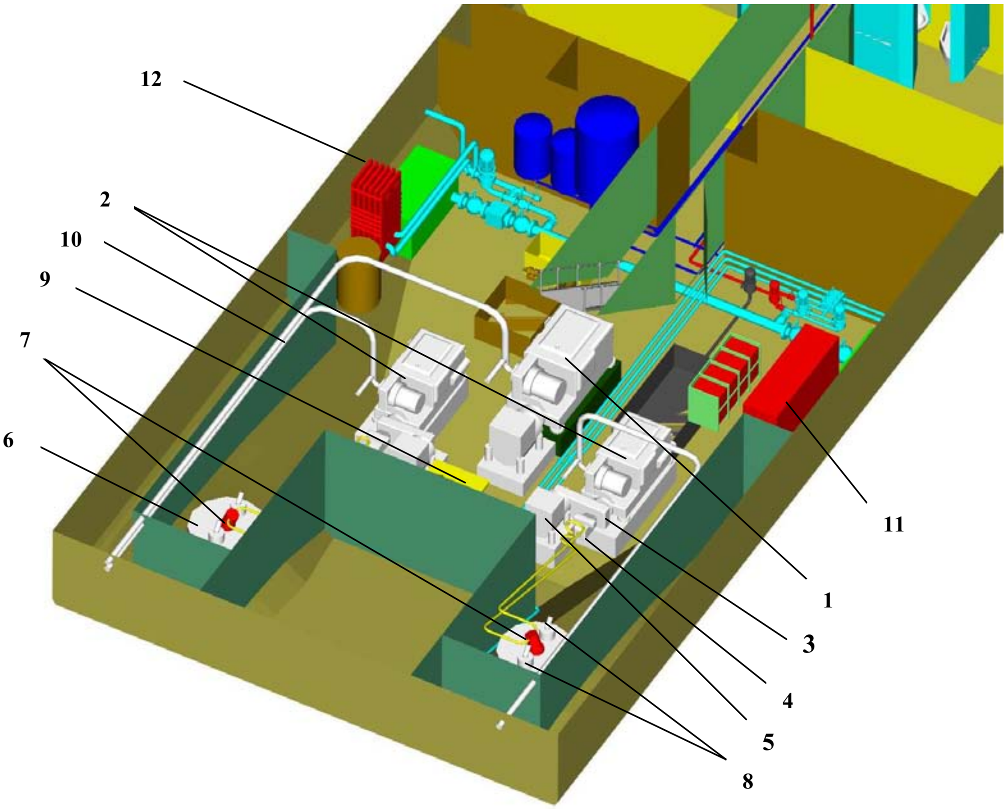

Fig. 5. View of an example arrangement of the main components of the combustion-hydraulic propulsion system. Notation: l – electric generating set, 2 - combustion engine, 3 - mechanical gear, 4 – the main pump unit to drive the propeller, 5 - electric generator, 6 - rotatable thruster, 7 - hydraulic motor driving the propeller, 8 - hydraulic motors to rotate the rotatable thruster around vertical axis, 9 – hydraulic oil supplying unit, 10 - exhaust piping with silencers, 11 – electric switchboard,12 - central " outboard water - fresh water " cooler

In Tab. 1 - 2 and diagrams (Fig.6) are presented some important data concerning the features and costs of the considered propulsion systems, which are supposed to make decision-taking easier.

Tabela 1. Parameters and prices (costs) of the units of the combustion-electric propulsion system

Name o unit	Gabarities	Number	Mass: of one unit /total [kg]	Volume [m3] / area [m^2]	Gross price: of one unit / total [EURO]
Electric generating set of 240 kW output **IVECO GE 8210SRM45**	2737x1150x1371	2	2820 / 5640	8.63 / 6.30	57050 / 114100
Electric generating set of 112 kW output **IVECO GE 8361SRM32**	2309x720x1280	1	1950 / 1950	2.13 / 1.66	37100 / 37100
Electric motors of 200 kW power **EMIT SVgm 315 mL4**	1210x600x800	2	1120 / 2240	1.16 / 0.96 not acounted for in calculations*	6500 / 13000

Frequency converter **Danfoss VLT**	370x420x1600	2	200 / 400	0,50 / 0.31	18000 / 36000
Hydraulic oil tank unit	500x500x700	1	300 / 300	0,15 / 0,25	
Azimuth thruster		2	910 / 1820		54000 / 108000
Total			/12350	11.41 / 8,52	/~308200

Tabela 2. Parametry i ceny zespołów systemu Diesel-hydraulicznego z przekładnią hydrostatyczną

Name o unit	Gabarities	Number	Masa: jednostkowa / łączna [kg]	Objętość [m^3] / powierzchnia [m^2]	Cena: jednostkowa / łączna [EURO]
Combustion engine of 220 kW **IVECO CURSOR 300**	1770x935x1030	2	900 / 1800	3,41 / 3.31	24500 / 49000
Electric generating set of 160 kW output **IVECO GE8210SRM36**	2975x1110x1940	1	2520 /2520	6.41 / 3.30	47160 / 47160
Hydraulic pump of 252 kW max. output **Rexroth A4VSG 180**	350x300x220	2	114 / 228	0,05 / 0.21	12000 / 24000
Hydraulic motor of 220 kW max. output **Rexroth A2FM 250**	224x280x250	2	73 / 146	0,03 / 0.13 not □enter□rs for in calculations*	5368 / 10736
Electric generator of 40kW output **Leroy – Somer 2.2VL8**	615x450x450	2	165 / 330	0,25 / 0.55	3000 / 6000
Hydraulic oil tank unit	1000x1000x1300	1	1050 / 1050	1.23/ 1	
Azimuth thruster	-	2	900 / 1800	-	54000 / 108000
Total			/ 7874	11.31 / 8.37	/~244900

- This unit does not occupy any useful space of the power plant

As far as the broadly understood ship's manoeuvrability is concerned the propulsion system with hydrostatic transmission shows more advantages out of which the following are most important:

- better protection of the propulsion system against overloading that results in much higher reliability and durability of its units especially the bevel gear;
- more accurately and faster realized □enter□rs that mainly results from many times smaller inertia moments of the hydraulic motors as compared with those of electric ones.

Successive advantages of the combustion-hydraulic system are its smaller weight and gabarites. They first of all result from many times smaller mass of the hydraulic motors and space occupied by them against those of the electric motors of the same power. As results from the data included in the tables the masses differ to each other almost fifteen times. Another source of the merits is the application of the much lighter high-speed combustion engines for driving the hydraulic pumps, having rotational speed much higher than that of the electric generating sets used in the combustion-electric propulsion system. It makes advantageous location of a □enter of gravity shifted in direction of the ship center. The features are especially favourable in the case of small vessels especially those intended for sailing in shallow waters. Another important advantage of the system fitted with hydrostatic transmission is its smaller initial cost amounting to less than 77% of that of the remaining systems in question.

The main drawback of the considered system is its higher operational costs. They mainly result from a lower efficiency of the system. From the so far performed analyses it results that the efficiency of the combustion-electric system is by about 5% higher than that of the combustion-hydraulic system, at rated values of their operational parameters. For this reason in the combustion-hydraulic system a somewhat higher total power output of combustion engines has been provided for. The need of periodical change of oil and filtering cartridges additionally rises operational costs.

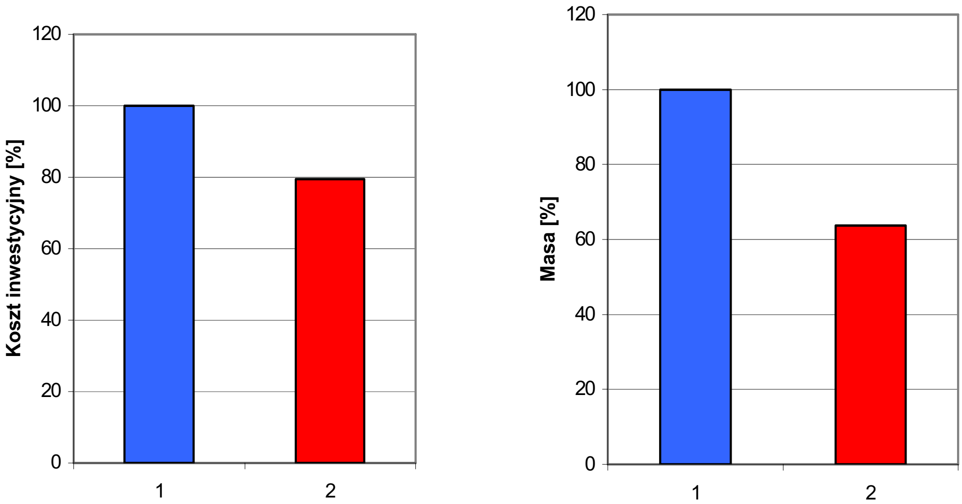

Fig. 6. Comparison of initial costs and mass of the both presented propulsion systems: 1 – Combustion-electric one, 2 – Combustion-hydraulic one

6. Final remarks

The both presented design variants of the ship propulsion systems satisfy the assumptions enumerated in introduction and each of them could be applied to the designed ship. To choose the most favourable one out them is not an easy task. However the author are convinced that the above presented analysis of basic features and costs of each of the systems certainly may help the principal designer of the ship in making a proper choice.

Bibliography

[1] Dymarski Cz., Skorek G., *Energy balance of conceptual design of propulsion system with hydrostatic transmission for inland and coastal vessel (in Polish)*. Faculty of Ocean Eng. and Ship Techn., Gdansk University of Technology. Research Report No 154/E/2004.

[2] Dymarski Cz., Rolbiecki R.: *Conceptual design of propulsion and control system with hydrostatic transmission for inland vessel (in Polish)*. Faculty of Ocean Eng. and Ship Techn., Gdansk University of Technology. Research Report No 164/E/2004.

[3] Dymarski Cz., *An azimuthing combustion-hydraulic propulsion system for inland vessel,* Marine Technology Transaction (Technika Morska), Vol. 16, 2005.

[4] Information pamphlets and offer materials of the following companies: KaMeWa, Lips, Schottel, Ulstein, Wartsila, Iveco Motors, Bosch Rexroth, Emit, Lcroy - Some.

TECHNICAL AND ECONOMICAL ANALYSIS OF COMBINED CYCLES OF GAS TURBINE – STEAM TURBINE ON PIPELINE COMPRESSOR STATIONS

Part I – Technical analysis

Marek Górecki

Inżynieria, Doradztwo, Ekologia IDEK sp. Z o.o.

Marek Dzida

Gdańsk Univeristy of Technology

Abstract

In this part there have been shown issues of combined cycle which are on Gas Compressor Stations, reclaiming steam blocks. In analysis of this issue there have been taken few variants of steam cycle configuration and few variants of part load of gas turbine. To steam cycles there have been taken all basis parameters, and then there have been made thermodynamic calculations, which result was value of possibility to make electric energy through steam turbine. In summarizing there have been made an opinion about profitability investment and compared economic results for separate variants.

Key words: *Pipeline Compressor Stations, Combined Cycle, Thermodynamic and Economic calculations*

1. Introduction

Transport of natural gas on big scale is mainly taken with help of gas pipeline systems. Length of those gas pipelines are measure in hundreds and even in thousands kilometers. In order to forward gas on those distances will be possible, there have to deal with problem of hydraulic resistance of gas pipeline. To deal with this on the way of gas pipeline there are built Gas Compressor Stations. The exhaust gases from gas turbine have considerable amounts of heat, which can be used to production of electric energy or heat. Energy which are in gases is a spin-off and its produce does not need to incur additional costs. Installation of recover block will allow on changing heat of gases into electric energy or heat which can be sold. It only made a question of financial investments which are connected with rebuild recover block and its exploitation if there are not exceeded of income from sale of energy production. This study is analysis of this investment and attempt of finding the answer on this above question. In first part there have been shown technical analysis of rebuild recover block on gas turbine which are working on Gas Compressor Stations. In second part there have been shown economic calculation.

2. Installation of recover steam block on Gas Compressor Stations

Installation of recover steam block is aim at using energy from exhaust gases of gas turbine. Because a lot of Gas Compressor Stations are in considerably distance from bigger cities or production factories it is no way to deliver heat energy which will be probably made. So it have been accepted that steam block will make electric energy.

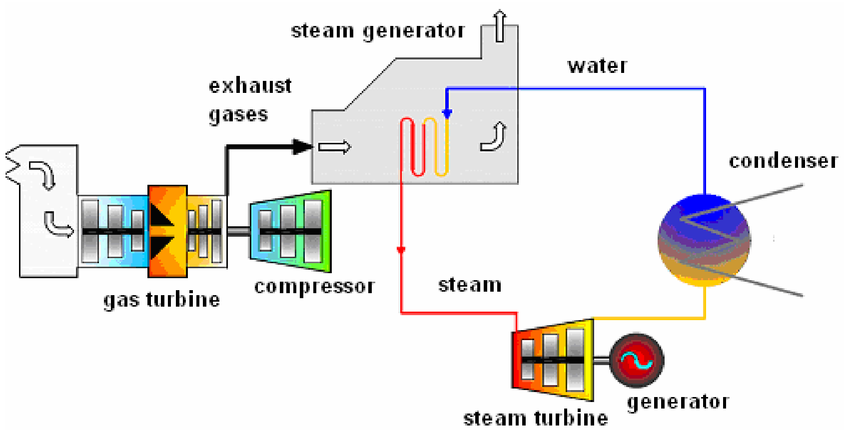

Fig..1. Visual diagram of combined cycle of gas turbine- steam turbine on Pipeline Compressor Stations

The analysis have been made on example of gas turbine ABB GT10B (Siemens SGT600), which is wide used on Gas Compressor Stations. It is double shaft construction with catalogue parameters, power output 25 MW and efficiency 34 %.

There have been analysed three types of steam system's configuration (variant A, B, C, Fig. 2÷4). All of three configurations have been projected and counted in two cases of gas turbine's overloads. The first case is in situation when gas turbine works all the time with full power. The second case consider turbine's work with part overload (from 55 % to 100 %).

2.1 Configuration of steam cycle

A) Single-Pressure System

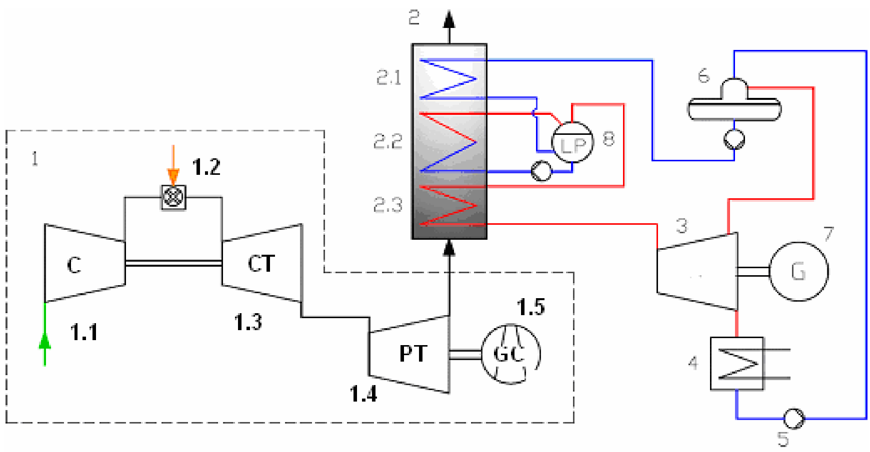

Fig. 2. Variant A of combined cycle plant
1 – Turbocompressor plant (1.1 – Compressor, 1.2 – Combustion Chamber, 1.3 –Compressor Turbine, 1.4 – Power Turbine, 1.5 – Gas Compressor), 2 – Heat Recovery Boiler, 2.1 –Economizer, 2.2 – Evaporator, 2.3 –Superheater, 3 – Steam Turbine, 4 – Condenser, 5 –Condensate Pump , 6 – Dearator, 7 – Generator, 8 – Boiler Drum

B) Single-Pressure System with a Low Pressure Evaporator as a Preheating Loop

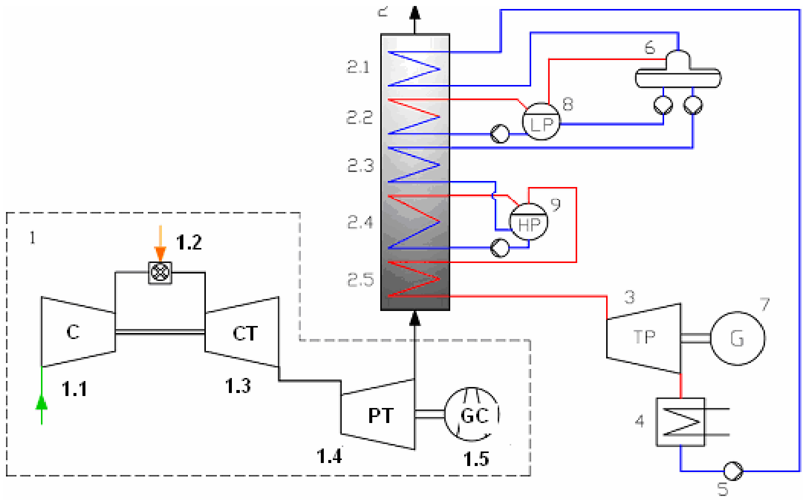

Fig. 3. Variant B of combined cycle plant : 1 – Turbocompressor plant (1.1 – Compressor, 1.2 – Combustion Chamber, 1.3 –Compressor Turbine, 1.4 – Power Turbine, 1.5 – Gas Compressor), 2 – Heat Recovery Boiler, 2.1 – Low Pressure Economizer, 2.2 –Preheating Loop (low pressure evaporator), 2.3 – High Pressure Economizer, 2.4 – High Pressure Evaporator, 2.5 –Superheater, 3 – Steam Turbine, 4 – Condenser, 5 –Condensate Pump , 6 – Dearator, 7 – Generator, 8 – Low Pressure Boiler Drum, 9- High Pressure Boiler Drum

C) Two-Pressure System

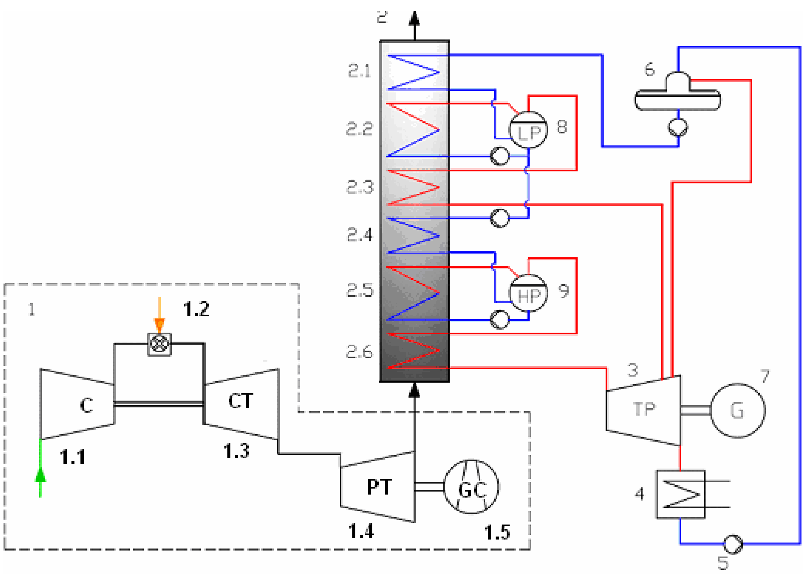

Fig. 4. Variant C of combined cycle plant: 1 – Turbocompressor plant (1.1 – Compressor, 1.2 – Combustion Chamber, 1.3 –Compressor Turbine, 1.4 – Power Turbine, 1.5 – Gas Compressor), 2 – Heat Recovery Boiler, 2.1 – Low Pressure Economizer, 2.2 – Low Pressure Evaporator, 2.5 –Low Pressure Superheater 2.4 – High Pressure Economizer, 2.5 – High Pressure Evaporator, 2.6 –High Pressure Superheater, 3 – Steam Turbine, 4 – Condenser, 5 –Condensate Pump , 6 – Dearator, 7 – Generator, 8 – Low Pressure Boiler Drum, 9- High Pressure Boiler Drum

2.2 Project assumptions and selection of system parameters

In case of analysis there have been made assumptions (joint for all three configurations) [1,2,4]:

- Range of gas turbine's power 55-100 %,
- Air intake temperature: 15˚*C*,
- Exhaust ducting pressure losses (including heat recover boiler) $\Delta p = 2\ kPa$,
- Difference between the fumes temperature after turbine and maximum live steam temperature: $\Delta T_1 = 25\ °C$ - single-pressure system ,
  $\Delta T_1 = 25\ °C$ - two-pressure system, section HP,
  $\Delta T_3 = 15\ °C$ - two-pressure system, section LP.
- pinch point temperature: $\Delta T_2 = 15\ °C$ - single-pressure system,
  $\Delta T_2 = 15\ °C$ - two-pressure system section HP,
  $\Delta T_4 = 15\ °C$ - two-pressure system, section LP.
- efficiency of economizer: $\eta_{ECO} = 0{,}9$ - single-pressure system,
  $\eta_{ECO\ LP} = 0{,}9$ - two-pressure system, section HP,
  $\eta_{ECO\ HP} = 0{,}95$ - two-pressure system, section LP.
- efficiency of steam turbine $\eta_{TP} = 0{,}9$ (steam turbine driving the generator directly),
- pressure in condenser $p = 0{,}005\ MPa$.

3. Calculations

Calculations are made in case of determination of optimal live steam pressure and term other parameters of system, all the power of steam turbine and efficiency of combined cycle. For organize all calculations are divided in the following variants:

- **Variant A1** – system A, load TG – 100 %,
- **Variant B1** – system B, load TG – 100 %,
- **Variant C1** – system C, load TG – 100 %,
- **Variant A2** – system A, load TG – changing,
- **Variant B2** – system B, load TG – changing,
- **Variant C2** – system C, load TG – changing.

3.1. Parameters of gas turbine

In Table 1 has been shown the parameters of gas turbine for part load.

*Table 1. Parameters of gas turbine for part load**

Load [%]	Power [*kW*]	Electric efficiency [%]	Exhaust Gas Temperature [˚*C*]	Exhaust Gas Flow [*kg/s*]
100	23557	32,69	550	80,66
90	21196	32,19	530	77,48
80	18833	31,46	511	74,14
70	16471	30,53	491	70,76
60	14108	29,31	473	67,07
50	11745	27,77	454	63,10

* Giving parameters are only when gas turbine powers electric generator; consider inlet and exhaust ducting pressure losses(also including heat recover boiler); are for all variants; air intake temperature 15˚*C*, atmospheric pressure 1,0132 *bar*.

3.2 Power of steam turbine and efficiency of combined cycle

Because of non-typical associational system, gas turbine is powered by gas compressor, and steam turbine is powered electric generator, efficiency of all system are been expressed such as electric efficiently. There have been accepted that gas turbine and steam turbine are powered electric generator.

Power of steam turbine:

$$N_{TP} = m \cdot \Delta i \cdot \eta_{mech} \cdot \eta_{gen}$$

were:

m - steam mass flow
Δi - steam turbine specific power
$\eta_{mech.}$ - mechanical efficiency (0,99)
$\eta_{gen.}$ - generator efficiency (0,985)

Efficiency of combined cycle:

$$\eta = \eta_{TG} \cdot \left(1 + \frac{N_{TP}}{N_{TG}}\right)$$

were:

η_{TG} - efficiently of gas turbine
N_{TP} - power of steam turbine
N_{TG} - power of gas turbine

3.3 Calculation results

In above tables there have been shown calculations results of optimal parameters of combined cycle for different variants. In Table 2 there have been shown calculation results for combined cycle with load 100 % of gas turbine, and with limit of steam quality on exit from steam turbine, x>0,9.

Table 2. Optimal parameters of combined cycle *with load 100 % of gas turbine*

Variant	Optimal live steam pressure [bar]		Power of steam turbine [kW]	Efficiency [-]	Exhaust gases temperature after boiler [$^\circ C$]
	LP	HP			
A1	-	40	12485	50,02	157
B1	-	40	12570	50,13	143
C1	4	30	14703	53,09	96

In Table 3 there have been shown optimal parameters of combined cycle in relation to load of gas turbine in range 55-100 % of power, with limit of steam dryness' degree after steam turbine, x>0,9. results of combined cycle have been made for different variants A, B and C in relation to load of gas turbine, but fresh steam pressure have been accepted as steady pressure in load of 55 % of gas turbine independent of analyse load.

Table 3. Optimal parameters of combined cycle *for 100 % load of gas turbine with steady live steam pressure independent of gas turbine load*

Variant	Optimal live steam pressure [*bar*]		Power of steam turbine [*kW*]	Efficiency [-]	Exhaust gases temperature after boiler [°*C*]
	LP	HP			
A2	-	22	12281	49,73	141
B2	-	22	12370	49,86	126
C2	4	16	13645	51,63	99

Fig. 5 and 6 have been shown efficiency and power output in function of gas turbine load (there have been accepted live steam pressure steady 55 % load of gas turbine independent of gas turbine load).

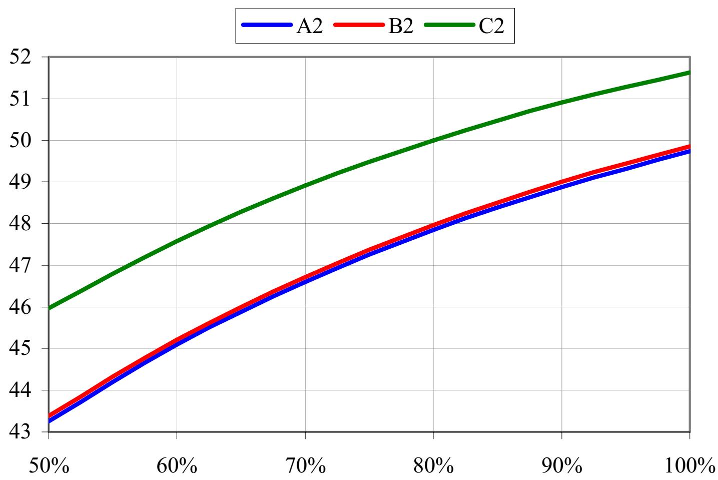

Fig. 5. Efficiency of combined cycle as a function of gas turbine load

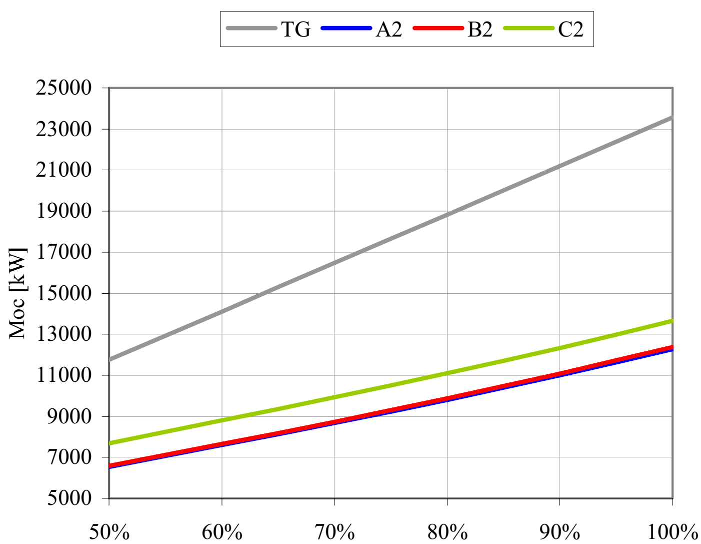

Fig. 6. Power output of gas turbine and steam turbine as a function of gas turbine load

4. Conclusion

From technical analysis of calculated variants there are following results. For variant with steady load of gas turbine, optimal live steam pressure is also maximum pressure. Futher increasing pressure is impossible because of reducing of steam quality (x) after steam turbine which should not be lower than 0,9 [1,4]. For system which are used to work with gas turbine working with changing loads, maximum live steam pressure conditions temperature of exhaust gases from gas turbine which is in minimum load. For variant A and B with load of 100 % power of gas turbine reducing steam pressure does not have a bigger influence on efficiency of combined cycle in comparison with calculated system without limits, while for two-pressure system it has considerably influence, see Tab. 2 and 3.

Exhaust gases temperature after boiler for variants A and B show that specific enthalpy of gases was not used exactly. Using variant C allows to reduce a gas temperature below $100^{\circ}C$, which of course gives obviously increase of efficiency in comparison with single-pressure systems.

Comparison calculation results for variant A and C shows that using additional section of boiler allows a little increase in using specific enthalpy of gases. The differences are not so big. It can be said that, in this range of power, there are omitted and also it should be remembered that recover boiler is equipped in two additional section which considerably increase investment cost.

Choosing optimal associational system needs economic analysis of optimal solutions which are achieved from thermodynamic calculations.

Additional issue without economic analysis which have influence on analysis combined cycle is check if slope of gas turbine's power is acceptable about 230 kW, which is created by additional installation of recover boiler.

References

[1] Boyce, M.P., *Handbook for cogeneration and combined cycle power plants*, ASME Press, USA 2006

[2] Kehlhofer, R., *Combined-Cycle Gas & Steam Turbine Power Plants*, The Fairmount Press INC., USA 1991

[3] Skorek, J., Kalina, J., *Gazowe układy kogeneracyjne*, Wydawnictwo Naukowo-Techniczne, Warszawa 2005

[4] Perycz, S., *Turbiny parowe i gazowe*, Wydawnictwo Politechniki Gdańskiej, Gdańsk 1988

TECHNICAL AND ECONOMICAL ANALYSIS OF COMBINED CYCLES OF GAS TURBINE – STEAM TURBINE ON PIPELINE COMPRESSOR STATIONS

Part II – Economic analysis

Marek Górecki

Inżynieria, Doradztwo, Ekologia IDEK sp. Z o.o.

Marek Dzida

Gdańsk Univeristy of Technology

Abstract

In this part there have been shown issues of combined cycle which are on Gas Compressor Stations, reclaiming steam blocks. In analysis of this issue there have been taken few variants of steam cycle configuration and few variants of part load of gas turbine. To steam cycles there have been taken all basis parameters, and then there have been made thermodynamic calculations, which result was value of possibility to make electric energy through steam turbine. In summarizing there have been made an opinion about profitability investment and compared economic results for separate variants.

Key words: *Pipeline Compressor Stations, Combined Cycle, Thermodynamic and Economic calculations*

1. Introduction

The goal of every business activity is to make financial profits. Profitability is the main criterion of investment assessment. Investor must be sure that the enterprise is for him profitable and make profit on appropriately size. In that case there must to be made essential economic and technical analysis, market resources and studies of viability on different stages, from beginning assessment of investment possibility to ending version of project.

Economic analysis which is shown here has a goal to show investment profitability of adding steam block to gas turbine on Gas Compressor Stations. This analysis is also to shown to compare (from economic point of view) technical analysis which was shown in Part I in this investment.

2. Method

Economic analysis was made with using NPV method [1, 2, 3]. It is dynamic method which is based on analysis of discounting cash flow in giving discount rate. Because this is approximate analysis there were not additional analysis of statistic methods, sensitivity resources etc. For assessment of investment profitability there were determined main economic rates.

a) NPV - net present value which can interpret as increase of investor wealth which result from realisation of investment with consider changing of money value in time.

$$NPV = \sum_{t=1}^{n} \frac{CF_t}{(1+R)^t}$$

were:

CF_t - cash flow in time *t*,
t - next years of exploitation (investment),
R - discount rate

b) IRR – internal rate of return; it is discount rate, which should be used in balance investment cost with future incomes connected with those costs. To calculate IRR value means to find discount rate which meet the following condition:

$$NPV = \sum_{t=1}^{n} \frac{CF_t}{(1+R)^t} = 0 \quad \Rightarrow R = IRR$$

Giving in this method value of discount rate it is the value of IRR index.

c) R – net present value ratio, which measure relation between essential capital outlay of project and getting current value of project. This index is to compare different variants of testing investment.

$$NPVR = \frac{NPV}{I_0}$$

were:

I_0 - all beginning outlays

3. Generally assumption

Economic analysis was made with the following assumptions:

a) investment will be realised in 2 years, but investment outlays in the first year will be 30 % of all outlays,
b) investment will be financed from own capital,
c) discount rate: R=12 %,
d) amortization of tangible assets: 7 %,
e) time of investment amortization is accepted on 15 years,
f) time of steam turbine work: 7000 hours per year,
g) own needs of electric energy of steam arrangement are accepted on 1,5 % of produced energy,
h) predictable selling price of electric energy: 40 USD/MWh,
i) income tax: 19 %.

4. Financial outlays

All costs which are shown here are assessed [1]. Individual contracts between order person and supplier will decide the real costs.

*Table1. Combined cycle in configuration **A** (see Part I)*

Investment outlays		
Administration costs (supervision in there)	[USD]	150 000
Project and author's supervision	[USD]	600 000
Arrangement of building place	[USD]	100 000

Building-installation works	[USD]	2 000 000
Supply of machines and devices	[USD]	9 400 000
Installation on Power Plant place	[USD]	600 000
Outside installations	[USD]	1 000 000
Reserve	[USD]	500 000
All together	[USD]	14 350 000
Exploitation costs		
Remunerations and remuneration services	[USD/year]	80 000
Materials, fuels and energy	[USD/year]	65 000
Renovation and maintenances	[USD/year]	287 000
All-plant costs	[USD/ year]	40 000
Taxies and charges	[USD/ year]	20 000
Others	[USD/ year]	9 000
All together	[USD/ year]	501 000

*Table 2. Combined cycle in configuration **B** (see Part I)*

Investment outlays		
Administration costs (supervision in there)	[USD]	150 000
Project and author's supervision	[USD]	600 000
Arrangement of building place	[USD]	100 000
Building-installation works	[USD]	2 000 000
Supply of machines and devices	[USD]	9 588 000
Installation on Power Plant place	[USD]	600 000
Outside installations	[USD]	1 000 000
Reserve	[USD]	500 000
All together	[USD]	14 538 000
Exploitation costs		
Remunerations and remuneration services	[USD/year]	80 000
Materials, fuels and energy	[USD/year]	65 000
Renovation and maintenances	[USD/year]	291 000
All-plant costs	[USD/ year]	40 000
Taxies and charges	[USD/ year]	20 000
Others	[USD/ year]	9 000
All together	[USD/ year]	505 000

*Table 3. Combined cycle in configuration **C** (see Part I)*

Investment outlays		
Administration costs (supervision in there)	[USD]	150 000
Project and author's supervision	[USD]	600 000
Arrangement of building place	[USD]	100 000
Building-installation works	[USD]	2 100 000
Supply of machines and devices	[USD]	11 280 000
Installation on Power Plant place	[USD]	615 000
Outside installations	[USD]	1 025 000
Reserve	[USD]	500 000
All together	[USD]	16 370 000
Exploitation costs		
Remunerations and remuneration services	[USD/year]	80 000

Materials, fuels and energy	[USD/year]	65 000
Renovation and maintenances	[USD/year]	328 000
All-plant costs	[USD/ year]	40 000
Taxies and charges	[USD/ year]	20 000
Others	[USD/ year]	9 000
All together	[USD/ year]	542 000

5. Counting of rates of economic effective

The detailed calculations are shown for variant A1. For others variants are shown only results. In case of changing loads of gas turbine made calculations for middle loads of 90 % and 80 % gas turbine's power.

5.1. Variant A1

Table 4. Energy production

Power of steam turbine	[MW]	12,485
Production of electric energy	[MWh/year]	87395
Selling	[MWh]	86084

Table 5. Calculations of cash flow (USD)

Proposition	Building		Exploitation			
	year 1	year 2	year 1	year 2	...	year 15
Selling income	0	0	3 443 363	3 443 363		3 443 363
Amortisation of tangible assests	0	0	1 004 500	1 004 500		287 000
Operational costs	0	0	1 505 500	1 505 500		788 000
Profit and loss account						
Pre-tax profit	0	0	1 937 863	1 937 863		2 655 363
Income tax	0	0	368 194	368 194		504 519
Profit after tax	0	0	1 569 669	1 569 669		2 150 844
Demand for working capital	0	0	414 997	414 997		414 997
Cash flow						
Ending netto value	0	0	0	0		414 997
Year's balance	-4 305 000	-10 045 000	2 159 172	2 574 169		2 852 841
Growing balance*	-4 305 000	-14 350 000	-12 190 828	-9 616 659		24 126 210

* Positive value of growing balance appears in 6 year of exploitation, will be calculated: 680 017 USD and will be increased gradually till ending value.

Table 6. Economy efficiency rate

NPV	[USD]	1 870 293
IRR	[%]	14,65
NPVR	[-]	0,130

IRR value bigger than discount rate and positive value of NPV mean that the investment is profitable. Achievement value of rates can say that profitability of investment is on quite good level, in giving assumptions [1, 2, 3].

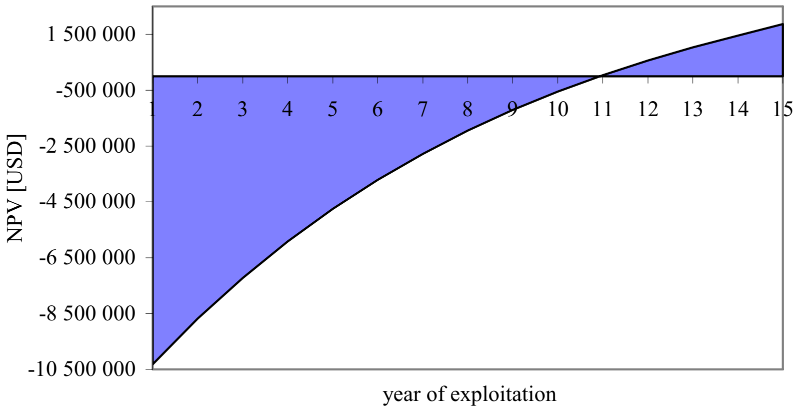

Fig. 1. Value of NPV rate for variant A1 as a function route of exploitation time

5.2. Result balance for all variants

Table 7. Balance of economic efficiency rate

variant	Middle loan TG	Power TP	NPV	IRR	NPVR
	[%]	[MW]	[USD]	[%]	[-]
A1	100	12,484	1870293	15	0,130
A2 90	90	10,987	72775	12	0,005
A2 80	80	9,808	-1341961	10	-0,094
B1	100	12,570	1812254	15	0,125
B2 90	90	11,068	9936	12	0,001
B2 90	80	9,883	-1411999	10	-0,097
C1	100	14,703	2821199	15	0,172
C2 90	90	12,321	-37071	12	-0,002
C2 80	80	11,098	-1504604	10	-0,092

How we can see not all variants are profitable. Negatively value of NPV means no meet of basic criterion of profitable of investment, Fig. 1.. The same is to IRR rate which value under 12 % (amount of discount rate) disqualify giving variant in economic assessment.

6. Conclusion

This shown analysis show that giving investment is profitable but it needs to implement some requirements. Above all gas turbine must constant work with full power or in the little range with changing power, which are decided about power produced by steam turbine. With economic seeing needed amount of energy should be produced from steam block, the middle load of gas turbine could not be lower than 90 %. Doing more precise analysis and specify datas which have been implied in this work, there can be calculated with big precision value of upper shown middle still of gas turbine loads. It should also be said that in giving case there will be always same value of description still and profitability of investment will be depended on it in the main measure.

For saying “profitably still” there will be also influence of type taking gas turbine in Gas Compressor Stations.

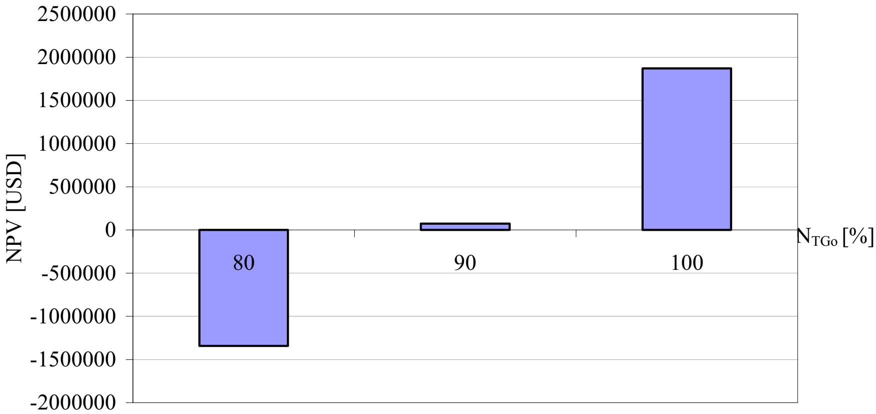

Fig. 2. Value of NPV rate for variant A2 in function of middle load of gas turbine

Very important thing is also energy selling. Significant thing has here the individual contracts between order person and supplier which have prices and amount of taking energy. In economic analysis there is taken the work time of steam block in size of 7000 hours/year.

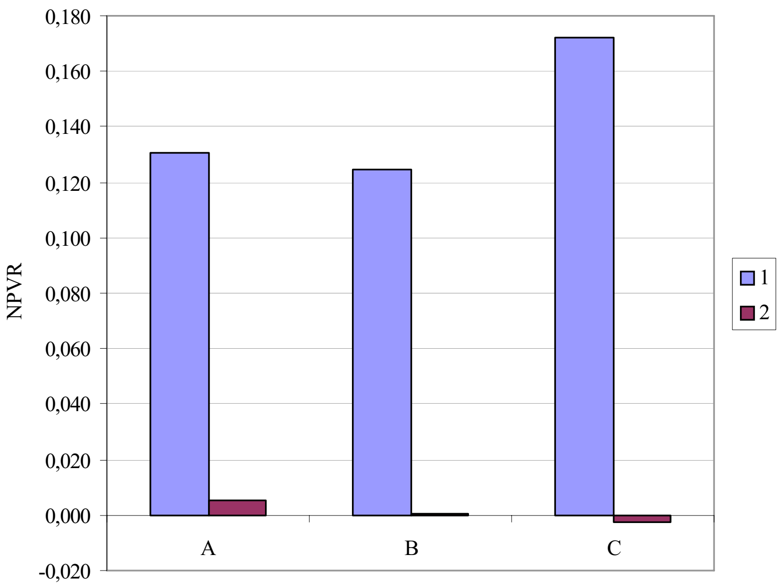

Fig. 3. Comparison of NPVR rate for variants A, B, C project with using of gas turbine working with full power (1) and with gas turbine working with changing loads – results for middle load 90% (2)

The most profitable variant from economic point of view is of course arrangement project to work with gas turbine which work with under full power, Fig. 2 and 3. In that case the most optimistic is project realization with using two-pressure system (variant C). It is very responded on changing load of Gas Compressor Stations. In fragmentary loads its efficiency is decreased and that is why this solution is not economic. In that case the most profitable solution is to use configuration of steam block and single-pressure system (variant A).

Using steam block in variant B gave a little increase of efficiency to variant A, but it is a little less profitable solution with economic point of view on account of buying cost of this arrangement. Those differences are not so big and can be results of not precise estimation of investment issues. It can be said that profits which are from efficiency increase are the same with expected additional costs. Variant A and B can be said that they are compared with themselves from the point of ending economic profit or less. But variant B is the most modern solution.

On Pipeline Compressor Stations usually there are more than one turbo-compressor block which allow on configuration 2+2+1 (two gas turbines, two heat recover boilers, one steam turbine) or 3+3+1. Power output of that variants will be the same like properly double taken 1+1+1 and thrice taken 1+1+1 and investment issues are little less because of steam turbine, generator, converter etc. which are a little less expensive than two or tree turbines with lower power.

References

[1] Skorek, J., Kalina, J., *Gazowe układy kogeneracyjne*, Wydawnictwo Naukowo-Techniczne, Warszawa 2005

[2] Ostaszewski, J., *Zarządzanie finansami w spółce akcyjnej*, Centrum Doradztwa i Informacji Difin sp. z o.o., Warszawa 2003

[3] Strona internetowa: „pl.wikipedia.org"

IMPROVEMENT IN PRELIMINARY DETERMINATION OF ENERGY DEMAND FOR MAIN PROPULSION, ELECTRIC POWER AND AUXILIARY BOILER CAPACITY BY MEANS OF STATISTICS AS AN EXAMPLE OF MODERN RO-RO VESSELS

Zygmunt Górski, Mariusz Giernalczyk

Gdynia Maritime University
83 Morska Street, 81-225 Gdynia, Poland
tel.: +48 58 6901307, +48 58 6901324
e-mail: magier@am.gdynia.pl, zyga@am.gdynia.pl

Abstract

The paper presents the method of estimated main propulsion power, electrical power and auxiliary steam delivery of the modern ro-ro vessels by using statistical method of calculations. The statistical researches were executed to determine dependencies among the main propulsion power, electric power and heating power as a function of selected basic ship parameters. The reference list of the modern ro-ro vessels was used in the analysis. The chosen ships were selected mainly from the studies of The Royal Institution of Naval Architects elaborated by the most eminent authors of the world shipping enterprise running their articles in a years issue SIGNIFICANT SHIPS OF YEAR. The chosen as the independent variables are the ship parameters being in a logical connection with the main propulsion power, electrical power and steam production of the vessel. Regression analyses were executed by means of the least squares method. Each determined formula was subjected to the statistical verification and the correlation coefficient between the obtained formula and analysed input data was determined.

Keywords: *ro-ro vessel, main propulsion power, electrical power, auxiliary steam delivery, statistics*

1. Introduction

On Ro-Ro ships cargo is rolled on and rolled off by lorries or trailers. The great advantage of this system is that no cargo handling equipment is required. The loaded vehicles are driven aboard by means of ramps through special stern and bow doors and properly secured for the passage. Upon arrival in the port of discharge, the vehicles are released and driven ashore to their destinations. Part of a Ro-Ro vessel's cargo may be loaded/discharged by gantry cranes, for example containers to/from the weather deck.

Various types of Ro-Ro vessels include ferries, cruiseferries, cargo ships, and barges. A true Ro-Ro's ramps can serve all of the vessel's decks; otherwise it is a hybrid type. New automobiles that are transported by ship around the world are often moved on a large type of Ro-Ro called a Pure Car Carrier (PCC) or Pure Car Truck Carrier (PCTC).

The acronym RoPax describes a Ro-Ro vessel equipped with cabins to accomodate passengers (fig. 1).

Sto-Ro (stowable Ro-Ro) is a modification of the ro-ro transport method where cargo is stowed directly into the ship's hold and the rolltrailer used for stowage does not accompany the cargo to the port of discharge. The sto-ro method is especially suitable for shipment of cargo such as paper reels.

Provisional analysis shows that:

- usually, the main propulsion of these vessels is multiengine type (mainly 4 engines), which drive two propellers trough gearbox,

- power plants are usually created by main engine-driven alternators and by three diesel-driven alternators,
- auxiliary steam is generated by main engines exhaust gas boilers (the amount of exhaust gas boilers is equal to the amount of engines) and by at least one oil fired auxiliary boiler.

Fig. 1. RoPax vessel at sea

The paper presents the method of estimated main propulsion power, electrical power and auxiliary steam delivery of the modern Ro-Ro vessels by using statistical method of calculations.

2. Method for the determination of energy demand for main propulsion, electric power production and boiler capacities for Ro-Ro ship.

Presently a number of methods are in use, which allow the approximate determination of demand for mechanical energy, electric power and auxiliary boiler capacity for seagoing vessels. For example the provisional determination of the ship main propulsion energy can be obtained by means of Papmiel, Guldhammer-Harvald, Hansen, Holtrop or Series 60 methods. These methods are based on arduous calculations and need the determination of the big number of coefficients and their further corrections without satisfactory accuracy in the final results. That is why there is an expectation for the method or ready given formulas, which can allow the estimation of energy demand for seagoing vessel during the preliminary designs in a quick and simple manner and with acceptable accuracy.

The target of research work was to obtain ready formulas by means of mathematical statistics. For this purpose "the list of similar vessels" (reference list) was prepared, in which the basic data of 61 modern Ro-Ro vessels built in last years or actually under construction are listed. Among the parameters the ones that are logically and functionally connected with energy demand for main propulsion, electric power and steam production are listed. The vessels placed in the reference list come from *The Royal Institution of Naval Architects*, where the most significant world representatives of the marine industry are published. Their works and designs are annually issued in the *SIGNIFICANT SHIPS OF YEAR*.

2.1. Determination of power for ship main propulsion

In the considered number of Ro-Ro vessels the power of main propulsion N_w was assumed as:

$$N_w = N_e - N_{pw}\ [kW] \tag{1}$$

where:

$N_e\ [kW]$ – main engine shaft power,
$N_{pw}\ [kW]$ – shaft generator power consumption.

The analysis of power demand for main propulsion of the vessel N_w was executed by means of Admiralty Formula, in which the main propulsion power depends on ship deadweight D, ship speed v and Admiralty Coefficient c_x regarding the geometric similarity of the hull:

$$N_w = \frac{D^{\frac{2}{3}} \cdot v^3}{c_x} \tag{2}$$

Using the formula (2) for $i=57$ vessels from the reference list the c_x coefficient was calculated and next used for calculation of main propulsion power at nine selected ship speeds *v=30, 28, 26, 24, 22, 20, 18, 16* and *14 knots*. Next the relationship between main propulsion power and deadweight $N_w = f(D)$ was determined for the whole vessel population at each a.m. speed. It was stated that for given speed the main propulsion power N_{wv} has a linear dependency on displacement:

$$N_{wv} = a_o + a_1 D \tag{3}$$

The calculations of coefficients a_{oi} and a_{1i} for each given speed were executed by linear regression based on the least squares method. The following dependencies were obtained:

$$\text{for:} \quad \left.\begin{array}{ll} v = 30\ w & Nw_{30} = 40234 + 1{,}04993\ D \\ v = 28\ w & Nw_{28} = 32712 + 0{,}85363\ D \\ v = 26\ w & Nw_{26} = 26191 + 0{,}68346\ D \\ v = 24\ w & Nw_{24} = 20600 + 0{,}53756\ D \\ v = 22\ w & Nw_{22} = 15857 + 0{,}41406\ D \\ v = 20\ w & Nw_{20} = 11921 + 0{,}31109\ D \\ v = 18\ w & Nw_{18} = 8691 + 0{,}22678\ D \\ v = 16\ w & Nw_{16} = 6104 + 0{,}15928\ D \\ v = 14\ w & Nw_{14} = 4089 + 0{,}10670\ D \end{array}\right\} \begin{array}{l} r^2 = 0{,}2632 \\ r = 0{,}5130 \end{array} \tag{4}$$

with the coefficient of determination $r^2 = 0{,}2632$, which confirms the linear nature of dependency $N_w = f(D)$.

Figure 2 presents the result of calculation for a speed of 22 *knots*.

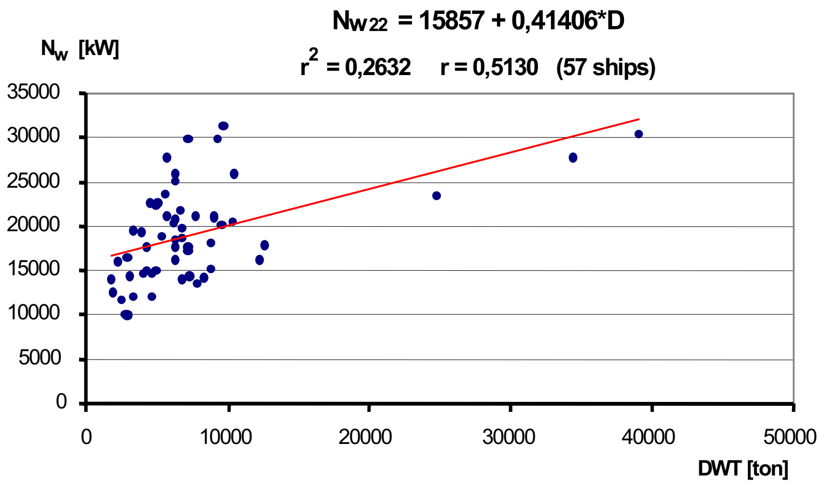

Fig. 2. Linear regression of dependency $N_w = f(D)$ for the speed 22 knots

The coefficients a_{oi} and a_{1i} in formulas (4) are functions of the vessel speed i.e.:

$$a_o = f(v)$$
$$a_1 = f(v) \qquad (5)$$

The determination of coefficients a_o and a_1 depending on ship speed was executed by means of power curve regression [2] of the function described as:

$$y = b\,x^{d} \qquad (6)$$

In this case coefficients of functions (4) are described as:

$$a_o = b_o\,v^{do}$$
$$a_1 = b_1\,v^{d1}$$

After the coefficients of regression b_i and d_i were calculated the functions (5) are:

$$a_0 = f(v) = 1{,}5886 * v^3$$
$$a_1 = f(v) = 0{,}00003488 * v^3$$

After the substitution of the above formulas into formula (3) the final form of main propulsion power equation was obtained. It is as follows:

$$\boldsymbol{Nw = (1{,}49042 + 0{,}00003888 * D) * v^3} \;\; [kW] \qquad (7)$$

where:

D [tons] – vessel deadweight,
v [knots] – vessel speed.

The correlation between the value of main propulsion power taken from the reference list and obtained according to the formula (7) is presented in figure 3. The linear regression of points location at the correlation area results as the straight line with the coefficient of the determination $r^2 = 0{,}8141$. However the Pearson linear regression coefficient of formula (7) with reference to the data from vessels reference list is $r = 0{,}9023$, which confirms the correctness of the above assumptions and calculations.

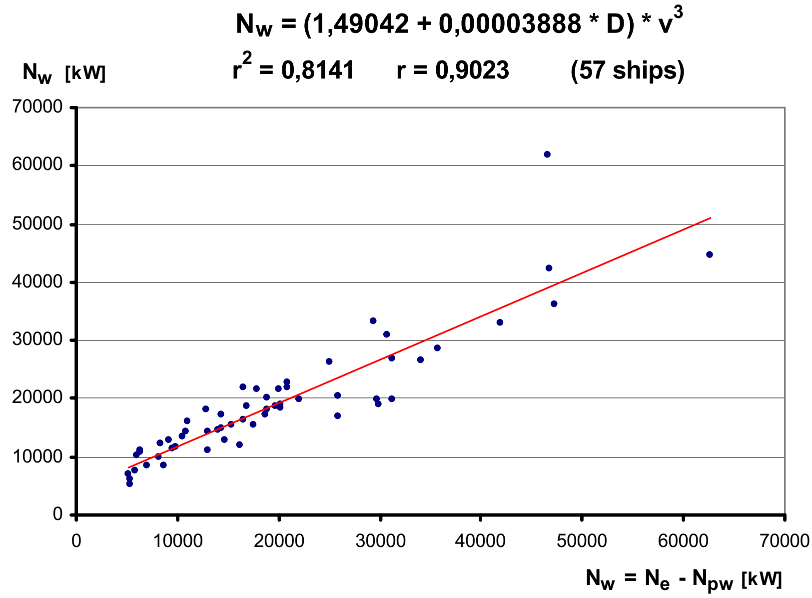

Fig. 3. Correlation area between main propulsion power obtained acc. to formula (7) and taken from reference list

2.2. Determination of total electric power demand

The accurate determination of electric power plant is not possible during the vessel preliminary design works due to lack of the final electric energy balance. Existing formulas [6, 9] regard to the vessels of older design and don't take into consideration new circumstances, which came as a result of ship construction development. It brought the necessity of modernising the existing formulas taking into consideration the new design trends according to the reference list of vessels.

During the determination of the electric power demand for the modern Ro-Ro vessels the principle that the total electric power ΣN_{el} *is* the function of main propulsion power N_w [6]. In that case linear dependence was assumed.

To show this relationship the linear regression was used with regarding to the least squares method. Total number of 56 vessels from the reference list was taken into consideration. As a result the following formula was obtained:

$$\Sigma N_{el} = 2432 + 0{,}14944\, N_w \quad [kW] \tag{8}$$

where: N_w *[kW]* – main propulsion power,

with the coefficient of determination $r^2 = 0{,}6387$. The graphical picture of formula (8) determination shows figure 4. Obtained Pearson linear regression coefficient of correlation between the values from formula (8) and values taken from the vessels reference list is $r = 0{,}7992$, which confirms the usefulness of formula in the preliminary calculations.

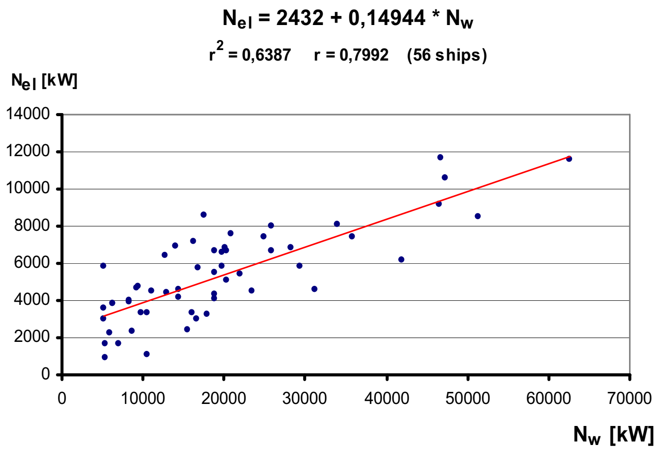

Fig. 4. Linear regression for determination of total electric power as the function of the main propulsion power

2.3. Determination of auxiliary boiler capacity

Similarly to the electric power the accurate determination of auxiliary boiler capacity is not possible during the vessel preliminary design works due to lack of the final heat energy balance.

During the determination of auxiliary boiler capacity for the modern Ro-Ro ships the principle that the auxiliary boiler capacity D_{blr} *is* the function of main propulsion power N_w [6] and that it is a linear dependence was assumed.

In this case the linear regression was also used with regarding to the least squares method.

Total number of 41 vessels from the reference list was taken into consideration. The following formula was obtained:

$$\boldsymbol{D_{blr} = 1382 + 0{,}15265\ N_w} \quad [kg/h] \tag{9}$$

where: N_w *[kW]* – main propulsion power,
with the coefficient of determination $r^2 = 0{,}5885$. The graphical picture of formula (9) determination shows figure 5. Obtained Pearson linear regression coefficient of correlation between the values from formula (9) and values taken from the vessels reference list is $r = 0{,}7671$.

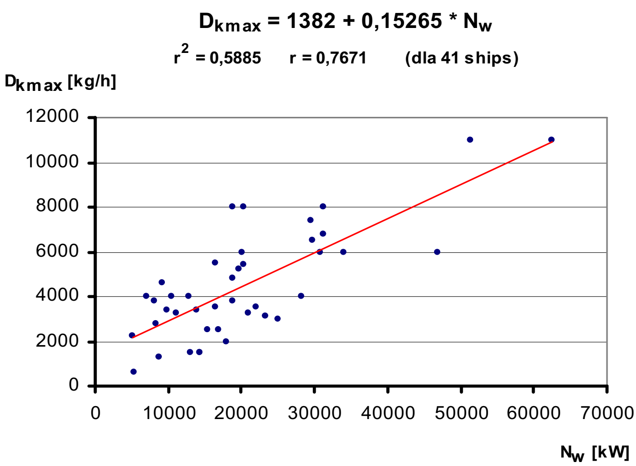

Fig.5. Graphical representation of formula (9) determination

3. Conclusion

The above discussion proves that statistic is very useful means for determination of energy demand for main propulsion, electric power and auxiliary boiler capacity in ship design preliminary calculations.

Authors of presented paper are concerned in this way of design calculations improvement. The method is to be used also in case of another types of sea going vessels. For example, for modern container vessels obtained formulas are as follows [2]:

$$N_w = (0{,}9179 + 0{,}00003412\, D)\, v^3 \quad [kW]$$

$$\Sigma N_{el} = 1077 + 0{,}1580\, N_w \quad [kW]$$

References

[1] Draper, N.R. and Smith, H., *An application of linear regression,* Warszawa (1973).

[2] Giernalczyk, M., Górski, Z., *Method for determination of energy demand for main propulsion, electric power production and heating purposes for modern container vessels by means of statistics,* Marine Technology Transactions, Marine Technology Commity of the Polish Academy of Sciences, Gdańsk 2004

[3] Giernalczyk, M., Górski, Z., *Improvement in the preliminary determination of energy demands for main propulsion, electric power and auxiliary boiler capacity by means of statistic: an example based on modern bulk carriers,* 9th BALTIC REGION SEMINAR ON ENGINEERING EDUCATION, Gdynia Maritime University 17-20 June 2005 pp 49-51

[4] Giernalczyk, M., Górski, Z., *A Statistics-based Method for the Determination of energy demands for main propulsion, electric power and auxiliary boiler capacity for modern crude oil and products tankers.Explo-ship 2006*, Szczecin Maritime University pp 183-192

[5] Hewlett Packard: *HP-65 Stat Pac 1.* Cupertino, California, (1976).

[6] Michalski, R., *Ship propulsion plants. Preliminary calculations,* Szczecin Technical University, Szczecin (1997).

[7] *Report – Energetic assessment of recent ship propulsion plants and means for theirimprovement. Research project no 9 T12D 033 17 of Government Research Comity Polish under management of Prof. Romuald Cwilewicz,* Gdynia Maritime University, Gdynia (2002).

[8] *Standardisation of calculation methods of motor ship engine room systems designing,* Study of Ship Techniques Centre (CTO), Gdańsk 1974

[9] *Unification of ship engine room. Part V. Ship power plant,* Study of Ship Techniques Centre (CTO), Gdańsk 1978.

[10] Zieliński, R., *Statistics Tables*. Scientific and Technical Publications (WNT), Warszawa 1978.

A NEW DESIGN OF ENERGETIC UNIT FOR SHIPS

Vladimír Hlavňa

University of Žilina
ul. Univerzitná 1, 010 26 Žilina, Slovak Republic
tel.: +421 41 513 2670, fax: +421 41 653016
e-mail: vladimir.hlavna@fstroj.utc.sk

Abstract

A new possibility of utilization of ICE cooling medium thermal capacity is its connection with the independent sorption cooling equipment by thermal pipe. Such a configuration avoids the use of a utilizable thermal gradient. This disadvantage of connection of the classical combustion engine with sorption cooling equipment is solved by a cooling internal combustion engine. Its basis lies in the fact that the chambers of the cooling jacket are simultaneously generator of the sorption cooling equipment. The classical engine becomes the sorption cooling equipment. Such an engine can be used for combined generation of electric energy, heat and cold. Cold can be used for the cooling of an engine charging air and for air conditioning of ships equipped with such an engine and cooling of food.

Keywords: *non-conventional energetic unit, cooling combustion engine, more efficient utilization of fuel energy*

1. Introduction

At a constructional realization of a ship it is necessary to deal with individual constructional parts so that the vessel can meet the requirements for safe and comfortable voyage and can feature required navigation and maneuvering abilities under varying loading conditions caused by outer influences.

Important parts of the vessel to be mentioned here are aggregates serving for driving and stabilization and as well as aggregates providing necessary kinds of energy both on board and below. The required kinds of energy (mechanical, electric, thermal, including cold) can be provided by means of the combustion engine in cooperation with suitable equipment. All kinds of energy can be distributed both on board and below. When secondary energies provided by the combustion engine are utilized in an efficient way, we can speak about an advantageous balanced utilization as well as about the aim to maximize the utilization of the fuel carried by the vessel. This fact consequently influences the assessment of the vessel from the point of view of its shipping weight and load capacity from which the total shipping capacity of the vessel results.

2. A new design of energetic unit

A new design of the energetic unit can provide the required kinds of energy, e. g. according to the scheme shown in Fig. 1. The system itself equipped with an appropriate control has to be able to distinguish priorities in the energy distribution. The energetic unit consists of the combustion engine being the primary source of energy for secondary cooperating devices. The devices use for their operation components of outer thermal balance of the combustion engine. An electro generator is used for transformation of mechanical energy into electric energy. Heat can be obtained from exhaust gases by means of an exhaust gases – water exchanger. Cold can be obtained from the thermal balance component which characterizes the combustion engine cooling system. Transformation of heat into cold is carried out by means of thermo compression. Thermo compression can be carried out indirectly, again, by means of an exchanger, or directly within the combustion engine block. For thermo compression to be carried out it is necessary to equip the combustion engine circuit with the sorption cooling system elements and to optimize the construction by creating conditions for its realization. The working substance of the sorption system flows directly within the combustion engine block. This block becomes the thermo generator of the cooling system based on the absorption principle [1].

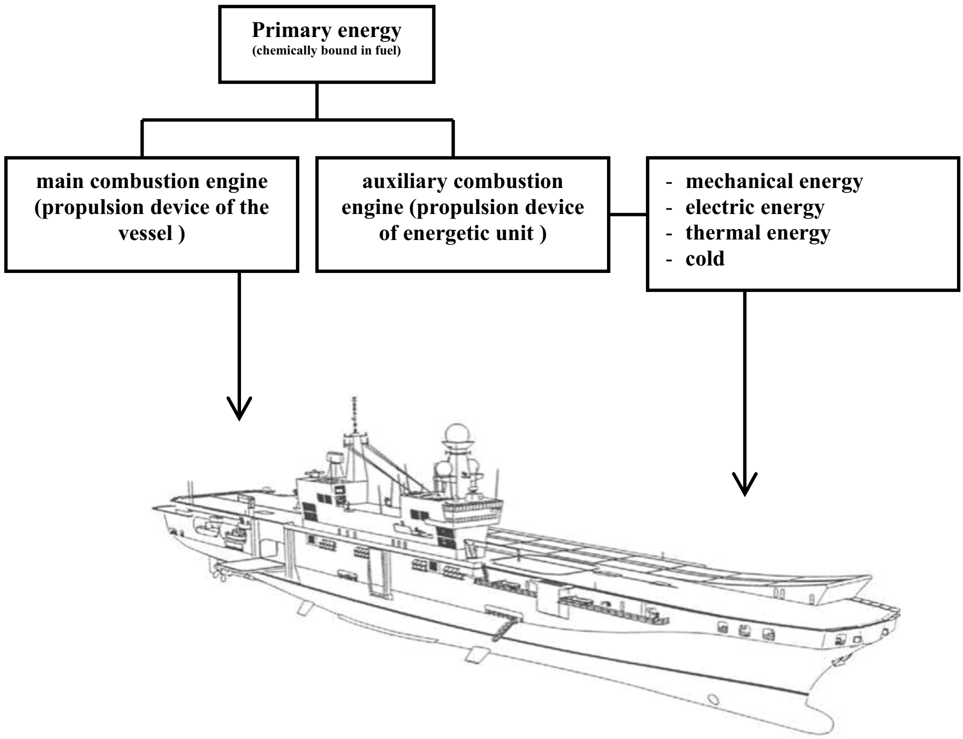

Fig. 1. Energetically provided vessel

For energetic assessment of the system it is possible to give the factor of thermal balance utilization (VTB) of the combustion engine:

$$VTB = \frac{Q_{VYF}\eta_{TE} + Q_{CH}\eta_{CH} + Q_E\eta_{EL}}{Q_P}, \qquad (1)$$

where:

Q_P – energy contained in the consumed fuel,
Q_{VYF} – energy of exhaust gases,
η_{TE} – efficiency of Q_{VYF} transformation into usable heat,
Q_{CH} – energy taken by the combustion engine cooling,
η_{CH} – efficiency of Q_{CH} transformation into cooling output,
Q_E – component characterizing the output on the crankshaft,
η_{CH} – efficiency of transformation Q_E into electric output.

The scheme of the new design of the energetic unit can be seen in Fig. 2 [1, 2], where the auxiliary combustion engine is the primary source of energy (Fig. 1).

The energetic unit scheme consists of a set of exchangers, regulating and control elements and measuring elements.

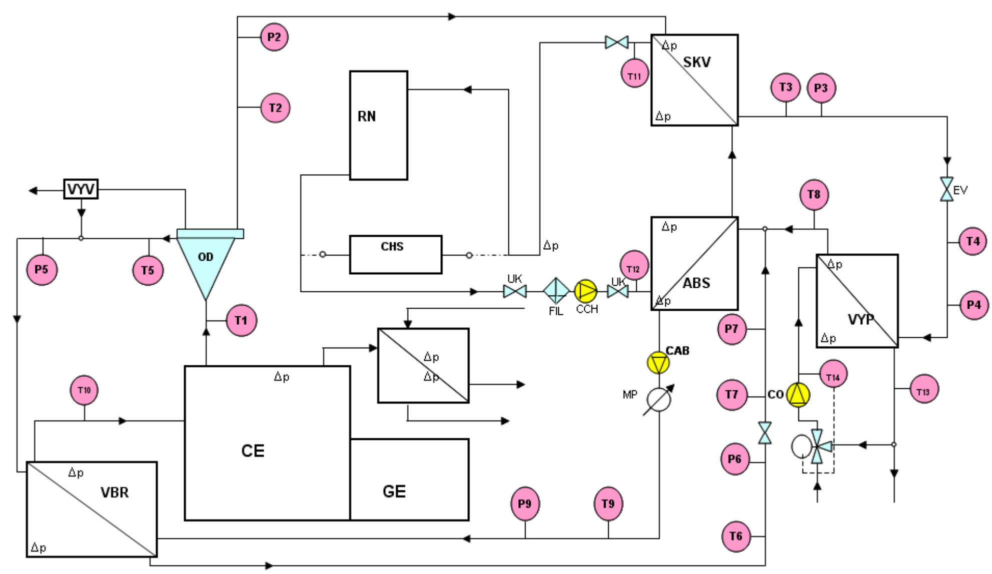

Fig. 2. Scheme of energetic unit. Exchangers: OD- evaporator, VBR- economizer, VYV- vacuum air pump, RN- retainer, CHS- cooler in which heat from sorption circle is obtained, CE – combustion engine, GE – electro generator, SKV- liquefier, ABS – absorber, VYP – evaporator, cooling of the coolant or environment and exchanger for heat from exhaust gases; Regulating and control elements: UK – closing valve, FIL – filter, CCH – circulating pump, CAB – regulating and circulating pump, MP – induction flow meter, CO – circulating pump, EV – expansion valve; Measuring elements: temperatures $T_{1\text{-}9}$, pressure $P_{1\text{-}9}$

When taking into consideration losses and efficiencies of individual circuits, the energetic unit of this type is able to make use of 86 % of primary fuel energy (energetic balance will be dealt with in more detail further). Fig. 3 presents a virtual design of an experimental non-conventional energetic unit. At present it is possible to present also a real laboratory model of the non-conventional energetic unit – Fig. 4.

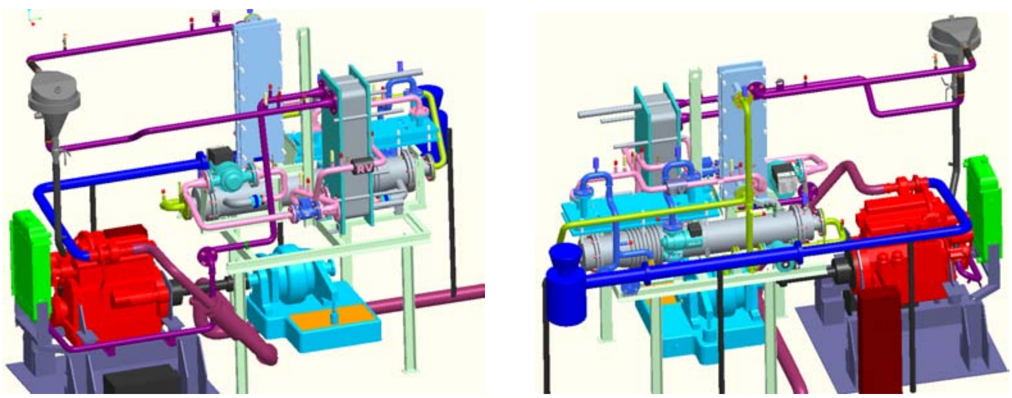

Fig. 3. Virtual energetic unit

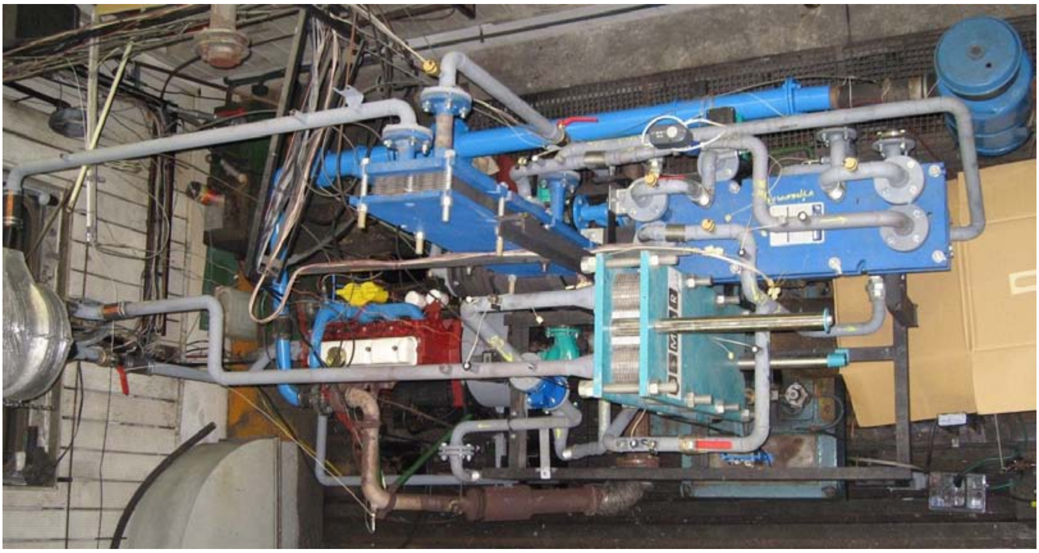

Fig. 4. Real construction of energetic unit

3. Conclusion

Output parameters of the energetic unit circuits (thermal circuit, circuit of the cooling and electric systems) are related to the engine output and its outer thermal balance. Another factor added to the above parameters is the efficiency of the physical principle of thermo compression within exactly stipulated pressure conditions, which exerts a substantial impact on the attainable cooling output usable on the vessel. This fact is assessed and observed by means of evaporation efficiency in the area of the evaporator. The output parameters of the non-conventional energetic unit are influenced also by its construction which is observed and assessed by means of its constructional efficiency.

So far we have carried out basic research of the equipment and by means of experiments we have verified basic axioms of operation within the given pressure and temperature conditions.

A direct use of the combustion engine in the circuit to provide cold represents a new attitude in the energetic unit realization. The objective is to achieve a more efficient utilization of the fuel primary energy, in this case, fuel carried by the vessel.

References

[1] Hlavňa, V. a kol., *Správy o riešení grantovej úlohy APVT-20-010302 a APVT-20-018404*, Ročné správy pre APVT, SjF ŽU v Žiline, Žilina 2003, 02004, 02005 a 2006.

[2] Sojčák, D., *ICE with the non-conventional cooling system,* In. XXI Science and Motor Vehicles 2007, Beograd.

The contribution was created within the framework of the project APVT – 20 – 018404, which is supported by the Agency for Support of Science and Technology of the SK.

ENERGETIC ASSESSMENT OF THE SHIP NON-CONVENTIONAL ENERGETIC UNIT

Dušan Sojčák, Peter Piroch, Vladimir Hlavňa

University of Žilina
ul. Univerzitná 1, 010 26 Žilina, Slovak Republic
tel.: +421 41 513 2670, fax: +421 41 653016
e-mail: dusan.sojcak@fstroj.utc.sk ; priroda.p@priroda.sk ; vladimir.hlavna@fstroj.utc.sk

Abstract

The paper deals with a non-conventional energetic unit equipped with a cooling combustion engine designed as an element for qualitatively new equipment to achieve a more efficient utilization of energy chemically bound in fuel of the combustion engine by transformation of heat into cold via thermocompression.

A simple example illustrates the advantage of a non-conventional energetic system from the point of view of a more efficient utilization of primary energy, i. e. the energy chemically bound in fuel.

Keywords: *non-conventional energetic unit, energetic assessment*

1. Introduction

Energy, the term generally expressing ability for a change of state or process of change of state, is the fundamental existential attribute of the world. One of its forms is an outer expression of the internal state of materials (inner energy), which is thermal energy, or, more exactly, given heat. Part of this form of energy is used by mankind in compliance with its interests, in thermal devices, machines, among which are also thermal engines and cooling devices, i. e. equipment carrying out a circular cycle within the framework of the second thermodynamic law.

2. Energetic assessment of the ship non-conventional energetic unit

Energetic efficiency assessment methods belong to important factors of comparison of energetic systems with thermal devices. General energetic, thermodynamic efficiency (EF) of energetic systems with thermal devices is given by the relation

$$EF = \frac{\sum E_u}{\sum E_u + \Delta E}, \tag{1}$$

where:

ΣE_u – sum of obtained energetic flows,
ΔE – unused energetic flow.

The rate of efficient utilization of thermal energy in these devices is characterized by thermal efficiency, exergy, anergy and by the coefficient of performance (COP). The rate of primary energy utilization (natural gas, liquid fuels, ...) in thermal devices, energetic units using the above mentioned machines, is expressed by a primary energy rate (PER).

The COP expresses attainable useful work of the combustion engine or useful cooling output of the sorption cooling device per one input unit of the given device. The higher the COP achieved by the device the less amount of primary energy consumed to provide the required output energetic flows. The COP can be though used only for comparison of similar devices in the application, i. e., for example, mutual comparison of either combustion engines or absorption devices.

The COP cannot be used for comparison of energetic efficiency of different kinds of devices. For these purposes the assessment by means of the PER is used. The lower the PER value, the higher the rate of primary energy utilization.

3. Energetic assessment

A simple example (for unit input) will be further used to illustrate the advantage of the utilization of the non-conventional energetic unit (presented in other part of the paper) on the ship mainly in relation to utilization of fuel primary energy [2]. The following boundary conditions are assumed for the mentioned example:

⇒ heat flows (input q_h) to the engine Q_M as well as to the cooling engine Q_{MCH} are equal, namely, 1 MJ,
⇒ mechanical work of the engine A_M as well as of the cooling engine A_{MCH} are equal, namely 0.25 MJ,
⇒ also output numbers of the engine COP_A and of the cooling engine COP_{ACH} are equal, namely 0.7,
⇒ input of the pressure pump is zero,
⇒ cooling takes away 30 % of heat (p = 0.3),
⇒ efficiency η_{ACH} of transformation of primary energy into thermal energy including transport into the cooling solution in the cooling engine generator is 0.9,
⇒ total thermal efficiency η_r expressing transport, transfer and transition of heat from the area of cylinder cooling of the independent engine to the working medium of the thermo generator of the independent sorption cooler is 0.85,
⇒ relative cold coefficient of the evaporator of the separate sorption cooler and the combustion engine is 0.85.

Assuming that:
⇒ heats from exhaust gases and from sorption processes are anergic,
⇒ temperatures in the thermo generator are identical in both devices

then the change in the coefficient of the primary energy utilization at its utilization in the cooling engine PER_{CHM} and in the separated aggregate of the combustion engine and sorption cooler PER_{AM} PER_{AM} is obvious from the below. For thermal flow to the cooling engine thermo compressor the following relation holds

$$Q_{GCH} = p \,.\, q_h \,.\, \eta_{ACH} = 0.27\ MJ\ . \tag{2}$$

The coefficient of primary energy utilization rate for the cooling engine can be then determined as follows:

$$COP_{MCH} = \frac{A_{MCH} + Q_{GCH}}{Q_{MCH}} = 0.52\,, \tag{3}$$

$$PER_{MCH} = \frac{1}{COP_{MCH}} = 1.92\ . \tag{4}$$

For the coefficient of primary energy utilization rate for the sorption cooler holds the following:

$$COP_{ACH} = \frac{Q_{OCH} + Q_{KCH} + Q_{ABCH}}{Q_{GACG} + P_{CCH}} \Rightarrow Q_{OCH} = 0.19\ MJ,$$

$$PER_{ACH} = \frac{1}{COP_{ACH}.\eta_{ACH}} = 1.58 \tag{5}$$

and the coefficient of primary energy utilization rate for the cooling engine is given by the relation:

$$PER_{CHM} = \frac{PER_{MCH}.A_{MCH} + PER_{ACH}.Q_{VCH}}{A_{MCH+Q_{VCH}}} = 1.76\ . \tag{6}$$

For the separated aggregates the coefficient of primary energy utilization rate can be determined in the following way:

$$\eta_{\mathrm{A}}.\eta_{\mathrm{ACH}}.\eta_{\mathrm{r}} = 0.77,$$

$$\mathrm{Q}_{\mathrm{GA}} = p.q_h.\eta_A = 0.23\ MJ. \tag{7}$$

for the motor then holds the following:

$$COP_M = \frac{A_M + Q_G}{Q_M} = 0.52,$$

$$PER_M = 1.92. \tag{8}$$

For the sorption cooler then holds:

$$COP_A = \frac{Q_O + Q_K + Q_{AB}}{Q_{GA} + P_C} \Rightarrow Q_O = 0.16\ MJ,$$

$$PER_A = \frac{1}{COP_A.\eta_A} = 1.85. \tag{8}$$

and for the separated aggregates the coefficient of primary energy utilization rate is as follows:

$$PER_{AM} = \frac{PER_M.A_M + PER_A.Q_V}{A_M + Q_V} = 1.9. \tag{9}$$

If the amount of cold is reduced to the value Q_{0CH} = 0.17 MJ, then, at the unchanged value of heat supplied for the cooling engine generator Q_{GCH} = 0.27 MJ, the amount of heat from the condenser will then be $Q_{KCH} = 0.44$ MJ. Then, for the same cooling engine using condensed heat the following will held:

$$COP_{MCH} = \frac{A_{MCH} + Q_{CH}}{Q_{MCH}} = 0.52,$$

$$PER_{MCH} = \frac{1}{COP_{MCH}} = 1.92,$$

$$COP_{ACH} \frac{Q_{OCH} + Q_{KCH} + Q_{ABCH}}{Q_{GACH} + P_{CCH}} = 2.17, \tag{10}$$

$$PER_{ACH} = \frac{1}{COP_{ACH} . \eta_{ACH}} = 0.51.$$

and the total coefficient of primary energy utilization rate of the cooling engine will be:

$$PER_{CHM} = \frac{PER_{MCH} . A_{MCH} + PER_{ACH} . Q_{VCH}}{A_{MCH} + Q_{VCH}} = 1. \tag{11}$$

3. Conclusion

From the above mentioned it is obvious that in the cooling engine there will be reduction of the PER (from value 1.9 to value 1.0), i. e., there will be increase in the efficiency of primary energy utilization. It is, therefore, quite realistic to use the non-conventional energetic unit with a cooling engine with more efficient utilization of primary energy, i. e. fuel energy, as a classical separated aggregate composed of a combustion engine and sorption cooler.

A more remarkable effect in utilization of fuel primary energy can be achieved when the obtained cold is utilized for the cooling of charging air behind the engine blower. If the charging air was cooled from 313 K to 288 K, a simplified calculation could show that the coefficient of primary energy utilization rate would fall to the value of 0.88.

References

[1] Sojčák, D., *Spaľovací motor s nekonvenčným chladiacim okruhom*, Strojnícka fakulta Žilinskej university v Žiline, doktorandska dizertačná práca, Žilina 2006.

[2] Piroch, P., *Efektívnejšie využitie energie paliva v nekonvenčnom spaľovacom motore*, Strojnícka fakulta Žilinskej university v Žiline, doktorandska dizertačná práca, Žilina 2006.

The contribution was created within the framework of the project APVT – 20 – 018404, which is supported by the Agency for Support of Science and Technology of the SK.

RUN REGULARITY IN DIESEL DRIVE CHAIN ELEMENTS

Antoni Iskra

Poznan University of Technology
ul. Piotrowo 3, 61-965 Poznan, Poland
tel.: +4861 665 2511, fax: +4861 665 2514
e-mail: antoni.iskra@put.poznan.pl

Abstract

Following paper presents efforts on deliberate modification of drive transmission elements vibrations aimed at limitation of their nuisance. Some effects of disadvantageous drive vibrations encountered during construction of a test rig will be presented as well. The proposed computational model is fully versatile and takes into account any number of inertia and drive transmitting stiffness. Stiffnesses can be described with any function corresponding to the real behaviour of joints and couplings, which generally are not linear. Damping which illustrate actual, most commonly non-linear characteristics of energy dissipation was also taken into consideration in the drive chain.

Keywords: *resonance vibrations, flying wheels, diesel run regularity*

1. Introduction

One of the IC engine shortcomings is cyclic character of torque transmitted to the power receiver. Due to that torsional vibrations appear which could not be eliminated. This makes that every engine has its characteristic vibrational and acoustic properties. Contemporary produced automobiles are equipped with engines of far limited operational inconveniences but it is impossible to design an engine completely free of vibrations. Term "culture of engine operation" exists in colloquial language as a result of this phenomenon. This idea describes an user's subjective feeling which relates to the range of rotational speeds when the engine emits discomfortable vibrations and noise. Following paper presents efforts on deliberate modification of drive transmission elements vibrations aimed at limitation of their nuisance

2. Characteristics of tested object

When analyzing engine crank mechanisms made of different producers one can conclude that there is no constant principle of reduction of vibration generated in any engine. Definitely this is a result of cyclic processes performed in reciprocating machine. An analysis of one of the most modern engines, namely the VW TDI R5 AXD proves about the range of undertakings aimed at the reduction of noise and vibrations generated by the engine. Fig. 1 presents engine crankshaft, Fig. 2 – composite flying wheel combined of two inertia wheels fixed with coupling of non-linear characteristics.

Fig. 1. General view of engine crankshaft, inertial vibration damper on the right

Fig. 2. General view of composite flying wheel

The composite flying wheel performs coupling of non-linear characteristics, presented in Fig. 3.

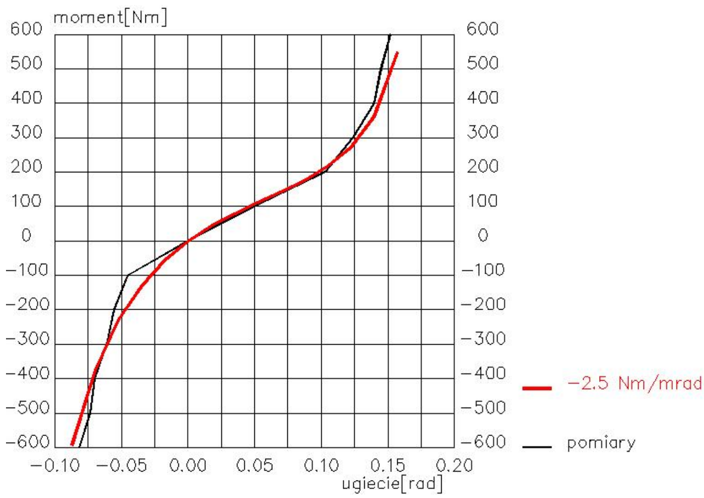

Fig. 3. Flying wheel coupling characteristics; measurements – black line, approximation of 2,5 Nm/mrad stiffness at the origin of the coordinate system – red line

3. Results of drive parameters computer simulation

The drive chain of presented unit performs minor vibrations within the whole operational range. Alas, any changes of inertia moment or stiffness in the drive chain could cause very disadvantageous changes in the drive characteristics. Definition of these parameters can be done using programs presented in literature [1]. The substitute model of vibrating unit has been presented in Fig. 4.

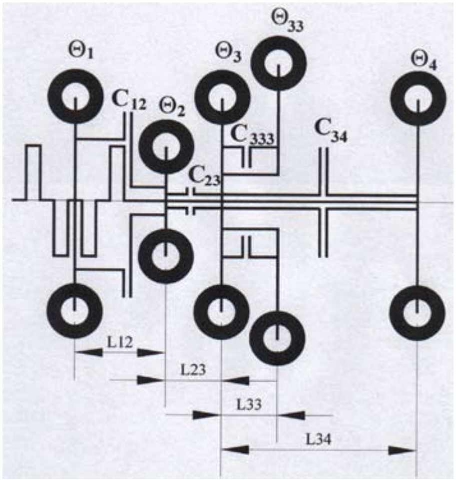

Fig. 4. The model of drive chain from crankshaft of Θ_1 equivalent polar inertia to the dynamometer rotor of Θ_4 polar inertia

According to Fig. 4 following notification of drive chain basic element parameters have been taken on:

– crankshaft of Θ_1 equivalent moment, L_{12} equivalent length and C_{12} damping,
– flying wheel of Θ_2 equivalent moment rigidly coupled to the crankshaft of L_{12} equivalent length and C_{12} damping transferring the torque to the additional flying wheel of Θ_3 polar inertia,
– dynamometer rotor of Θ_4 polar inertia coupled to the flying wheel with an articulated shaft of L_{34} equivalent length.

The articulated shaft has been presented in Fig. 5 and its characteristics – in Fig. 6.

Fig. 5. Engine–to–dynamometer articulated coupling

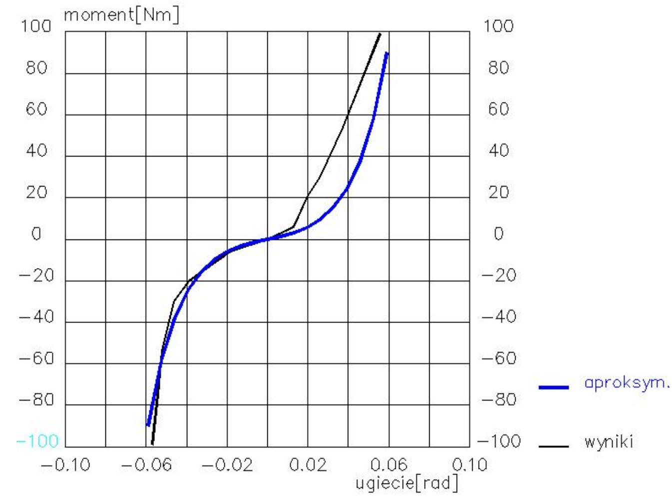

Fig. 6. Characteristics of the articulated coupling presented in Fig. 5; measurements–black line, approximation–blue line

There are very complicated resonance phenomena in the drive chain, which above all affect the engine speed irregularity but also are the source of noise and in extreme case could initiate the instantaneous torque far higher than the static one. Fig. 7 presents the course of engine speed momentary value for average conditions of operation.

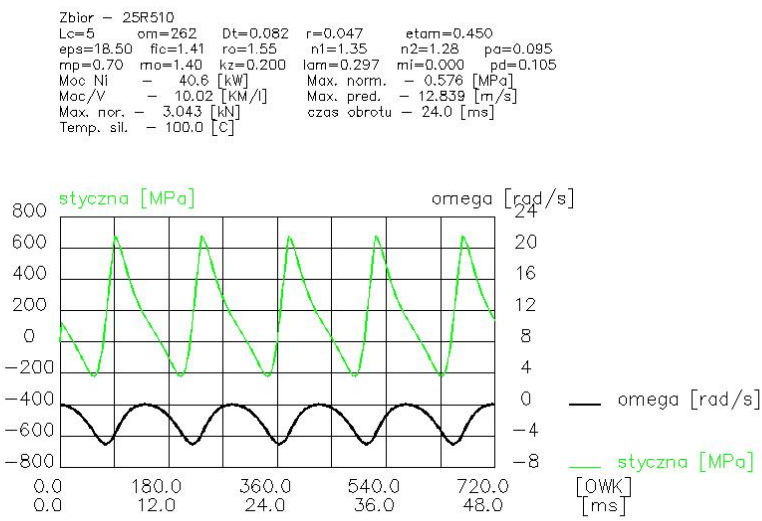

Fig. 7. Course of the TDI R5 AXD engine instantaneous speed variations for conditions presented above; green line–the course of tangential force giving angular speed variations of δ = 1/52 level of irregularity

A disadvantageous phenomenon of increase in engine speed irregularity resulting from the superposition of gaseous and inertia force phases has been encountered in the case of 5–cylinder engine tested. A 4–cylinder engine of similar size and thermodynamics performs almost two times better δ level of irregularity because δ=1/93.

The course of change in momentary value of angular speed of drive chain individual elements schematically presented in Fig. 4 can be seen in Fig.8.

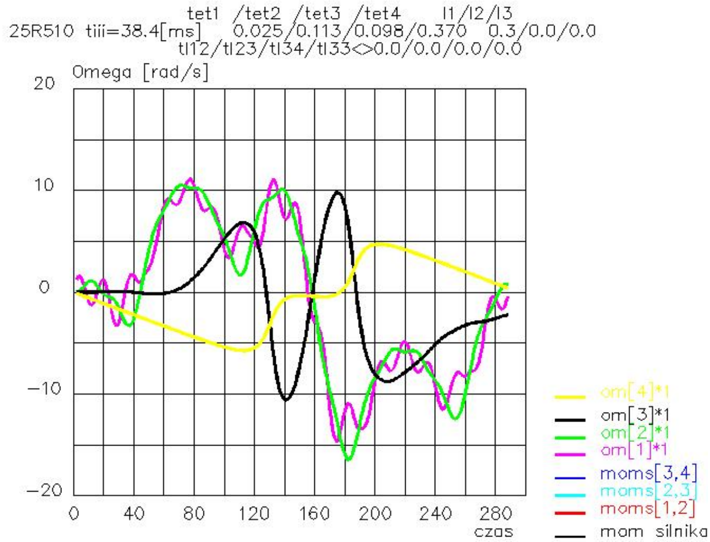

Fig. 8. Course of engine shaft angular speed variation – pink line; of Θ_2 flying wheel firmly fixed to the engine shaft – green line; of Θ_3 flying wheel flexibly coupled to the engine shaft – black line, and of Θ_4 dynamometer rotor –yellow line

Presented in Fig. 8 changes in rotational speed generate the coupling torques in Fig. 9.

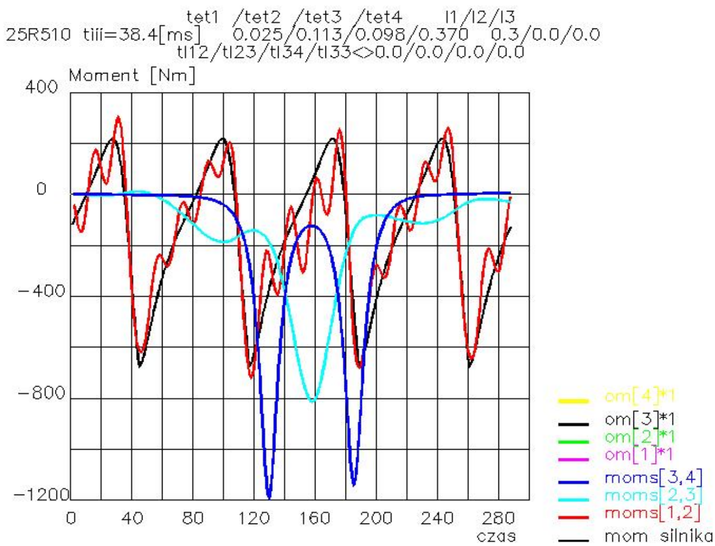

Fig. 9. Course of variations of the TDI R5 AXD engine generated torque – black line and of coupling torques within sections of equivalent shaft (see Fig. 4) – L12 – red, L23 – light blue and L34 – blue

In the analyzed drive chain the course of torque in the joint presented in Fig. 5 develops particularly unfavorably that lead to the failure of pin joint [2].

4. Possibilities of run irregularity level correction

In the case of tested engine – power receiver system the speed irregularity level might be significantly improved and particularly the torque transmitted to the power receiver could be reduced if the coupling characteristics of composite flying wheel was changed. Fig. 10 presents the coupling parameters graph from Fig. 9 but for the flying wheel coupling characteristics taken from Fig. 11.

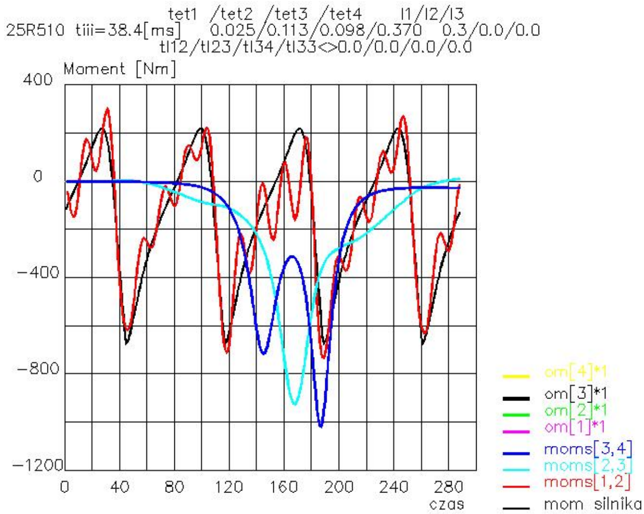

Fig. 10. Course of the TDI R5 AXD engine generated torque variations after the modification of flying wheel set coupling characteristics

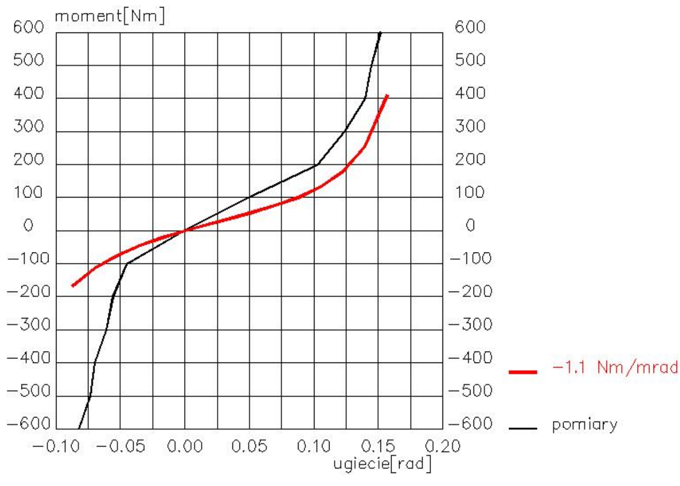

Fig. 11. Flying wheel set coupling characteristics; measurements – black line, approximation with the 1.1 Nm/mrad rigidity at the origin of coordinate system — red line

Comparing graphs in Figs. 9 and 10 one can notice an apparent reduction in maximum value of torque transmitted to the power receiver. However, the flying wheel coupling torque rises by about 10% which does not make a problem, nevertheless the coupling springs of flying wheel set should be appropriately replaced.

5. Conclusions

- One of the fundamental disadvantages of reciprocating engines is the irregularity of torque transmitted to the power receiver, which is the cause of resonance vibrations and noise. Torque transmission by a set of flexibly coupled flying wheels could cause a unfavorable torque increase at the drive chain elements like joints correcting the coaxiality of engine and dynamometer.
- Individual selection of joint characteristics enables the possibility of ease the resonance phenomena but on the other hand reducing the negative effects of resonance for certain parameters of engine operation could lead to the increase of coupling torque in other regions of engine run.

References

[1] Iskra, A. i zespół., *Redukcja obciążenia środowiska spowodowanego biegiem jałowym silnika samochodu w warunkach utrudnionego ruchu miejskiego, Reduction in Environmental Burden Caused by the Automotive Engine Idle Run,* Nr projektu Komitetu Badań Naukowych - 5 T12D 040 25, Poznań 2006.

[2] Iskra, A., *Problemy drgań elementów przeniesienia napędu w fazie rozruchu silnika, Problems of Drive Train Elements Vibrations at Engine Start,* Ogólnopolskie Sympozjum Naukowe – Rozruch silników spalinowych – SYMROZ'2007, 23-25.04.2007 – Szczecin, Malmö, Kopenhaga.

REAL POSSIBILITIES OF CONSTRUCTION OF CI WANKEL ENGINE

Antoni Iskra

Poznan University of Technology
ul Piotrowo 3, 60-965 Poznań, Poland
tel.:+48 61 6652511, fax: +48 61 6652514
e-mail:Antoni.Iskra@put.poznan.pl

Maciej Babiak

Poznan University of Technology
ul Piotrowo 3, 60-965 Poznań, Poland
tel.:+48 61 6652049, fax: +48 61 6652514
e-mail:Maciej.Babiak@doctorate.put.poznan.pl

Abstract

In the paper deliberations on constructing the CI Wankel engine and some problems of using this kind of combustion system are presented. Many problems have been known for years but their solution seems to be available nowadays. Special meaning will probably have electronically controlled injection systems which fast evolution and common use in CI reciprocating engines could be seen during last few years. Also use of numerical methods with taking advantages of newest computers in designing process will be helpful. The CI Wankel engine with advantages of rotary engine and virtues of CI combustion system could become an attractive powertrain for passenger cars. This kind of construction could have a chance of finding its place in the market and increasing its popularity in this hard times for rotary engine.

Keywords: internal combustion engine, rotary engine, CI combustion system

1. Introduction

The first run of rotary combustion engine took place in 1957 in NSU research and development center. Author of the project and main constructor was German engineer Felix Wankel. The prototype was four-stroke SI gasoline engine. Information about successful tests of first rotary engine made producers of combustion engines interested in this kind of construction and it was predicted that the era of reciprocating engines is about to end. In that time reciprocating engines already were sophisticated constructions and their constructors had rich experience in range of constructional solutions and materials. This referred both types of engines, SI which were the most popular powertrain for passenger cars and CI which, owing to development of more perfect injection systems and turbocharging, have been founding more and more wider possibilities of their use. Research and development centers of many producers started intensive works on rotary engine and the main goal was to start as soon as possible serial production of the Wankel engine. It was obvious that conceptions of rotary engine and CI combustion system used together could be the turning point in designing of internal combustion engines. Quite early rotary engine revealed its main disadvantages such as high value of specific fuel consumption and low durability of trochoid surface and rotor sealing elements. During designing the CI Wankel engine the main problem was disadvantageous shape of the combustion chamber. For that and many other problems conception of the CI Wankel engine was discontinued without correctly working prototype. However the progress that proceeded during last decade in sphere of turbocharging and electronic control of CI engines permits to put a question if it is possible to construct the CI Wankel engine which parameters like wattage rating, torque, emission of toxic exhaust gases would meet today's standards.

2. Problems connected with shape of combustion chamber and possibilities of their solution

As it was noticed in introduction the main problem for constructors was the shape of combustion chamber which in CI engines is essential for quality of fuel/air mixture and as a result course of combustion process. Combustion chamber has to ensure as good as possible mixing quality of drops with air mainly by swirling the fresh charge so the combustion air factor would guarantee the highest value of total efficiency. What is more it is desirable to shorten the self-ignition delay so the maximum values of pressure and temperature, which in CI engine occur during kinetic phase of combustion process, can be reduced. In Wankel engine there are not many ways of improving the shape of combustion chamber because of its basic geometry. Long shape of combustion chamber in rotary engine do not allow to fulfill earlier specified requirements connected with formation of fuel/air mixture in CI engine. This shape is also unfavourable because of the volume to field of surface ratio. The less is value of this ratio the higher are losses of heat to the cooling system so thermal and total efficiency get worse. This means that the value of specific fuel consumption of the Wankel engine is higher than for reciprocating engine of comparable power.

The only way of forming combustion chamber in Wankel engine is making recesses in rotor and this solution is also applied in the SI Wankel engines. Adding recesses can improves quality of the fuel/air mixture but unfortunately the value of volume to field of surface ratio remains poor. In SI engine this kind of treatment is possible because the maximum value of needed compression ratio is $\varepsilon = 11$ while in CI engine it is much higher what decides of its better total efficiency. Moreover the temperature after compression stroke in CI engine has to be high enough for self-ignition of the fuel. In the Wankel engine the maximum value of compression ratio depends on Z parameter which is defined as:

$$Z = \frac{R}{e}. \tag{1}$$

The e parameter specifies value of the journal eccentricity and the R parameter specifies the distance between rotor's centre of symmetry and its apex. The greater is the value of Z parameter the highest value of maximum compression ratio is available but in the same time the shape of combustion chamber gets worsen which becomes longer and thinner. This means that it is needed to make greater recesses in the rotor in order to optimize the combustion chamber shape. Value of Z parameter has its influence on apex seal angle of attack which is connected with maximum difference of the pressure in adjacent chambers. Higher value of Z parameter allows to increase the difference of pressures which is very important for CI engine. The combustion chamber shape without recesses for two Z parameter examples are shown on Fig. 1.

In 1972 the Rolls-Royce company built the CI Wankel engine with configuration of two rotors where first larger rotor was used to initial compress of the air and also to use energy from expanding exhaust gases for getting power. Combustion process where the exhaust gases and main part of the engine power were produced took place in smaller second rotor. Because of complicated construction and problems with course of combustion process this conception was not developing any longer [2].

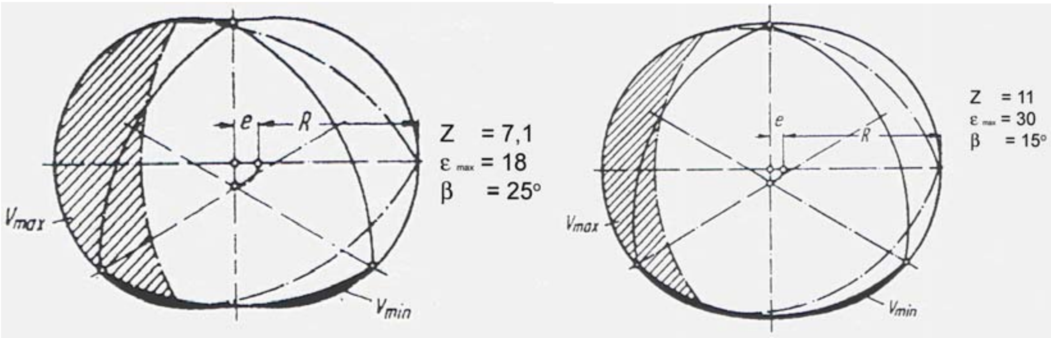

Fig. 1. The combustion chamber shape for two values of Z parameter [1]

Observing development of modern reciprocating CI engines a tendency of decreasing geometrical compression ratio can be noticed. This allows to increase the supercharching pressure. The use of modern turbocharger with variable geometry of turbine guide vanes in CI engine gathers great meaning because besides of obvious increasing output power it betters conditions of combustion process and increase total efficiency of the engine. The turbocharger increases the pressure at the beginning and at the end of the compression stroke, what in spite of lower compression ratio makes the temperature of the fresh charge, where the fuel is being injected, higher. The higher temperature accelerates the self-ignition process what allows to attain greater engine speed.

Summing up, it seems that with use of high pressure turbocharging it is possible to obtain suitable thermodynamic parameters in Wankel engine combustion chamber for fuel self ignition with maintaining the correctability of combustion chamber shape.

3. Modern injection systems of CI engines in aspect of the Wankel engine

During last decade a tendency of increasing CI engines share in automotive market could be observed. Two deciding factors were application of high pressure electronically controlled injection systems and development of turbochargers construction. Advantages of new technologies have led to considerable improvement of engine parameters with simultaneous reduction of toxic gases emission and bettering so called culture of work.

In field of injection systems two competitive systems have appeared: common-rail system and injection unit system which have been promoting by Volkswagen company because of its higher injection pressure. However features of common-rail system like easiness of controlling fuel injection course and cost of production have decided that most CI engines from the smallest one for passenger cars to the biggest marine are supplied with this type of injection system. Also in the CI Wankel engine common-rail system seems to be the most suitable. The latest generation of common-rail system is characterized with maximum injection pressure of 1800 bar and application of piezoelectric injectors which allow to divide fuel dosage on five parts. This allows to precise control of combustion process course in CI engine. Partition of fuel dosage, especially usability of extremely small and precisely measured pilotage dose, could be very useful in the CI Wankel engine. Because in Wankel engine combustion chamber rotates with the rotor it is necessary to choose number and moment of injection particular doses so the optimum form of fuel/air mixture is provided. Proper fuel atomization is obtained by high pressure of injection. The goal of using pilotage dose is to prepare and better conditions in combustion chamber before the main dose is injected. Apart from recesses shape in the rotor the combustion chamber of the Wankel engine will always have oblong shape so it is possible that usage of two fuel injectors for injection to different combustion chamber areas will be necessary. With today's processor capacity it is not a problem to determine in real time moment and duration of injection for particular dose in both injectors. Parameters of injection have to be optimized dependent on combustion chamber shape, engine speed, engine load and other parameters that have their influence on combustion process course. If the optimization process is done properly it should be possible to obtain required CI engine cycle parameters. These are theoretically brief foredesign which firstly should be put on many simulation tests and next confirmed on test bed. Special attention should be focused on combustion chamber and swirl optimization because it is very important for injection system design process.

4.Rotor sealing

The rotor of the Wankel engine is sealed in two ways. First is side seal which makes the fresh charge and exhaust gases impossible to move between adjacent chambers. It also prevents the lubricating oil flowing from rotor bearing to combustion chamber. Second type of seal, which always has been much more problematic for constructors, is the apex seal.

All functions of piston packing of reciprocating engine in the Wankel engine have to be fulfilled by only one apex seal on each rotor vertex. It is not possible to separate functions of tightening and oil film thickness controlling. In everyday use, when the engine is running often in cold stage, the apex seal is the weakest element and in short time lead to worsen parameters of the engine and next to destruction rotor housing trochoid surface.

In the CI Wankel engine another problem is greater difference of pressures in adjacent chambers, because when in one chamber intake stroke is about to end in the adjacent chamber power stroke begins and the combustion pressure reach its maximum value. For CI engine with direct injection maximum pressure exceeds 10 MPa while for SI engine it is usually of 6 MPa. Greater pressure difference puts higher requirements for apex seal which has to ensure proper separation of chambers and not generate high friction looses in oil film. The worst situation is when the oil film is ruptured because of the forces that push the apex seal to the rotor housing. This means that apex seal is in direct touch with the trochoid surface what leads to early wear of rotor housing and sealing elements. For this reason oil film parameters course during full engine cycle should be subject of precise studies. Designing reliable sealing system, appropriate combustion chamber and injection system are the main problems that need to be solved during designing the CI Wankel engine.

5. The newest CI Wankel engine achievements

Wankel Super Tec GmbH company has started their researches on designing the CI Wankel engine. Brief foredesign are similar to this one that authors of the paper have mentioned. The injection system will be based on common-rail system with partition of fuel dosage. Self-ignition assist device is also planed to be used but no specific information about this device were published. Cross-section design of CI Wankel engine with visible position of injector is shown on Fig. 2.

Two other examples of different combustion chambers and injectors positions, which were also studied and tested by mentioned company, are presented on Fig. 3. It is worth to pay attention on draft on the right where very complicated injection system with more than two injectors is visible.

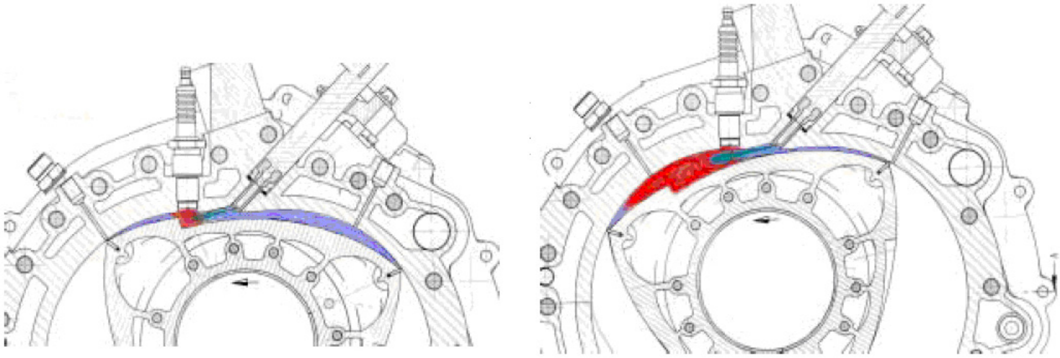

Fig. 2. Cross-section of the CI Wankel engine designed by Wankel Super Tec GmbH [3]

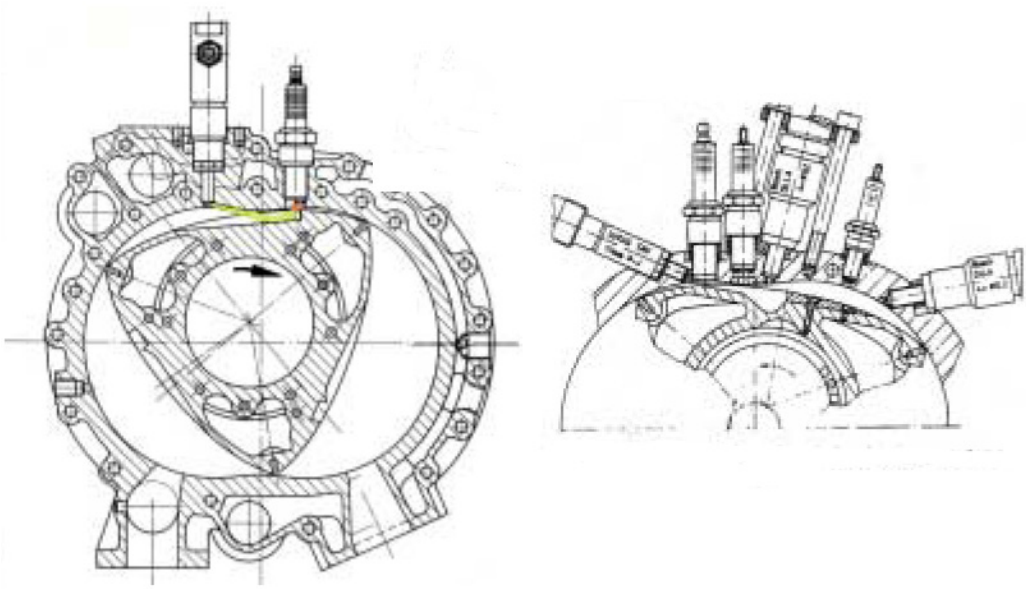

Fig. 3. Different possibilities of combustion chamber shape and injectors position tested by Wankel Super Tec GmbH [3]

Wankel Super Tec GmbH company had announced start of mass production the CI Wankel engine in 2006 but although it is 2007 now no information were published. It is more than certain that during design process much more problems occurred than it was first expected.

6. Conclusions

Both the Wankel engine and CI engine characterize with many advantages, and theirs connection could be a chance to create new alternative for passenger cars powertrain. Many problems are very interesting science challenge and their solving can be much improvement in understanding of many phenomena which are connected with combustion and lubrication processes in internal combustion engine both reciprocating and rotary. Great example is injection system which thanks to evolution in reciprocating engines can find their application in rotary engine. It is probable that evolution of rotary engine will bring achievements that could be used in reciprocating engines. Scientific success could be an impulse to intensify researches by commercial companies which goal is to get a profit. If science centers and of automotive industry would join their efforts vision of properly working CI Wankel engine and its application as a passenger car powertrain could be very realistic.

References

[1] Bernhard, M., *Silniki spalinowe o tłokach obrotowych*, Wydawnictwa Komunikacji i Łączności, Warszawa 1964.
[2] www.der-wankelmotor.de
[3] Wankel Super Tec GmbH press materials

OPTIMIZATION OF OPERATING TASKS ASSIGNED FOR ENGINE ROOM STAFF

Piotr Kamiński

Maritime University of Gdynia
Department of Mechanical Engineering
e-mail: pkam@am.gdynia.pl

Abstract

The present work shows the two approaches to the problem according to the situation in which the engineer is made to take certain decisions. In formulation of the two most substantial operating states of a ship like lay time in port and sea voyage, knapsack algorithms and task scheduling algorithms were applied. For both approaches was formulated objective function, decision variables and constrains.

Keywords*: task scheduling, knapsack problem, ship power plant, decision making*

1. Introduction

According to many experts' opinion proper management of engine room presents serious difficulties for decision – making engineers. This is caused by among others:

- increasing number of automated ship's systems,
- many work processes performed simultaneously,
- information shortage which allow fast familiarization with Engine Room systems and work scheduling,
- frequent change of ship staff,
- increasing safety requirements for staff, ship and environment.

Moreover the changes of international maritime law put on the engine room staff many additional works relating new procedures and report them.

That state creates situations, which large number of factors do decision making difficult and the engineer's knowledge and experience can be not enough to make a correct decision. Decision making relating of Engine Room management could be irrelevant or irrational, causing the different kind of loss. For example - the loss of time, what increase the general cost of ship used.

To eliminate that situations engineer could use a computer application, as a tool supporting him at managing of task scheduling in Engine Room.

Nowadays a lot of ships have computer systems supporting a ship engineers in power plant management being installed or functioning. The chief engineer has by himself to analyze all information's and make the proper decision about scheduling the operation tasks.

The objective of such tool would be to solve the following problem:

Knowing a set of tasks to be performed and taking into consideration all accessible resources (technical, human, time) as well as ship operating states, make a choice of such tasks, which make use of resources most effectively.

In other words, the idea is to take rational decisions referring to above-mentioned tasks, what will be the best from operating viewpoint at a certain time, and assigning them to suitable E.R. staff. Such "a tool" can be a computer-aided program of E.R. management supporting a chief engineer in making those decisions.

2. Operating task scheduling

2.1 Problem formulation

The solution of decision – making problem what a chief engineer deals during E.R. managing is a rational schedule of tasks which are important to be performed in a certain operating situation.

Analyzing situations, which a chief engineer is likely, to be made to solve a decision – making problem described above, a few situations depending on operating condition of a ship can be distinguished.

For example, the ship is on a long sea voyage. In this case there are no strict time restrictions in completing either operating process in E.R. or a particular operating task. Therefore the decision – making problem can be formulated as a tasks scheduling with no time limits. So the tasks must be scheduled with optimum application of accessible human and material, also concerning execute moment of a certain task imposed by external factors such as: producer of marine machineries, classification societies, port controls (*Port State Control*), etc.

Another situation is when time limits occur, e.g. during stay in port time. The exact departure time is known and the number of tasks to be completed exceeds considerably E.R. staff capabilities. Situation like this, the chief engineer has to take decision which operating tasks are to be completed in the allowed time and which tasks can be postponed for further term. Making inappropriate decisions at this moment can lead to execute failure tasks. Result of this can be detention of the ship by port control (*PSC, FSC*) or break off of normal operating process of E.R. (e.g. *black out*) in further. Decision – making problem in this situation can be formulated as a choice of the most relevant tasks from viewpoint of E.R. operating and scheduling them so as to make the most of the available time.

There are a lot of other situations in ship operating process, e.g. anchoring, manoeuvres, passing through a channel etc., when an engineer could be made to the decisions on task scheduling. However, these states make a tiny percentage of the overall operating time of a ship, they occur very seldom in her operating process. Otherwise the situation demands immediate decision about the method of acting (e.g. port manoeuvres), computer aided system is unlikely to be used. Therefore the two first specified situations have been taken into account: stay time in port, sea voyage.

In general theory of decision making the decision problem is the situation, when the decision-maker faces before necessity of choice one from at least two possible variants of working. In Engine Room the chief engineer has to decide, what variant with all decision variants (schedule of operation task) will be the best. According with definition of this problem chief engineer must from among all operation tasks, which are to execute, choose and schedule for operators these which are the most important in particular operation situation consider all occurrent condition and constraint.

The decision making process of chief engineer relating the scheduling tasks of the operators in E.R. can distinguish tree of the principle stages:

- accumulation and processing all accessible and necessary information [4],
- selection tasks, which realization be limited by the every operation constraints and conditions in what the decision be making [3],
- assigning of the tasks to the E.R. staff according with his competences (qualifications), so to the schedule was the best [1][2].

2.2. Application of knapsack algorithm

In present work described the last stage, so the allotment of the operation tasks to operators in this situation. The strategy of allotment of these tasks in such situation can go to two aims:

maximization of the schedule value, what is the choice of the most important tasks, or the best use of the available time.

Problem of the tasks scheduling in E.R. in both aims, it similarly how many industrial problems, could be implemented as packing problem (knapsack problem), being a special case of 0-1 linear programming.

Many authors describe several methods and algorithms of scheduling, which concerned of varied special types of problems [5][7]. But these models are general the most comprehensive in relation to reality problems and not account many different practical conditions.

Standard knapsack problem depend on completion the limited knapsack volume, by "packs" which volumes and weight are different, in such way that, the knapsack get maximum worth.

In analogous it is possible to formulate a scheduling problem of chief engineer. Specific situations like e.g. short stay in port or short sea voyage, where the operation tasks are assigned to E.R. staff in such to execute the most important tasks and to use available time maximally also.

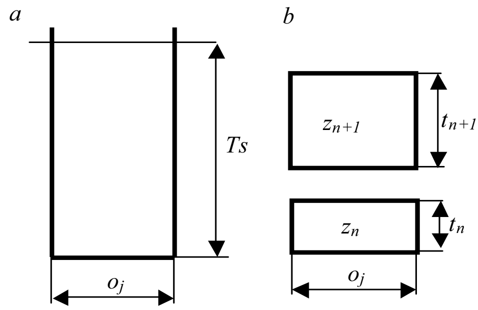

Fig.1. Graphic representation of knapsack problem

2.3. Application of multi-knapsack algorithm in task scheduling in Engine Room

The problem of scheduling operation tasks to all operators in *E. R.*, could be possible to consider as multi-knapsacks problem (*in shortcut: 0-1 MKP*) [6]. The operators o_j (*E. R.* staff) are representing by "knapsacks". Theirs height is available time T_S (e.g.: short stay in port or short sea voyage). The competence (qualification) $k_j=o_j$ what possess the operator is symbolize by width of the knapsack (fig.1a).

The tasks are representing by "packs" (fig.1b), which are placed in knapsacks. Every task possess few parameters:

- competence what need operator to do it, it's a width of pack,
- time t_i necessary to do it, it's a height of pack,
- task weight wg_i, what is the validity of the task, with operation of view point, it's worth of pack.

The solution of that introduced problem will be tasks schedule, what need to realized for every of accessible operators in this situation in Engine Room, with fulfilling all constraints.

2.4. Mathematical model

Fundamental elements of chief engineer decision-making as packing problem are:

- tasks with the parameters (e.g.: task weight wg_i, realization time t_i, etc.),
- operators with possess competence k_i,
- available time T_S.

In presented scheduling operation tasks in E.R. approach was accepted few general foundations and constrains:

- every operator can execute only one task in the same time,
- every task can be executed by one operator only,
- number of execrable tasks in the E.R. is larger then operators can realize,
- every tasks possess few parameters keeping in database or appointing in earlier [1][2],
- assigning of the tasks will be execute accordantly whit the professional qualification.

A big number of operating tasks, which should be used to scheduling, bring many solutions filling all restrictions. In order to point out the optimum task planning from operating viewpoint, determination of importance indicator of each task and determination of quantity indicator *Fj* of each solution (objective function of optimization problem) are necessary.

Objective function

In this problem we admit two optimization's criterions. The first, should be execute the most important tasks fj_1 (eq.1). Such schedule should consist the tasks attached of all operators whit possibly the largest weight coefficient wg_i. Second, the best utilization the available time differently fj_2 (eq.2).

$$fj_1 = wg_1 x_{1j} + wg_2 x_{2j} + ... + wg_n x_{nj} = \sum_{i=1}^{n} wg_i x_{ij} \tag{1}$$

$$fj_2 = x_{1j}\frac{t_1}{T_S} + x_{2j}\frac{t_2}{T_S} + x_{3j}\frac{t_3}{T_S} + ... + x_{nj}\frac{t_n}{T_S} = \frac{\sum_{i=1}^{n} t_i x_{ij}}{T_S} \tag{2}$$

where:

$i = 1, 2, 3, ..., n$ - number of tasks,
$j = 1, 2, 3, ..., o$ - number of operators,
wg_i – weight of task importance,
x_{ij} - *0 or 1*, if task *i* is assigned to operator *j*,
t_i - execute time of task *i*,
T_S – available time for execute of tasks.

According with principles of formulating the objective function [8] in problem like this, was accepted as scalar combination this two criterions. Generally it's definite as valid sum: the coefficients of tasks weight and time, what occupy there execute.

In that case this is two-criterions optimization problem. To equation introduced coefficients of weight's criterions ρ_1 and ρ_2, what gives to user the possibility of choice which criterion is more important. A chief engineer chooses dependence which criterion is the most important in this moment. Coefficients ρ_1 and ρ_2 can admit value from compartment <0,1>, and their sum always has to be equal 1. The most often takes it like $\rho_2=(1-\rho_1)$.

Objective function of this problem is as follows:

$$Fj = \max\sum_{j=1}^{o}\sum_{i=1}^{2} sk\cdot\rho_i\cdot fj_i(o_j) = \sum_{j=1}^{o}\left(sk\cdot\rho_1\cdot\sum_{i=1}^{n} wg_i x_{ij} + (1-\rho_1)\frac{\sum_{i=1}^{n} t_i x_{ij}}{T_S}\right) \tag{3}$$

where:

ρ_1– weight of criterion,
sk – scale coefficient.

Such form of objective function possesses some imperfection. The schedule folds many low weight tasks (less important) and a short of execute time. It can have larger value of objective function, then schedule which folds high weight tasks (very important) and longer time of execute.

Is proposed modified this form of objective function to eliminate that imperfection. It depends on addition to the first of criterions fj_1 (eq.1), a coefficient of task relative size kw_i (eq.4). This is represented by the product of execute relative time and relative competence. In notation of knapsack problem it's represented by the size of pack (height × width) in relation to knapsack's size where is placed in.

$$kw_i = t_{wzgl} \cdot k_{wzgl} = \frac{t_i}{T_S} \cdot \frac{k_i}{k_o} \tag{4}$$

where:

kw_i – relative size coefficient,
k_i – necessary competence to execute the task,
k_o – operator competence.

Objective function follows as:

$$Fj = \max \sum_{j=1}^{o} \left(sk \cdot \rho_1 \cdot \sum_{i=1}^{n} wg_i kw_i x_{ij} + (1-\rho_1) \frac{\sum_{i=1}^{n} t_i x_{ij}}{T_S} \right) \tag{5}$$

Decision variables and constrains

The decision variables in that formulated problem are the facts whether the tasks will go into consider schedule, or not. It is defined by indicator x_{ij}, which can accept one of two values 1 or 0 (eq.6). The decision-maker decides, which of tasks the foundling oneself in created schedule as well as, in what the orders should be realized.

$$x_{ij} = \begin{cases} 1 & \textit{if the task go into the schedule} \\ 0 & \textit{if the task is skip in schedule} \end{cases} \tag{6}$$

Four of principle constrains appear in such approach:

- the total of execute time for every of operators can not be larger than available time T_S:

$$\sum_{i=1}^{n} t_i x_{ij} \le T_S \qquad \forall i, \forall j : i \in Z_Z, j \in Z_O \tag{7}$$

  where:

  Z_Z – tasks collection,
  Z_O –operators collection.

- the task attached only once in schedule:

$$\sum_{i=1}^{m} x_{ij} \in H \le 1 \qquad \forall i \in Z_Z \tag{8}$$

  $x_{ij} \in H$ – the task *i* belongs in schedule *H*.

- the way of assign the tasks to individual operator is definite as following:

$$k(o_p) \le k(o_j) \qquad \forall x_{ij} \in H \tag{9}$$

  where:

  $k(o_j)$ – competence of operator, who is assigned the task in schedule ***H***,
  $k(o_p)$ – competence of operator, who has attached the task in duties.

The task can be assign to operator o_j in schedule who has a competence equal or larger then operator o_p who has it attached in duties.

- every of tasks could be executed by once of operators only,

$$\sum_{i=1}^{m} o_n\left(x_{ij}\right) \leq 1 \qquad \forall n \in Z_O \tag{10}$$

2.5. Choice of computational method to solution of problem

To solution of task scheduling in E.R. optimization problem was chosen the indirect review method called also the review with recurrences method. Cause of simplicity, contains basic steps almost all review methods and simultaneously is the one of the quickest among them [6].

The review with recurrences algorithm finds the solution of the problem by systematic searching whole space of acceptable solutions. It uses the representation of the space solutions in the figure of tree. In this every of decision variables are represented by tree level. Every of tree nodes can have two branches only, what accept value 0 or 1 only (fig.2a). The method depends on searching of solutions space through creating first the left branch. When search after left side achieves finish, is created right branch and search moves on this side. Such method of creating tree's nodes is very thrifty and despite of this does not skip any node, which would lead to better solution.

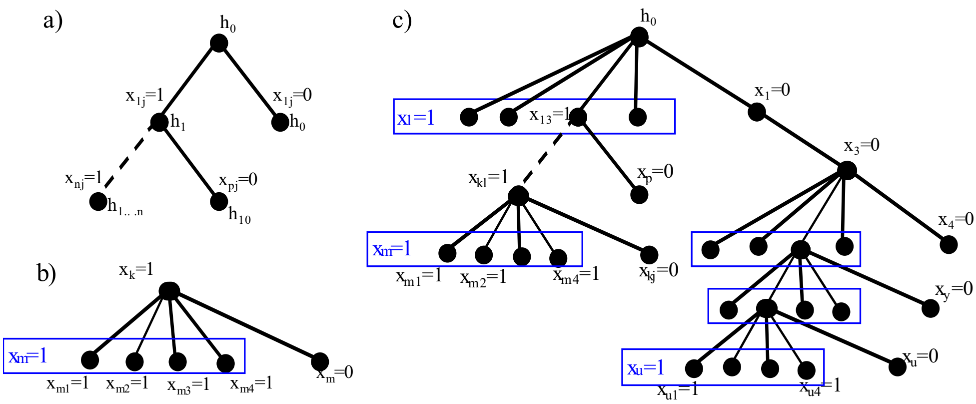

Fig. 2. Modify method for searching solutions tree for multi-knapsack problem

In Engine Room we have to assign tasks to large number of operators therefore also introduced algorithm requires modification. To next considerations was accepted the most often situation in E.R. - four operators who are assigned tasks.

Spread of operators number (four) causes, that every task, if the constrains permit, could be assign to every of four operators. So, in a situation, when the task parameter x_{ij} admits value 1, we have four additional solution variants (fig.2b).

The searching of the possibility solutions for many operators is started like for one. The assigned is begun from operator who possesses the smallest competences to execute the task. If any of constrains do not permit to assign it to him, the task is tried to assign next of operator, who has one larger competence from among remaining operators'.

The assigning the task to operator gives the new admissible solution. For this is checked the value of the objective function (sum of tasks' weights for every of operators) and compared with the best result obtain to this time. If the appointed value of objective function is larger then exists so far, the new value and the solution (Schedule) are stored as the best.

3. Computer application of tasks scheduling in engine room

In order to check presented the mathematical model of this problem and way to solution of decision-problem what meet chief engineer was implemented prototype of computer application.

On the figure 3 is shown, that interface of which consists the parameters, defined individual for users in tasks scheduling before starting the process of search the problem solution.

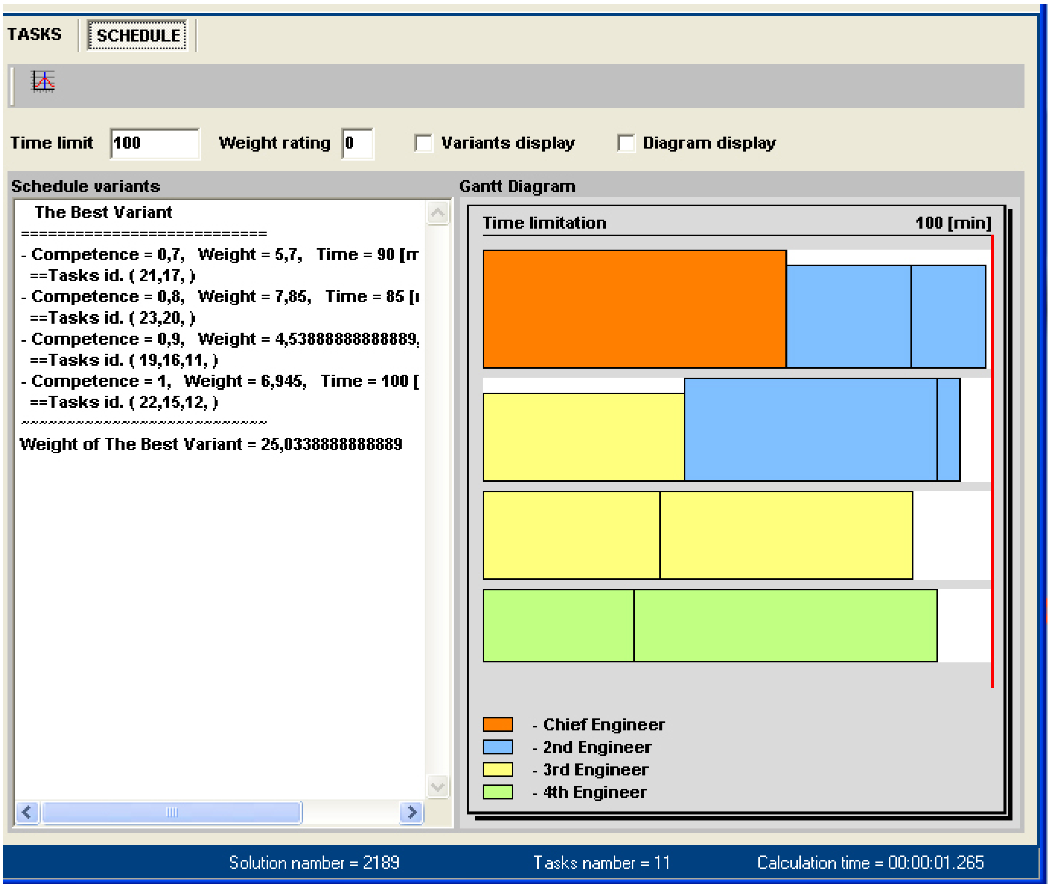

Fig. 3. Fragment of application interface representative the best solution and Gantt's diagram of assigning few operating tasks optimization

The two fundamental for optimization process parameters it:

- "Limit time", that is the time, when the tasks have to execute (e.g.: time to leave the port, etc.),
- "Weight rating", that is weight criterions (parameter ρ in equations 3 and 5).

The main area of this interface is partite on two units. The best result is displayed in first "Schedule variants" of them. There are displayed the following information:

- there are displayed the assigned tasks, for checks correctness of working are displayed the identification number only,
- sum of the really tasks executed times for every of operator,
- sum of the task weights for every of operator,

the sum of weights for total schedule also, which is the coefficient of quality of the solution.

In the second "Gantt Diagram" are showed the visualizations of received results in form of Gantt's graphs for every of operators. Every of operators have appeared as e white "rectangle", which dimensions illustrate:

- available time (the length of rectangle),
- competence what possesses the operator (the height of rectangle).

In "State bar" being in bottom edge of interface, are displayed three additional information needed to analysis of received results: number of analyzed solutions, the number of analyzed tasks, the time of calculations what use the process to finding the best solution.

4. Conclusions

It is described the mathematical model of two-criterions optimization of operation tasks assign in Engine Room and the searching the best from among admissible solutions and in peculiarly:

- objective function consider the most essential element, what chief engineer makes allowance for during tasks scheduling, as: weight of task, competence every operators, the available time,
- defined elementary constrains, what appear during schedule of operational tasks in E.R.,
- the searching algorithm for four operators was chosen and modified,
- prototype of computer application what uses introduction mathematical model was implemented.

In the next works will be checked whether the objective function and constrains are sufficient for solution this problem. As well whether the accepted method of solution search will be sufficiently and fast to use in tasks scheduling in Engine Room.

References

[1] Kamiński, P., *Formulation objective function of the decision - making problem in ship power plant*, Materiały IV Konferencji Engineering design in integrated product development, Zielona Góra 2006.

[2] Kamiński, P., *Identyfikacja elementów problemu decyzyjnego zarządzania siłownią okrętową,* Materiały Konferencyjne - Polioptymalizacja i CAD, Mielno 2006.

[3] Kamiński, P., *Wybrane zagadnienia związane z zarządzaniem eksploatacją siłowni okrętowej*, Materiały Konferencyjne – Projektowanie i zarządzanie realizacją produkcji, Zielona Góra 2005.

[4] Kamiński, P., Tarełko, W., Podsiadło, A. *Źródła informacji wykorzystywane w systemie wspomagającym zarządzanie siłownia okrętową*, XXV Międzynarodowe Sympozjum Siłowni Okrętowych, Gdańsk 2004.

[5] McDiarmid, C.J.H., *The Solution of a Timetabling Problem*, Journal Institute Mathematics Applications 9, s. 23-34, 1972.

[6] Sysło, M.M., Doe, N., Kowalik, J.S., *Algorytmy optymalizacji dyskretnej*, PWN, Warszawa 1995.

[7] Szwed, C., Toczyłowski, E., *Optymalizacja rozdziału zasobów lokalowych w warunkach elastycznego studiowania*, Materiały Konferencyjne Polioptymalizacja i CAD, Mielno 2000.

[8] Tarnowski, W., *Symulacja i optymalizacja w MATLAB'ie*, Wydawnictwo WSM, Gdynia 2001.

INCREASE IN THE FUEL TEMPERATURE OF AN INJECTOR BODY OF A SELF-IGNITION ENGINE IN THE THERMAL-CATALYTIC FUEL TREATMENT

Oleh Klyus

Maritime University of Szczecin
ul. Wały Chrobrego 1/2, 70-500 Szczecin, Poland
tel.: +48 91 4809425, fax: +48 91 4809575
e-mail: olegklus@o2.pl

Abstract

This article presents an analysis of thermodynamic processes taking place in the fuel nozzle holder equipped with a fuel preheating system containing catalytic material. The analysis results show that it is possible to raise the effectiveness of self-ignition engine operation and, at the same time, to reduce the emission of toxic compounds into the atmosphere.

Keywords: *self-ignition engine, fuel injector, catalytic and thermal fuel treatment*

1. Introduction

The reduction of toxic compound emission into the atmosphere and decreasing fuel consumption are at present basic directions in combustion engine developments. Designs of engines and their systems have reached limits in terms of working process parameters and possible control of these processes. However, future standards of exhaust gas toxicity and fuel consumption are expected to be even stricter. Research done at the Institute of Technical Operation of Marine Power Plants, Maritime University of Szczecin (4T12D06029) also includes the application of methods which will make it possible to reduce exhaust gas toxicity and fuel consumption in self ignition piston engines without introducing significant changes in the construction of fuel injectors. To this end preliminary thermal and catalytic fuel treatment may be applied directly before the fuel is sprayed into the combustion chamber.

2. Catalytic fuel treatment

It is known that obtaining better operational parameters of internal combustion engines is possible by increasing the speed of initial chemical reactions in fuel in the process of ignition lag. These reactions in internal combustion engines are characterized by dehydrogenation and can be accelerated by contacting fuel with catalytic material (mostly metals belonging to the platinum group) [1]. The process can be made possible in the nozzle holder by allowing contact between the fuel flowing through injector passages and catalytic material placed directly on the surface of fuel passages. Besides, in order to increase the contact area in injector passages additional elements can be put in, such as balls, wire or springs coated with a catalyst. It should be underlined that the catalyst action is accelerated at higher temperatures. Therefore, a new positive effect of enhancing the engine performance parameters can be gained by simultaneous action of catalytic material and increased fuel temperature.

3. Effect of temperature of injected fuel on the combustion process

A positive effect of injecting preheated fuel on the processes occurring in the combustion chamber of a self-ignition engine has been presented in works [1, 4, 6]. The following parameters have been observed to decrease: rate of pressure increase and maximum combustion pressures in cylinders, exhaust gas smoke content , as well as unit fuel consumption.

As fuel temperature increases, reactions of fuel cracking in the combustion chamber accelerate; besides, due to shortened fuel heating time, the ignition lag period is reduced. In addition, injecting preheated fuel into the combustion chamber causes the intensity of toxic compound emission to lower. This is explained by the fact that the toxic emission level in exhaust gases, particularly soot, is connected with the process of cooling off the flame by cold fuel injected into the combustion chamber. Another reason for soot content decrease is the increased combustion rate, which is equivalent with the reduction of heated fuel combustion period, so that the time of possible burning of soot in the engine chamber increases.

However, fuel preheating systems have not been used in internal combustion engines so far. This can be explained mostly by the fact that fuel in these systems is heated before the injection pump in high pressure pipes or directly before the injector. This changes working conditions of those elements through which preheated fuel flows, thus the working conditions of precision elements change, because the clearances are changed and so does the durability of construction materials [7]. This leads to accelerated wear of injection system components as well as engine elements and nodes. However, the most negative effect on engine performance characteristics in such fuel heating system turns out to occur after a change in fuel injection characteristics [3, 8].

The research [6] showed that the best effect from using preheated fuel can be achieved when an engine works at power output up to 50% of its maximum power, where each load condition corresponds to a specific temperature of injected fuel. Heating of fuel leads to changes in its thermodynamic parameters, which in fact means that physical properties of the fuel are changed: density, viscosity, surface tension decrease; compressibility, volatility and other properties increase; as a result:

- lowered viscosity and surface tension enhance the quality of atomizing;
- increased volatility is basically connected with load changes, i.e. engine thermal conditions;
- increased compressibility at higher temperature results in the reduction of pressure waves in pipes, which combined with increasing leaks in discharging steam changes the characteristic of fuel injection, increase of injection lag period and fuel injection time.

Enhancing the effectiveness of engine performance at low loads by heating the fuel can be explained by the fact that the quality of atomization and combustion is of major importance, whereas worsened operating parameters when loads are higher than 50% are due to the major role of the injection lag and increase in fuel injection time.

It has been found [6] that the variation of heated fuel temperature which results in better effectiveness of diesel engines ranges from 40 to 60 °C (Fig. 1).

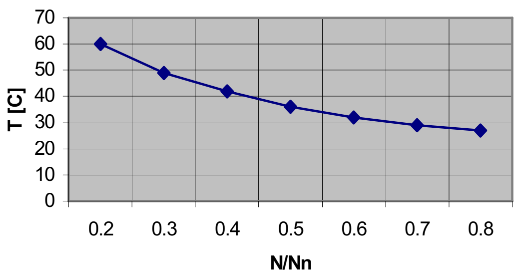

Fig. 1. Recommended change in temperature of injected fuel dependent on combustion engine load [6]

4. Heating fuel in the nozzle holder

From the point of view of heating fuel, it is better to use a system that would be placed outside the area of precision elements, which is achieved in the case of heating fuel directly in the nozzle holder (Fig.2) [3,7].

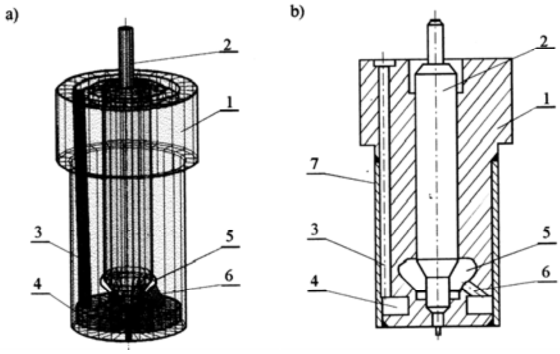

Fig. 2. Diagram (a) and cross-section (b) of an injector with cooling-heating fuel system 1 – nozzle holder, 2 – needle, 3 – inlet passage, 4 – ring passage, 5 – under-needle space, 6 – connecting passage, 7 – external skirt

Heating fuel is possible when one fuel feeding passage is joined with a ring passage made in the lower part of the holder and with outlet from that ring passage to the under-needle space. As a result of such modifications, fuel flows into the ring passage where it absorbs heat from the hottest parts of the holder cooling it at the same time. Fuel then goes to the under-needle space and due to increased pressure it raises the needle as it happens during the normal process of fuel injection.

In order to calculate the quantity of fuel flowing through the cooling passages of the atomizer the general Bernoulli's equation for fluid flow was used [5]. Considering two cross-sections of the injector at the passage 3 inlet and passage 6 outlet (Fig. 2) we can write:

$$\frac{v_1^2}{2g}+\frac{p_1}{\gamma}=\frac{v_2^2}{2g}+\frac{p_2}{\gamma}, \tag{1}$$

where:

g – gravitational acceleration,
v_1, v_2, p_1, p_2 – velocity and pressure of fuel at the inlet (1) and outlet (2) of passages,
γ - fuel specific gravity.

After a transformation, we obtain:

$$\frac{\Delta p}{\gamma}=\frac{v_2^2-v_1^2}{2g}. \tag{2}$$

The following condition has to be satisfied for the fuel to flow through cooling passages of the atomizer:

$$\frac{\Delta p}{\gamma}=\sum h_{str}, \tag{3}$$

where: $\sum h_{str}$ – sum of linear and local losses of flow through cooling passages.

Comparing the right-hand sides of the equations 2 and 3 we can calculate the quantity of fuel flowing through the circuit of cooling passages.

Knowing the fuel flow rate in cooling passages of the injector we can calculate the change in temperature of injected fuel. To do this, the finite elements method was used as it allows to determine the temperature in computational nodes and formulas defining the absorption of heat in a heat exchanger:

$$t_2 = T - \left(T - t_1\right)e^{-\frac{kF}{Qc}}, \tag{4}$$

where:

t_1 and t_2 – fluid temperatures at the inlet and outlet from the exchanger;
T – heating surface temperature F,
k – convection coefficient,
Q – fluid flow intensity,
c – fluid specific heat.

To determine the temperature of the atomizer body (heat exchanger) the finite elements method was used, assuming that the temperature at the combustion chamber corresponds to a specific engine load. For a pintle injector of a DN0SD type the temperature distribution is presented in Fig. 3.

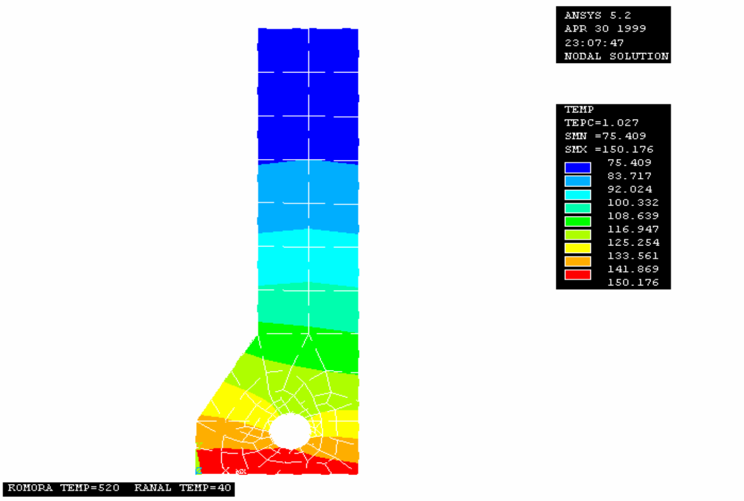

Fig.3. Distribution of temperatures in an injector element for the temperature in the fuel passage T=40°C and the temperature in the combustion chamber T_{ks}=520°C

Analytical research aiming at the determination of quantities of fuel flowing through passages and the changes in its temperature in the nozzle holder was done in two series: at continuous fuel flow and taking into account fuel stoppage in injector passages due to cyclical character of the injection process. The variable parameters were the dose of fuel injected and the temperature of heat exchanger (i.e. nozzle holder), depending on the engine load (temperature in the combustion chamber).

The results of this investigation which made use of the equations (1) – (4) are presented in the form of temperature field in Fig. 4. It should be emphasized that the recommended temperature change of injected fuel aimed at obtaining the most effective indicators of engine performance (Fig. 1) is located in that field.

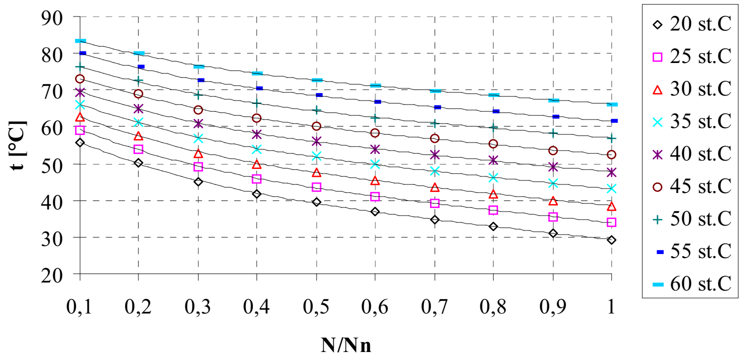

Fig. 4. Changes in the temperature of injected fuel dependent on fuel temperature at the inlet to nozzle holder passages

Conclusions

The following conclusions can be drawn from the analysis:

- application of a cooling system in the fuel injector using injected fuel allows to reduce the working temperature of the precision elements:- needle-nozzle holder body, and at the same time increasing the temperature of injected fuel;
- heating fuel fed into the atomizer eliminates a number of negative phenomena connected with heated fuel flow through the fuel devices as in this solution the heating of fuel takes place directly before the injection of fuel into the combustion chamber;
- up to 50% of the fuel injected into the engine combustion chamber can flow through the cooling passages;
- the temperature of fuel used for the heating of injector cooling passages can range from 40 °C to 60 °C, recommended to improve the effectiveness of engine performance in its working conditions nor higher than 50 % of the maximum power output.

Literature

[1] Гаврилов, Б.Г., *Химизм предпламенных процессов в двигателях,* Изд. Ленинградского университета, 1970, 98с..

[2] Klyus, O., *Termiczna i katalityczna obróbka paliwa w silnikach z zapłonem samoczynnym,* Wyd. KGTU, Kaliningrad, 2006, 154s.

[3] Klyus, O., Niziński, S., Wierzbicki, S., *Obniżenie temperatury rozpylaczy silników z zapłonem samoczynnym,* Sil-Woj'95, Materiały konferencyjne, Warszawa 1995, s. 164-171.

[4] Kowalczyk, M., *Wpływ temperatury wtryskiwanego paliwa na wybrane wskaźniki procesu cieplnego silnika wysokoprężnego,* Silniki spalinowe Nr.2/1975, 2. 14-19.

[5] Лышевский, А.С., *Системы питания дизелей,* Машиностроение, Москва 1981, 179с.

[6] Маркова, И.Б., Циулин, В.Н, *Повышение экономичности дизеля на долевых режимах,* Труды КТИРПиХ, Калининград, 1991, с. 79-97.

[7] Niziński, S., Klyus, O., Wierzbicki, S., *Sterowanie warunkami cieplnymi wtryskiwaczy,* Autoprogres'95, Materiały konferencyjne, Jachranka 1995, s. 98-107.

[8] Орлин, А.С., Круглов, М.Г., *Двигатели внутреннего сгорания.* Т 2, Машиностроение, Москва 1984, 297с.

UNIT EMISSION OF THE EXHAUST GAS COMPONENTS DETERMINED BY MEANS OF THE SIMPLIFICATION METHOD

Czesław Kolanek, Zbigniew Sroka, Wojciech Walkowiak

The Technical University of Wrocław
Wybrzeże Wyspiańskiego 27, 50-370 Wrocław, Poland
tel., fax.: +48 71 34 77 918
e-mail: czeslaw.kolanek@pwr.wroc.pl; zbigniew.sroka@pwr.wroc.pl; wojciech.walkowiak@pwr.wroc.pl

Summary

Toxicity of the combustion engines is determined by means of the procedures that result from their size group and appropriation, determining a measurement mode (a type of test) and a calculation method, and lead to the determination of the so-called unit emissions of the particular components. The paper aims at presenting the differences in the unit emission value determined for a compression-ignition engine complying with the full procedure which includes the corrections resulting from a state of atmosphere and a type of the component observed, and are calculated in a simplified way omitting corrections.

***Key words**: combustion engines, toxicity, unit emission, and calculations*

1. Introduction

Nowadays, the research on the exhaust gas emissions is carried out based on the rules presented in the Polish standard: Measurement of the exhaust gas emissions; Measurement of emissions of the gas components and stable particles in a research station (PN-EN ISO 8178-1), which is identical with EN ISO 8178-1:1996, and the standard PN-EN ISO 8178-2: Measurement of the exhaust gas emissions; Measurement of emissions of the gas components and stable particles at an installation place.

In order to assess the possibility of simplification of the calculation procedures, the calculations have been performed which have enabled estimation of the differences resulting from the assumed different types of procedure.

2. Research

The results of the research on a propulsion motor of a river pusher-tug have been assumed as the basis. The research has been realized according to a cycle of an E3 type (heavy-duty motors intended for ship drive; PN-EN ISO 8178-4: Measurement of the exhaust gas emissions; Research cycles of the engines of different applications).

The research cycle phases and weight coefficients have been specified in Table 1.

Tab. 1 Research cycle components

Phase number	1	2	3	4
Rotational speed, %	100	91	80	63
Power, %	100	75	50	25
Weight coefficient	0.2	0.5	0.15	0.15

The permissible deviations of the instruments intended for measurement of the motor operation parameters have been specified in Table 2.

Tab. 2 Permissible deviations of the measuring instruments

Specification	Permissible deviation	
	acc. to 8178-1	acc. to 8178-2
Motor rotational speed	± 2 %	± 2 %
Torque	± 2 %	± 5 %
Power	± 2 %	± 5 %
Fuel consumption	± 2 %	± 4 %
Expenditure of air	± 2 %	± 5 %

The standard PN-EN ISO 8178-2 determines accuracy of determination of the gas component emissions provided in g/kWh at a level of ± 9 %.
The conditions and results of the research and calculations have been specified in Table 3.

3. Result analysis

Fuel typical coefficient for the calculation of F_{FW} wet exhaust gas flow

Pursuant to Appendix A to the Standard 8178-1, the F_{FW} coefficient can be calculated from the following equation (A.51):

$$FFW = 0.05557 \text{ x } ALF - 0.00011 \text{ x } BET - 0.00017 \text{ x } GAM + \\ + 0.0080055 \text{ x } DEL + 0.006998 \text{ x } EPS$$

where:

ALF – H content in fuel, % (m/m); for diesel oil (ON) H = 13.6 (Table 7)
BET – C content in fuel, % (m/m); for ON: C = 86.2
GAM – S content in fuel, % (m/m); for ON: S = 0.17
DEL – N content in fuel, % (m/m); for ON: N = data missing
EPS – O content in fuel, % (m/m); for ON: O = 0,
or to assume a value of 0.749 (PN-EN ISO 8178-1 Table. 7).

The value calculated according to the formula (A.51), with an assumption that DEL = 0, amounts to FFW = 0.746 (for three decimal places).
Simplification of the formula (A.51) to the following form:
FFW = 0.0556 x ALF – 0.0001 x BET – 0.0002 x GAM + 0.0080 x DEL + 0.0070 x EPS
gives a value of FFW' = 0.748.
A relative error of the value calculated in such a way (0.748) compared to the value 0.749 amounts to 0.13 %, and compared to the value 0.746 – 0.27 %, respectively.

Humidity correction coefficient for NO_x, K_{HDIES}

A humidity correction coefficient for NO_x is described in chapter 13.3 of the Standard.
A value of the coefficient for the reference humidity amounting to 10.71 g/kg proposed by the standard originator amounts to K_{HDIES} = 0.9914**.**

Tab. 3 Conditions and results of the research

Phase number	1	2	3	4	Remarks
Rotational speed, %	100	91	80	63	
Maximum power for a given motor rotational speed P_m, kW	147	110	74	37	
Volumetric intensity of wet inlet air flow V_{AIRW}, m^3/h	599.4	547.5	479.5	379.6	
Volumetric intensity of wet exhaust gas flow V_{EXHW}, m^3/h	620.1	564.5	487.9	384.5	
Mass intensity of fuel flow G_{FUEL}, kg/h	27.7	22.8	11.2	6.5	
Typical fuel coefficient for the calculation of wet exhaust gas flow F_{FW}, 1	0.749	0.749	0.749	0.749	
CO concentration $conc_{CO}$, %	0.44	0.14	0.10	0.085	
NO_x concentration $conc_{NOx}$, %	0.088	0.098	0.106	0.098	
Atmospheric absolute pressure p_B, kPa					101.3
Steam saturation pressure in the inlet air p_a, kPa					3.166
Absolute temperature of the inlet air T_a, K					298
Relative humidity of the inlet air R_a, %					50
Humidity correction coefficient for NO_x, K_{HDIES}, 1					0.9914
Mass intensity of CO emissions $M_{GAS\ CO}$, kg/h	3411	988	610	409	
Mass intensity of NO_x emissions $M_{GAS\ NOx}$, kg/h	1120	1136	1062	774	
w coefficient for CO for NO_x	 0.00125 0.002053	 0.00125 0.002053	 0.00125 0.002053	 0.00125 0.002053	
CO unit emission GAS_{CO}, g/kWh	-	-	-	-	11.96
NO_x unit emission GAS_{NOx}, g/kWh	-	-	-	-	9.60
Accuracy, %					± 9

The permitted possibility of inclusion of the measurement conditions (for the presented example, the value of the reference humidity amounts to 9.88 g/kg) results in changing to the value of K'_{HDIES} = 1.0007.

The relative error for the suggested value of K_{HDIES} = 1

compared to K'_{HDIES} = 1.0007 amounts to 0.07 %

and, compared to K_{HDIES} = 0.9914 amounts to 0.86 %.

Thus, K_{HDIES} = 1 can be assumed, which means resignation from such a coefficient.

‘w’ correction coefficient

The ‘w’ correction coefficient amounts, respectively, to:

CO: w = 0.00125;

NO_x: w = 0.002053.

The suggested ‘rounded’ ‘w’ values and the corresponding relative error amount to:

CO: w’ = 0.0013; error 4 %,

NO_x: w’ = 0.0021; error 2.3 %.

The permissible deviations of the instruments intended for measurement of the motor operation parameters have been specified in Table 4.

Tab. 4 Permissible deviations of the measuring instruments

Item	Specification	Permissible deviation referred to maximum motor values
1	Motor rotational speed	± 2
2	Torque	± 5
3	Power	± 5
4	Fuel consumption	Diesel oil: ± 4
5	Expenditure of air	± 5
6	Component concentration	± 5

Assuming an unfavourable coincidence, the calculations of the unit emission for the permissible values of the measurement instruments have been carried out.. Their impact on the unit emission values has been provided in Table 5.

Tab. 5 Impact of the deviations on the unit emission values

Item	Specification	Deviation, %	Unit emission change, %	
			CO	NO_x
	Power	- 5	+ 2.04	+ 2.04
	Fuel consumption	+ 4	+ 2.16	+ 2.15
	Expenditure of air	+5	+ 7.11	+ 7.12
	Component concentration	+5	+ 12.47	+ 12.47

In the presented situation, the maximum deviation of the determined unit emission exceeds 12.4 % at an accuracy, assumed pursuant to the standard (or permissible dispersion) at a level of 9 %.

4. Conclusions

1. The maximum deviation of the determined unit emission in g/kWh exceeds 12.4 %.
2. Determined by the standard PN-EN ISO 8178-2, the accuracy of determination of the gas component emissions provided in g/kWh, at the level of ± 9 % is insufficient.
3. In order to make the unit emission determination procedures more user-friendly, they can be simplified through reduction of the significant decimal places in the humidity correction coefficient or, alternatively, through assuming the value of 1 for the coefficient and reduction of the significant decimal places in the ‘w’ correction coefficient.

Bibliography

[1] PN-EN ISO 8178-1:1999 Piston combustion engines -- Exhaust gas emission measurement -- Measurement of emissions of the gas components and stable particles in a research station

[2] PN-EN ISO 8178-2:1999 Piston combustion engines -- Exhaust gas emission measurement -- Measurement of emissions of the gas components and stable particles at an installation place.

[3] PN-EN ISO 8178-4:1999 Piston combustion engines -- Exhaust gas emission measurement -- Research cycles of the engines of different applications.

[4] PN-EN ISO 8178-5:2000 Piston combustion engines -- Exhaust gas emission measurement -- Research fuels.

[5] PN-EN ISO 8178-6:2003 Piston combustion engines -- Exhaust gas emission measurement -- Part 6: Report on the research and measurement results.

[6] PN-ISO 8178-10:2005 Piston combustion engines -- Exhaust gas emission measurement -- Part 10: Research cycles and procedures of the operational measurements of exhaust gas smokiness of the compression-ignition engines which operate in the undetermined conditions.

[7] PN-ISO 8178-3:1997 Piston combustion engines -- Exhaust gas emission measurement – Definitions and methods of the exhaust gas smokiness measurement in the determined operational conditions.

[8] PN-ISO 8178-7:2002 Piston combustion engines -- Exhaust gas emission measurement -- Part 7: Determination of the engine family.

[9] PN-ISO 8178-8:2002 Piston combustion engines -- Exhaust gas emission measurement -- Part 8: Determination of the engine group.

[10] PN-ISO 8178-9:2005 Piston combustion engines -- Exhaust gas emission measurement -- Part 9: Research cycles and procedures of the exhaust gas smokiness measurements for the compression-ignition engines which operate in the undetermined conditions in a research station.

THE INFLUENCE OF SOME SELECTED PARAMETERS ON THE THERMODYNAMIC CHARACTERISTICS OF A CHP PLANT WITH A GAS TURBINE

Janusz Kotowicz[1], **Tadeusz Chmielniak**[2]

Silesian University of Technology
ul. Konarskiego 18, 44-101 Gliwice, Poland
tel.: +48 32 2371368, fax: +48 32 2372680
[1]*e-mail: janusz.kotowicz@polsl.pl*
[2]*e-mail: tadeusz.chmielniak@polsl.pl*

Abstract

The paper presents ways of determining the thermodynamic characteristics of a CHP plant with a gas turbine. Special attention has been paid to the average annual efficiency of transforming the chemical energy of fuel into electricity and heat (the so-called Energy Utility Factor – EUF) and Primary Energy Savings (PES). Two different systems were analyzed, viz. the installation of a gas turbine with a waste-heat boiler and a heat and power generating plant. Concerning the former one the influence of the parameters of steam (temperature and pressure) generated in the waste-heat boiler on the values of PES and EUF was determined. Concerning the latter one, the methods of investigating the effect of the thermal power of heat exchangers on the characteristics have been presented. This will facilitate the proper choice of heat exchangers.

Keywords: *CHP plant, heat and power generating plants, thermodynamic characteristics, primary energy saving*

1. Introduction

The application of gas turbines in CHP plants contributes to:

a) a decreased noxious effect of these installations on the environment, mainly thanks to
- the elimination of the emission of SO_2 and dust;
- an essential restriction of CO_2 and NO_X emission;
- reduced losses of water,

b) a more effective consumption of the chemical energy of fuel associated with an increased efficiency of generating electricity and heat,

c) decreased capital costs and a shorter time of constructing the required installations,

d) a shorter starting time from all states (cold, warm and hot).

Small and middle-sized installations of CHP plants with gas turbines are nowadays an important alternative for bigger units to meet the demand for heat and electricity. Thanks to the advantages mentioned above the number of such systems increases constantly, particularly in developed countries. New installations replace mainly old coal-fired boiler houses. Their final technological structures as well as the way and scope of automation are determined basing on the kind and number of consumers, and also on special requirements of the users.

More and more often, particularly in the course of the recent ten years, in Poland disused heat-generating units of medium and large power, which do not come up to the standards of environment protection, are being replaced by gas-and-steam systems. Similarly as in the case of smaller installations, the aforesaid advantages and economical analyses are of decisive importance.

2. Fundamental work indices in the thermodynamic assessment of CHP plants

An important index in the assessment of the work of the analyzed systems is the instantaneous gross watt-hour efficiency of the CHP plant, determined also as the unit capacity of the chemical energy of fuel, expressed by the formula:

$$\eta_C = \frac{N_{el} + Q}{m_{1p} W_d} \tag{1}$$

where:

N_{el} – power rating of the system, Q – flux of heat emitted by the system, m_p – flux of fuel, W_d – net calorific value of the fuel.

Having at our disposal the relations N_{el}, Q = f(τ) (where τ - time), and knowing the annual time of generating electrical energy (T_{el}) and heat (T_c), we can determine the production of electricity (E_{el}) and heat $(Q_g)_r$ per year:

$$E_{el} = \int_0^{T_{el}} N_{el} d\tau \tag{2}$$

$$(Q)_r = \int_0^{T_C} Q d\tau \tag{3}$$

These quantities permit to determine the average efficiency of transformation of the chemical energy of fuel into electricity and heat:

$$\eta_{ecr} = \frac{(Q_g)_r + E_{el}}{B \cdot W_d} \tag{4}$$

The quantity $B \cdot W_d$ in this equation determines the yearly consumption of chemical energy of the fuel, basing on the known fuel flux (m_{1p})

$$B \cdot W_d = \int_0^{T_{el}} (m_{1p} W_d) d\tau \tag{5}$$

The quantity determined by means of equation (4) is also called Energy Utility Factor or energy efficiency of CHP. It may also be expressed as

$$\eta_{ecr} = \eta_{er} + \eta_{cr} \tag{6}$$

where:

$\eta_{er} = \frac{E_{el}}{BW_d}$ - average ampere-hour efficiency per year (the efficiency of the cogeneration of electric energy)

$\eta_{cr} = \frac{(Q_g)_r}{BW_d}$ - average annual efficiency of cogeneration of heat

The decree of the Minister of Economy, Labour and Social Policy of May 30th, 2003concernicg the scope of duties connected with the purchase of electricity and heat from renewable sources and its amendments of December 19th, 2004 obligate power stations to buy electrical energy cogenerated in compliance with $\eta_{ecr} \geq 70\,\%$ [6].

The energy efficiency of the considered installations is assessed taking also into account the instantaneous cogeneration coefficient

$$\sigma = \frac{N_{el}}{Q} \tag{7}$$

Another coefficient is the Primary Energy Savings

$$PES = 1 - \frac{1}{\frac{\eta_{er}}{\eta_e^{Ref}} - \frac{\eta_{cr}}{\eta_c^{Ref}}} \tag{8}$$

where:

$\eta_e^{Ref}, \eta_c^{Ref}$ - efficiency reference value for separate electricity and heat production.

Equation (7) is based on the definition of relative savings of the chemical energy of fuel, attained by cogeneration, compared with the consumption of the chemical energy of the same kind of fuel in separate establishments (power station and heating plant).

The Directive 2004/8/WE EU introduces the term "high-efficiency cogeneration". If the value of PES is not lower than 10%, this term can be used.

It still remains an open question which part of the produced electrical energy will be considered to belong to the technology of high-efficiency cogeneration. The conditions of the classification of the total production of electricity as high-efficiency cogenerations have been quoted in the Directive 2004/8/WE: PES≥10% and η_{ecr}≥75% (80%).

3. The influence of the parameters of steam on the thermodynamic characteristics of a gas turbine installation with a waste-heat boiler

There are many possible structures of power stations (heat and power generating plants) with a gas turbine, e.g. [1], [2], [3]. The considerations discussed in the present paper concern merely installations of a gas turbine with a waste heat boiler and a gas and steam power station.

The installation of a gas turbine with a waste heat boiler presented in Fig.1 consists of a compressor (SP), the combustion chamber (KS), the gas turbine (TG), generator (G), air filter (F) and the waste heat boiler.

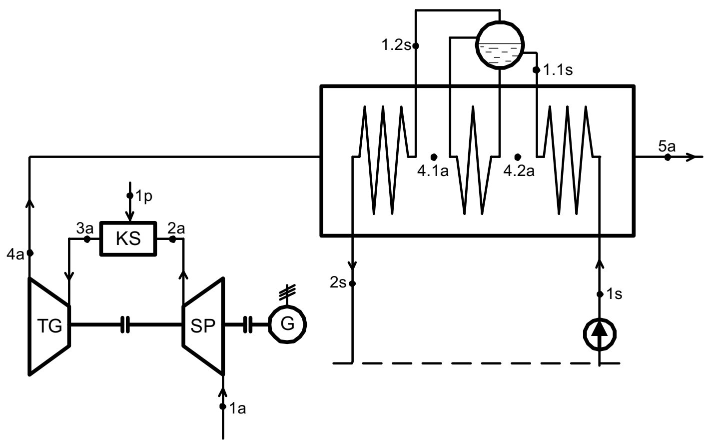

Fig.1. Thermal diagram of the investigated system

Under nominal conditions (i.e. ambient temperatures, respectively equal to t_{1a}=15°C and p_{1a}=101,325kPa) the parameters of the gas turbine are known, viz. power rating – 15,42 MW, pressure ratio – 11,11, flux fuel and combustion gases m_{1p}=0,968 kg/sec, m4a=51,74 kg/sec (the applied indices concern Fig.1) and temperatures of the combustion gases t_{3a}=1060°C and t_{4a}=544,7°C. In the waste heat boiler steam is generated. The temperature of the water feeding the boiler is known (t_{1s}=80°C), the pinch point (Δt_{pp}) and approach point (Δt_{ap}) are equal to 10K. The temperatures of the generated steam (t_{2s}, p_{2s}) affecting the fundamental operation characteristics of the power station have been determined. The results of calculations $\eta_c = f(t_{2s}, p_{2s})$ have been presented in Fig.2, the characteristics of $PES = f(t_{2s}, p_{2s})$ in Fig.3 (assuming that $\eta_e^{Ref} = 55\%$, $\eta_c^{Ref} = 90\%$). The flux of steam generated in the boiler results from the balances of the evaporator and superheater:

$$m_{2s} = \frac{c_p \{T_{4a} - [T_n(p_{2s}) + \Delta t_{pp}]\}}{h_{2s} + c_w \Delta t_{ap} - h'_{2s}} \tag{9}$$

where:

c_p, c_w - specific heat capacity of combustion gases and water, $T_n(p_{2s})$ - saturation temperature at the pressure p_{2s}, h_{2s}, h'_{2s} - enthalpy of steam and enthalpy of saturation.

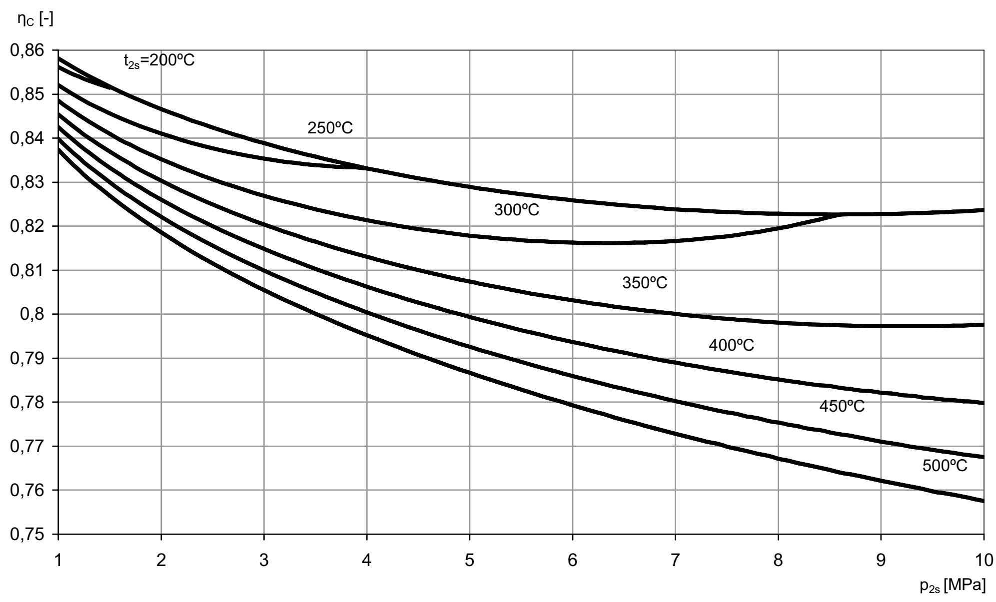

Fig.2. The relation $\eta_C = f(t_{2s}, p_{2s})$

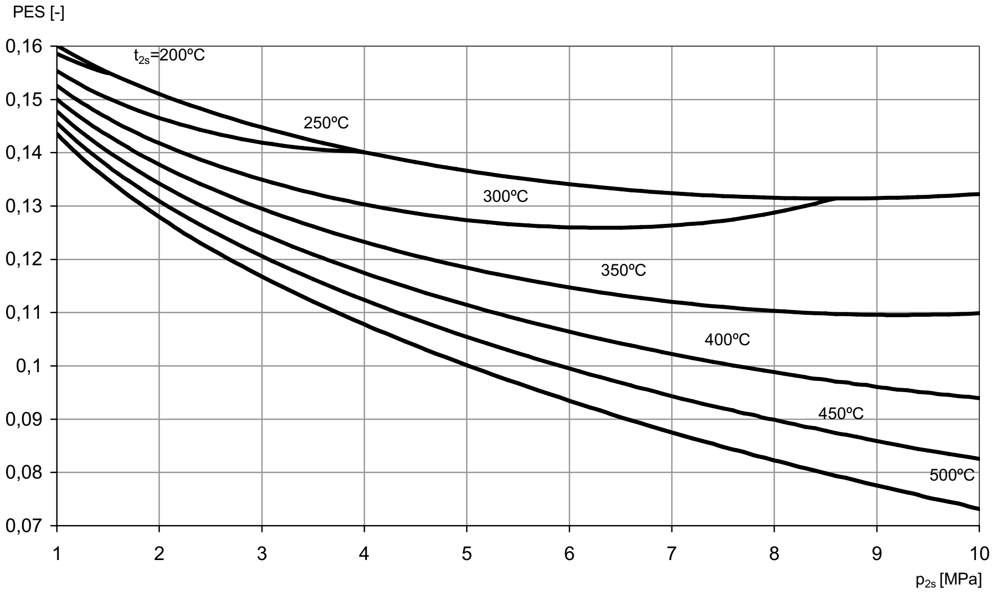

Fig.3. The relation $PES = f(t_{2s}, p_{2s})$

4. The influence of the thermal power of heat exchangers on the thermodynamic characteristics of gas and steam power stations

The analyzed system of a heat and power generating plant is to be seen in Fig.4, where also its characteristic points have been denoted. This system consists of a gas-steam unit and water boilers [8]. The gas-steam unit consists of a simple gas turbine and a double-pressure waste heat boiler with a condensing-extraction turbine. The thermodynamic parameters of the system are known in all its characteristic points under nominal conditions. The power rating of the system amounts to 235 MW (in compliance with ISO at t_{1a}=15°C). The ambient temperature (t_{1a}) influences substantially the fundamental parameters of the gas-steam unit and also the demand for heat. Hence, the necessity of modeling the operation of the system and its analysis in the entire range of changes of the ambient temperature. The gas turbine was modeled basing on the parameters of the industrial turbine Siemens V.94.2. The characteristic quantities describing this turbine are: the temperature at the outlet of the combustion chamber t_{3a}=1226°C, the compression ratio 11, the maximum isentropic efficiency of the air compressor 0,913 and the isentropic efficiency of the turbine 0,936, the efficiency of the combustion chamber 0,992, the ratio of the flux of air cooling the turbine to the flux at the inlet to the compressor 0,205. The double-pressure waste heat boiler generates steam with the following parameters: : $p_{3s(h)} = 8078\,kPa$, $t_{3s(h)} = 525^o C$ in the high-pressure part, $p_{3s(l)} = 540 kPa$, $t_{3s(l)} = 217^o C$ in the low-pressure part (the indices coincide with the denotations of the points in Fig.4). The minimum pinches of temperature (Δt_{pp}) in the boiler amount to 9 and 11K, respectively, for the high-pressure and low-pressure part. The steam generated in the boiler is passed to the turbine. The isentropic efficiencies of the high-pressure and low-pressure part of the steam engine amount to 0,905 and 0,8, respectively. The pressure in the condenser amounts to $p_{4s(l)} = 5\,kPa$, and in the deaerator to $p_{13s} = 130\,kPa$. The temperature of the feed water is $t_{WZ} = 76\,^o C$, thanks to the application of a preheater of the condensate. The applied heat exchanger consisted of two parts, one of which was being fed with steam from the controlled bleeder valve. The other part constitutes the last heating surface in the waste heat boiler. This permits to cool the combustion gases leaving the waste heat boiler to a temperature of $t_{5a} = 85\,^oC$. When the demand for heat exceeds the capacity of the heat exchanger, the connected water boilers are fired with coal.

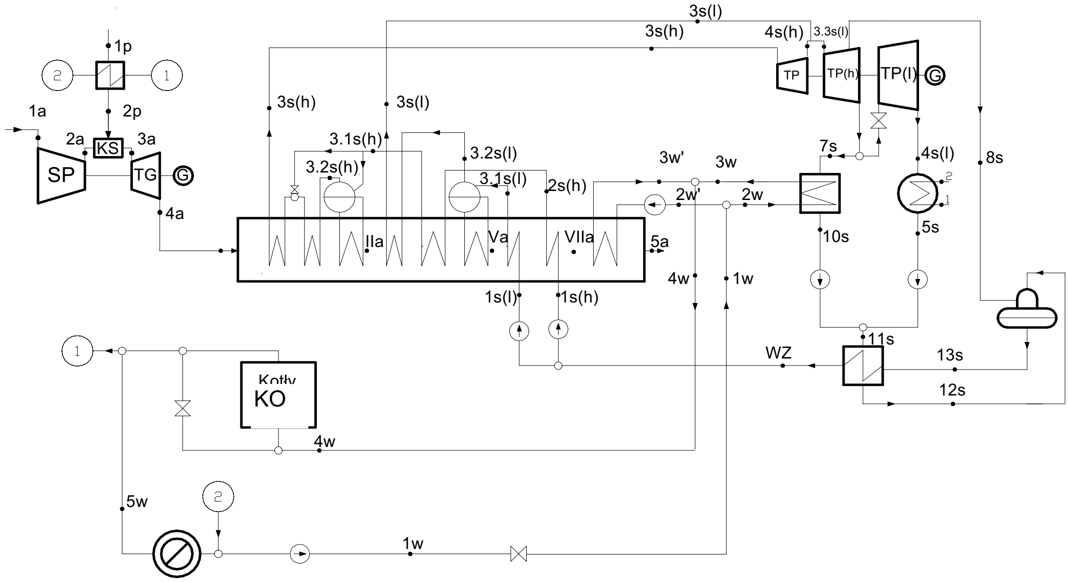

Fig.4. Thermal diagram of the investigated system (SP – compresor, KS – combustion chamber, G – generator, TP – steam turbine, KO – waste heat boiler)

The maximum demand for heat (at an ambient temperature of $t_{1a} = -20\,^oC$) has been assumed as $(Q_{ec})_{\max} = 400\ MW$, as is to be seen in Fig.5. Generally, a linear dependence of the flux of heat (Q_{ec}) on the ambient temperature is assumed during the heating season [9]. In other seasons the system operates with a constant thermal power of 10% of the maximum demand, producing warm water for household purposes. The gas-steam unit of the considered heat and power generating plant provides heat (Q_g) in compliance with the diagram of demand. Peak loads $(Q_{ec} - Q_g)$ are taken over by the water boiler with a power rating of $Q_{KW} = (Q_{ec})_{\max} - (Q_g)_{\max}$. Fig.5 presents the relation $Q_{ec} = f(t_{1a})$ based on the data quoted above. It also shows the relation $Q_g = f(t_{1a})$, assuming that most of the heating season the heat exchangers of the gas-steam unit operate with a constant calorific effect of $Q_g = (Q_g)_{\max} = 120\ MW$ (which may also be called design power rating of these heat exchangers). For the assumed process $Q_g = f(t_{1a})$ the power rating of the gas-steam unit is determined as $N_{el} = f\lfloor Q_g(t_{1a}), t_{1a}\rfloor$ [10].

Thermodynamic calculations were carried out making use of the programme GateCycle, changing the ambient temperature within the range -20°C ≤ t_{1a} ≤ 28°C in steps of 1°C. The thermodynamic parameters were determined in all the points denoted in the diagram, basing on which the quantities quoted below have been determined. Making use of the systematic diagram of the ambient temperature as a function of time, Fig.6 presents the determined dependences of the power rating of the unit and thermal power on time (τ). Knowing the time of operation of the gas-steam unit (T_{el}=T_c), the relation $N_{el}, Q_{ec}, Q_g = f(\tau)$ permits to determine the annual production of electricity (E_{el}) and heat $(Q_g)_r$.

The annual consumption of gaseous fuels is determined by means of the known or calculated characteristics of the flux of fuel depending on the ambient temperature $m_p = f(t_{1a})$ [8,10] and the systematic diagram of temperature, applying the relation [5].

These quantities will make it possible to determine also $\eta_{ecr,} \eta_{er,} \eta_{cr,} PES$, making use of the relations (4), (5) and (8). For this purpose the time of operation of the unit in the course of one year has been assumed to amount to 8200 hours.

Further on the same calculations were applied for changing values of *(Qg)max*.

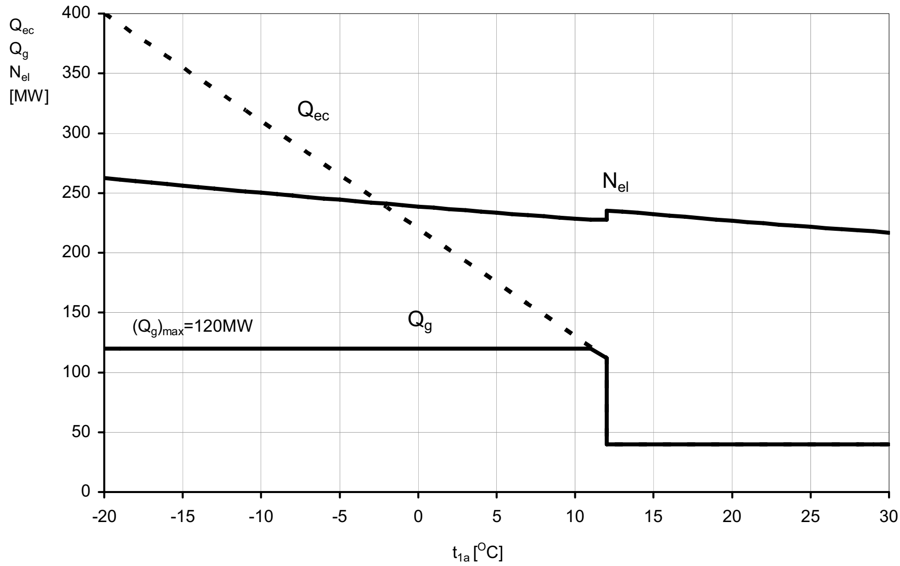

Fig.5. Dependence of the flux of heat generated in the heat and power generating plant (Q_{ec}) and the gas-steam unit (Q_g) and of the power rating of the unit (N_{el}) on t_{1a}

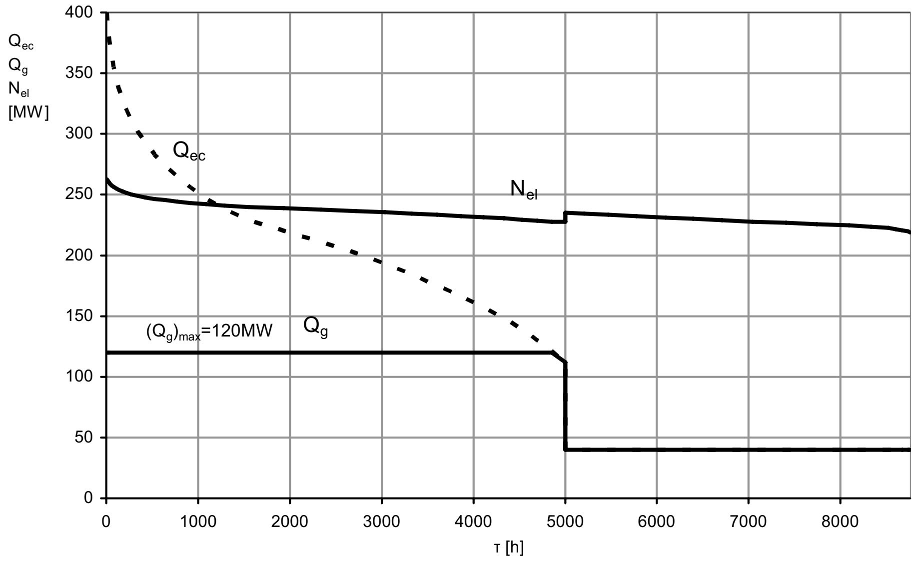

Fig.6. Dependence of the flux of heat generated in the heat and power generating plant (Q_{ec}) and the gas-steam unit (Q_g) and of the power rating of the unit (N_{el}) on the time of its occurrence τ

Calculations were carried out for $110\ MW \le (Q_g)_{max} \le 180\ MW$ in steps of 10 MW. The upper limit results from the required minimum value of the flux of steam flowing through the last stages of the turbine. It has been assumed that this flux constitutes 7% of the flux of steam flowing through the condenser in the case of carrying out merely condensation operations. The most important results of calculations have been gathered in the form of characteristics $\eta_{ecr,} \eta_{er,} PES = f\lfloor (Q_g)_{max} \rfloor$, as presented in Fig.7. In order to render it more perspicuous in the value of η_{er} were multiplied by 1,5.

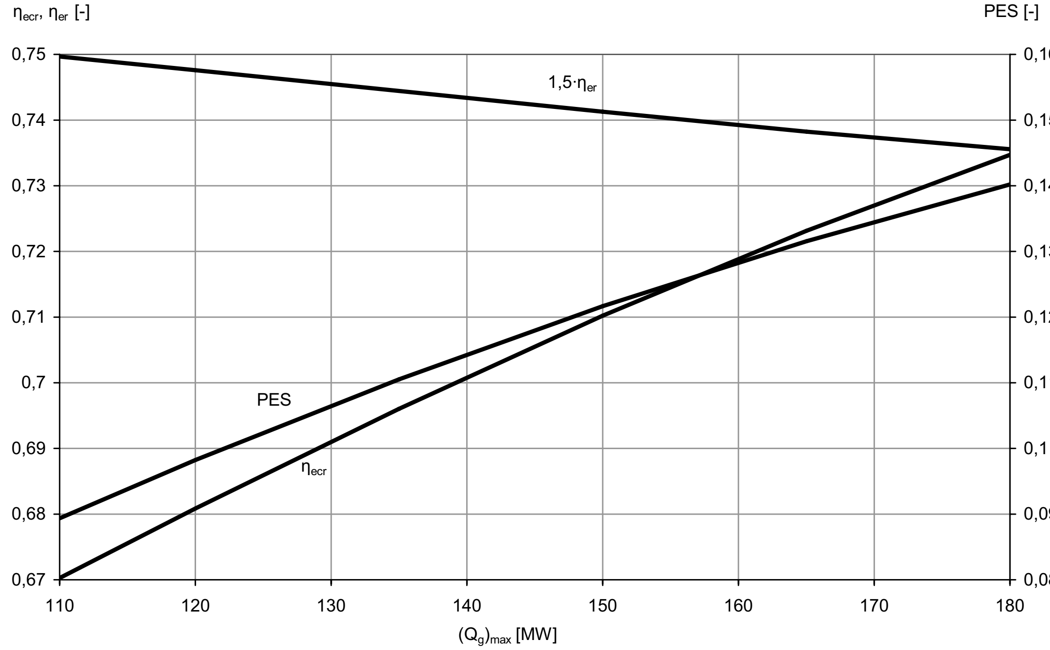

Fig.7. The relation $\eta_{c,} PES = f\lfloor (Q_g)_{max} \rfloor$

Summary

- The installation of a gas turbine with a waste heat boiler generating steam even with very high parameters attains an Energy Utility Factor (EUF) exceeding 80%. In the case of high parameters of the steam (e.g. at t_{2s}=500°C, p_{2s}=5MPa) the primary energy savings (PES) are lower than 10%.
- The indices EUF and PES concerning the investigated gas and steam power station increase with the growth of the thermal power of the heat exchangers $(Q_g)_{max}$. It is possible to choose such a $(Q_g)_{max}$ which would permit to attain PES≥10% and simultaneously also EUF>70%. In compliance with the Directive 2004/8/WE EU this is high-efficiency generation. Not all the generation of electricity, however, can be classified as high-efficiency generation, because EUF<80%. Therefore, attempts should be made to reduce the time of operation of the heat and power generating plant (T_{el}<8200 h/year) during the summer season.

References

[1] Chmielniak, T., *Energetistic Technologies*, Wydawnictwo Politechniki Śląskiej, Gliwice 2004.
[2] Marecki, J., *Combined Heat and Power*, WNT, Warszawa 1991. (in Polish)
[3] Zaporowski, B., *Analiza efektywności ekonomicznej skojarzonego wytwarzania energii elektrycznej i ciepła w elektrociepłowniach opalanych gazem ziemnym,* Rynek Energii nr 3, 2004
[4] Kotowicz, J., *Analyses of the Effectiveness of Some Selected Systems with a Gas Turbine,*. Zeszyty Naukowe Politechniki Śląskiej, Energetyka, z.138, Gliwice 2003. (in Polish)
[5] Chmielniak, T., Rusin, A., Czwiertnia, K., *Gas Turbine*. Ossolineum, Wrocław 2001. (in Polish)
[6] Kotowicz, J., Lepszy, S., *The Influence of Some Chosen Parameters on the Characteristics of Operation of Combined Cycles Heat and Power Plan,*. Rynek Energii nr 5, 2005. (in Polish)
[7] Szargut, J., Ziębik, A., *Fundamentals of Thermal Engineering*, PWN, Warszawa 2000. (in Polish)
[8] Kotowicz, J., Lepszy, S., The Influence of the Ambitne Temperature and the Heat of Fluxes on the Thermodynamic Characteristics of a CHP Plant, Inżynieria Chemiczna i Procesowa, nr 26, 2005. (in Polish)
[9] Malko, J., Augusiak, A., *Zagadnienia ekonomiczno-prawne w elektrociepłowniach,* Materiały konferencji „Skojarzone wytwarzanie ciepła i elektryczności". Wydane przez Polski Komitet Naukowo-Techniczny FSNT NOT ds. Gospodarki Energetycznej, Warszawa 2004.
[10] Zaporowski, B., *An Analysis of Energy Effectiveness of Electricity and Heat Cogeneration in Steam CHP Plants and Power Plants,* Archives of Energetics, Vol.XXXVI, 2006. (in Polish)
[11] Directive 2004/8/Ecof the European Parliment and of the Council of 11 February 2004 on the promotion of cogeneration based on useful heat demand in the internal energy market. Official Journal of the European Union, L52/50, 2004.
[12] Ziębik, A., *Combined Heat and Power in Poland According to the EU Directive on Promotion of Cogeneration,* Archives of thermodynamics, Vol.27, No 4, 2006.

The investigations presented in this paper were carried out within the frame of the research project No. 1410/T02/2006/30, sponsored by the Ministry of Education and Science.

HEAT TRANSFER MODEL FOR MARINE TWO STROKE ENGINE CYLINDER

Jerzy Kowalski
Wieslaw Tarelko

Gdynia Maritime University
ul. Morska 81-87, 81-225 Gdynia, Poland
tel.: +48 58 6901331
e-mail: jerzy95@am.gdynia.pl; tar@am.gdynia.pl

Abstract

This paper deals with modeling of heat flow through cylinder structural components of a marine two-stroke engine. Especially, we paid attention on simulating of temperature distribution for the wet cylinder liner. Multidimensional equations for the transient heat conduction with the Dirichlet and Fourier boundary conditions have been applied. In particular, we applied local values for the convective and radiative heat transfer coefficients using the Fourier boundary conditions determined in a space of cylinder volume and a cooling space of the cylinder. In order to determine the temperature distribution for considered spaces, we applied the radiosity method. Simulation results have been presented in the form of a temperature field for cylinder structural components depended on the crankshaft position angle. Application of the iterative calculation method for solving differential equations of energy balance allowed us for using software easy to get. We carried out all iterative computations using MS Excel spreadsheet. This way, we could decrease the simulation cost significantly.

Keywords: *marine engine, radiosity method, heat transfer, cylinder liner, thermal state,*

1. Introduction

Many researches show us that approximately 25 % energy produced by a combustion process is lost to the engine cooling system [1]. In order to increase the piston engine effectiveness, we should recognize the heat-releasing phenomenon from an engine cylinder volume. The knowledge makes it also possible to determine thermal stresses in particular elements of cylinder, as well as to model emission of toxic compounds contained in exhaust gas [2].

It is necessary to express that working features of piston engines, for example cyclic changes of combustion process parameters depended on crankshaft positions, can cause to additional difficulties in describing such a process in appropriate quantitative and qualitative way. Therefore, in order to identify the amount of heat lost, we should determine not only parameters occurring in the combustion chamber and cooling volume, but also geometrical features (sizes and shapes) of a cylinder liner. Additionally, it should be stressed that structural elements of engine cylinders are massive units with complex shapes and – in the case of marine engines – of large dimensions as they have to withstand large mechanical and thermal loads. For this reason, they are capable of accumulating a large amount of heat energy, which may cause detrimental effects such as thermal overloading which – in extreme cases – may result in engine failures.

The presented work has been aimed at developing a multi-dimensional model of heat conduction through structural elements of piston engine cylinder, with a use of one of the numerical methods of solving heat conduction problems, namely the radiosity method [3]. Such a model has been applied to visualize temperature distribution of the mentioned components for the laboratory two-stroke engine installed in Gdynia Maritime University.

2. Modeling of the heat transfer coefficient

The heat transfer rate from the combustion gases to the combustion chamber wall is usually expressed by the Newton's law [4]. It uses, *inter alia*, the term of the experimental heat transfer coefficient. Many models proposed various ways to obtain such a coefficient. They assumed that the heat flux is the same for all surfaces in construction elements of the engine combustion chamber.

First of them is Nusselt's model [5]. It assumed steady state heat transfer and shows dependence of amount of the heat transfer coefficient on the mean piston speed, the temperature difference, the cylinder gas pressure and a gas and the wall emissivity. Based on the same parameters, Sitkei [6] proposed a different experimental equation for four-stroke, indirect injection diesel engines. Eichelberg [5] proposed very simple model for two and four-stroke engines and Hohenberg studied the heat transfer for six engine types [7]. Wiebe's proposal presented in [8], makes a value of the overall heat-transfer coefficient dependent on geometrical sizes of a cylinder volume, average speed of a piston, and stage parameters of a mixture averaging for the total volume of a cylinder space. A value of such a coefficient changes according to the crankshaft position. Woshni proposes the similar dependency in [9]. He developed it adding variable coefficients, which vary with different phases of the engine cycle. Annand cited in [10] proposed other approach. He determined amount of heat transferred to cylinder walls by means of adding heat conveying trough the convection and radiation phenomena. However, he made the accuracy of results received with using of this method dependent on the correct determination of so-called calibrating constants. As a rule, these constants can be obtained by means of laboratory tests. The presented correlation dependencies can be helpful in setting up the total energy balance of piston engines because they require only a small number of the input data. Nevertheless, the accuracy of results received in this way depends on calibrations made every time for the specific engines. The comparison of values of the heat-transfer coefficients determined for a laboratory engine by using the described methods is presented in [11]. Results received by these methods have the sufficient discrepancy, reaching almost 80% for beginning and throughout of a combustion process. However, the mentioned dependencies describe only the overall heat quantity transferred from the cylinder liner or the whole engine and they are not able to describe the local and transient flow of heat [12].

Therefore, they are not suitable to describe thermal stages of structural components of an engine cylinder. In last years, models describing of the multidimensional flow of heat through cylinder walls have been developed according to the progress made in the field of the turbulent combustion of fuel. It is obvious that these models take into consideration the changeable conditions of a combustion process in various points of a cylinder volume.

3. Heat transfer through construction elements of the engine

Construction elements of the cylinder of large marine two-stroke engine have usually cylindrically shapes. Therefore, in this case use of the cylindrical arrangement of equations is more adequate. The heat flow balance for an elementary geometrical area of engine cylinder structural element (Fig.1) can be presented as energy balance as follows:

$$Q_V + \sum_{i=1}^{n} Q_i = 0, \tag{1}$$

where:

Q_V – an internal heat source,
Q_i – amount of heat flow from a neighboring elementary geometrical area,

n – a number of neighboring areas.

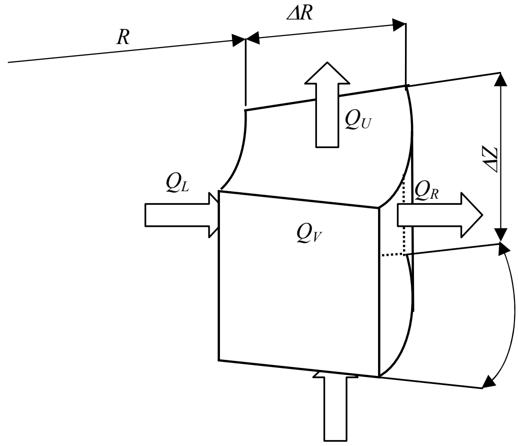

Fig 1. An elementary volume of a cylinder liner structural component

According to Fourier's law of heat transfer, the heat flux is proportional to the local temperature gradient in any direction:

$$Q = -\lambda \cdot \nabla T \,, \tag{2}$$

where:

λ – thermal conductivity of material [W/(m·K)],
∇T – temperature gradient [m·K].

Assuming that properties of structural material are isotropic in all directions, we can state that there is no heat source inside the considered area and the heat exchange process is stationary. The heat flux across walls of the elementary component can be presented by the following equations:

$$Q_{V \Rightarrow U} = \left(R + \frac{\Delta R}{2} \right) \Delta R \cdot \Delta \varphi \cdot \lambda \left(\frac{T_V - T_U}{\Delta Z} \right), \tag{3}$$

$$Q_{V \Rightarrow R} = \left(R + \Delta R \right) \Delta Z \cdot \Delta \varphi \cdot \lambda \left(\frac{T_V - T_R}{\Delta R} \right), \tag{4}$$

$$Q_{D \Rightarrow V} = \left(R + \frac{\Delta R}{2} \right) \Delta R \cdot \Delta \varphi \cdot \lambda \left(\frac{T_D - T_V}{\Delta Z} \right), \tag{5}$$

$$Q_{L \Rightarrow V} = R \cdot \Delta Z \cdot \Delta \varphi \cdot \lambda \left(\frac{T_L - T_V}{\Delta R} \right), \tag{6}$$

where:

T – temperature [K],
$_{L,\,R,\,U,\,D}$ – indexes of neighboring areas temperatures (see Fig. 1),
λ – thermal conductivity of material [W/(m·K)].

Substituting of Eq. (3) to Eq. (6) and next into Eq. (1) and taking into account that $\Delta Z = \Delta R = X$, we obtained the following relation:

$$T_V = \frac{1}{4}T_U + \frac{1}{4}T_D + \left(\frac{R+X}{4R+2X}\right)T_R + \left(\frac{R}{4R+2X}\right)T_L, \tag{7}$$

Eq. (7) for modeling of heat flow through an engine cylinder liner could not give correct results due to the unstable heat transfer through the cylinder liner structural components resulting from the cyclic engine work. Moreover, thermal energy accumulation in the cylinder liner structural components complements such a kind of phenomena. In this case, we converted the Eq. (1) to the following form:

$$Q_{D\Rightarrow V} - Q_{U\Rightarrow V} - Q_{R\Rightarrow V} + Q_{L\Rightarrow V} = Vol \cdot c_p \cdot \rho \cdot \frac{T_V^{+1} - T_V}{\Delta t}, \tag{8}$$

where:

Vol – volume of the elementary component [m^3], equals $\left(R + \frac{1}{2}\Delta R\right)\Delta R \cdot \Delta\varphi \cdot \Delta Z$,

c_p – specific heat at constant pressure[J/(kg·K)],
ρ – density of the elementary control volume [kg/m^3],
Δt – considered time interval [s],
T_V^{+1} – temperature after Δt time [K].

Using the notion of the Fourier discrete number ΔFo for two-dimensional heat flow [13] inside elementary area, we can express the temperature T_V^{+1} by the following equation:

$$T_V^{+1} = T_V(1 - 4\Delta Fo) + \Delta Fo\left(T_U + T_D + T_R\frac{R+X}{R+0.5\cdot X} + T_L\frac{R}{R+0.5\cdot X}\right), \tag{9}$$

where:

ΔFo – the Fourier discrete number [–], equals $\dfrac{\lambda \cdot \Delta t}{c_p \cdot \rho \cdot X^2}$.

In the iterative solutions, the steady-state condition should be met. It can be expressed by the following inequality:

$$\Delta Fo > \frac{1}{4}, \tag{10}$$

4. A model of temperature in the engine construction elements

The input data for a thermal state model are the boundary conditions on borders of the cylinder liner structural components and initial conditions determined by means of the experimental measurements or modeling of a combustion process in the cylinder volume. Both the boundary and the initial conditions determine a thermal state for structural component boundaries. All calculations were carried out for the one-cylinder, two-stroke, and crosshead laboratory engine with the straight-through scavenging. The fresh water flowing through the wet cylinder liner cools its cylinder volume. The main parameters of this engine are; the piston stroke 350mm, a diameter of the cylinder 220mm, the actual rotational speed 200 rpm and the actual power output 17kW. The structural similarity to the large-size marine engines was the reason of its selection as the modeling item. Using design documentation of the mentioned engine, we have divided the cylinder liner structural components into the elementary components with a size 2 mm of their sides (parameter X in relative Equations). Taking into mind axial-symmetrical shapes of the modeled elements, we limited our modeling to the two-dimensional areas located in the longitudinal section. These elementary control patches allow us to describe the temperature field for the following components: the engine piston together with its rings considered as the uniform structural component, the cylinder liner, the cylinder block with under-piston chamber and the cylinder head together with its exhaust valve and injector.

For describing the heat exchange phenomena, the following forms of boundary conditions were applied:

- Dirichlet's conditions for a surface between the structural component walls and the surrounding air, which were obtained by determination of the wall temperature equals to the air temperature measured during the experimental study,
- Dirichlet's conditions for a surface of under-piston chamber which were obtained by calculation of compression in this area during the engine working [14],
- Fourier's condition for a surface between the structural component walls and the cooling volume,
- Fourier's condition for a surface between the structural component walls and the combustion chamber.

The Fourier boundary condition was obtained with the use of heat transfer coefficients, which are calculated individually for local conditions. The convective heat transfer coefficient was determined by the following semi-empirical equation:

$$\alpha_C = 0{,}023 \cdot \left(\frac{C \cdot X}{\nu} \right)^{0,8} \cdot \left(\frac{c_{pa} \cdot \nu}{\lambda_a} \right)^{0,4} \cdot \frac{\lambda_a}{X}, \tag{11}$$

where:

C – speed of gas in a combustion chamber assumed as a mean piston speed or mean speed of water in a cooling volume, calculated by Poiseuille formula [m/s],

ν – a kinematic viscosity [m^2/s], assumed $\nu = 6 \cdot 10^{-11} \cdot T^2 + 7 \cdot 10^{-8} \cdot T - 1 \cdot 10^{-5}$ for gas in a cylinder and $8{,}60 \cdot 10^{-5}$ m^2/s for the cooling water,

λ_a – thermal conductivity of material [W/(m·K)], assumed $\lambda = -2 \cdot 10^{-8} \cdot T^2 + 8 \cdot 10^{-5} \cdot T + 0{,}0037$ for gas in a cylinder and 0,612 W/m·K for the cooling water,

c_{pa} – specific heat at constant pressure[J/(kg·K)], assumed $c_p = 3 \cdot 10^{-7} \cdot T^2 + 0{,}1974 \cdot T + 938{,}14$ for gas in a cylinder and 4178 J/kgK for the cooling water.

The radiative heat transfer coefficient determined on the basis of Newton's and Stefan-Boltzmann's laws can be described as follows:

$$\alpha_{Ri} = \frac{\varepsilon \cdot C_C}{T_i - T_V} \left(T_i^{\,4} - T_V^{\,4} \right), \tag{12}$$

where:

ε – a relative emissivity determined for „grey” flame and „lusterless” surface of cylinder walls equals ε=0,79,
C – a Stefan-Boltzmann’s constant, equals Cc= $5{,}67 \cdot 10^{-8}$ W/($m^2 \cdot K^4$),
T_i – a temperature of a combustion chamber and a local temperature in the cooling volume [K].

The sum of convective and radiative heat transfer coefficient was take into account to describe Fourier’s condition for surfaces. The correct value of T_V temperature of elementary area was obtained by using the iterative method, whereas the input data regarding temperature T_i in a combustion chamber were taken from the combustion process model presented in [14].

5. Results of modeling

Solving Eq. (9) for each of elementary control patches, we can obtain a temperature field picture for cylinder components in cylindrical arrangement. All necessary calculations we performed for the described laboratory engine. The engine thermodynamic state varied according to its crankshaft position angle. It is represented by changes of temperature in a combustion chamber. Values of these temperatures are presented in [15]. Taking it into account, we carried out calculations beginning from the angle equal 8º before and ending at 88º after the top dead centre (TDC). Moreover, we performed these calculations in interval 8º, what gave the time interval of 6 [ms] at the set rotational speed. Using of such intervals together with the assumed sizes of elementary components allowed us to meet the condition expressed by Eq. (10). This, in turn, ensured the convergence of several iterative solutions. Bearing in mind the unstable character of this heat transfer, we applied the input data in the form of a temperature field resulting from the previous crankshaft position in order to calculate temperatures of cylinder liner structural components. Only the starting calculations for an angle 8º before TDC, we carried out with using Equation (7) assuming the steady heat transfer.

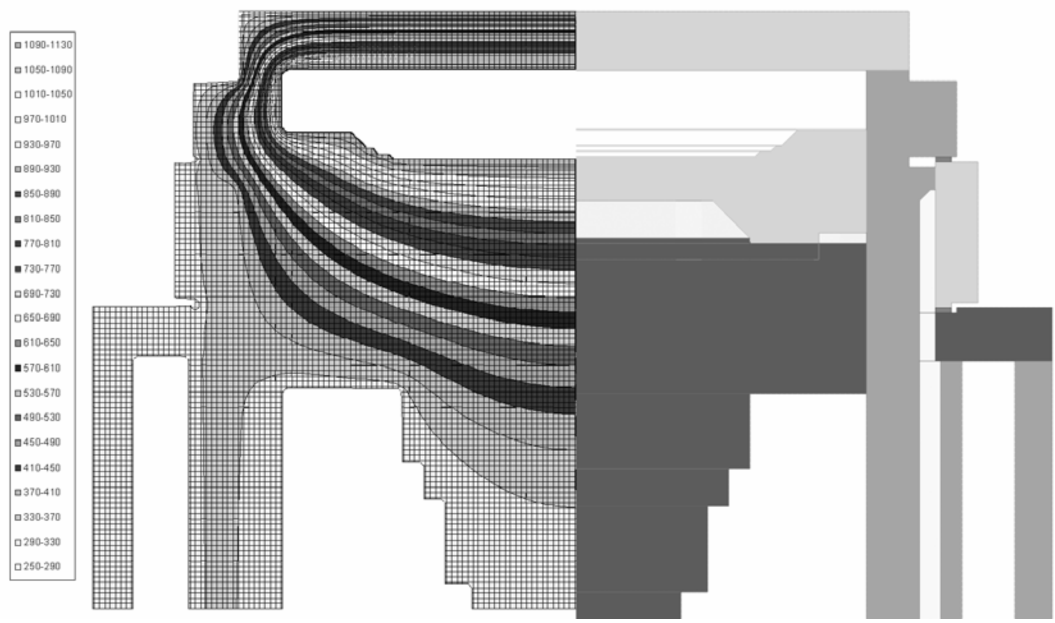

Fig 2. The example of temperature field in engine structural components shown in axial cross-section (left side) and schematic view of an upper part of the engine cylinder (right side)

In the left side of Fig. 2, the example of modeling results is presented in the form of the temperature field of engine structural components shown in axial cross-section. Due to the large number of elementary areas, the obtained modeling results are presented in the form of multi-color map. Borders of particular colors correspond with the isotherms dividing the cylinder construction areas into the temperature intervals of 40 K. The right side of Fig. 2 presents the schematic axial cross-section of engine cylinder construction applied in modeling the temperature field within particular structural compo nets.

Depiction of the modeled cylinder in its longitudinal section and temperatures of its structural components are presented in Table 1. The distinguished points plotted on its individual structural components are related to layouts of the elementary components for which of temperature values were calculated. Based on these results, we observed considerable differences of temperatures between furthest geometrical points of the cylinder reaching even 820 K, but in one point differences of temperatures did not exceed 12 K (point 2). It resulted from thermal inertia of construction components represented by the Fourier discrete number *ΔFo*. High temperature in upper side of cylinder elements is observed. The reason of this fact is modeling of temperature in start of combustion process by using Eq. (7), without considering a thermal inertia of cylinder construction components.

Tab. 1. The modeled cylinder and temperatures of its structural components

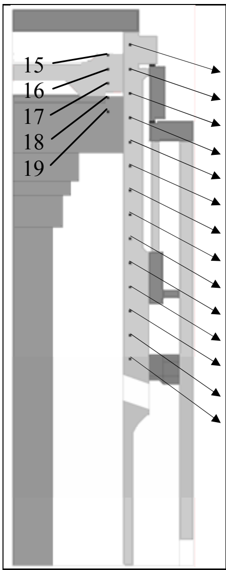

Number of comp.	Temperature [K] in elementary components in crankshaft position												
	-8º	0º	8º	16 º	24 º	32 º	40 º	48 º	56 º	64 º	72 º	80 º	88 º
1	861	861	861	861	861	865	865	865	865	865	865	865	865
2	638	638	638	638	638	640	640	640	640	640	640	640	640
3	455	455	455	455	455	456	456	456	456	456	456	456	456
4	386	386	386	386	386	387	387	387	387	387	387	387	387
5	342	342	342	342	342	342	342	342	342	342	342	342	342
6	316	316	316	316	316	316	316	316	316	316	316	316	316
7	314	314	314	314	314	314	314	314	314	314	314	314	314
8	314	314	314	314	314	314	314	314	314	314	314	314	314
9	313	313	313	313	313	313	313	313	313	313	313	313	313
10	307	307	307	307	307	307	307	307	307	307	307	307	307
11	302	302	302	302	302	302	302	302	302	302	302	302	302
12	301	301	301	301	301	301	301	301	301	301	301	301	301
13	301	301	301	301	301	301	301	301	301	301	301	301	301
14	301	301	301	301	301	301	301	301	301	301	301	301	301
15	1119	1122	1121	1121	1120	1120	1119	1119	1118	1118	1117	1117	1116
16	894	894	894	894	894	895	895	895	895	895	895	895	895
17	720	720	720	720	720	721	721	721	721	721	721	721	721
18	595	595	595	595	595	596	596	596	596	596	596	596	596
19	504	504	504	504	504	505	505	505	505	505	505	505	505

6. Conclusions

The presented paper deals with a model of heat transfer through structural components of the engine cylinder. Results obtained during modeling allowed us for the qualitative estimation of a thermal state of the engine cylinder. Nevertheless, the lack of experimental verification does not permit to carry out the quantitative estimation of such a state. Moreover, simplification made in representation of a cylinder structure within the piston and cylinder head makes impossible to obtain the high accuracy of such a modeling. Therefore, in order to increase the model adequacy, we should increase an accuracy of representation of a structure of the considered areas by means of modeling friction nodes: a piston - piston rings - a cylinder liner. It, in turn, entails the necessity to decrease geometrical sizes of elementary control patches. The modeled temperature in certain points seems to be too high. The reason of this fact probably is modeling of temperature in start of combustion process without considering a thermal inertia of components. In order to remove this problem, modeling of temperature of elements should be begin from start of compression process. The obtained modeling results may contribute to an increase of modeling accuracy of the phenomena occurring within the engine combustion chamber, accompanied by a significant decrease of the modeling cost associated with using special computer software. Such a model makes possible to develop guidelines for designing of the engine cylinder structure taking into account decreasing of thermal stresses by optimization of temperature distribution in the cylinder components. As far as combustion process models are concerned, the modeling of temperature distribution within cylinder walls may effectively contribute to an increase of engine efficiency – on the one hand – due to the decrease of total heat flowing out to the engine cooling space and – on the other hand – due to the possibility of forming the heat flow in complex areas of a cylinder space. Moreover, the obtained results may be used in teaching the subjects associated with combustion engines, i.e. analysis of thermal stresses and temperature distribution within engine elements.

References

[1] Heywood J. B., *Internal Combustion Engine Fundamentals*, McGraw-Hill, 1988.

[2] Zhiyu Han, Reitz R. D., *A temperature Wall function formulation for variable-density turbulent flows with application to engine convective heat transfer modelling,* Int. J. Heat Mass Transfer Vol. 40, No. 3, pp. 613-625, Elsevier Science, 1997.

[3] Nagórski Z., *Modelowanie przewodzenia ciepła za pomocą arkusza kalkulacyjnego*, Wydawnictwo Politechniki Warszawskiej, Warszawa, 2001.

[4] Incropera F. P., DeWitt D. P., *Fundamentals of Heat and Mass Transfer*, Wiley, 2001.

[5] Wu Y-Y., Chen B-Ch, Hsieh F-Ch., *Heat transfer model for small-scale air-cooled spark-ignition four-stroke engines*, Int. J. Heat Mass Transfer Vol. 49, pp. 3895–3905, Elsevier Science, 2006.

[6] Borman G., Nishiwaki K., *Internal-combustion engine heat transfer*, Prog. Energy Combust. Sci, No. 13, pp. 1–46, Elsevier Science, 1986.

[7] Hohenberg G.F., *Advanced approaches for heat transfer calculations*, Diesel Engine Thermal Loading, SAE SP-449, 1979, pp. 61–79.

[8] Nguien H., *A simulation model of heat exchange in the ship diesel engine cylinder – environment system*, Polish Maritime Research, No 1(31), Vol. 9, pp. 9-14. Gdańsk, 2002.

[9] Woschni G., *A universally applicable equation for the instantaneous heat transfer coefficient in the internal combustion engine*, SAE paper No. 670931, SAE Trans. Vol. 76, 1967.

[10] Heywood J. B., Sher E., *The two-stroke cycle engine, its development, operation and design*, Taylor & Francis, Philadelphia, 1999.

[11] Ghojel J., Honnery D., *Heat release model for combustion of diesel oil emulsions in DI diesel engines*, Applied Thermal Engineering Vol. 25, pp. 2072-2085. Elsevier Science, 2005.

[12] Rychter T., Teodorczyk A., *Modelowanie matematyczne roboczego cyklu silnika tłokowego*, PWN, Warszawa, 1990.

[13] Galindo J., Lujan J.M., Serrano J.R., Dolz V., Guilain S., *Description of heat transfer model suitable to calculate transient processes of turbocharged diesel engines with one-dimensional gas-dynamic codes*, Applied Thermal Engineering, Vol. 26, pp. 66-76, Elsevier Science, 2006.

[14] Kowalski J., Tarelko W., *Modeling aspects of nitric oxides emission from the two-stroke ship engine*, Explo-Diesel & Gas Turbine 2003, pp. 329-338, Miedzyzdroje-Lund, 2003.

[15] Kowalski J., Tarelko W., *The thermal state modelling of cylinder liner of marine two-stroke combustion engine*, Polish Maritime Research, No 2(48), pp. 15-20, Gdańsk 2006.

PRESSURE AND CAPACITY CHANGES IN SLIDE JOURNAL BEARING FOR LAMINAR UNSTEADY OIL FLOW

Paweł Krasowski

Gdynia Maritime University
ul. Morska 81-87, 81-225 Gdynia, Poland
tel.: +48 58 6901331, fax: +48 58 6901399
e-mail: pawkras@am.gdynia.pl

Abstract

This paper presents numerical solutions of the modified Reynolds equation of laminar unsteady lubrication in a cylindrical slide journal bearing. Laminar, unsteady oil flow is performed during periodic and unperiodic perturbations of bearing load or is caused by the changes of gap height in the time. Above perturbations occur during the starting and stopping of machine. The particular solutions are limited to the isothermal models of bearing with infinite length and lubricated by Newtonian oil with the dynamic viscosity dependent on pressure. The disturbances are related to the unsteady velocity of oil flow on the sleeve and on the surface Diagram shows the results of hydrodynamic pressure and capacity forces in the dimensionless form in time intervals of displacement duration.

Keywords: *journal bearing, unsteady laminar lubrication, pressure distribution, capacity forces*

1. Introduction

This article refers to the unsteady, laminar flows issue, in which [4,5] modified Reynolds number $Re^*=Re\psi$ is smaller than 2 or Taylor number $Ty=Re\sqrt{\psi}$ is smaller than 41,1. Laminar, unsteady oil flow is performed during periodic and unperiodic perturbations of bearing load or is caused by the changes of gap height in the time. In this article following problems were also mentioned: lubricated oil disturbance velocity on the pin and on the bearing shell. Velocity perturbations of oil flow on the pin, are caused by torsion vibrations during the rotary movement of the shaft. Perturbations are proportional to torsional vibration amplitude and to pin radius of the shaft. Oil velocity perturbations on the shell surface can be caused by rotary vibration of the shell together with bearing casing. This movement can be consider as kinematic constraint for whole bearing friction node. Isothermal bearing model can be approximate to bearing operation in friction node under steady-state thermal load conditions for example bearing in generating set on ship. In considered model flow [1,5,6] we assume small unsteady disturbances and accordingly to the laminar flow, oil velocity V_i^* and pressure p_1^* are sum of time dependent quantities $\widetilde{V}_i$; $\widetilde{p}_1$ and time independent quantities $V_i; p_1$ from time [1,2,3] in following form:

$$V_i^* = V_i + \widetilde{V}_i \qquad \mathrm{i} = 1,2,3$$
$$p_1^* = p_1 + \widetilde{p}$$

(1)

Unsteady components of dimensionless oil velocity and pressure we show [1,5] in following form of infinite series :

$$\widetilde{V}_i(\varphi;r_1;z_1;t_1)=\sum_{k=1}^{\infty} V_i^{(k)}(\varphi;r_1;z_1)\exp(j\,k\omega_0\,t_0 t_1)$$

$$\widetilde{p}_1(\varphi;z_1;t_1)=\sum_{k=1}^{\infty} p_1^{(k)}(\varphi;z_1)\exp(j\,k\omega_0\,t_0 t_1) \qquad \text{i=1,2,3} \tag{2}$$

where:

ω_0 – angular velocity perturbations in unsteady flow,
j - imaginary unit: $j=\sqrt{-1}$.

Reynolds equation describing total dimensionless pressure p_1^* (sum steady and unsteady components) in oil journal bearing gap [1,2] by unsteady, laminar, isotherm Newtonian flow along with disturbances of peripheral velocity V_{10} on the journal and V_{1h} on the sleeve and disturbances of velocity on journal length V_{30} on the journal and V_{3h} on the sleeve has following form:

$$\frac{\partial}{\partial\varphi}\left\{\frac{(h_1)^3}{e^{Kp_1}}\left[\frac{\partial p_1^*}{\partial\varphi}-K\left(p_1^*-p_1\right)\frac{\partial p_1}{\partial\varphi}\right]\right\}+\frac{1}{L_1^2}\frac{\partial}{\partial z_1}\left\{\frac{(h_1)^3}{e^{Kp_1}}\left[\frac{\partial p_1^*}{\partial z_1}-K\left(p_1^*-p_1\right)\frac{\partial p_1}{\partial z_1}\right]\right\}=$$
$$=6\frac{\partial h_1}{\partial\varphi}+\frac{1}{2}\frac{\rho_1}{\eta_1}\mathrm{Re}^* n\left\{\frac{\partial}{\partial\varphi}\left[h_1^3\left(V_{10}+V_{1h}\right)\right]+\frac{1}{L_1^2}\frac{\partial}{\partial z_1}\left[h_1^3\left(V_{30}+V_{3h}\right)\right]\right\}\sum_{k=1}^{\infty}A_k+ \tag{3}$$
$$-6\left\{\frac{\partial}{\partial\varphi}\left[h_1\left(V_{10}+V_{1h}\right)\right]+\frac{1}{L_1^2}\frac{\partial}{\partial z_1}\left[h_1\left(V_{30}+V_{3h}\right)\right]-2\left(V_{1h}\frac{\partial h_1}{\partial\varphi}+\frac{1}{L_1^2}V_{3h}\frac{\partial h_1}{\partial z_1}\right)\right\}\sum_{k=1}^{\infty}B_k$$

where $0\le\varphi\le\varphi_e$; $0\le r_1\le h_{p1}$; $-1\le z_1\le 1$; $0\le t_1\le t_k$; $p_1^*=p_1^*(\varphi;z_1;t_1)$

Components of oil velocity V_φ, V_r, V_z in cylindrical co-ordinates r,φ,z have presented as V_1, V_2, V_3 in dimensionless form:

$$V_\varphi=UV_1^* \qquad V_r=\psi UV_2^* \qquad V_z=\frac{U}{L_1}V_3^* \tag{4}$$

Dynamic oil viscosity η is depended on pressure by Barrus formula [1] and has following form:

$$\eta=\eta_0 e^{\alpha(p-p_a)}\approx\eta_0 e^{\alpha p}=\eta_0\eta_1 \tag{5}$$

where:

η_o- the dynamic oil viscosity for atmospheric pressure $p=p_a\approx 0$
η – the dynamic oil viscosity function,
α – the pressure influence piesocoefficient of the oil viscosity ,
η_1 – dimensionless dynamic viscosity depending on pressure $\eta_1=\exp(\alpha p)$.

Parameter K characterize dimensionless oil dynamic viscosity change caused by pressure(if K=0 dynamic oil viscosity is constant and independent from pressure):

$$K=\alpha p_0 \qquad p_0=\frac{U\eta_0}{\psi^2 R} \tag{6}$$

where:

p_0 - characteristic value of pressure

Sum for series $\sum_{k=1}^{\infty} A_k$ and $\sum_{k=1}^{\infty} B_k$ in right hand side of Reynolds equation (3) are results from conservation of the momentum solutions and were define in work [1,2]. Nomenclature has been placed in the end of the paper. Specific explanation to above Reynolds equation were define in works [1,2,3]. Quantity of oil peripheral velocity perturbations on the whirling pin surface with ω velocity caused by forced torsion vibration of shaft with the angular velocity ω_o and angular amplitude φ_0 can be present in the following dimensionless form:

$$V_{10} = \varphi_0 n \ , \qquad n = \frac{\omega_0}{\omega} , \tag{7}$$

In this torsion vibrations case of engine, n number depend on the cylinder number c and on engine type: two-stroke (s=2) or four-stroke (s=4):

$$n = \begin{cases} c & s = 2 \\ \dfrac{c}{2} & s = 4 \end{cases} , \tag{8}$$

Rest of the symbols and quantities which apply to Reynolds equation (3) have been precisely define and describe in work [1,2,3].

2. Pressure distributions

The equation solution (3) for bearing with infinity length determine total dimensionless hydrodynamic pressure function in following [2,3] (K>0) form:

$$\begin{aligned} p_1^*(\varphi) = \frac{1}{1-Kp_{10}} \Bigg[& -\frac{1-Kp_{10}}{K} \ln\left|1-Kp_{10}\right| + p_{10}\left(V_{1h}-V_{10}\right)\sum_{k=1}^{\infty} B_k + \\ & +\frac{1}{2}\rho_1 \operatorname{Re}^* n\left(V_{10}+V_{1h}\right)\left(\varphi - h_{1e}^3 \int_0^{\varphi} \frac{d\varphi}{h_1^3} - K\int_0^{\varphi} p_{10} d\varphi \right) \sum_{k=1}^{\infty} A_k \Bigg] , \end{aligned} \tag{9}$$

$$\text{for} \qquad 0 \le \varphi \le \varphi_e , \quad 0 \le t_1 \le t_k , \quad p_1^* = p_1^*(\varphi; t_1)$$

Pressure p_{10} is located in the oil gap by steady flow and by constant oil dynamic viscosity (K=0):

$$p_{10}(\varphi) = 6 \int_0^{\varphi} \frac{h_1(\varphi) - h_{1e}}{h_1^3(\varphi)} d\varphi \ , \qquad \text{for} \quad 0 \le \varphi \le \varphi_e \tag{10}$$

Dimensionless total pressure by disturb flow and by constant oil dynamic viscosity independent from pressure (K=0):

$$p_1^*(\varphi) = p_{10} + \frac{1}{2}\rho_1 \operatorname{Re}^* n\left(V_{10}+V_{1h}\right)\left(\varphi - h_{1e}^3 \int_0^{\varphi} \frac{d\varphi}{h_1^3} \right) \sum_{k=1}^{\infty} A_k + p_{10}\left(V_{1h}-V_{10}\right)\sum_{k=1}^{\infty} B_k \ , \tag{11}$$

Disturbance pressure in unsteady flow part can be presented with common formula for constant (K=0) and variable dynamic viscosity $(K \ge 0)$:

$$\tilde{p}_1 = \frac{1}{1-Kp_{10}}\left[\frac{1}{2}\rho_1 \operatorname{Re}^* n(V_{10}+V_{1h})\left(\varphi - h_{1e}^3\int_0^{\varphi}\frac{d\varphi}{h_1^3} - K\int_0^{\varphi} p_{10}d\varphi\right)\sum_{k=1}^{\infty} A_k + p_{10}(V_{1h}-V_{10})\sum_{k=1}^{\infty} B_k\right], \quad (12)$$

Presented equations (9),(11),(12), which describe total pressure course and perturbation pressure course, have following conclusions: pressure in dependence on velocity perturbations quantity V_1 and on direction with relation to pin peripheral velocity U. In this equations, two components occur in dependence on the sum and on the difference of velocity perturbations on the pin and on the bearing shell. That is way in presented graphs characteristic cases of perturbations with different and equal values were shown.
Numerical calculation results are presented by following tangential velocity perturbations:

1. velocity perturbations on the journal V_{10}=0,05 and on the sleeve V_{1h}=0,
2. velocity perturbations on the journal V_{10}=0,05 and on the sleeve V_{1h}=0,025,
3. velocity perturbations on the journal V_{10}=0,05 and on the sleeve V_{1h}=0,05,
4. velocity perturbations on the journal V_{10}=0,05 and on the sleeve V_{1h}=-0,05

In numerical calculation example, oil with constant density was assume, equivalent to quantity ρ_1=1. In presented calculation way an expression value is assumed $n\rho_1\text{Re}^*$ = 12, what is approximately equivalent to force over first frequency torsion vibrations force of six cylinder engine shaft. This take place by laminar unsteady flow. Time of reference t_o is a period of velocity disturbances dispersion. Examples apply to bearing with constant dependent eccentricity λ=0,6.

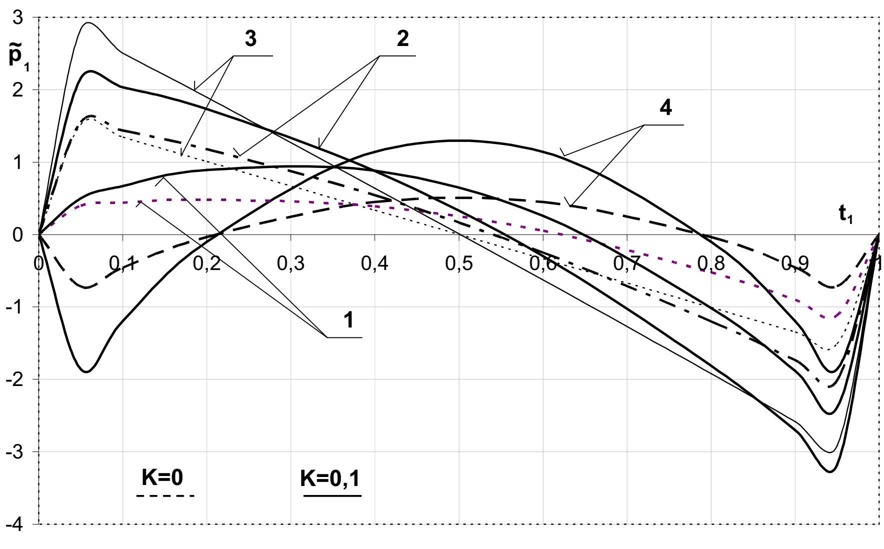

Fig.1. Pressure distributions $\tilde{p}_1$ in place φ=145° in the time t_1 for constant oil viscosity (K=0) and for oil viscosity in dependence on pressure (K=0,1) by velocity perturbations: 1)V_{10}=0,05; V_{1h}=0; 2) V_{10}=0,05; V_{1h}=0,025; 3) V_{10}=0,05; V_{1h}=0,05; 4) V_{10}=0,05; V_{1h}=-0,05

Unsteady pressure is changing due velocity perturbations time and it is in function of time and position on the journal. It is a periodic function with the following lasting period of velocity perturbation. Pressure perturbation course in point φ=145° on the journal surface in dimensionless time function in case of velocity perturbation on the journal and on the sleeve is presented by four variant on Fig. 1. Above graphs are made for constant viscosity and for viscosity in dependence on pressure where K=0,1. When oil velocity perturbations on the journal are compatible to journal tangential velocity, the perturbation pressure increase, otherwise the pressure decrease. In this case decrease is considerably bigger than increase and it last shorter than half of perturbation period. In case of velocity perturbation on the sleeve it is opposite. There is a lack of graphs for this example. Periods of pressure increase and decrease are non-symmetrical in case of different perturbation velocity values (graph 2). When perturbations velocity values are equal and directions are the same or opposite then the perturbation pressure is symmetrical in time (graph 3 and 4, Fig.1). Pressure perturbation distribution by wrapping angle is changing in time, giving in different time periods maximal or minimal pressure. Maximal and minimal pressure distribution in considered velocity perturbation examples are presented on Fig.2. In order to compare influence of viscosity variable in dependence on pressure (graph b),pressure distribution for oil with constant viscosity (K=0) which is independent from pressure, were plotted (graph a). In case where velocity perturbations on the pin and on the bearing shell have the same signs and pressure, perturbations values are maximum (graph 3). When viscosity is in dependence of pressure it causes an increase of steady pressure and perturbation pressure on both maximal and minimal pressure sides. Steady pressure flow sum up with perturbation pressure and total distribution of maximal and minimal pressure by bearing wrapping angle is received. This are the border pressure distribution for given type of perturbation.

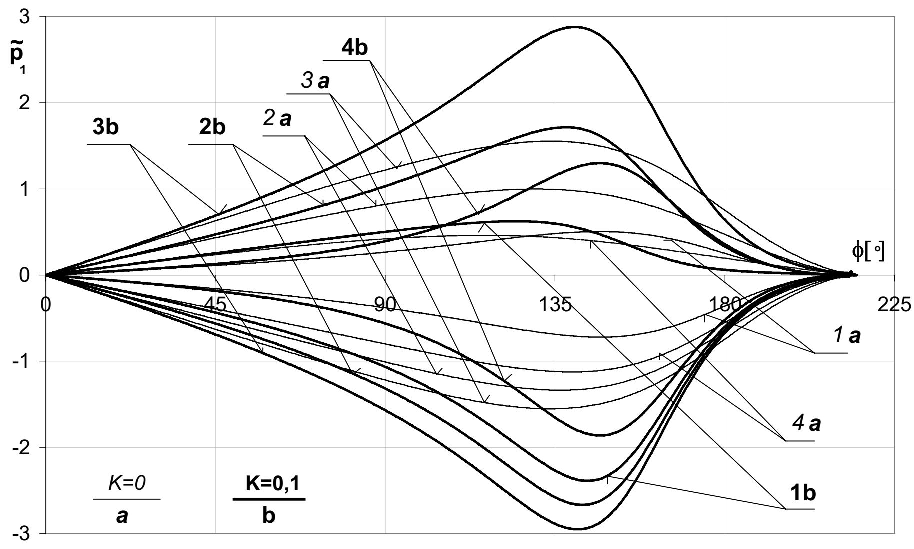

Fig.2. Unsteady part maximal and minimal pressure distributions $\widetilde{p}_1$ in direction φ a) for constant oil viscosity (K=0), b) for oil viscosity in dependence on pressure (K=0,1) by velocity perturbations 1) V_{10}=0,05; V_{1h}=0; 2) V_{10}=0,05; V_{1h}=0,025. 3) V_{10}=0,05; V_{1h}=0,05;4) V_{10}=0,05; V_{1h}=-0,05

3. Capacity forces

Capacity force W for cylindrical slide journal bearing has following components W_x and W_y to be determined [2,5] in the local co-ordinate systems in Fig. 3. Thus dimensionless components W_{1x} and W_{1y} of capacity forces W_1 are as follows [2]:

$$W_{1x} = \frac{W_x}{W_0} = -\int_0^{\varphi_k} p_1 \cos\varphi d\varphi, \qquad W_{1y} = \frac{W_y}{W_0} = -\int_0^{\varphi_k} p_1 \sin\varphi d\varphi \ , \tag{13}$$

$$W_1 \equiv S_o = \sqrt{W_{1x}^2 + W_{1y}^2} = \frac{W}{W_0}$$

where:

W_0 - characteristic value of capacity force $W_0 \equiv 2Rbp_0$,
S_o – Sommerfeld Number for slide journal bearing.

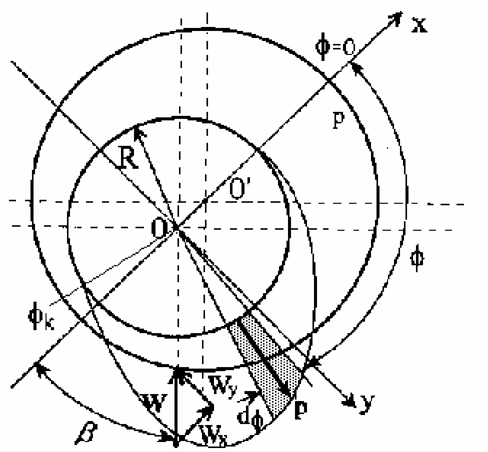

Fig. 3 Capacity force W and components W_x and W_y in the local co-ordinate system

Hydrodynamic capacity force change caused by the pressure perturbation is calculate from:

$$\widetilde{W}_1 = W_1^* - W_1 \ , \tag{14}$$

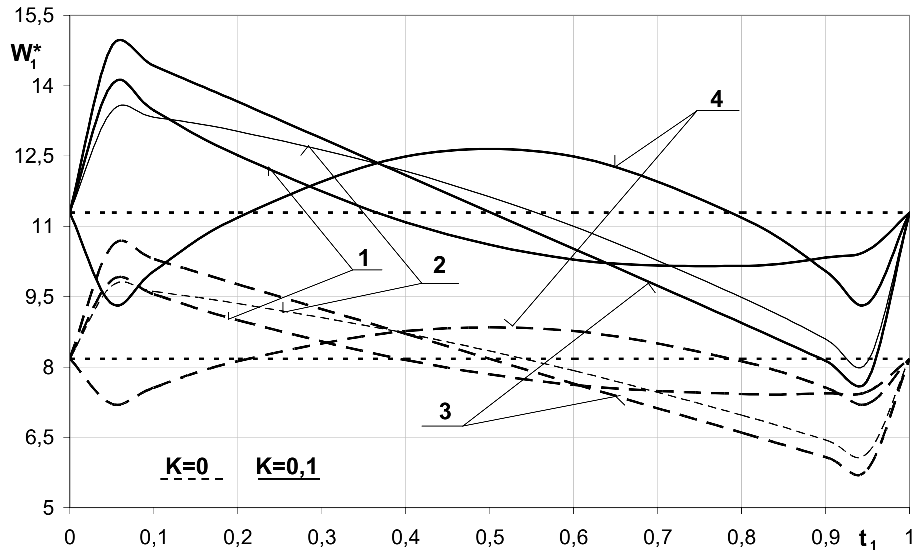

Fig.4. The dimensionless capacity forces W_1^* of slide journal bearing in the time t_1 by velocity perturbations:1) V_{10}=0,05; V_{1h}=0;2) V_{10}=0,05; V_{1h}=0,025;3) V_{10}=0,05; V_{1h}=0,05;4) V_{10}=0,05; V_{1h}=-0,05

Pressure in the bearing during the perturbation is a total of stationary flow pressure and perturbation pressure according to (1). According to mentioned equation (2) if we provide stationary flow pressure p_1 we will obtain capacity force W_1. On the other hand if we provide summary pressure p_1^* we will receive capacity force W_1^* as a result of this distribution.

Figure 4 presents hydrodynamic capacity W_1^* in the time function t_1 for perturbation velocities cases marked with graphs 1,2,3,4. Figure 4 also presents capacity calculation results for oil with constant viscosity (K=0). Capacity force in stationary flow is marked by horizontal lines with dots. Hydrodynamic capacity force W_1^* changes periodically with a period equal to perturbation velocity. In case of velocity perturbation in the bearing pin, increase of capacity force above the stationary condition value last no longer than half of the perturbation period and the increase of capacity force is bigger than the decrease in the remaining time. When perturbation of velocity on the bearing pin is in the same direction as a peripheral velocity of the pin it causes then bigger increase of capacity force than decrease. It is opposite in case of oil peripheral velocity perturbation on the shell surface, but his diagrams are not presented in his article. The case 2 effects are shown on the diagram 4. Capacity force course in time is not symmetrical for different perturbation of velocity quantities on the pin and on the shell. . Presented modification of dimensionless capacity force W_1^* illustrate also a change of Sommerfeld Number So in the bearing node model.

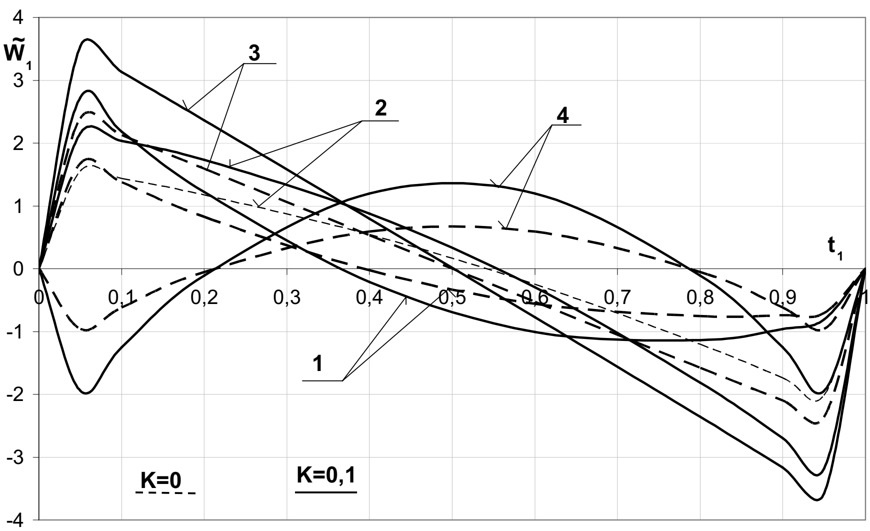

Fig.5. The dimensionless capacity forces $\widetilde{W}_1$ of slide journal bearing in the time t_1 by velocity perturbations:1) V_{10}=0,05; V_{1h}=0; 2) V_{10}=0,05; V_{1h}=0,025 3) V_{10}=0,05;V_{1h}=0,05; 4) V_{10}=0,05; V_{1h}=-0,05

Capacity force W^* is situated in the co-ordinate angle φ_w from a angle φ=0 calculated for film origin (Fig. 3):

$$\varphi_w = \pi - \beta = \pi - arctg\left|\frac{W_{1y}^*}{W_{1x}^*}\right|, \tag{15}$$

Figure 6 presents contact angle of a bearing hydrodynamic capacity force in dimensionless time function t_1 in four considered perturbation of velocity cases marked same as before. By stationary flow angle is marked with dot line φ_w angle defines capacity force position changes periodically and the period is equal to perturbation of velocity period. In all considered cases of perturbation velocity the φ_w angle change in time is not bigger than four degrees. Only in case 4 (graph 4 Fig.6) for oil with constant viscosity the position angle is uniform (constant). Capacity force angle change for viscosity in dependence on pressure is insignificant comparing to change with constant viscosity and equals below one degree. Viscosity dependence on pressure causes angle φ_w increase for stationary flow.

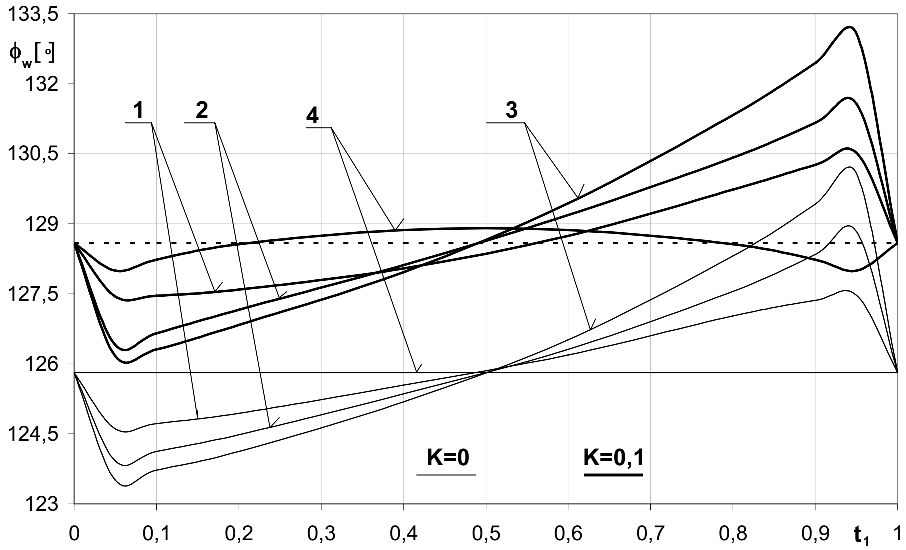

Fig. 6. Angle φ_w situated capacity force W_1^* in slide journal bearing in the time t_1 by velocity perturbations: 1) V_{10}=0,05; V_{1h}=0 2) V_{10}=0,05; V_{1h}=0,025. 3) V_{10}=0,05; V_{1h}=0,05; 4) V_{10}=0,05; V_{1h}=-0,05

5. Conclusions

Unsteady perturbation of velocity on the journal and the sleeve have influence on the hydrodynamic pressure distribution and the hydrodynamic capacity forces in the lubricated gap. The influence is stronger when the oil viscosity depends stronger on pressure. Summary pressure, perturbation pressure change and capacity forces are periodical equal to perturbation of velocity period and the size of change depends on perturbation of velocity. When the perturbation of velocity on the journal has the same direction as peripheral velocity of the pin then the perturbation pressure is positive. When the peripheral velocity is in the opposite direction then the perturbation pressure is negative and it decrease summary pressure. Pressure increase and decrease is not symmetrical during the perturbation time. Although presented case consider isothermal bearing model with infinity width the results can be useful in preliminary pressure distribution estimation by laminar unsteady lubrication of cylindrical journal bearings with infinity width. Presented results will going to be used as a comparison quantities in case of laminar unsteady flow of Non-Newtonian fluids in cylindrical bearing gap.

Notation

b - length of the journal
ε - eccentricity
h - gap height $h = \varepsilon h_1$
h_1 - dimensionless gap height $h_1 = 1+ \lambda \cos\varphi$

L_1 - dimensionless bearing length $L_1 = \frac{b}{R}$
p - hydrodynamic pressure $p = p_0\, p_1$
p_o - characteristic value of pressure
p_1 - dimensionless hydrodynamic steady pressure
p_1^* - dimensionless hydrodynamic summary pressure
$\tilde{p}_1$ - dimensionless hydrodynamic unsteady pressure
r - radial co-ordinate $r = R(1+\psi r_1)$
r_1 - dimensionless radial co-ordinate
R - radius of the journal
Re - Reynolds Number $\mathrm{Re} = \frac{U\rho_0\varepsilon}{\eta_0 R}$
Re* - modified Reynolds Number $\mathrm{Re}^* = \mathrm{Re}\psi$
S_o - Sommerfeld Number for slide journal bearing
t - time $t = t_0\, t_1$
t_o - characteristic value of time
t_1 - dimensionless time
Ty - Taylor Number $\mathrm{Ty} = \mathrm{Re}\sqrt{\psi}$
U - peripheral journal velocity $U = \omega R$
V_{10} - dimensionless velocity of perturbation in direction φ on the journal
V_{1h} - dimensionless velocity of perturbation in direction φ on the sleeve
V_{30} - dimensionless velocity of perturbation in direction z on the journal
V_{3h} - dimensionless velocity of perturbation in direction z on the sleeve
W_0 - characteristic value of capacity force $W = 2Rbp_0$
W - capacity force $W = W_0\, W_1$
W_1 - dimensionless capacity force
W_x , W_y - components of capacity force W
W_{1x} , W_{1y} - dimensionless components of capacity force W_1
z - co-ordinate in length of the journal $z = b\, z_1$
z_1 - dimensionless co-ordinate in length of the journal
ε - radial clearance
η - dynamic oil viscosity $\eta = \eta_0\eta_1$
η_o - characteristic value of dynamic oil viscosity
η_1 - dimensionless dynamic oil viscosity
λ - dimensionless eccentricity ratio
ρ - oil density $\rho = \rho_0\rho_1$
ρ_o - characteristic oil density
ρ_1 - dimensionless oil density
φ_0 - the angular amplitude torsional forced vibrations of the shaft
φ_e - the angular co-ordinate for the film end
φ_w - the angular co-ordinate situated capacity force
ψ - dimensionless radial clearance $\psi = \frac{\varepsilon}{R}$; $10^{-4} \le \psi \le 10^{-3}$
ω - angular journal velocity
ω_o - angular velocity of perturbations

References

[1] Krasowski, P., *Modelling of laminar unsteady and unsymmetrical oil flow in slide journal bearing gap,* Tribologia 5/2002 (185), pp. 1425-1436.

[2] Krasowski, P., *Capacity forces and pressure in slide journal bearing by laminar unsteady lubrication,* ZAGADNIENIA EKSPLOATACJI MASZYN, 2(146), Vol.41 2006, pp. 83-94.

[3] Krasowski, P., *Pressure in slide journal bearing for laminar, unsteady lubrication by variable viscosity oil,* Journal of KONES Internal Combustion Engines. Vol.12 No.1-2, pp.175-182, Warsaw 2005.

[4] Teipel, I., Waterstraat, A., *The Reynolds equation for lubrication under unsteady conditions,* Proceedings The IX Canadian Congress of Applied Mechanics, pp. 497-502, University of Saskatchean 1983.

[5] Wierzcholski, K., *Theory unconventional lubricant slide journal bearing,* Technical University Press, Szczecin 1995.

[6] Wierzcholski, K., *Mathematical methods in hydrodynamic theory of lubrication,* Technical University Press, Szczecin 1993.

FRICTION LOSSES AT CRANK MECHANISM BEARINGS OF A DIESEL ENGINE

Anna Krzymień

Institute of Combustion Engines and Transportation
Poznań University of Technology
ul. Piotrowo 3, 60-965 Poznań, Poland
phone: +48 61 665 22 39
e-mail: anna.krzymien@put.poznan.pl

Abstract

From the point of user it is important to minimize engine friction losses because it means the reduction in fuel consumption and emissions. Among all losses encountered during energy transformation a significant part relate to the friction in crank mechanism, in particular in bearing nodes.

This paper presents results of calculation of averaged friction losses generated at the main and crank bearings of a diesel operating in a wide range of rotational speeds. A main bearing served as an example for demonstration of utilization of obtained results to an analysis of friction losses from the perspective of their relation against engine certain constructional (dimensions, clearances, lubricating oil viscosity) and operational (speed, load, oil properties) parameters. Total power required for overcoming friction resistance at main and crank bearings has been presented in relation to the variable rotational speed.

Keywords: *friction, IC engine, friction losses, slide bearings*

1. Introduction

It is important to minimize the friction losses of a running engine because they substantially affect fuel consumption and emissions. One of the ways toward the effective reduction in fuel consumption and improvement of a number of indices like engine durability and reliability is minimization of friction losses through proper engine design and operation.

In the literature on friction losses one can find various percentage share of individual friction nodes in total losses generated by the engine. According to Martin [9] losses encountered at the "piston-rings-pin-cylinder" assembly account for about 44%, bearings 22% and valve train another 6%, which gives about 72% of all mechanical losses. Other authors associate the volume of friction losses with rotational speed. Fig. 1 presents a typical division of friction losses in relation to the crankshaft rotational speed taking into account a number of considerable factors [1]. A significant shear in total mechanical losses of modern engine have an auxiliaries drive. Losses relative to the valve train drive prevail at low speeds, while those connected with piston-cylinder assembly and crank mechanism quickly increase with the increase in rotational speed.

Both constructional and operational factors affect friction losses connected with main and crank bearings operation. The most important are: bearing dimensions, clearance, mass of engine moving parts, rotational speed, lubricating oil (its viscosity in particular). Friction losses can be determined analytically utilizing relevant computational procedures, above all forces in crank mechanism and hydrodynamic parameters of slide bearings as well as carrying the test stand measurements.

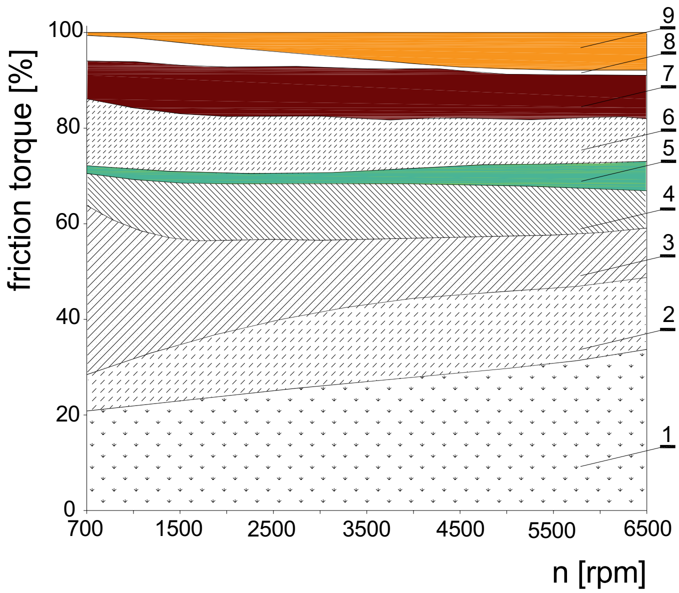

Fig. 1. Friction losses of engine individual subassemblies and auxiliaries: 1 – piston-cylinder node, 2 – crank system, 3 – valve train, 4 – oil pump, 5 – alternator, 6 – water pump, 7 – auxiliary pump, 8 – vacuum pump, 9 – balancing shafts, 10 – fuel pump (GDI engines) [1]

2. Friction losses at crank mechanism bearings

Besides the hydrodynamic lift due to lubricating wedge, dynamically loaded bearings of engine crank mechanism experience hydrodynamic lift due to lubricant squeeze when the journal displaces relatively to the bush. Superposition of both these phenomena is utilized to determine the characteristic parameters of bearing operation (see Fig. 2), including friction losses.

Total friction losses of dynamically loaded bearings equal:

$$N_t = N_k + N_w, \tag{1}$$

where:

N_k – friction losses due to rotation (wedge effect),
N_w – friction losses resulting from displacements (squeeze effect).

The friction losses understood as the flux of energy absorbed as the result of overcoming the resistance to motion, have the dimension of friction power. The friction power N_k (wedge) consists of a part resulting from shear due to speed gradient in lubricant layer between surfaces of journal and bush for angular velocities ω_1 and ω_2, respectively. The friction power N_w (squeeze) results in turn from the work of dumping the journal displacement relative to bush performed by the lubricant squeezed from bearing.

In order to determine the friction forces acting on surfaces of journal and bush, balance of forces acting on an element of lubricant in lubricating gap should be analyzed. This balance of friction forces and pressures acting on an element of lubricant has been presented in Fig. 3.

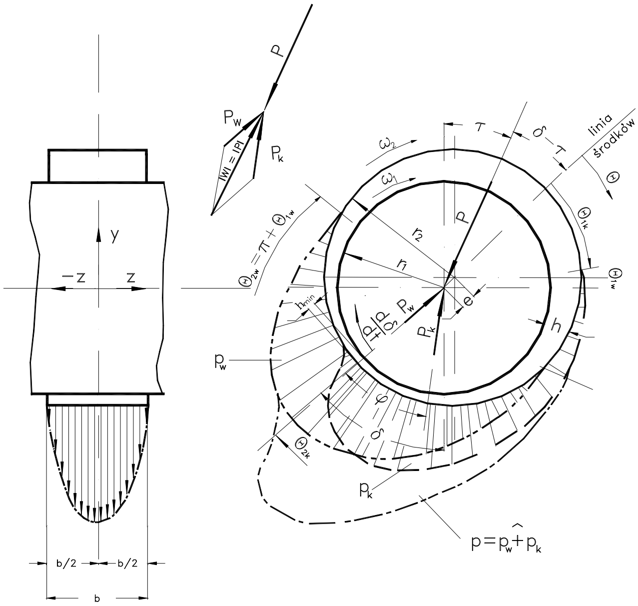

Fig. 2. Schematic of a cylindrical slide bearing, geometric marking and a principle of lift summation: P – bearing load, P_k – oil film reaction due to wedge effect, P_w – oil film reaction due to squeeze effect, r_1 – journal radius, r_2 – bush radius, e – eccentricity, h – lubricating gap variable height, b – bush effective length, τ – angle of load direction, δ – angle of centers line direction, φ – angle between P_k and P_w, Θ – angular coordinate measured from the thickest layer of lubricant (indexes mark respectively beginning and end of the region of individual effects), ω – angular velocity of journal (1) and bush (2), $d\partial/dt$ – angular velocity of line of centers

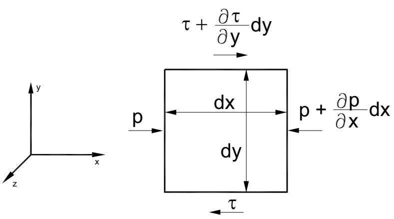

Fig. 3. Balance of forces acting on a lubricant element in lubricating gap

According to Fig. 3:

$$p \cdot dy + \left(\tau + \frac{\partial \tau}{\partial y} dy \right) dx - \left(p + \frac{\partial p}{\partial x} dx \right) dy - \tau dx = 0 \ , \tag{2}$$

where:

p – hydrodynamic pressure,

$\tau = \eta \frac{\partial u}{\partial y}$ – shear in lubricant layer (η – lubricant dynamic viscosity, $\frac{\partial u}{\partial y}$ – velocity gradient in direction of lubricant layer thickness).

From Eq. (2) it comes:

$$\frac{\partial \tau}{\partial y} = \frac{\partial p}{\partial x} \ , \tag{3}$$

and after substitution of τ to (2)

$$\frac{\partial^2 u}{\partial y^2} = \frac{1}{\eta}\frac{\partial p}{\partial x}. \tag{4}$$

As result of double integration of (4) relative to y, we receive:

$$u = \frac{1}{2\eta} \cdot \frac{\partial p}{\partial x} \cdot y^2 + C_1 \cdot y + C_2. \tag{5}$$

Integration constants can be defined using boundary conditions that are as follows:
for $y = 0$ $u = u_2$ which corresponds to the bush circumferential speed,
for $y = h$ $u = u_1$ which corresponds to the journal circumferential speed.
Hence

$$u = \frac{y(y-h)}{2\eta} \cdot \frac{\partial p}{\partial x} + \frac{h-y}{h} \cdot u_2 + \frac{y}{h} \cdot u_1. \tag{6}$$

Elementary force of friction in the layer of lubricant

$$dS = \tau \cdot dx \cdot dy. \tag{7}$$

Substituting (6) to (7), we receive:

$$\begin{aligned} dS &= \eta \cdot \frac{\partial u}{\partial y} dx \cdot dz = \eta \cdot \frac{\partial}{\partial y}\left[\frac{y(y-h)}{2\eta} \cdot \frac{\partial p}{\partial x} + \frac{h-y}{h} \cdot u_2 + \frac{y}{h} \cdot u_1\right] dxdz = \\ &= \eta \cdot \frac{\partial}{\partial y}\left[\frac{1}{2\eta} \cdot \frac{\partial p}{\partial x}\left(y^2 - yh\right) + \left(u_1 - u_2\right)\frac{y}{h} + u_2\right] dxdz, \end{aligned} \tag{7}$$

and after differentiation

$$dS = \left(\eta\frac{u_1 - u_2}{h} - \frac{h}{2}\frac{\partial p}{\partial x} + y\frac{\partial p}{\partial x}\right) dxdz. \tag{8}$$

For $y = 0$ – bush slide surface:

$$dS_2 = \left(\eta\frac{u_1 - u_2}{h} - \frac{h}{2}\frac{\partial p}{\partial x}\right) dxdz, \tag{9}$$

and for $y = h$ – journal slide surface:

$$dS_1 = \left(\eta\frac{u_1 - u_2}{h} + \frac{h}{2}\frac{\partial p}{\partial x}\right) dxdz. \tag{10}$$

Friction force on the journal surface is bigger than on the bush surface, hence the friction power should be calculated using the S_1 force.

Taking into consideration the difference in circumferential speeds of journal and bush that equals $u_1 - u_2 \approx r(\omega_1 - \omega_2) = r \cdot \omega_s$ and introducing the circumferential coordinate $\partial x = r \cdot \partial\Theta$, the friction force in the lubricant layer adjoining to the journal surface

$$S_1 = r\int_{-\frac{b}{2}}^{+\frac{b}{2}}\int_{\Theta_{1k}}^{\Theta_{2k}}\left[\eta \cdot \frac{r \cdot \omega_s}{h} + \frac{h}{2} \cdot \frac{\partial p}{r \cdot \partial\Theta}\right] d\Theta dz. \tag{11}$$

Hence [8]:

$$S_1 = \frac{b \cdot d \cdot \eta \cdot \omega_s}{\psi} \cdot \frac{\pi}{\sqrt{1-\varepsilon^2}} + \psi \cdot \frac{\varepsilon}{2} P_k \cdot sin\varphi , \tag{12}$$

where – besides earlier introduced indications, ψ is a bearing relative clearance and ε – relative eccentricity.

Due to periodical changes in position of journal center relative to bush center (dynamically loaded bearing) the friction force changes periodically as well.
Friction power:

$$N_t = \frac{1}{m \cdot \pi} \cdot \frac{d}{2} \cdot \omega \cdot \int_0^{m\pi} S_1(\alpha) d\alpha , \tag{13}$$

where: m = 2 for two stroke engine and m = 4 for four stroke engine, d – bearing nominal diameter, ω – crankshaft angular velocity, α – crankshaft angle. The friction force S is being numerically integrated.

3. Results of calculation and analysis

In order to determine the friction losses (friction power) at the engine crank mechanism bearing a method presented in the previous chapter has been utilized. The computations have been carried out using earlier formulated computer programs. A turbocharged diesel of nominal power N_e = 66 kW and maximum torque M_o = 195 Nm has been selected for calculations [5]. A part of technical data have been provided by the manufacturer, other were found during engine tests at test bed (indication diagrams) and previously conducted computer calculations of bearing loads and hydrodynamic parameters of bearing operation [4, 10]. Computations have been carried out for following speeds: idle run (800 rpm), maximum torque (2500 rpm) and maximum power (4100 rpm).

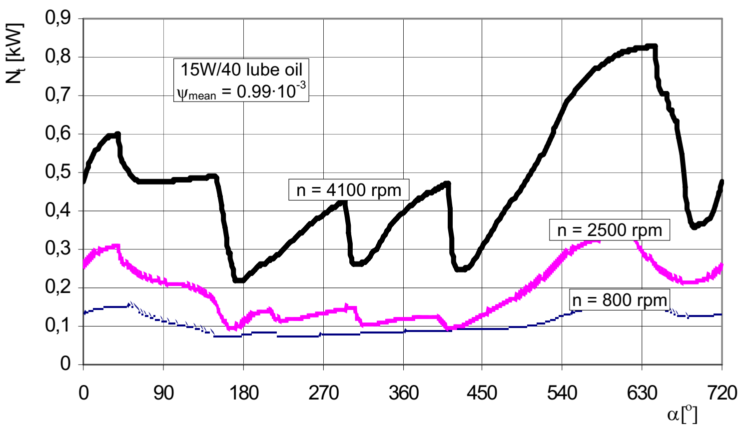

Fig. 4. Course of momentary friction power at B main bearing vs. crank angle for various speeds

Eventually presented results concern the highly loaded main bearing B. Fig. 4 presents the course of momentary power dissipated at the bearing as a result of friction against the crank angle within the full cycle. The mean friction power is: N_{tmean} = 0,10 kW, 0,19 kW and 0,47 kW at n =800, 2500 and 4100 rpm, respectively.

For the further analysis of the relation between certain parameters and magnitude of friction losses at the bearing, an averaged value of friction power within the entire cycle has been assumed. When analyzing the effect of bearing size on friction losses a length to nominal diameter ratio (b/d) was taken into consideration. Since the bearing half bush has the circumferential groove, an effective length (b_c) has been taken into account. Fig. 5 presents the course of friction loss change vs. bearing length b_c (and b/d ratio as well) for various rotational speeds.

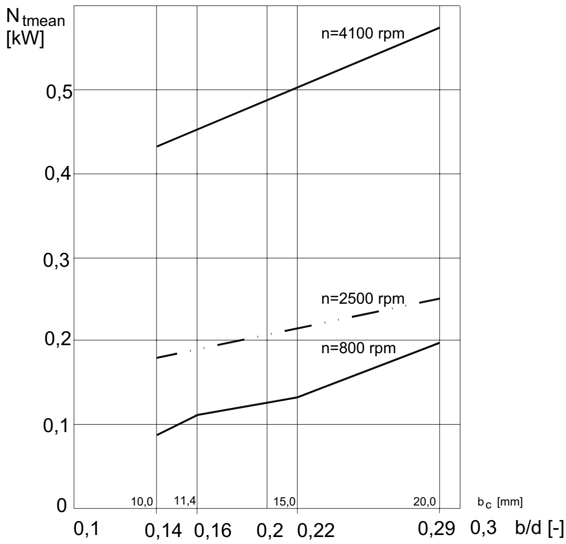

Fig. 5. Mean friction power vs. length of main bearing (bearing nominal diameter d = 0.070 m, half of grooved bearing effective length b = 0.01142 m)

The bearing clearance is another parameter influencing the friction losses. For the speeds analyzed, there is a close relation between the value of bearing clearance and friction losses as it has been presented in Fig. 6. Along with the increase in bearing clearance the friction losses insignificantly decline. A considerable drop in friction losses can be observed in the range of minimum and medium clearances for the speed of idle run (n = 800 rpm). All calculations have been carried out for the SAE 15W/40 mineral lube oil. In the case of minimal bearing clearance a replacement of SAE 15W/40 oil with the synthetic 5W/40 one would be advantageous because the friction losses could be diminished by about 60% (from 0.3 kW to 0.12 kW).

The grade of lubricating oil, especially its viscosity is an important factor influencing the friction losses at bearing. Three types of the Lotos lube oil, namely synthetic, semisynthetic and mineral ones (the last fresh and used) have been chosen for calculations. Their viscosity corresponds to the manufacturer's data and in the case of used oil its viscosity remains within the predicted range (increase or drop in viscosity by 40 and 20 percent, respectively) [6]. Fig. 7 presents the friction losses depending on oil grade (calculated for bearing mean clearance) for different rotational speeds. Despite the oil grade friction losses at the bearing are very similar for the same speed (2500 and 4100 rpm). In the case of idle run use of the 5W/40 synthetic oil brings about definitely lower losses. Comparing losses resulting from application of fresh and used 15W/40 mineral oil, an insignificant fall in their value could be observed for the used oil.

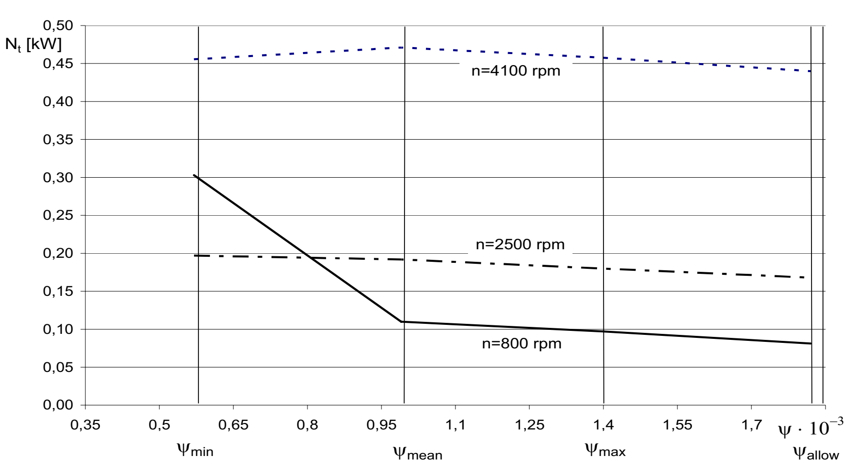

Fig. 6. Mean friction power vs. bearing clearance for various crankshaft speeds

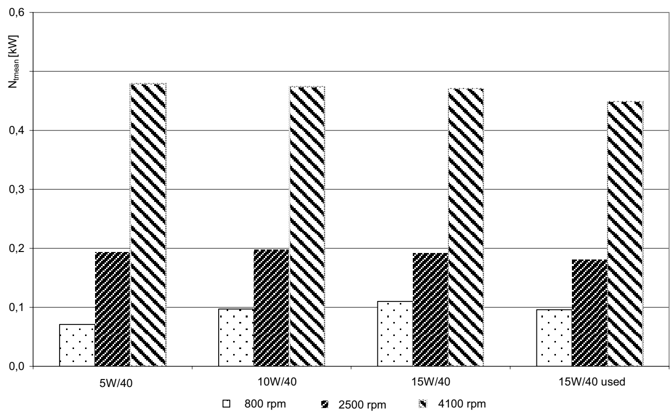

Fig. 7. Bearing mean friction losses for tested oils and speeds

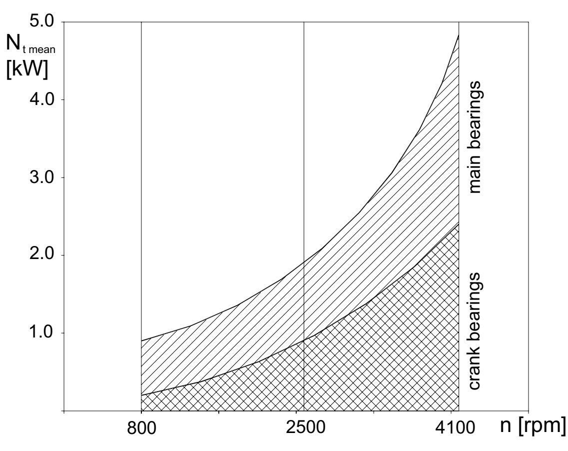

Fig. 8. The course of change in friction losses at engine main and crank bearings

Fig. 8 presents a diagram summarizing friction losses at all main and crank bearings vs. crankshaft speed. Curves representing friction losses combine friction power calculated for individual main (five fold) and crank (four fold) bearings. Calculations were carried out for a mean relative clearance and for SAE 15W/40 grade lube oil.

4. Conclusions

The friction losses calculated for running crank mechanism bearings allow to conclude that the rotational speed affects them to the highest degree. For the idle run speed the losses at crank bearings are a half of those generated at main bearings. However, along with the increase in speed they increase as well and for the speed of 4100 rpm are comparable to the losses at main bearings.

For the most loaded bearing (the B main bearing) the friction losses:

– increase with the increase in bearing length,
– decrease slightly with the increase in bearing clearance, while the significant drop in their value could be observed for 800 rpm within the clearance range ψ_{min} and ψ_{mean},
– are almost the same for oils analyzed at the same crankshaft speeds; in case of synthetic oil far lower friction losses correspond to the idle run speed. This is why this kind of oil is recommended for cold starts.

Eventual works on friction losses should take into consideration higher number of factors affecting the power necessary to overcome friction resistance at main and crank bearings. Then the decrease of those losses could be achieved thanks to the proper design and optimization, what in turn results in lower fuel consumption and lower toxic emissions.

References

[1] Gaberscik, G., Meldt, W., Tripolt, W., Trzesniowski M., *Durch Reibungsoptimierung zur Verbrauchsreduktion,* MTZ, 03/2006.

[2] Kozłowiecki, H., Krzymień, A., *Łożyska mechanizmu korbowego tłokowych silników spalinowych i ich smarowanie*, Wyd. Politechniki Poznańskiej, Poznań 1997.

[3] Krzymień, A., *An influence of bearing length on its performance data*, Journal of Kones, Internal Combustion Engines, Vol. 12, No 1-2, p.183-186, Warszawa 2005.

[4] Krzymień, A., *Reliability evolution of crank mechanism bearings of a supercharged automotive diesel*, III International Scientific-Technical Conference EXPLO-DIESEL & GAS TURBINE '03, pp. 347-354, Gdańsk – Lund 2003.

[5] Krzymień, A., Krzymień, P., *Analysis of the lube oil viscosity effect on selected operational parameters of the vehicle engine crank mechanism sidle bearings*, PTNS Kongres – 2005, PTNS PO5-C046-Paper, Bielsko-Biała / Szczyrk 2005.

[6] Krzymień, A., Krzymień, P., *Wpływ lepkości oleju silnikowego na hydrodynamiczne parametry pracy łożysk głównych przy zmiennym luzie łożyskowym*, Archiwum Motoryzacji, Wydawnictwo Naukowe PTNM, Nr 3, s. 289-298, Radom 2006.

[7] Krzymień, A., Krzymień, P., *Wpływ lepkości oleju smarującego na wybrane wskaźniki pracy łożysk mechanizmu korbowego,* Czasopismo Techniczne, Silniki Spalinowe, z.6-M/2004, s. 437-443, Wydawnictwo Politechniki Krakowskiej 2004.

[8] Lang, O., Steinhilper, W., *Gleitlager,* Springer Verlag, Berlin, Heidelberg, New York 1978.

[9] Martin, F.A., Friction in internal combustion engine bearings, I Mech E, C67/85, pp. 1-17, London 1987.

[10] Praca zespołowa, *Opracowanie programów obliczeniowych łożysk hydrodynamicznych,* praca niepublikowana, Politechnika Poznańska, Poznań 1999.

STRATIFIED CHARGE COMBUSTION MODEL INCLUDING NO_X FORMATION

Kazimierz Lejda, Paweł Woś

Rzeszów University of Technology
al. Powstańców Warszawy 8, 35-959 Rzeszów, Poland
tel.: +48 17 8651805, fax: +48 17 8543112
e-mail: klejda@prz.edu.pl, pwos@prz.edu.pl

Abstract

The paper presents a brief of mathematical model describing a two-zone, quasi-dimensional combustion in Diesel engine chamber. In order to simulate NO_X emission, the simplified Zeldovitch mechanism was applied in nitric oxide formation model. An outline of the model can also be applied for engines of other types, where stratified charge is formed, e.g. in GDI spark ignition engines. In case of Diesel engines with direct fuel injection, the model includes injection sub-model that allows investigation of injection rate effect on NO_X emission. This important advantage may be very useful for pre-fixing injection strategy in Common-Rail systems prior test bed fine research.

Keywords: *stratified charge combustion, mathematical modeling, NO_X emission, fuel injection model*

1. Introduction

In combustion engine exhaust a lot of toxic compounds such as carbon monoxide CO, hydrocarbons HC, nitric oxides NO_X, particles PM, and many others can be found. Most of them might be easily eliminated in exhaust system by use of filters and catalytic converters. But some might be not. It goes for NO_X. The main cause of NO_X formation is presence of oxygen O_2 and nitrogen N_2 molecules in combustion zone in the cylinder. There, during combustion, in very high temperature, a dissociation process occurs and free atoms of nitrogen and oxygen are released. These atoms are characterized by very high chemical activity and get quickly in reaction each other and with rest of N_2 and O_2 molecules, what results in NO and NO_2 formation. This is mainly thermal process - the higher combustion temperature the higher NO_X formation rate [4].

The NO_X formation during in-cylinder combustion with atmospheric air can't be avoided. However, it can be limited by two manners - to affect combustion process in such a way that excessive growth of NO_X emission should not be allowed; or to eliminate just formed NO_X from exhaust by a catalytic converter. The second way is used for homogenous charge, stoichiometric combustion engines rather. In diesel engines and other ones, where stratified charge, lean combustion proceeds, use of standard three-way catalytic converters does not give a good results because of high exhaust oxygen concentration. Thus, the most suitable and almost the only manner to limit NO_X emission for this type of engines seems to be a proper regulation of the combustion process.

The working cycle in the piston engines is very complex, especially a combustion stage, when many phenomena combine together in the same time and area. For example, in Diesel engines simultaneously occurs injection, fuel atomization and vaporization, induction of ignition, burning and many others chemical processes. All of them take only a few milliseconds. That is why full combustion optimization needs performing a lot of time- and fund-consuming experimental tests. The injection process has a fundamental influence on combustion, and finally on performance and ecological parameters of the engine. Knowledge of these mechanisms should allow helping in combustion control. It can be achieved not only in experimental way, but also by mathematical modeling of engine working cycle. Additionally, analytical methods allow fully arbitrary analyzing and are more time and cost efficient.

2. Description of a combustion model

All working cycle mathematical models can be sorted as follows [5]:

1) as regards dimensions, we have:
   - zero-dimensional models,
   - quasi-dimensional models,
   - multi-dimensional models;

2) as regards number of marked zones, we have:
   - one-zone models,
   - two-zone models,
   - multi-zone models.

Above segmentation defines a model complexity and fidelity in reflection of reality in the model. It is also connected with complication in mathematical tools used for simulation. The fundamental problem to select a proper type of the model is to agree to a compromise between accuracy and labor consumption needed to describe all phenomena. A priority here is the goal of analysis. As a rule, for comparative and/or quantitative research, a simplified model can be used giving good results; for qualitative investigations more precise model should be worked out instead.

Here will be presented an example of two-zone, quasi-dimensional model of combustion applied for DI Diesel engine. Split of the combustion chamber into two zones, although complicates a mathematics, yet makes much better fidelity in representation of phenomena proceeded inside the cylinder of this type of the engine. The scheme of physical and chemical processes is shown on Fig. 1.

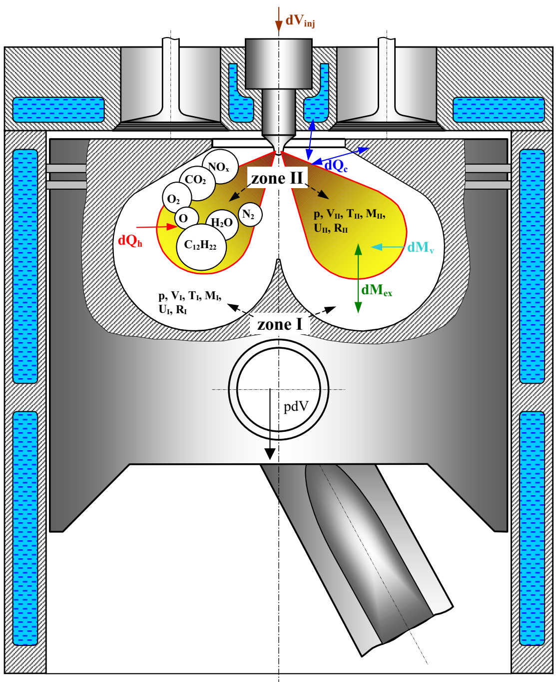

Fig. 1. The scheme of physical and chemical processes proceeded in combustion chamber in DI Diesel engine [6] (denotations are explained in the chapter below)

Inside the cylinder of volume V and pressure p, where at the end of intake stroke there is a fresh charge of a mass M_{ch}, at the moment determined by the start of injection angle a fuel dose begins to be injected. The fuel volume flow rate is $dV_{inj}/d\varphi$. Here, $d\varphi$ means increment of an independent variable of crank angle. A part of the fuel begins to evaporate with the rate equals $dM_v/d\varphi$. It forms streams of fuel-air mixture of total volume V_{II}. Through that, the combustion chamber is divided on two zones: the first one (I) of rest of fresh charge, and the second one (II) of fuel-air mixture. After short time of autoignition delay τ_o, process of evaporated fuel combustion begins with the burning rate equals $dM_h/d\varphi$. It results in a heat flux $đQ_h/d\varphi$ that is supplied into the zone II. Between both zones (I and II) mass transfer occurs ($dM_{ex}/d\varphi$), similarly between cylinder walls and both zones heat transfer of the rate $đQ_c/d\varphi$ occurs. The whole system gives an elementary mechanical work equals $pdV/d\varphi$. Except of fundamental combustion reaction, in both zones process of dissociation of some compounds runs, as well as NO_X formation. Finally, seven chemical species are considered.

On the basis of above physical model, taking indispensable assumptions into consideration, a mathematical model of engine working cycle was formulated. The essential equation for energy conversion inside the cylinder is differential equation of the first law of thermodynamics for open systems:

$$\frac{dU}{d\varphi} = \frac{đQ}{d\varphi} - p\frac{dV}{d\varphi} + \frac{dH}{d\varphi} \tag{1}$$

where:

U - internal energy of the system [J],
Q - heat delivered to/derived from the system [J],
V - system volume [m^3],
p - system pressure [Pa],
H - enthalpy delivered to/derived from the system [J],
φ - crank angle [deg].

Above equation is valid for both zones, and for both must be developed further. According to the assumptions taken in the physical model, we can write (detailed evaluation can be found in [6]):

- for heat fluxes:

$$\frac{đQ_I}{d\varphi} = -\frac{đQ_{c\,I}}{d\varphi} \quad \text{and} \quad \frac{đQ_{II}}{d\varphi} = -\frac{đQ_{c\,II}}{d\varphi} + \frac{đQ_h}{d\varphi} - \frac{đQ_v}{d\varphi} \tag{2}$$

- for mass transfers:

$$\frac{dM_I}{d\varphi} = \frac{dM_{ex}}{d\varphi} \quad \text{and} \quad \frac{dM_{II}}{d\varphi} = \frac{dM_v}{d\varphi} - \frac{dM_{ex}}{d\varphi} \tag{3}$$

- and for enthalpy fluxes:

$$\frac{dH_I}{d\varphi} = h_{ex}\cdot\frac{dM_{ex}}{d\varphi} \quad \text{and} \quad \frac{dH_{II}}{d\varphi} = h_v\cdot\frac{dM_v}{d\varphi} - h_{ex}\cdot\frac{dM_{ex}}{d\varphi} \tag{4}$$

where:

I, II - subscripts referred to zone I and II in order,
Q_c - heat of cooling [J],
Q_h - heat generated by combustion [J],
Q_v - heat consumed by vaporizing fuel [J],
M_{ex} - mass transferred between both zones [kg],
M_v - mass of evaporated fuel [kg],
h_{ex} - specific enthalpy of transferred mass; it is specific enthalpy of I or II zone depending on direction of mass flow [J/kg],
h_v - specific enthalpy of fuel vapor [J/kg],

Total internal energy of any thermodynamic system can be expressed by multiplying specific internal energy u and system mass M. Thus, we can also differentiate this multiplication, what gives:

$$\frac{dU}{d\varphi} = \frac{d(M \cdot u)}{d\varphi} = u \cdot \frac{dM}{d\varphi} + M \cdot \frac{du}{d\varphi} \tag{5}$$

If we consider, that specific internal energy u for various compounds mixture can be calculated as $u = \sum_i (u_i \cdot g_i)$ then, assuming $\sum_i \left(u_i \cdot \frac{dg_i}{d\varphi} \right)$ is almost zero, we get:

$$\frac{du}{d\varphi} = \frac{dT}{d\varphi} \cdot \sum_i \left(g_i \cdot \frac{\partial u_i}{\partial T} \right) \tag{6}$$

where:

u_i - specific internal energy for a "i"component [J/kg],
g_i - mass fraction of a "i" component in whole system [kg/kg],
T - system temperature [K].

After substitution all above equations into the fundamental equation (1) for both zones, we get a system of two differential equations with three unknowns: $dT_I/d\varphi$, $dT_{II}/d\varphi$, and $dM_{ex}/d\varphi$:

$$\begin{cases} \left[\sum_i (u_{Ii} g_{Ii}) - h_{ex} \right] \frac{dM_{ex}}{d\varphi} + M_I \sum_i \left(g_{Ii} \frac{\partial u_{Ii}}{\partial T} \right) \frac{dT_I}{d\varphi} = \frac{đQ_I}{d\varphi} - p \frac{dV_I}{d\varphi} \\ \left[h_{ex} - \sum_i (u_{IIi} g_{IIi}) \right] \frac{dM_{ex}}{d\varphi} + M_{II} \sum_i \left(g_{IIi} \frac{\partial u_{IIi}}{\partial T} \right) \frac{dT_{II}}{d\varphi} = \frac{đQ_{II}}{d\varphi} - p \frac{dV_{II}}{d\varphi} - \left[\sum_i (u_{IIi} g_{IIi}) - h_v \right] \frac{dM_v}{d\varphi} \end{cases} \tag{7}$$

The other differentiates, such as $đQ_I/d\varphi$, $đQ_{II}/d\varphi$, $dV_I/d\varphi$, $dV_{II}/d\varphi$, $dM_v/d\varphi$, can be calculated using separated sub-models. To resolve above system algebraically, $dM_{ex}/d\varphi$ must be eliminated and expressed by other known components. To do that, we use an overall assumption that pressure p in both zones is equal:

$$p_I = p_{II} \tag{8}$$

According to ideal gas law equation of Clapeyron it also means that:

$$\frac{M_I \cdot R_I \cdot T_I}{V_I} = \frac{M_{II} \cdot R_{II} \cdot T_{II}}{V_{II}} \tag{9}$$

where the symbols refer to both zones, such as subscript indicates, and there are:

M - mass of the zone [kg],
R - universal gas constant for whole zone [J/(kg·K)],
T - average temperature of the zone [K],
V - zone volume [m^3].

Going ahead, at any time a mass of the first zone is a sum of initial mass of fresh charge M_{ch} and transferred mass M_{ex}, and for the second one it is a mass of evaporated fuel M_v from which transferred mass M_{ex} is subtracted. Then transferred mass can be evaluated as follows:

$$M_{ex} = \frac{M_v \cdot R_{II} \cdot T_{II} \cdot V_I - M_{ch} \cdot R_I \cdot T_I \cdot V_{II}}{R_I \cdot T_I \cdot V_{II} + R_{II} \cdot T_{II} \cdot V_I} \tag{10}$$

To differentiate it relatively to crank angle variable φ, we receive a formula for component $dM_{ex}/d\varphi$ as a function expressed by the other differentiates:

$$\frac{dM_{ex}}{d\varphi} = f\left(\frac{dT_I}{d\varphi}, \frac{dT_{II}}{d\varphi}, \frac{dV_I}{d\varphi}, \frac{dV_{II}}{d\varphi}, \frac{dM_v}{d\varphi}\right) \tag{11}$$

Now, replacing the component $dM_{ex}/d\varphi$ in the system of equations (7) with the above function we receive a new system of two differential equations with two unknowns $dT_I/d\varphi$, $dT_{II}/d\varphi$ only, i.e.:

$$\begin{cases} A \cdot \dfrac{dT_I}{d\varphi} + B \cdot \dfrac{dT_{II}}{d\varphi} = C \\ D \cdot \dfrac{dT_I}{d\varphi} + E \cdot \dfrac{dT_{II}}{d\varphi} = F \end{cases} \tag{12}$$

where A, B, C, D, E, F contains expressions of known variables, which can be evaluated by use of separated sub-models and/or formulas. In this shape of the system, the unknowns $dT_I/d\varphi$, $dT_{II}/d\varphi$ can not be calculated by any of numerical methods. These methods need explicit from of equations. To get it, the system (12) has to be transformed (solved algebraically) relatively to $dT_I/d\varphi$, $dT_{II}/d\varphi$. For instance, applying the method of Cramer determinants we have:

$$\begin{cases} \dfrac{dT_I}{d\varphi} = \dfrac{B \cdot F - E \cdot C}{B \cdot D - E \cdot A} \\ \dfrac{dT_{II}}{d\varphi} = \dfrac{C \cdot D - A \cdot F}{B \cdot D - E \cdot A} \end{cases} \tag{13}$$

Above computer simulation friendly form of equations has been implemented to perform all calculations.

In the model of NO_X formation, the two of reversible Zeldovitch's reactions have been used [1, 2]:

$$O + N_2 \quad \leftrightarrow \quad NO + N \tag{14}$$
$$N + O_2 \quad \leftrightarrow \quad NO + O \tag{15}$$

On the base of chemical kinetic theory, the formula to calculate the NO formation rate according to the above reaction scheme is following:

$$\frac{1}{V} \cdot \frac{dn_{\mathrm{NO}}}{dt} = 2k_1 [\mathrm{O}][\mathrm{N}_2] \tag{16}$$

where:

V - volume of reaction zone [m^3],
n_{NO} - mole number of NO [mole],
t - time [s],
k_1 - kinetic constant of the first Zeldovitch reaction in forward direction [m^3/(mole·s)],
[O], [N_2] - molar concentration of O-atoms and N_2-molecules inside the reaction zone [mole/m^3].

It follows that the formation rate is controlled by the first reaction of Zeldovitch. Atoms of oxygen come mainly from dissociation $O_2 \leftrightarrow 2\,O$, and its concentration can be calculated as follows:

$$[\mathrm{O}] = \left(K^c{}_{\mathrm{O}} \cdot [\mathrm{O}_2]\right)^{\frac{1}{2}} \tag{17}$$

where:

$K^c{}_{\mathrm{O}}$ - equilibrium constant of oxygen dissociation reaction referred to the concentration [mole/m^3],
[O], [O_2] - molar concentration of O-atoms and O_2-molecules inside the reaction zone [mole/m^3].

Finally, the NO formation rate formula (16) takes following shape (all denotations are as same as above):

$$\frac{1}{V} \cdot \frac{dn_{\mathrm{NO}}}{dt} = 2k_1 \cdot K_{\mathrm{O}}^{c\,\frac{1}{2}} \cdot [\mathrm{O}_2]^{\frac{1}{2}} \cdot [\mathrm{N}_2] \tag{18}$$

The same formula can express a mass flux of NO in kilograms, such as to be used directly in model equations. It should be changed as follows:

$$\frac{dM_{\mathrm{NO}}}{d\varphi} = \frac{\mu_{\mathrm{NO}} \cdot V}{6000 \cdot n} \cdot \left[2k_1 \cdot K^c{}_{\mathrm{O}}^{\frac{1}{2}} \cdot [\mathrm{O}_2]^{\frac{1}{2}} \cdot [\mathrm{N}_2] \right] \tag{19}$$

where:

μ_{NO} - molar mass of nitric oxide [g/mole]; $\mu_{\mathrm{NO}} = 30{,}0061$,
n - engine speed [rev/min],
- remaining denotations are as same as above.

The constants $K^c{}_{\mathrm{O}}$ and k_1 can be gathered from the bibliography sources [1, 5], and were slightly modified to achieve validated results. The initial values of them can be equal to:

$$k_1 = 7{,}6 \cdot 10^7 \cdot exp\left(\frac{-38000}{T}\right) \quad \left[\frac{\mathrm{m}^3}{\mathrm{mole} \cdot \mathrm{s}}\right] \tag{20}$$

$$K^c{}_{\mathrm{O}} = \frac{10^{5+0{,}310805 \cdot ln(T) - \frac{12954}{T} + 1{,}07083 - 0{,}738336 \cdot 10^{-4} \cdot T + 0{,}344645 \cdot 10^{-8} \cdot T^2}}{\overline{R}T} \quad \left[\frac{\mathrm{mole}}{\mathrm{m}^3}\right] \tag{21}$$

3. Model estimation and calculation results

Described in brief, the model has been validated using a test stand. The stand was supported by the single-cylinder, direct injection diesel engine SB 3.1. The full scheme of the bench is shown on Fig. 2.

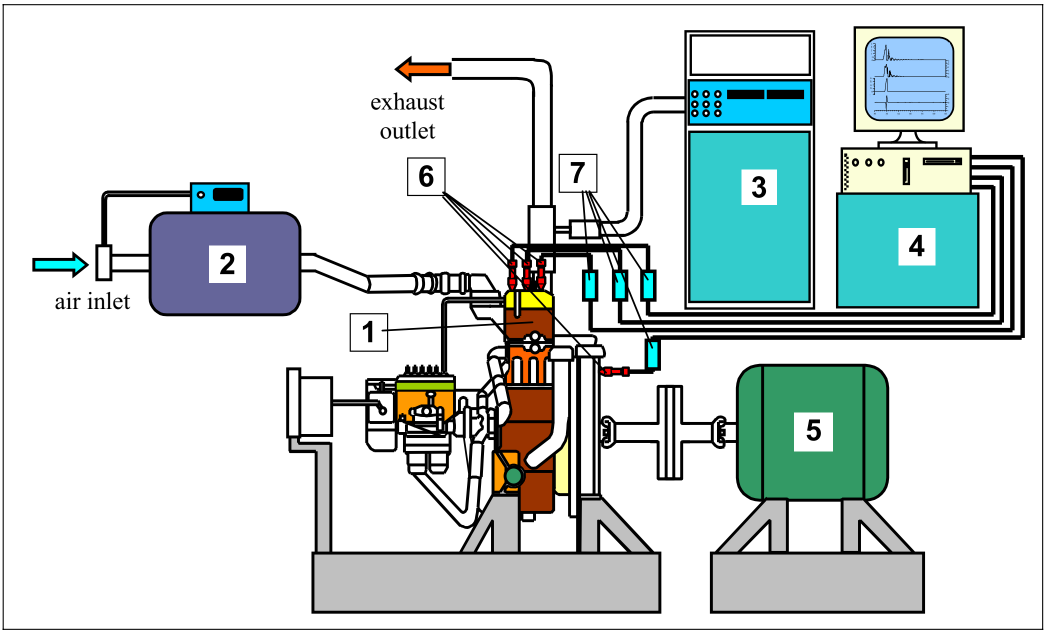

Fig. 2. The scheme of the test bench [3]: 1 - test engine SB 3.1, 2 - air consumption meter, 3 - Pierburg NOx analyzer, 4 - control computer with fast data acquisition card, 5 - eddy-current dynamometer, 6 - AVL pressure, lift, and crank angle sensors, 7 - amplifiers

The main acquired parameters were: injector needle lift, fuel pressure before the injector, pressure inside the combustion chamber, exhaust concentration of NO_X, and fuel and air consumption. The injector needle lift and fuel pressure data were used to calculate fuel injection rate, and NO_X concentration and exhaust flux data were used to calculate NO_X emission.

Some of parameters in the model have had to be tuned up to achieve satisfactory conformity between calculated results and experiments. It is common feature of all semi-empirical models and cannot be avoided in the process of parameter estimation. The sample results (Fig. 3) show that the convergence in the field of NO_X emission was not worse than 10%. It can be considered as a good result, seeing that the model contains many simplifications and assumptions.

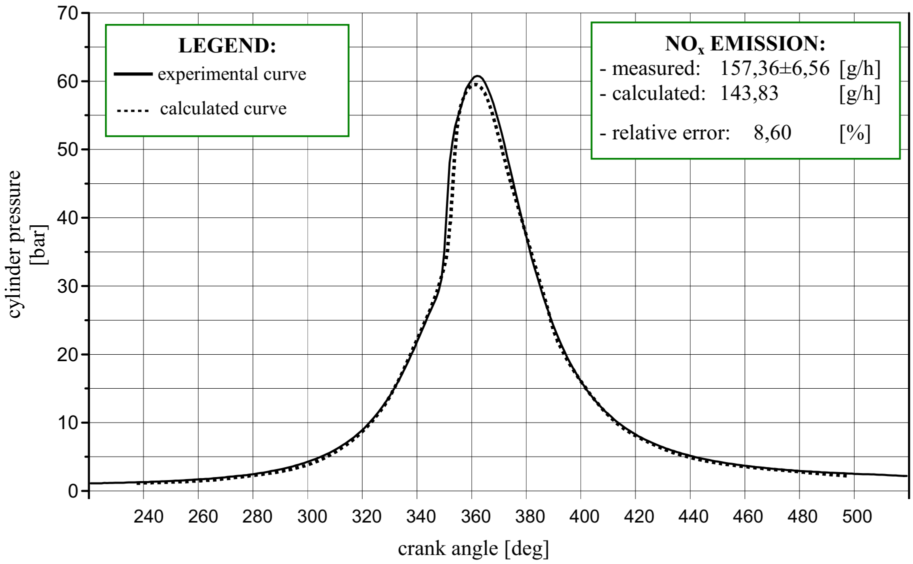

Fig. 3. Experimental and simulated results comparison [6] (engine speed n = 1000 rev/min, half load)

4. Conclusion

The mathematical model of combustion presented in the paper includes a lot of phenomena. Here, from among of rich set, only the formulas for thermodynamic energy conversion and NO_X formation were selected for presentation. Many of physical and chemical effects occurred in reality have been omitted in the model or included in reduced form because of impossibility in exact mathematical representation. Surely, it influences model accuracy, but is also partially compensated in parametric estimation process. This way of model validation has the disadvantage that must be anew performed for each engine taken into simulation. Nevertheless, the model is a valuable research tool, which can be used for extensive studies of combustion in stratified charge engines.

References

[1] Heywood, J. B., *Internal Combustion Engines Fundamentals,* McGraw Hill Co., New York 1988.

[2] Kafar, I., Piaseczny, L., Merkisz, J., *Mathematical Model of Toxic Compound Emissions in Exhaust Gases Produced by Marine Engines,* Journal of KONES, vol. 5, No 1, Warsaw - Gdańsk 1998.

[3] Lejda, K., Woś, P., *Effect of fuel injection rate on NO_X emission in Diesel engine*. Machine Engineering, vol. 8, book 4, Publishing Agency of Wroclaw Board of FSNT NOT, Wrocław 2003, (in Polish).

[4] Merkisz J., *Ecological Problems of Combustion Engines*. Publishing by Poznań University of Technology, Poznań 1999, (in Polish).

[5] Rychter, T, Teodorczyk, A., *Mathematical Modeling of Piston Engine Working Cycle,* PWN, Warsaw 1990, (in Polish).

[6] Woś, P., *An Analysis of Fuel Injection Rate Effect on NO_X Emission from Direct Injection Diesel Engine,* Doctor Thesis, Rzeszów University of Technology 2003, (in Polish).

THE APPLICATION OF THE PHOTO OPTIC TORQUE METER TO ESTIMATION OF TORQUE AND ROTATIONAL SPEED FLUCTUATIONS ON THE PROPELLER SHAFT OF A SHIP

Leszek Morawski

Gdynia Maritime University
83 Morska Str., 81-225 Gdynia, Poland
tel.: +48 58 6901256, fax: +48 58 6219938
e-mail: lmoraw@am.gdynia.pl

Zbigniew Szuca

Enamor Ltd.
83 Morska Str., 81-225 Gdynia, Poland
tel.: +48 58 6901751, fax: +48 58 6901701
e-mail: zbigniew.szuca@enamor.com.pl

Abstract

The paper presents the method of measuring instantaneous torque and rotational speed fluctuations on the propeller shaft of a ship. The measured data are significantly deformed, therefore spectral analysis and filtering are used for estimating the real signals. The microprocessor torque meter ETNP-8 described in the paper was designed to measure not only mean values of the torque and rotational speed on the ship's propeller shaft, but also instantaneous fluctuations of the torque and engine rotational speed as a function of the shaft rotation angle. Displaying time-histories of those parameters on the monitor screen of an external PC computer gives the operator an opportunity to make a preliminary performance assessment for each individual cylinder in the engine, and for the drive system as a whole. As an example, the analysis and processing of the measured torque and rotational speed fluctuations are presented. The measurements were done on the training ship m/s Horyzont II, owned by the Gdynia Maritime University.

Keywords: *propeller unit ,main engine, torque measurement, torque fluctuation, torque meter*

1. Introduction

In the Gdynia Maritime University and Research-Production Enterprise for Maritime Industry Enamor Ltd., a device (bearing a symbol ETNP-8) is manufactured for measuring torque, rotational speed, and power at the ship's main drive propeller shaft. Optionally, it also can calculate other ship performance indices, such as fuel consumption per nautical mile, per unit of power, etc.[2]. The torque meter was designed not only for measuring mean values of the torque and rotational speed on the propeller shaft of the ship but also to measure instantaneous fluctuations of the torque and engine rotational speed as a function of the shaft rotation angle. A new version of the torque meter reveals better characteristics than the older ones. One of the first manufactured devices was installed on the board of the training ship m/s Horyzont II. The analysis and processing of the measured data of torque and rotational speed fluctuations is presented below.

2. Measuring torque and rotational speed fluctuations

The general idea of the torque and rotational speed measurement makes use of the torsion angle measurement executed on a shaft section using a photo-optical technique. Two discs with machined teeth are fixed on the propeller shaft at distance L (approx. 400 mm). They are designed in such a way that their teeth are in the same plane. The teeth of these two discs can rotate in (and through) a gap of a transoptor based measuring head (Fig. 1a). The shaft torsion, proportional to the loading torque, makes the teeth of the two discs move with respect to each other, as is shown in Fig. 1b. At the output of the measuring head a rectangular wave is obtained with variable pulse-width modulation (Fig. 1c).

The torque measurement bases on measuring the difference in the time duration of two successive pulses, recorded by the transopting head, that correspond to the clearances between the disc teeth.

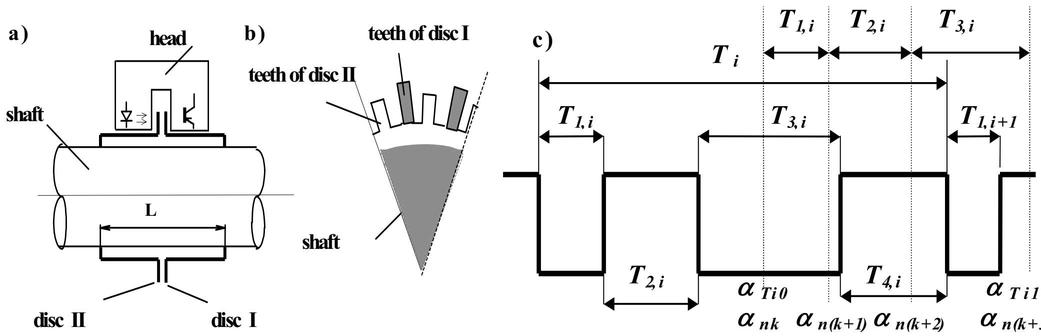

Fig. 1. Principle of the shaft torsion angle measurement: a) method of disc fastening on the propeller shaft; b) cross sections of toothed disc portions; c) time-history of output signal from transoptor head.

One tooth on one disc has a narrow gap to mark a selected shaft position angle. Other shaft position angles are determined by counting pulses transmitted by the transoptor head (Fig. 1c). When the pulse from the narrow gap is estimated, the torque meter starts measuring the passing times T_{1i}, T_{2i}, T_{3i}, T_{4i} (Fig. 1c) of consecutive clearances between the teeth during a given number of revolutions. The results of the time measurements are stored in the RAM memory of the torque meter electronic unit. Then, after the measurement is completed, the data are transmitted to the external computer. Actual values of the torque and rotational speed fluctuations are computed in the off-line mode.

Assuming that the values of the torque and rotational speed are constant during the time when the transporting head passes two consecutive teeth and two clearances, the instantaneous torque is determined from the formula:

$$T_T\,(\alpha_{Ti,j}) = \pm\, k_T \cdot \frac{\left|T_{3,i} - T_{1,i+j}\right|}{T_{1,i+j} + T_{2,i+j} + T_{3,i} + T_{4,i}} \;=\; \mathrm{T_{Tji}} + \mathrm{T_{Tjip}} \quad [\%] \quad j=0,1 \tag{1}$$

while the instantaneous rotational speed of the shaft is computed from the formula:

$$n\,(\alpha_{nt,i}) = k_n \cdot \begin{cases} 1/(T_{1,i} + T_{2,i} + T_{3,i} + T_{4,i}) & t=0 \\ 1/(T_{1,i+1} + T_{2,i} + T_{3,i} + T_{4,i}) & t=1 \\ 1/(T_{1,i+1} + T_{2,i+1} + T_{3,i} + T_{4,i}) & t=2 \\ 1/(T_{1,i+1} + T_{2,i+1} + T_{3,i+1} + T_{4,i}) & t=3 \end{cases} \quad [\text{rev/min}] \tag{2}$$

where:

i - number of teeth in one disc,
k_T - proportionality coefficient resulting from the nominal torque, the amorphous elasticity coefficient of the shaft, the shaft diameter, the length of the twisted shaft section, and the unit scaling,
k_n - proportionality coefficient resulting from the unit scaling;
$\alpha_{Tj,i}$ - torque measurement angles (j=0,1),
$\alpha_{nt,i}$ - rotational speed measurement angles (t=0,1,2,3),
$T_{tj,i}$ - torque resulting from the shaft tension angle,
$T_{Tj,ip}$ – average torque correction resulting from the distribution of clearances in the rest position.

It should be stressed here that the number of points corresponding to one shaft revolution during which the torque is measured is equal to the double number of teeth (i) in one disc, while for the rotational speed the number of points is four times as big as the number of teeth.
The mean values of the shaft torque and rotational speed are calculated using formulas (1) and (2) for an integer number of shaft revolutions.

3. Results of measurements on real objects

The measurements were done on the training ship m/s Horyzont II, owned by the Gdynia Maritime University (L=56m; main engine: 4-stroke Sulzer–Cegielski 8S20U, nominal power 1280 kW, nominal rotational speed 1000 rev/min; reduction gear 3.115:1; propeller shaft diameter 180 mm; four-blade variable pitch propeller; number of teeth of the torque meter disc 48). Below the analysis and data processing of the measured torque and rotational speed fluctuations are given.

As is well known, the force which is generated by the combustion gas pressure and is tangent to the engine crank creates the torque and determines the power delivered by particular engine cylinders to the crankshaft. Since the energy transmitted by each individual cylinder is usually a function of the rotation angle, the time-history of the total torque transmitted to the propeller shaft and its rotational speed reveal a periodical nature. The reduction gear and vibration damper significantly limit the torque and rotational speed fluctuations on the shaft. The torque fluctuation curves computed, using formula (1), for two different loads and shaft rotations, are shown in Figs 2 and 3.

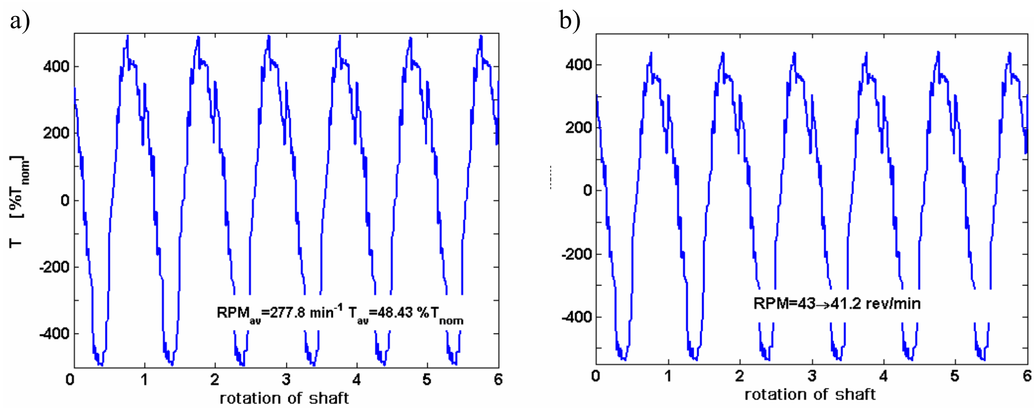

Fig. 2. Propeller shaft torque fluctuations:
a) for n_{av}=277.8 rev/min, torque T_{av}=48.43 $\%T_{nom}$, b) for n_{av}=41.2-43 rev/min, T_{av}=-0.32 $\%T_{nom}$.

The second case corresponds to the situation when the shaft was decoupled from the engine and the shaft rotation was only provoked by the moving ship. The value of the torque was near zero. The both presented signals are significantly deformed. The main source of deformations is an inaccuracy in manufacturing and installing the toothed discs on the shaft, but it can also include possible resonances of free torsion vibrations of the propeller shaft, vibrations of the shaft deflection, propeller load fluctuations, etc. The possibility of free resonances of mechanical parts of the torque meter cannot be neglected as well.

The two presented torque time-histories are similar to each other, with the first harmonics being the dominating component. Its most possible source is the lack of symmetry in fastening of the two halves of the toothed disc, cut apart before the assembly, on the shaft. As is seen in Fig. 2, this component exceeds 400% of the nominal torque. This and other spectrum components deforming the measurement results can be eliminated using a method of spectral analysis which was presented in [1] and [2]. The below presented direct method in time domain consists in cyclic subtracting from the analysed time-histories 96 values (2*number of teeth in one disc), being the torque corrections corresponding to the distribution of gaps and teeth when the torque is equal zero. The torque corrections for the full revolution of the propeller shaft are calculated as averaged over a number of revolutions, following the formula:

$$T_{cor}(\alpha_{Tt,j}) = \frac{1}{n}\sum_{k=1}^{n}\left(T_k(\alpha_{Ti,j}) - T_{kav}\right) \tag{3}$$

where:

$T_k(\alpha_{Ti,j})$ – calculated instantaneous value of the torque for the propeller shaft rotation angle $\alpha_{Ti,j}$ in k-th shaft revolution,
T_{kav} – real mean value of the torque in k-th shaft revolution.

Figure 3 presents the torque correction time-history for the full propeller shaft revolution, based on 96 correcting values determined in the above described way. Corrections determined for other loads and rotational speeds differ by no more than 0.3%. Figure 4 shows the torque time-histories from Figs 2a and 2b after taking into account the correction curves. They are still deformed by high-frequency effects, which, however, can be eliminated using a forward-backward type filter, which gives zero phase shift due to double filtering. The filter used here was the third-order low-pass Butterworth filter, with the cutting frequency $\omega=0.88\pi\cdot i/n$ (i- number of teeth in one disc, n-shaft rotational speed, in rad/s).

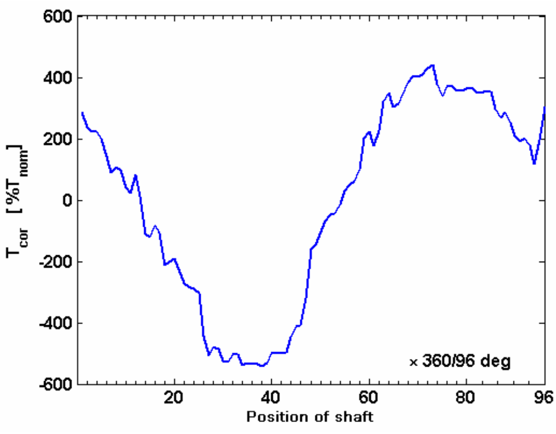

Fig. 3. Torque correction factor for one propeller shaft revolution

The filtered torque time-histories are marked in Fig. 4 as thicker lines. What is noteworthy is torque fluctuations with the amplitude of about 2.5% of the nominal torque (Fig. 4a). Those fluctuations are generated by the running engine and residual torque fluctuations on the engine crankshaft, which were not completely damped. This estimation is confirmed by the torque time-history shown in Fig. 5, significant components of which are the harmonics corresponding to the full cycle of propulsion engine operation (2 crankshaft revolutions). A very small amplitude component, marked with an arrow, which is generated by individual cylinders is significantly damped (the operation of all 8 cylinders during two crankshaft revolutions). In the figure the frequency scale unit is related to one full revolution of the propeller shaft.

Figure 4b shows the time-history of the instantaneous torque measured on the propeller shaft 50 seconds after decoupling it from the propulsion engine. The propeller is rotated, together with the shaft and the gear, by the water flowing down the ship's hull, which moves by its own inertia. That is why the fluctuations caused by the engine in operation are missing in Fig. 4b. The observed low fluctuations are likely to be generated by irregular stream of water flowing down the propeller and friction torques in shaft bearings. The load was approximately equal to 0.4% of the nominal torque.

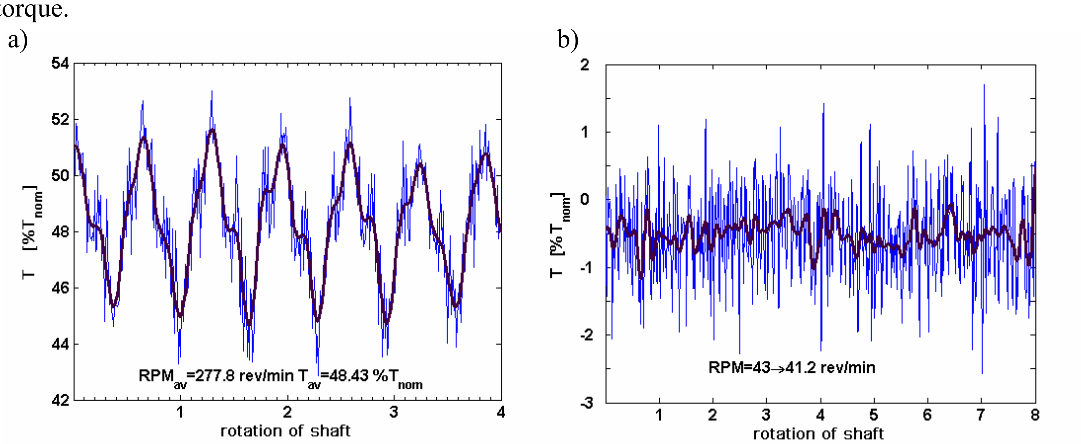

Fig.4. Torque time-histories in consecutive shaft revolutions, taking into account corrections and filtering: a) RPM_{av}=277.8 rev/min; b) RPM_{av}≈41-43 rev/min

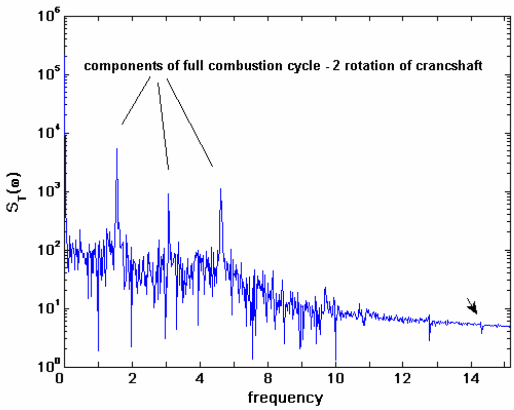

Fig.5. Frequency spectrum of the torque shown in Fig.4a

A similar methodology of measurement data analysis was applied for shaft rotational speed time-histories. Figure 6 presents rotational speed time-histories calculated using formula (2). They correspond to the same measurement cycles as for the torque. Like for Fig. 4, the frequency scale unit is related to one full revolution of the propeller shaft.

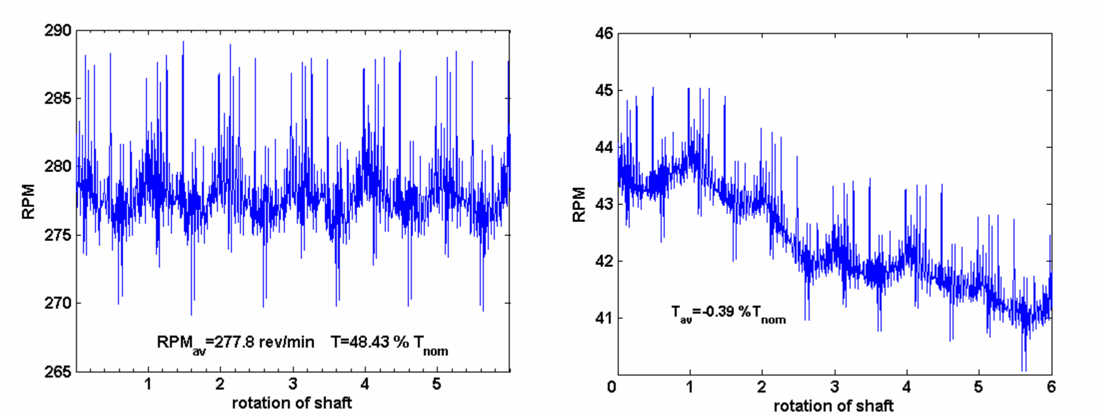

Fig.6. Fragments of rotational speed time-histories for different engine loads

The shape of the angular speed correction curve taking into account the inaccuracy of toothed disc machining and assembly is shown in Fig. 7. It is related to the mean value of the rotational speed in the measurement cycle being the basis for its calculation. The figure shows two, identical in practice, correction curves which were calculated using two different data samples recorded at different mean shaft rotational speeds. The way in which the correction was calculated is similar to that used for torque correction.

$$n_{cor}(\alpha_n(i)) = \frac{1}{n \cdot n_{av}}\left(\sum_{k=1}^{n}\left(n_k(\alpha_{Ti,j}) - n_{kav}\right)\right) \tag{4}$$

As results from formula (2) the amplitude of the correction curve is directly proportional to the shaft rotational speed. For higher shaft rotational speeds the same geometrical inaccuracies of toothed disc machining lead to higher amplitudes of disturbances, which is confirmed by the rotational speed time-histories shown in Fig. 6.

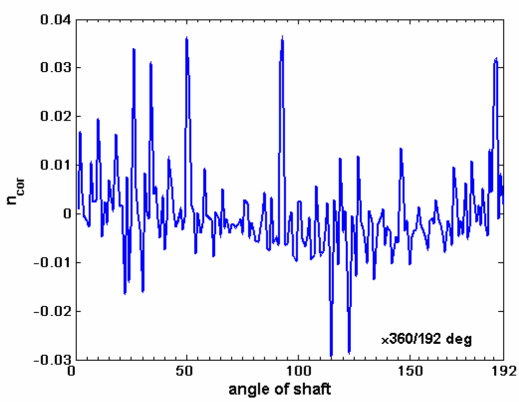

Fig.7. Relative values of propeller shaft speed correction factor

The rotational speed time-histories taking into account the calculated corrections are given in Fig. 8. The figure purposely preserves the same scale of the Y-axis to better illustrate the scale of reduction of the disturbances.

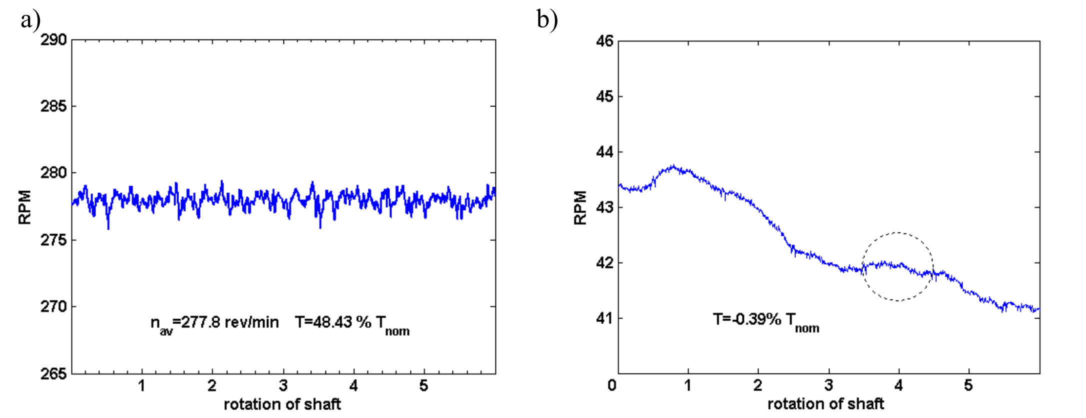

Fig. 8. Time-histories of the propeller shaft rotational speed after taking into account the correction from Fig.7: a) the coupling connected; b) the coupling disconnected

The propeller shaft rotational speed fluctuations shown in Fig. 8a result from power transmission from the engine to the propeller. When the propeller shaft is decoupled from the propulsion engine, the amplitude of fluctuations is significantly lower (Fig. 8b). The time-histories of instantaneous values of shaft rotational speed can also be filtered using the forward-backward method. The result of this filtering, applied to selected fragments of time-histories from Fig. 8, is shown in Fig. 9.

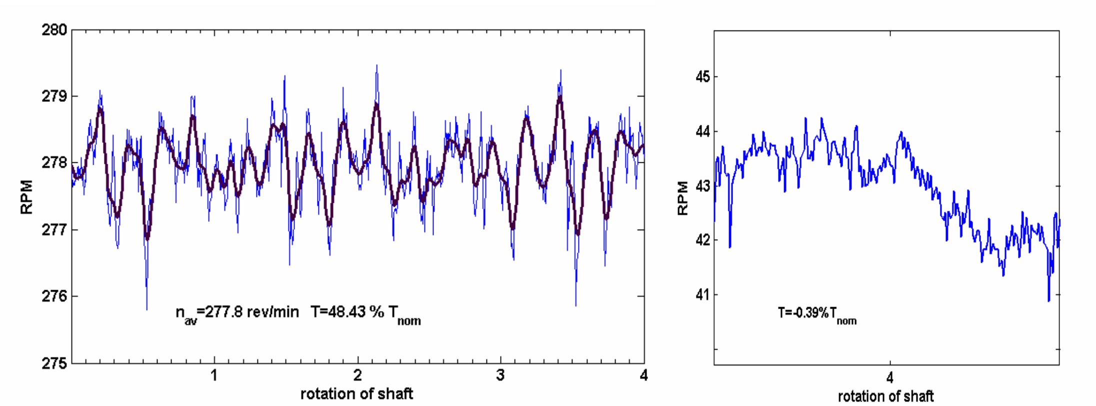

Fig.9. Detailed fragments of rotational speed time-histories shown in Fig.8

4. Final conclusions

The presented results of measurements of instantaneous torque and rotational speed, and the methodology of their processing confirm much higher measuring potential of the newly developed torque meter ETNP-8. The ship on which the measurements were done has a 4-stroke medium speed engine and the power transmission system which to a considerable extent damps torque and rotational speed fluctuations. The analysed time-histories reveal basic harmonics corresponding to the full cycle of engine operation (2 crankshaft revolutions). The components corresponding to the operation of individual cylinders are not recognised in the analysed spectra.

The experience gained from numerous measurements of operating parameters of the power transmission system, performed with the aid of specialised measuring instrumentation on sea-going cargo vessels, allows concluding that along with typical application for continuous measurements of moment and rotational speed, the presented torque meter ETNP-8 can also be used by the measuring staff for diagnostic measurements. Easy use in the operating mode „Diagnostics" allows the machine crew to perform on-line measurements, with their immediate analysis, data storage, and transmission to the shipowner.

References

[1] Morawski, L., Szuca, Z., *Urządzenie nowej generacji do pomiaru momentu i prędkości obrotowej na wale okrętowego silnika średnio/wolnoobrotowego, z możliwością identyfikacji zmian stanu technicznego zespołu napędowego oraz wstępnej diagnostyki silnika napędu głównego*, Raport końcowy-Projekt celowy KBN Nr 6T12 2003C/06267, Akademia Morska w Gdyni, PBP ENAMOR marzec 2006.

[2] Morawski, L., Sikora, M., *Wykorzystanie mikroprocesorowego urządzenia mierzącego moment i prędkość obrotową wału śruby do monitorowania pracy układu napędu głównego statku*, Pomiary Automatyka Kontrola, nr 7 (lipiec) 1998, str.272-277, rys.10 bibl. 6.

[3] *Dokumentacja techniczna urządzeń na statku Horyzont II,* Stocznia Północna, Gdańsk, 1998.

GASEOUS EROSION AND CORROSION OF TURBINES

Bartosz Olzak, Janusz Szymczak, Andrzej Szczepankowski

Air Force Insitute of Technology
ul. Księcia Bolesława 6, Skr. poczt. 96, 01-494 Warszawa 46, Polska
tel.:+48 22 6852210, e-mail: assz@op.pl

Abstract

The paper presents main service problems of turbomachinery users. These are gaseous erosion and corrosion of turbine elements specifically in jet aero engines.

The factors that have an influence on this phenomena initiation and development have been described. The illustrated examples show the development of turbine elements degradation caused by them. The influence of this phenomena on jet engine reliability and flying safety has been analyzed.

One of the basic jet engine health diagnostics method (during service) has been presented.

Keywords: *turbine, diagnostics, erosion and gaseous corrosion*

1. Introduction

Fatigue cracks, mechanical and thermal deflections, overheating, burning, chemical corrosion and mechanical and gaseous erosion are main causes of decreasing turbomachinery lifetime and if undetected can be a real threat for users safety.

Considering this endoscope testing has a great number of advantages. It doesn't need tested machinery disassembling into parts. Used tools don't interact with tested object. Moreover, obtained data gives an ability for fast damage source detection and periodic observation of developing parts degradation. This all made it one of the main Non-Destructive Testing (NDT) methods used in air transport. It is necessary both from economical and technical point of view because together with decreasing present technical state identification time the costs decreases and maintenance safety increases. [1].

Continuous visual testing (endoscope) and connected with it engine parts health analysis give an ability to make some simplifies about damages and its initiation. That's why the main source of compressor blades damage is Foreign Object Debris (FOD). In armed aviation it can be caused by random accidents, the need of operating from temporary airfields or lack of needed cleanness around jet inlet or airfield surface. It can also be caused by badly done blade coating and following erosion damage.

A great influence on observed damages hale also working environment e.g. air dustiness, salinity or chemical contamination.

By analysis of weighted average of damages number we can observe that the number of compressor parts damage (in Polish Air Force) is not the highest part. Developing degradation of engine hot parts is 22% of all damages number and is another part (with the compressor) that should be periodically tested by endoscopic technique.

This also makes possible to early detect and correct other damage premises including badly organized combustion processes because of injectors damage. That problem can cause in existence of non-uniform and unsteady temperature field upwind to turbine. The source of this can be:

- fuel metering unit control system failure,
- wrong combustion chamber geometry design,

- fuel chemical composition change,
- fuel storage problems.

These are only a few problems that occur in hot section of jet engine. They can be also a source of others (more dangerous) which are many cases of gaseous corrosion and erosion.

That's why the diagnostics engineer must have a wide knowledge not only about engine structure and design but also about processes that take place in hot parts of an engine (combustion, flow, structural and manufacturing technology).

2. Jet engine turbine parts destruction

In most cases damage dimensions that can be passed (for service) are included in technical user's manual of an engine. But during long service some other damages that are not a key factor for safety decrease (and are not included in tech. manual) are observed. Then the knowledge about effects carried by phenomena that take place in engines, is a key to prognose the exact part lifetime and service conditions limitations. As an example we can see what happened with turbines on Fig.1.

The source of this was badly organized combustion which caused local, short duration combustion area (flame) downwind shift (up to turbine blades). It caused a situation in which during start-up procedure fuel-air mixture combustion could occur at turbine stator vane area and increase temperature there rapidly.

This process periodic disturbances are illustrated by noticed changes of surface state. It should be mentioned that combustion chamber section structure corresponds with these disturbances. That's because the axes of injectors are directed to turbine inlet stator vane hub. It occurred by burning insulation coating and then by developing blade material loss (fig. 1c). The stator blades internal cooling didn't slow this process down.

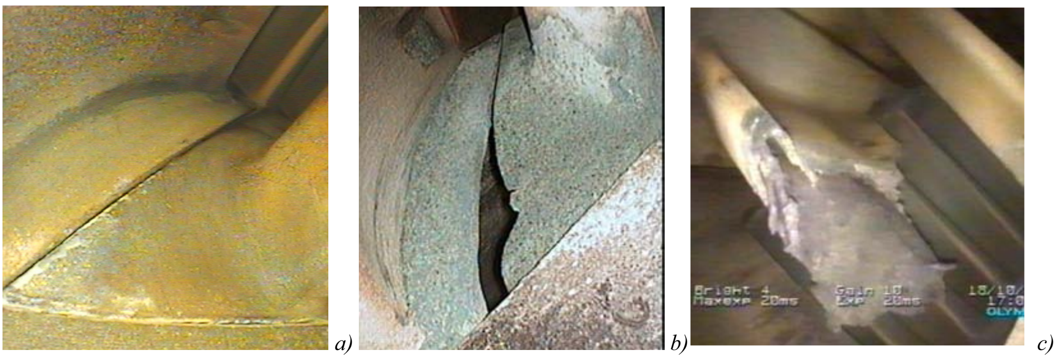

Fig. 1. The part of jet engine HP turbine stator vane [7]
Gaseous corrosion. a) ÷ c) corrosion and erosion material „washing out" form two of stator blades hub

Moreover, the signs of gaseous corrosion show that the whole process is a long lasting one and started when the engine got into service (fig 1b). It was accelerated by existence of some parts of W, Mo, Co and some sulfur compounds in the fuel. Corresponding to military norm for JET A-1 (or F-35) fuel the sulfur compounds fraction is up to 0.3 % by volume. It can cause that carbon-dioxide fraction in combustion products (exhaust emission) can get about 0.014% by volume [3]. So, the higher sulfur fraction in the fuel the higher SO_2 and SO_3 fraction in the exhaust emission – the threat of turbine damage increases.

However, we can say that produced fuels correspond with norms in a range of tolerance. The same think we can say about engines. We can say that this situation is somehow a closed circle.

Engine manufacturers are supported on fuel norm and design engine corresponding to them. They have to make a choice between structure complexity and engine production, overhaul and service costs. This is based on their knowledge and experience. The fuel producers are not going to make the norms tougher because there is no need from the engine user. They all forget that all of this causes our environment.


a)
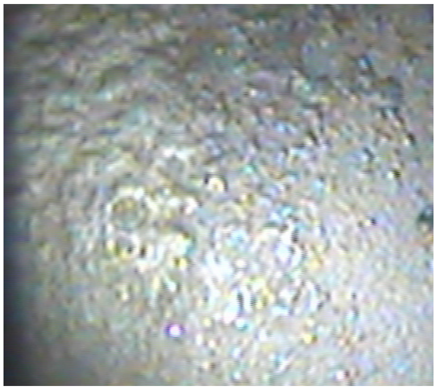
b)

Fig. 2. The view of pressure side of turbine rotor blade of a jet engine used in high salinity environment [7] Two following stages of a) ÷ b)oxidation and sulphidation.

The lack of coating surfaces making precision during production and especially overhaul can cause a case illustrated in Fig. 2. It is certified by their placement (blade pressure side and leading edge LE). Also working environment that is a high salinity one (low level flights over sea) had an influence on this. On the upper example [4] we can observe early stage of oxidation (fig. 2a) characterized by small area of changes and increasing oxidants bubbles (low roughness change). In fig. 2b we see developing phenomena of oxidants bubble rise and their area development (high roughness changes). The chromium depletiation from lower alloy surfaces had started.

One of delay methods of his process is engine clearing but its frequency should be determiated during endoscopic testing.

Describing turbine alloys corrosion development we should divide this process into parts They would be: metal-oxidants, oxidants-atmosphere chemical reactions and reagents diffusion through products layer. At first we should find out if we deal with strong (as in Fig. 2) or with porous (like in Fig. 3) oxidants layer. In the first case the oxidants layer is a protection and the corrosion speed is dependent from reagents diffusion in oxidants layer (speed is inversely proportional to its thickness).

Together with corrosion development on chromium-nickel-steel alloy surface the characteristic products layer is growing. On its border appears an eutectic mixture layer Ni_3S_2 – Ni, over this appear additions like Cr, Al, Ti, W, Mo and below this we can observe sulfurs [5]. The composition of sulfurs in nickel alloys with increased strength for corrosion is different than in alloys which corrode with high speed. In the second one we observe such corrosion products like $(Cr, Ti)_3S_4$, CrS, $(Cr, Ni, Ti)_3S_4$, $(Cr, Ni)_3S_4$, $(Cr, Al, Mo)_3S_4$ and Ni_3S_2. The first three are more stable than another. So, in order to obtain high intensity growing of corrosion products (including sulfurs Ni_2S, Ni_3S_2,$(Cr, Al, Mo)_3S_4$) the sulfur activity in working environment should be increased [5].

When we start-up and cut-down turbomachinery for many times we can get products of incomplete combustion that form soot in some engine parts (combustion chambes sections, turbine blades, injectors). Because of this we observe exact part material “washing out” as a cause of high temperature corrosion.

Despite morfologic signs of corrosion we can observe in such layer oxidants (in external layer) and sulfurs (by the pure alloy). When the time is passing by we observe mixing of them in both of these layers. This is how we explain an eutectic mixture Ni_3S_2 – Ni appearance on corrosion layer and pure alloy border. When it develops fast the upper explanation is also good enough for oxidants NiO and $NiMo_4$ existence. They are also “washed out” by sulfur exhaust Ni_3S_2.

a)

b)

Fig. 3. A part of HP turbine blade of turboprop [7].
a) Sulfur-oxidant corrosion source at LE;
b) Corrosion cracks and lack of material made by LE „washing out”

The other form of tested damage is intercrystalline corrosion which changes alloys chemical composition at crystal borders. It appears in salted working environment with temperature higher than 1050 K on Ni, Co, Fe matrix alloys. More Cr in alloy decreases this trend. When machinery service in different temperatures and periodic exceeds its temperature limit (chromium composition decrease in overheated area) increases the ability of this phenomenon appearance. It can lead to coating products spalling by hot exhaust flow (Fig. 2 and 3).

These changes should be followed by new blades production technology and material development (multiple layer coating, ceramic coating). But it only can slow the whole process down. As an example we can see the turbine destruction process (Fig. 4).

In figure 4 (a ÷ b) coating damage on blades LE – its area increases (by the blades hight) together with turbomachinery service time (fig. 4b). The lack of not only coating but also insulating layer can be observed after another 25 service hours (fig. 4c). We know that summarized service time for this engine is not higher than 80 hours. Described damage was observed for 80% of blades in this turbine rotor vane. It could be caused by turbine cooling system malfunction.

The mentioned engine is still in service because our experience shows that before destruction we will first see cracks in pure alloy of a blade (fig. 4e) – this is dangerous for fighter jet service.

It is still not known at which phase the engine should be taken out of service.

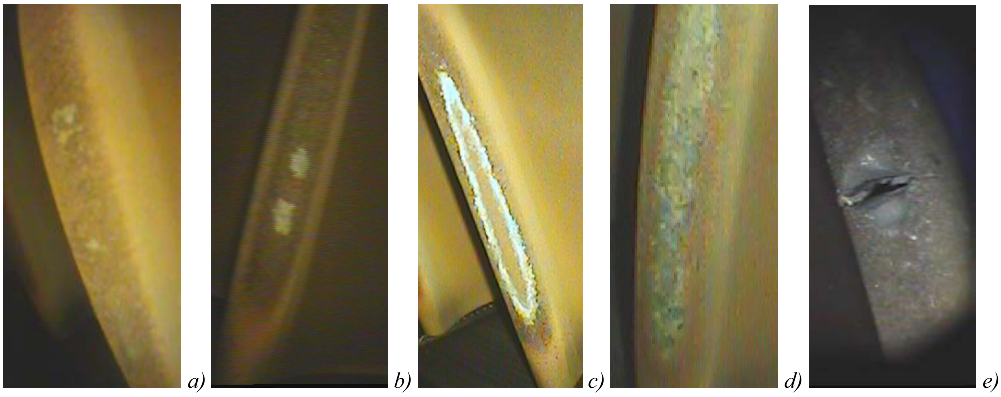

Fig. 4. A view from LE of HP turbine rotor blade of jet engine [7]. Following stages a) ÷ e) of damage

3. Diagnosing

There are many algorithms that determinate NDT frequency [3] but most of them were designed for stationary turbomachinery or air transport jet engines – the machinery with known fatigue cycle number. It's more difficult for military jets where the load on engine parts is dependent from mission type, its duration and pilots habituations.

It's very important to equip engine in start-up number and flight duration acquisition unit. All limitations passes (including g-force) should also be registered. Basing on them it is possible to find an endoscope testing frequency. All previous flights parameters (that are available) are also considered.

In a computer engine health monitoring systems (used in Polish Air Force) the subjective way of diagnosing is used. Data analysis and the knowledge of persons who make it determinates an effect. This is because the mentioned systems don't have automated symptoms identification and analysis applications. They only illustrate needed parameters. The analysis is made by technicians and its effects are based on their knowledge and experience. It is very important in case of a few over-limits existence. So, basing only on flight recorders data it is very hard to identify the time period to the next testing.

The knowledge of engine structure is also a key for a good visual testing. Not only the ability of measurement system usage but also the analysis of noticed pictures is needed.

That's why the safe horizon of turbomachinery health monitoring (basing on endoscopic visual inspection) is based on: mentioned knowledge and experience, statistic each type of machinery damage data and acceptable level of critical damage existence level [6].

4. Conclusions

So, every not defined by manufacturer turbomachinery damage case should by analyzed separately, including known and common cases experience and basic knowledge about effects of such damage on other parts of an object.

There is of course the ability of some analysis data obiectivity but it needs some procedures of automated or half-automated large sort of damage data processing. It also needs development of knowledge about material fatigue properties, and correlation between damage propagation with data obtained during structural experiments.

References

[1] Szymczak, J., Szczepankowski, A., *Badania endoskopowe w ocenie degradacji elementów wewnętrznych wirnikowych maszyn przepływowych*, X Jubileuszowy Kongres Eksploatacji Urządzeń Technicznych, Stare Jabłonki 2005.

[2] Szymczak, J., Szczepankowski, A., *Endoskopia w diagnostyce turbinowych silników odrzutowych*, VIII Międzynarodowa Konferencja *Diagnostyka Samolotów i śmigłowców*, Warszawa 2005.

[3] Norma obronna NO-91-A200, Warszawa 1991 oraz MIL-T-5624P z 29.09.1992 r. i MIL-T-83133D z 29.01.1992 r.;

[4] Pratt & Whitney Canada, *Instrukcja obsługi technicznej numer 3032142*, *Przegląd Silnika* - karta 72-00-00.

[5] Nikitin, W. I., *Korrozija i zaszczita łopatok gazowych turbin*, Leningrad 1987.

[6] Olzak, B., Szymczak, J., Szczepankowski, A., *Badania endoskopowe wirnikowych maszyn przepływowych*, Szczyrk 2006.

[7] Archiwum Zakładu Silników Lotniczych ITWL.

MARINE ENGINES OF NATO NAVIES AND ECOLOGICAL PROBLEMS OF THEIR EXPLOITATION

Malgorzata Pawlak
Leszek Piaseczny

Naval University of Gdynia
ul. Smidowicza 69, 81-103 Gdynia

Abstract

Imposing the legal regulations aims at extorting restrictions of harmful substances in marine engines exhaust gases emissions. An Annex VI of MARPOL73/78 Convention, being ratified in 2005, lays commercial ships under an obligation of the reduction of emissions of sulphur and nitrogen oxides that are formed when combusting marine fuels. And although navy vessels are excluded from performing that obligation, a great number of studies on emission reduction methods applicable at NATO navies have been carried out. It is worth noticing that in relation to the sulphur level in marine fuel, the NATO ships fulfil the requirements specified by Annex VI, because the fuel used by naval ships is of low sulphur level. However, the admissible NO_x emission levels in naval ships exhaust gases is much higher comparing to the one in commercial ships.

Keywords: *marine engines, exhaust gas emission, NATO navies*

1. Introduction

Environmental protection issues are important for NATO Nations. A great number of studies and research have been carried out, many reports and scientific publications have been prepared. One of the main tasks of Special Working Group for Marine Environment Protection (SWG/12), of the NATO Naval Armament Group (NNAG) is implementation of international organizational, technical and legal standards concerning marine environment protection against pollution from ships.

In 1995, Special Working Group SWG/12 conducted a study for the „NATO Environmentally Sound Ship of the 21st Century". Its objectives were to determine the methods of effective shipboard waste management and treatment to be fully compliant with current and future regulations for the protection of the maritime environment. The document deserves attention as historically the first study in NATO concerning maritime environment protection issues.

Gaseous wastes can be divided into four key groups:

- exhausts from marine main diesel engines (main and auxiliary);
- exhausts from marine gas turbine engines and steam boilers (main and auxiliary);
- ozone depleting substances (halons and freons);
- volatile organic compounds (VOCs).

In the paper, only two first categories will be discussed, i.e. exhausts from marine diesel engines (DE) gas turbine engines (GT) and steam boilers (ST).

2. Gaseous emissions of engine exhaust gases in the US Navy

U.S. Navy estimated the exhaust gases emissions resulting from burning the hydrocarbon fuel on American vessels (for the year 1994), such as: nitrogen oxides (NO_x), sulphur oxides (SO_x), carbon dioxide (CO_2), carbon monoxide (CO), unburned hydrocarbons (HC) and particulate matter (PM). The evaluation was encompassing 44 ship classes and 256 ships (Table 1).

Tab. 1. Exhaust gases emission estimates in the U.S. Navy marine engines in 1994 [1]

Class	No. of ships	Main propulsion		Auxiliary propulsion		Estimated total class exhaust emissions [t/yr]					
		Type	Power [kW]	Type	Power [kW]	NO_x	SO_x	CO_2	CO	HC	PM
AD37	2	ST	29 800	ST	NA	57.8	176.5	57 219	68.5	5.6	4.0
AD41	4	ST	59 700	ST	NA	97.2	296.2	96 040	137.2	11.3	8.0
AE21	2	ST	23 900	ST	NA	28.9	86.6	28 083	54.9	4.5	3.2
AE23	2	ST	23 900	ST	NA	17.8	53.7	17 424	54.9	4.5	3.2
AE27	7	ST	114 800	ST	NA	181.2	543.4	176 181	263.9	21.7	15.3
AFS1	3	ST	49 200	ST	NA	59.0	175.9	57 024	113.1	9.3	6.6
AO177	5	ST	89 500	ST	NA	149.2	446.8	144 856	205.7	16.9	12.0
AOE1	4	ST	298 300	ST	NA	204.0	612.2	198 477	685.6	56.3	39.8
AOR1	5	ST	119 300	ST	NA	173.5	518.7	168 188	274.2	22.5	15.9
AR5	1	ST	8 600	ST	NA	34.0	101.9	33 030	19.8	1.6	1.1
AS 33	2	ST	29 800	ST	NA	26.9	82.3	26 670	68.5	5.6	4.0
AS 36	2	ST	29 800	ST	NA	18.2	55.4	17 972	68.5	5.6	4.0
AS 39	3	ST	44 700	ST	NA	24.2	73.6	23 856	102.7	8.4	6.0
CG16	2	ST	126 800	ST	NA	48.3	144.6	46 873	291.4	23.9	16.9
CG26	3	ST	190 200	ST	NA	45.2	137.2	44 483	437.2	35.9	25.4
CV59	2	ST	417 600	ST	NA	349.1	1040.5	337 355	959.8	78.8	55.8
CV63	3	ST	626 400	ST	NA	734.5	2191.8	710 655	1439.7	118.1	83.7
CV67	1	ST	208 800	ST	NA	0.0	0.0	0.0	0.0	0.0	0.0
FF1052	8	ST	208 800	ST	NA	32.5	98.4	31 900	479.9	39.41	27.9
LCC19	2	ST	32 800	ST	NA	58.1	175.6	56 926	75.4	6.2	4.4
LHA1	5	ST	261 000	ST	NA	296.1	884.9	286 898	599.9	49.2	34.9
LHD1	2	ST	104 400	ST	NA	148.8	444.2	144 031	240.0	19.7	13.9
LKA113	1	ST	16 400	ST	NA	0.6	1.8	579	37.7	3.1	2.2
LPD1	1	ST	17 900	ST	NA	19.8	60.1	19 489	41.1	3.4	2.4
LPD4	11	ST	196 900	ST	NA	378.6	1135.2	368 075	452.6	37.1	26.3
LPD7	1	ST	17 900	ST	NA	20.4	61.3	19 887	41.1	3.4	2.4
LPH2	5	ST	85 800	ST	NA	164.6	491.9	159 475	197.2	16.2	11.5
LSD 36	5	ST	89 500	ST	NA	144.0	430.8	139 682	205.7	16.9	12.0
MCSC	1	ST	17 900	ST	NA	1.6	4.8	1 541	41.1	3.4	2.4
DDG51	2	GT	149 100	GT	15 000	345.9	296.7	98 567	289.3	18.4	18.5
DDG993	4	GT	238 600	GT	24 000	386.6	386.1	127 939	439.9	35.3	24.1
DD963	31	GT	1 849 400	GT	186 000	3198.5	3349.3	1 110 327	3803.6	306.6	208.9
CG47	25	GT	1 491 400	GT	165 000	3153.6	3120.0	1 039 093	3455.1	216.6	195.5
FFG7	51	GT	1 521 300	DE	204 000	5003.1	2421.6	790 535	4078.2	413.2	254.1
ASR7	1	DE	2 200	DE	NA	20.8	5.2	1 877	3.5	0.4	0.6
MSO427	4	DE	6 800	DE	NA	17.5	2.6	950	10.5	2.8	0.4
AS 31	2	DE	17 400	DE	6 200	321.5	26.0	9 385	436.3	23.0	2.8
ASR21	1	DE	4 500	DE	2 000	212.5	26.0	10 679	436.3	23.0	2.8
ATS1	3	DE	13 400	DE	3 600	320.6	43.6	15 732	45.1	9.3	3.9
ARS38	5	DE	9 100	DE	4 500	190.6	64.2	23 123	20.5	2.5	6.8
ARS50	4	DE	12 500	DE	9 600	336.3	103.3	37 233	30.7	9.0	12.1
MCM1	10	DE	17 900	DE	13 000	255.9	45.2	16 280	59.6	26.3	5.0
LST1179	10	DE	123 000	DE	24 000	2267.5	493.1	177 662	490.1	68.5	42.9
LSD 41	8	DE	220 100	DE	45 600	2986.3	295.7	106 549	213.3	121.0	24.2
Total	**256**		**9 217 100**			**22 531.3**	**21 204.9**	**6 978 802**	**21 469.4**	**1 904.4**	**1 247.8**

(ST – steam turbine, DE – diesel engine, GT – gas turbine engine, NA – data not available)

To estimate exhaust emissions, the U.S. Navy used two general methodologies: a fuel-based method and an operating profile-based method [2,3]. Due to the fact that operating power profiles and individual boiler emission factors were not available for steam turbine powered ships, estimation of the exhaust emissions for these vessels was made on the basis of the amount of fuel consumed by each ship, in compliance with the U.S. EPA fuel-based emission factors. For each class of diesel powered or gas turbine powered ships and for each pollutant type, an operational based emission factor (including the generator engines) was developed, based on the operating power profile and the emission data of installed engines. This factor was multiplied by the number of underway hours per year for each ship. In addition, there were estimated the emissions for the generators running in port or at anchor, when the generators were required to be operated.

3. Exhaust gas emissions from marine engines of NATO Navies in 1995-96

Table 2 shows the installed propulsion power distribution in the ships of different NATO Navies in the years 1995-96.

Tab. 2. Propulsion power distribution summary in selected NATO Navies in 1995-96 [1]

NAVY	Total Power [MW]	DE						GT				ST			
		<1	1-5	5-10	10-20	>20	**Total**	<10	10-20	>20	**Total**	<10	10-20	>20	**Total**
BELGIUM	98	7	34	0	0	0	**41**	0	57	0	**57**	0	0	0	**0**
CANADA	772	7	32	72	0	0	**111**	0	0	502	**502**	0	47	112	**159**
DENMARK	333	17	79	37	0	0	**133**	144	55	0	**199**	0	0	0	**0**
FRANCE	1247	45	138	344	117	64	**707**	0	0	69	**69**	0	0	471	**471**
GERMANY	1307	13	245	343	208	0	**808**	0	0	342	**342**	0	0	157	**157**
GREECE	1110	24	83	174	203	0	**485**	0	0	243	**242**	5	0	377	**382**
ITALY	1310	25	100	255	62	0	**442**	19	22	664	**705**	0	0	162	**162**
NETHERLANDS	755	10	35	102	15	0	**162**	0	0	593	**593**	0	0	0	**0**
NORWAY	250	6	72	113	0	0	**1910**	0	0	0	**0**	0	59	0	**59**
PORTUGAL	345	16	45	108	59	0	**228**	0	0	119	**119**	0	0	0	**0**
SPAIN	645	20	108	47	96	0	**271**	4	0	218	**222**	0	33	129	**162**
TURKEY	1129	41	78	179	183	98	**579**	10	18	45	**73**	0	0	478	**478**
UK	2097	44	233	130	152	0	**558**	0	0	1452	**1452**	0	87	0	**87**
US	10925	205	76	385	137	248	**1051**	28	936	6169	**7133**	0	858	185	**2742**
TOTAL	**22332**	**480**	**1358**	**2289**	**1232**	**410**	**5767**	**205**	**1088**	**10416**	**11709**	**5**	**1084**	**1770**	**4559**

As it results from the table, those days all the Navies had diesel powered ships and nearly all (excluding Norway) had gas turbine powered ships. Some of them (Belgium, Denmark, Netherlands and Portugal) did not have steam propulsion installed.

4. Estimation of the NATO Navies future exhaust gas emissions

It is possible to estimate the future exhaust emissions from NATO marine engines. There are two factors that are expected to influence the level of those emissions.

The first one involves the changes in exhaust emission levels of new engines which will be driven mainly by changes in emission regulations. Some changes in marine engine regulations will undoubtedly affect the ship exhaust emission levels directly. An example of such types of changes are the regulations of the International Marine Organisation (IMO), concerning the acceptable levels of NO_x and SO_x emissions by marine diesel engines. Other expected changes are those in regulations for other applications, such as land based power generations or mechanical drive applications, which will affect the ship exhaust emission levels indirectly if the same engine model is used both in land and marine applications. This is generally the case for gas turbines.

The second factor that will influence future naval ship exhaust emission levels is the changes to the force structure of the navies, such as decrease in overall number of ships, modernisation of some vessels by changes in propulsion power types or lowering the power levels, or replacement of older ships with the more modern ones.

To illustrate the changes in emission levels caused by the above mentioned factors, there was analysed some data of the future exhaust emission estimates for the U.S. Navy in 1994. Table 3 contains the 1994 U.S. Navy ship exhaust emission estimates previously shown in Table 1, together with revised estimates to account for changes expected to occur by 2010.

Tab. 3. Exhaust emission levels estimated for the U.S. Navy engines in 2010 [1]

U.S. Navy Class	No. of ships	Main propulsion		Auxiliary propulsion		Estimated total class exhaust emissions in 2010 [t/yr]					
		Type	Power installed [kW]	Type	Power installed [kW]	NO_x	SO_x	CO_2	CO	HC	PM
AD 37	2	ST	29 800		NA	57.8	176.5	57 219	68.5	5.6	4.0
AD 41	4	ST	59 700		NA	97.2	296.2	96 040	137.2	11.3	8.0
AR 8	1	ST	8 600	ST	NA	34.0	101.9	33 030	19.8	1.6	1.1
AS 33	2	ST	29 800	ST	NA	26.9	82.3	26 670	68.5	5.6	4.0
AS 36	2	ST	29 800	ST	NA	18.2	55.4	17 972	68.5	5.6	4.0
AS 39	3	ST	44 700	ST	NA	24.2	73.6	23 856	102.7	8.4	6.0
Subtotal 1	**14**		**202 400**			**258.4**	**785.8**	**254 787**	**465.2**	**38.2**	**27.0**
Subtotal 1 rev.	**13**	**less AR 5**	**193 800**			**224.4**	**684.0**	**221 757**	**445.4**	**36.5**	**25.9**
AE21	2	ST	23 900	ST	NA	28.9	86.6	28 083	54.9	4.5	3.2
AE23	2	ST	23 900	ST	NA	17.8	53.7	17 424	54.9	4.5	3.2
AE27	7	ST	114 800	ST	NA	181.2	543.4	176 181	263.9	21.7	15.3
AFS 1	3	ST	49 200	ST	NA	59.0	175.9	57 024	113.1	9.3	6.6
AO177	5	ST	89 500	ST	NA	149.2	446.8	144 856	205.7	16.9	12.0
AOR1	5	ST	119 300	ST	NA	173.5	518.7	168 188	274.2	22.5	15.9
Subtotal 2	**24**		**420 600**			**609.6**	**1825.1**	**591 756**	**966.7**	**79.3**	**56.2**
Subtotal 2 rev.	**18**	**1/2 GT**	**420 600**			**851.9**	**1472.3**	**481 008**	**997.0**	**81.8**	**57.9**
AOE 1	4	ST	298 300	ST	NA	204.0	612.2	198 477	685.6	56.3	39.8
Subtotal 3	**4**	**No change**	**298 300**			**204.0**	**612.2**	**198 477**	**685.6**	**56.3**	**39.8**
CG16	2	ST	126 800	ST	NA	48.3	144.6	46 873	291.4	23.9	16.9
CG26	3	ST	190 200	ST	NA	45.2	137.2	44 483	437.2	35.9	25.4
FF1052	8	ST	208 800	ST	NA	32.5	98.4	31 900	479.9	39.41	27.9
Subtotal 4	**13**		**525 800**			**126.0**	**380.2**	**123 257**	**1208.5**	**99.2**	**70.2**
Subtotal 4 rev.	**9**	**only GT**	**525 800**			**226.2**	**233.2**	**77121**	**1284.2**	**105.4**	**74.6**
CV 59	2	ST	417 600	ST	NA	349.1	1040.5	337 355	959.8	78.8	55.8
CV 63	3	ST	626 400	ST	NA	734.5	2191.8	710 655	1439.7	118.1	83.7
CV 67	1	ST	208 800	ST	NA	0.0	0.0	0.0	0.0	0.0	0.0
Subtotal 5	**6**		**1 252 800**			**1083.6**	**3232.3**	**1 048 011**	**2399.5**	**196.9**	**139.4**
Subtotal 5 rev.	**3**	**1/2 Nuclear**	**626 400**			**541.8**	**1616.2**	**524 005**	**1199.8**	**98.4**	**69.7**
LCC19	2	ST	32 800	ST	NA	58.1	175.6	56 926	75.4	6.2	4.4
LHA1	5	ST	261 000	ST	NA	296.1	884.9	286 898	599.9	49.2	34.9
LHD1	2	ST	104 400	ST	NA	148.8	444.2	144 031	240.0	19.7	13.9
LKA113	1	ST	16 400	ST	NA	0.6	1.8	579	37.7	3.1	2.2
LSD 36	5	ST	89 500	ST	NA	144.0	430.8	139 682	205.7	16.9	12.0
MCSC	1	ST	17 900	ST	NA	1.6	4.8	1 541	41.1	3.4	2.4
Subtotal 6	**16**		**522 000**			**649.1**	**1942.0**	**629 657**	**1199.8**	**98.4**	**69.7**
Subtotal 6 rev.	**12**	**all LHA/LHD**	**626 400**			**741.0**	**2214.0**	**717 826**	**1439.7**	**118.1**	**83.7**
LPD1	1	ST	17 900	ST	NA	19.8	60.1	19 489	41.1	3.4	2.4
LPD4	11	ST	196 900	ST	NA	378.6	1135.2	368 075	452.6	37.1	26.3
LPD7	1	ST	17 900	ST	NA	20.4	61.3	19 887	41.1	3.4	2.4
LPH2	5	ST	85 800	ST	NA	164.6	491.9	159 475	197.2	16.2	11.5
Subtotal 7	**18**		**318 500**			**583.4**	**1748.5**	**566 926**	**732.0**	**60.1**	**42.5**
Subtotal 7 rev.	**12**	**only DE**	**318 500**			**6678.6**	**1522.4**	**550 323**	**1384.2**	**226.5**	**80.4**
DDG51	2	GT	149 100	GT	15000	345.9	296.7	98 567	289.3	18.4	18.5
DDG993	4	GT	238 600	GT	24000	386.6	386.1	127 939	439.9	35.3	24.1
DD963	31	GT	1 849 400	GT	186000	3198.5	3349.3	1 110 327	3803.6	306.6	208.9
CG47	25	GT	1 491 400	GT	165000	3153.6	3120.0	1 039 093	3455.1	216.6	195.5
FFG7	51	GT	1 521 300	DE	204.000	5003.1	2421.6	790 535	4078.2	413.2	254.1
Subtotal 8	**113**		**5 249 800**			**12 069.8**	**9 573.7**	**3 166 461**	**12 086.2**	**990.1**	**701.2**
Subtotal 8 rev.	**113**	**1/4 new GT**	**5 249 800**			**11 390.9**	**9 573.7**	**3 166 461**	**12 086.2**	**990.1**	**701.2**

ASR7	1	DE	2 200	DE	NA	20.8	5.2	1 877	3.5	0.4	0.6
MSO427	4	DE	6 800	DE	NA	17.5	2.6	950	10.5	2.8	0.4
AS 31	2	DE	17 400	DE	6200	321.5	26.0	9 385	436.3	23.0	2.8
ASR21	1	DE	4 500	DE	2000	212.5	26.0	10 679	436.3	23.0	2.8
ATS 1	3	DE	13 400	DE	3600	320.6	43.6	15 732	45.1	9.3	3.9
ARS38	5	DE	9 100	DE	4500	190.6	64.2	23 123	20.5	2.5	6.8
ARS50	4	DE	12 500	DE	9600	336.3	103.3	37 233	30.7	9.0	12.1
MCMI	10	DE	17 900	DE	13000	255.9	45.2	16 280	59.6	26.3	5.0
LST1179	10	DE	123 000	DE	24000	2267.5	493.1	177 662	490.1	68.5	42.9
LSD 41	8	DE	220 100	DE	45600	2986.3	295.7	106 549	213.3	121.0	24.2
Subtotal 9	**48**		**426 900**			**6929.5**	**1105.1**	**399 471**	**1745.8**	**285.7**	**101.4**
Subtotal 9 rev.	**48**	**1/4 new DE**	**426 900**			**6409.7**	**1105.1**	**399 471**	**1745.8**	**285.7**	**101.4**
TOTALS	**256**		**9 217 100**			**22 513.3**	**21 204.9**	**6 978 802**	**21 469.4**	**1 904.1**	**1 247.6**
TOTALS REV.	**232**	**about 2010 r.**	**8 688 500**			**27 288.5**	**19 032.8**	**6 336 449**	**21 248.0**	**1 998.8**	**1 234.7**
% change	**-9.4**	**1994 to 2010**	**-5.8**			**+21.1**	**-10.2**	**-9.2**	**-1.0**	**5.0**	**-1.0**

(ST – steam turbine, DE – diesel engine, GT – gas turbine engine, NA – data not available, rev. – revised estimates)

In making the above projection there were made the following assumptions:

- All estimates in regard to future U.S. Navy force levels and its force structure are based on publicly available information;
- Although over the last decades there has been made a significant reduction in the number of U.S. navy ships, the number of fossil fuelled surface ships is not expected to be reduced substantially below the 1994 level by 2010. However, older ships are expected to be replaced with more modern ships, majority of which will be powered by either gas turbine (GT) or diesel engines (DE). Exceptions to this will be a few (about five) additional steam (ST) powered LHD vessels.

To facilitate predicting force composition changes, the U.S. Navy ships were divided into 9 subgroups, as it is indicated by the subtotals in Table 3. In estimating the change in exhaust emissions for each subgroup, the following rationale was applied:

- Subgroup 1: For this group of ST powered ships, only little change in exhaust emission is predicted.
- Subgroup 2: It is assumed that 12 of 24 ST powered resupply ships will be replaced by 6 new more capable GT powered ships (e.g. of the AOE 6 class). However, the total power level of that 18 ship subgroup will not change.
- Subgroup 3: No change is predicted for these four AOE 1 class ships.
- Subgroup 4: It is expected that these ST powered cruisers and frigates will be replaced by GT powered combatants. It is assumed that a one for one replacement for the cruisers and a one for two replacement for the frigates will take place. The total power will remain the same.
- Subgroup 5: It is expected that three of the six ST carriers will be replaced by nuclear powered carriers.
- Subgroup 6: Nine amphibious ships other than the LHAs and LHDs will be replaced by five additional LHDs.
- Subgroup 7: It is predicted that these 18 ST powered LPDs and LPHs will be replaced by LPD 17 class amphibious assault ships, which will probably be DE powered.
- Subgroup 8: It is estimated that about one-fourth of these GT powered ships will be replaced by new vessels of the same propulsion type.
- Subgroup 9: It is assumed that a one-fourth of these DE powered ships will be replaced by new vessels of the same propulsion type.

The method used to estimate the emissions of replacement ships assumed the following:

- For DE or GT powered ships replacing ST ships, the replaced ships emissions estimates were multiplied by factors based on the ratios of the overall average emission rates for all the 1994 ST, DE and GT powered ships on a per unit installed propulsion power basis.

- All new DE powered ships were estimated as indicating 30% lower NO_x emissions than the DE powered ships from 1994, which is in accordance with the regulations of the VI Annex of MARPOL 73/78 Convention, and one-fourth of new GT powered ships were estimated as indicating 90% lower NO_x emissions than the GT powered ships from 1994, reflecting dry low emission combustors in those engines. No retrofit of dry low emission combustors in existing GT powered ships was predicted.

Analysing the results of obtained data, it can be remarked that:

- The increase in NO_x emissions is primarily due to decrease in the number of steam powered ships being replaced by diesel powered ships.
- The decrease in SO_x and CO_2 emissions, which are directly related to fuel consumption, is due to older steam powered ships being replaced by new, more efficient diesel or gas turbine ships.

These examples show how the changes in exhaust emission levels of new engines, as well as the changes in naval force structures can affect the future exhaust emission levels.

5. Exhaust harmful substances generation rates

From the data concerning the U.S. Navy ships, presented in Table 3, the overall rates of exhaust harmful substances generation were calculated for each type of propulsion – DE, ST and GT. These rates were normalised on a per unit installed propulsion power basis, but include auxiliary engine emissions (Table 4).

Tab. 4. Unit exhaust gas harmful substances emission rates [1]

U.S. Navy propulsion type	Estimated unit emission rates [t/(MW-year)]					
	NO_x	SO_x	CO_2	CO	HC	PM
DE	15.3	2.0	730	4.1	0.75	0.19
GT	2.3	1.8	605	2.3	0.19	0.13
ST	1.0	3.0	965	2.2	0.18	0.13

The rates illustrated in Table 4 are useful for making gross estimates of naval ships emissions but as they include many different ship types with different operating profiles, they should be used only for rough estimations. Also, it ought to be mentioned that all of the U.S. Navy emission estimates were made assuming the use of MIL-F-16884/NATO F76 distillate fuel of 0.5% sulphur content and of a carbon to hydrogen ratio of 1.8, and the SO_x and CO_2 emission rates are directly proportional to fuel consumption rates. However, as operation power profiles were included in the estimating process, the fuel consumption rates for different ship types are not directly proportional to the specific fuel consumption rates of the propulsion engines. For instance, the estimated overall SO_x and CO_2 emission rates for GT powered ships are lower than for DE powered ships, although the unit fuel consumption for DE is generally lower than for GT. It is so, because the majority of GT powered naval ships have a large amount of installed propulsion power (in order to provide a relatively high top speed capability), but most of the time they operate at relatively low speeds, which require only a small percentage of the installed power. Therefore, a typical naval GT average operating power as a percentage of the total installed power is much lower than for a typical naval DE.

For CODOG or CODAG[1] ships, the GT operates at a higher percentage of the installed power rating but generally the operating time is much shorter than for the associated DE, so on a yearly basis, the overall waste generation rates might be expected to be somewhat similar to those for all GT powered ships or all DE powered ships in terms of emissions per year per unit installed power.

[1] CODOG or CODAG – Combined Gas Turbine and/or Diesel ships

Since the U.S. Navy estimates did not include any CODOG or CODAG ships, the exhaust emission estimates of NO_x and CO_2 were calculated for an Italian Navy CODOG frigate (Table 5).

Tab. 5. Comparison of exhaust gas harmful substances generation rates [1]

Propulsion type	Estimated unit emission rates [t/(MW-year)]			
	NO_x		CO_2	
	U.S. Navy	CODOG	U.S. Navy	CODOG
DE	15.3	14.2	730	997
GT	2.3	2.0	605	373

Table 6 shows the relative compositions of exhaust gases generated by naval high- and medium-speed DE, GT and ST engines, when using fuel MIL-F 16884H/NATO F76.

Tab. 6. Unit emission of exhaust gases and engine noise [1]

Parameters	Units	DE	GT	ST
NO_x	g/(kW·h)	8 - 15	2 - 5	1 - 4
CO	g/(kW·h)	1 - 1.5	0.1 - 1.5	2
SO_x	g/(kW·h)	3 - 4.5	3 - 4.5	3 - 4.5
HC	g/(kW·h)	0.3 - 0.6	0.3 - 0.6	0.8
PM	g/(kW·h)	0.4 - 0.7	0.2 - 0.4	0.4
Smoke	Opacity [%]	10 - 15	-	-
Noise (level)	dB	90	-	-

6. Conclusion

World-wide trends of decreasing the human harmful influence on the natural, including maritime, environment, do no exclude navies. It can be remarked especially over the past few years. Ratification of the Annex VI of MARPOL73/78 Convention in 2005, lays commercial ships under an obligation of the reduction of emissions of sulphur and nitrogen oxides that are formed when combusting marine fuels. And although navy vessels are excluded from performing that obligation, a great number of studies on emission reduction methods being carried out in many countries (the United States of America, Great Britain, the Netherlands) bear evidence of the opportunities and will to expand those regulations over NATO navies. Moreover, some countries (the United States of America and partly France) have already introduced the obligation of meeting the regulations of MARPOL73/78 Convention, including all its annexes.

In relation to the sulphur level in marine fuel, the NATO ships fulfil the requirements specified by Annex VI, because the fuel used by naval ships is of low sulphur level. The problem appears however when considering admissible NO_x emission levels. The MARPOL Convention regulates the NO_x emission levels for diesel engines, which are commonly installed on commercial vessels, but more rarely on naval ones due to their size and weight. What is more, the MARPOL Convention excludes navies from performing that obligation, so even though admissible sulphur oxides concentration levels in exhaust gases is not exceeded, the nitrogen oxides concentration in exhaust gases of these ships exceeds the admissible levels regulated by the Annex VI. Such a situation occurs not only in Polish Navy, and the problem seems to be world-wide [3,4].

Therefore, do the naval vessels should reduce the exhaust gases nitrogen oxides emission? Taking into account that naval vessels do not operate only in case of war, but also peace (e.g. training), they should be treated as any other vessels and thus, laid under the obligation of protecting the natural environment.

A modern naval ship is the vessel that fulfils not only military requirements, but also integrates up-to-date technologies enabling operating on all water regions, even those requiring severe environmental protection regulations. An interest of NATO navies in this problem shows that they do tend to solve ecological problems of their development.

References

[1] NATO Environmentally Sound Ship of the 21st Century, 1995 NATO Unclassified.

[2] Bergier T., Piaseczny L., *Zakres i warunki badań emisji związków toksycznych w spalinach silników tłokowych napędu głównego okrętów,* Zeszyty Naukowe AMW, Nr 1/136/1998.

[3] Markle S.P., Brown A.J., *Naval Ship Engine Exhaust Emission Characterization,* Naval Engineers Journal, September 1996, s. 37-46.

[4] Schnohr O., Frederiksen P., *NOx optimizing of auxiliary engines 21 st.* Int. Congress on Combustion Engines, Cimac, Interlaken 1995.

PERFORMANCE OF THE ADVANCED AND SIMPLIFIED VARIANTS OF A NON-LINEAR OBSERVER OF A TURBOJET ENGINE, COMPARISON OF RESULTS

Wojciech I. Pawlak, Jarosław Spychała

Air Force Institute of Technology
ul. Księcia Bolesława 6, 01-493 Warszawa 46, skr. poczt. 96, Poland
tel.: +48 (0-22) 6 852 182
e-mail: PawlakIzydor.Wojciech@acn.waw.pl

Abstract

Non-linear observers have got great potentialities in the fields of turbojet engine control, monitoring and diagnosing. They may prove of particular suitability for measuring actual values of the so-called difficult-to-measure parameters, e.g. temperature of the working medium at the combustion chamber outlet, thrust, etc. For this reason, reliability and accuracy of results of the performance of observers should be given careful consideration. The paper has been intended to deliver comparison between results gained with two variants of a non-linear observer of the SO-3 engine. It has been assumed in the computational algorithm of the first variant that the working medium in the engine duct is a perfect gas. In the second variant, the working medium has been considered a semi-perfect gas. Both the variants of the observer have been tested using real data from tests of the SO-3 engine on a ground-based engine test bench.

Key words: *turbojet engine, mathematical modelling, non-linear observer*

Nomenclature

Cp_{12} - average specific heat of the working medium in the compressor duct
Cp_{23} - average specific heat of the working medium in the combustion chamber
Cp_{34} - average specific heat of the working medium in the turbine duct
D - convergent nozzle
G2 - mass flow of the working medium at the compressor outlet
$G2_r$ - reduced mass flow of the working medium at the compressor outlet
G3 - mass flow of the working medium at the combustion chamber outlet
G3t - reduced mass flow of the working medium through the turbine
I_o – polar moment of inertia of the spool of the turbine-compressor assembly
k_{12} – mean value of the isentropic exponent of the working medium in the compressor
k_{34} - mean value of the isentropic exponent of the working medium in the turbine
k_{45} - mean value of the isentropic exponent of the working medium in the nozzle
KS - combustion chamber
M - Mach number (here: air speed)
n - rotational speed of the spool
N_s - input power of the compressor
n_{sr} - reduced rotational speed of the compressor
n_{start} - initial rotational speed of the spool
N_t - turbine power
n_{tr} - reduced rotational speed of the turbine
Pi_1 – actual value of the ‘i’ parameter calculated with the non-linear observer no. 1

Pi_2 – actual value of the ‘i’ parameter calculated with the non-linear observer no. 2
P0 - total pressure of the working medium at the engine inlet
P1 - total pressure of the working medium in front of the compressor
$P2_{start}$ - initial average total pressure of the working medium behind the compressor
P4 - total pressure of the working medium in the convergent nozzle
$P4_{start}$ - initial average total pressure of the working medium in the convergent nozzle
PH - ambient pressure
Pks_{start} - initial average total pressure of the working medium in the combustion chamber
Q - rate of fuel flow
Q_start - initial rate of fuel flow
R - engine thrust
Rg - gas constant
T1 - total temperature of the working medium in front of the compressor
T2 - total temperature of the working medium behind the compressor
T3 - total temperature of the working medium in front of the turbine
T3start - initial total temperature of the working medium at the combustion-chamber outlet
T4 - total temperature of the working medium behind the turbine
T4start - initial total temperature of the working medium in the nozzle
u_1, u_2, u_3, u_4, u_5 - errors of iteration
w_1, w_2, w_3, w_4, w_5 - factors of amplification of iterative loops
Wo - fuel calorific value
Wu - air bleed coefficient
ΔPi - percentage difference between actual values of the ‘i’ parameter, calculated by means of both versions of the observer
ΔT12 - increment of temperature of the working medium due to compression
Δt - interval of sampling the inputs and results of computations
Π - pressure ratio (of the compressor)
ε - pressure ratio of decompression of the working medium while flowing through the turbine
ϕ - rate-of-flow coefficient of a convergent nozzle
η_{ks} - efficiency of heat emission in the combustion chamber
η_{ms} - coefficient of mechanical efficiency of compressor
η_{mt} - coefficient of mechanical efficiency of the turbine
η_s - isentropic efficiency of the compressor
η_t - isentropic efficiency of the turbine
σ_{01} - the total-pressure-retention coefficient for the compressor flow
σ_{23} - the total-pressure-retention coefficient for the combustion-chamber flow

1. Introduction

The suggested variants of a non-linear observer of a one-spool turbojet engine [1, 2, 4, 6, 8] differ in their scopes of directly measured parameters. Among these variants one should be distinguished, i.e. one featured with that a minimum number of such parameters are required for the performance thereof [8]. These parameters are as follows: flight altitude (H), air speed (M), total temperature of air at the engine inlet (T0), rotational speed of the spool (n).

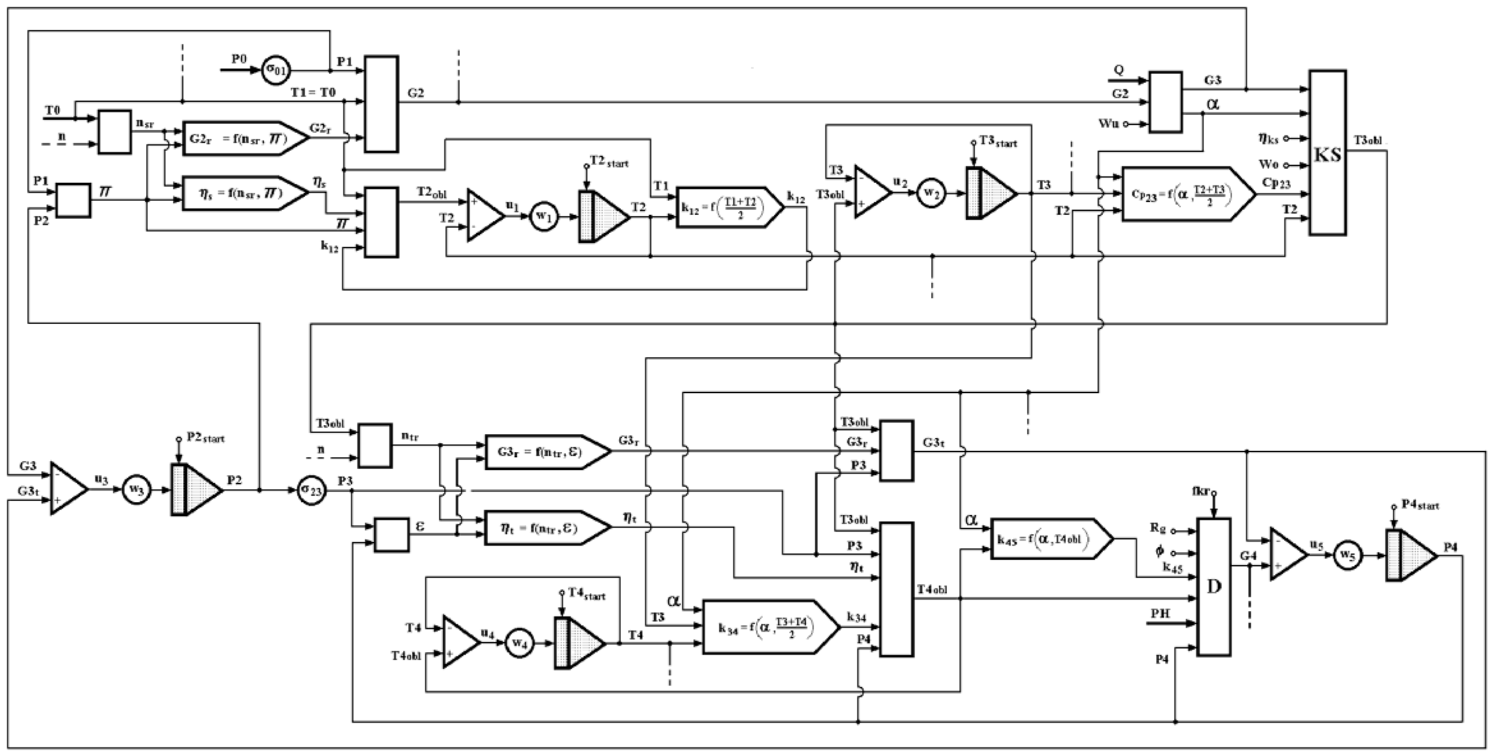

Fig. 1a. An analogue diagram of the observer no. 1. The block of the iteration-based solving of a system of non-linear algebraic equations that describe actual values of parameters of the working medium in the engine duct

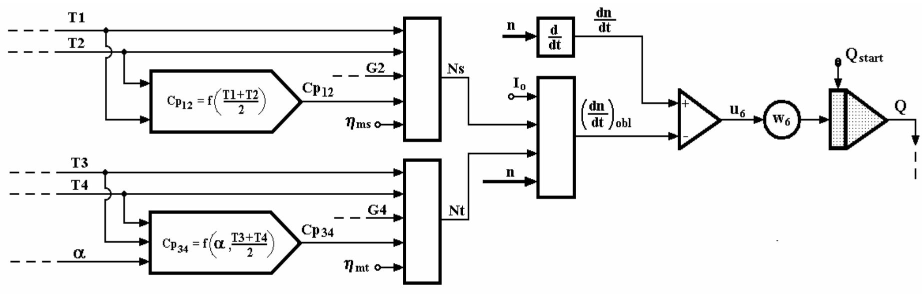

Fig. 1b. An analogue diagram of the observer no. 2. A block to calculate actual values of turbine power, compressor power, and the rate of fuel flow

In practice, there are a number of potential applications for this variant of the observer. Among other ones, the following should be mentioned:

- In procedures to monitor degradation of turbojet performance throughout the engine's operational use [5] – as the reference while evaluating the rate of degradation;
- In failure detection systems of sensors to control turbojet engine's operation – as comparative data to evaluate errors of measurements of engine parameters taken with digital electronic control systems of the FADEC class;
- In systems to automatically detect unstable operation of compressors of turbojets [4];
- In systems to detect other dangerous modes of turbojet's operation, e.g. uncontrolled flameout or incorrect shut-down.

The above-mentioned potentialities for practical applications of the observer generate demand for investigating into the accuracy of results gained with this observer. This paper has been intended to examine the effect of a simplifying assumption that the working medium in the engine duct is a perfect gas upon the observer's accuracy. Therefore, two versions of the observer have been developed for the same engine.

In version no. 1 it has been assumed that the working medium is a semi-perfect gas. In practice it means that variable values of specific heats (Cp) and isentropic exponents (k) have been assumed in equations which describe parameters of the working medium flow. Non-linear functions inserted in the observer's algorithm, which describe dependences of isentropic exponents and specific heats of the working medium on temperature and the excess-air coefficient have been shown in Figs 1a and 1b. Fig. 1a shows a diagram of the block intended for the iteration-based solving of a system of non-linear algebraic equations, which describe parameters of the working medium flow. Fig. 1b shows a diagram of the block intended to calculate an actual value of power generated by the turbine (Nt), input power of the compressor (Ns), and the rate of fuel flow (Q).

In version no. 2 isentropic exponents and specific heats of the working medium remain constant. The respective values are as follows: $k_{12} = 1.40$, $k_{34} = 1.33$, $k_{45} = 1.33$, $Cp_{12} = 1.0048$ kJ/(kg·K), $Cp_{23} = 1.0886$ kJ/(kg·K), $Cp_{34} = 1.1723$ kJ/(kg·K).

Simplifying assumptions made to satisfy the needs of a mathematical description of the observer are exactly the same as those made for the simulation-based model of the SO-3 engine [3]. To make this paper more consistent, it has been decided NOT to present all mathematical equations used to construct the algorithm. Instead, special attention has been paid to detailed presentation of analogue diagrams that illustrate the method of the iteration-based solving of the system of non-linear algebraic equations.

2. Results of the processing of data from the ground testing of the SO-3 engine

The intention was to compare results gained from the processing, with each of both versions of the observer, of exactly the same plot (Fig. 6) of how the rotational speed of the spool was changing.

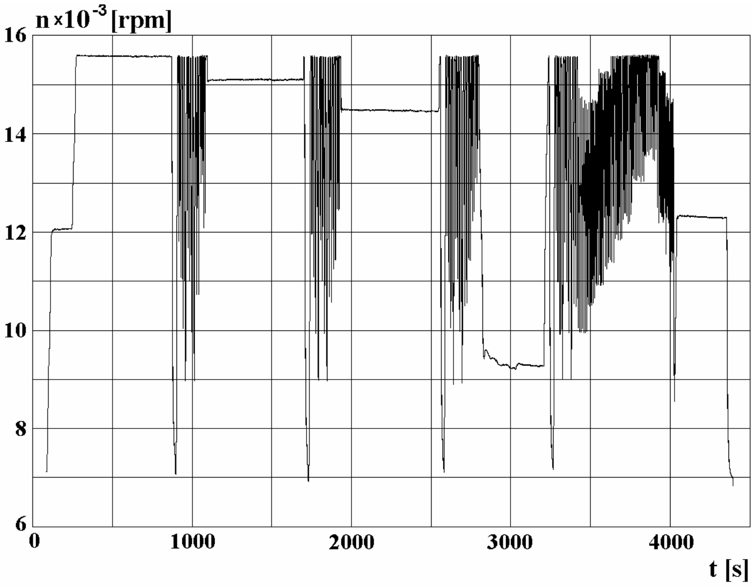

Fig. 2. Rotational speed of the spool changing in the course of ground testing of the SO-3 engine

Files with results of the processing carried out with each of both versions of the observer have been completed with actual values of thrust (R) and fuel consumption per unit (Cj). Not to be found in the diagrams, these values have been calculated in some obvious way using another values of parameters shown in Figs 1a and 1b.

Percentage differences between results gained with both versions of the observer (ΔPi(t)) have been calculated in the following way:

$$\Delta Pi(t)\ [\%] = 100\ [Pi_1(t) - Pi_2(t)]\ /\ Pi_1(t), \quad (1)$$

where:

$Pi_1(t)$ - an actual value of the ‘i’ parameter calculated with the observer no. 1;
$Pi_2(t)$ - an actual value of the ‘i’ parameter calculated with the observer no. 2.

Tab. 1. Times of the processing

Version of observer	Time of processing [s]	Time interval Δt [s]	Number of samples	Time of a real process [s]
No. 2	3245	0.02	215800	4316
No. 1	4865			
No. 2	2060	0.04	107900	
No. 1	2975			

The processing was carried out using a PC furnished with the Pentium processor (R), a system clock of 3.0 GHz and RAM of 1.0 GB. Table 1 shows times of the processing with each of both versions of the observer. Codes of computer programs have been written in Turbo-Pascal.

3. Results

Exemplary plots of actual values of parameters of engine performance, calculated with version no. 1 of the observer, have been shown as functions of a directly measured rotational speed of the engine (Figs 3 ÷ 6). The idea of directly presenting the actual values of parameters of the engine performance, calculated with version no. 2 of the observer, has been given up. Instead, two exemplary plots of percentage differences discussed in 2. have been shown in Figs 7 and 8.

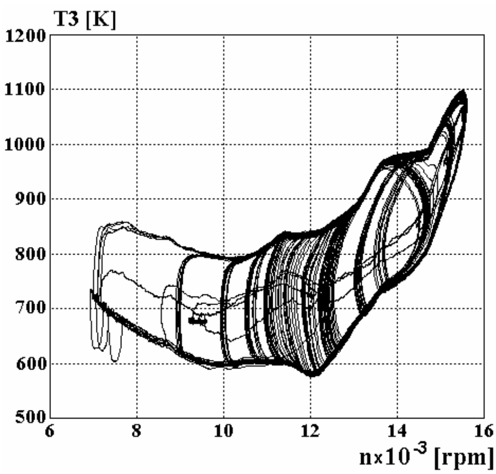

Fig. 3. An actual value of total temperature of the working medium at the combustion-chamber outlet, as calculated with the observer no. 2 – against rotational speed of the spool

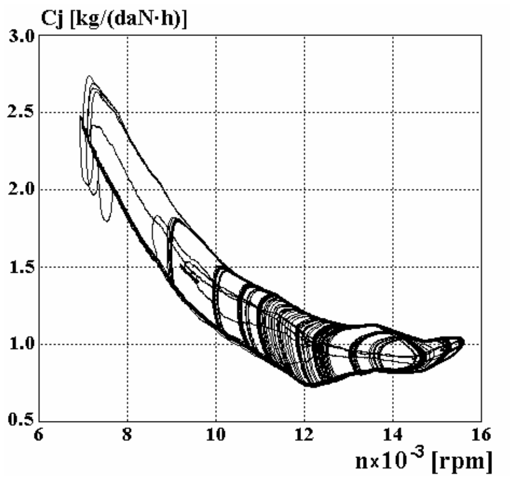

Fig. 4. An actual value of specific fuel consumption, as calculated with the observer no. 2 - against – rotational speed of the spool

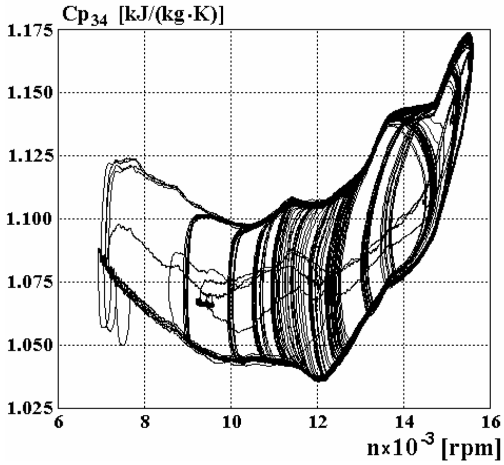

Fig. 5. An actual value of specific heat of the working medium in the turbine, as calculated with the observer no. 1 – against rotational speed of the spool

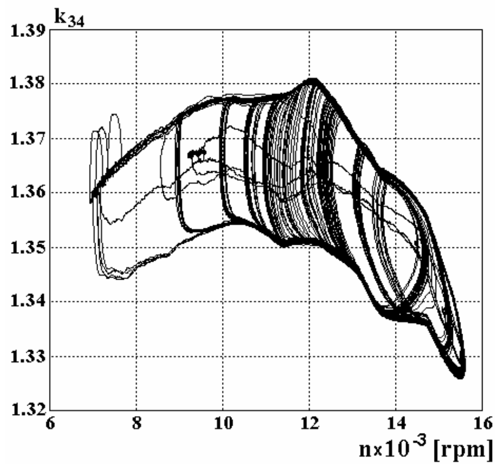

Fig. 6. An actual value of the isentropic exponent of the working medium in the turbine, as calculated with the observer no. 1 – against rotational speed of the spool

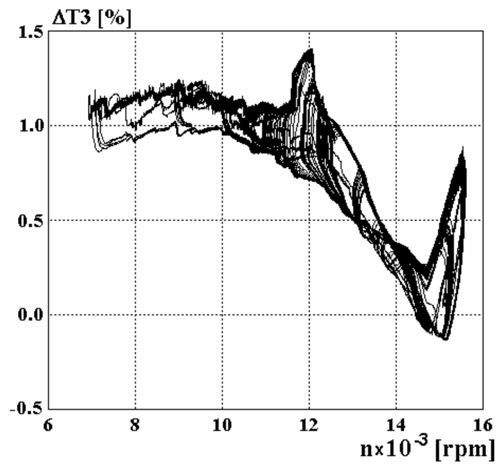

Fig. 7. How actual values (measured with both versions of the observer) of difference in the average total temperature of the working medium at the combustion-chamber outlet change - against rotational speed of the spool

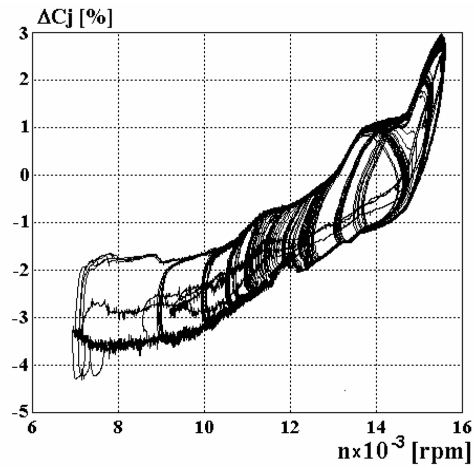

Fig. 8. How actual values (measured with both versions of the observer) of difference in the specific fuel consumption change - against rotational speed of the spool

4. Conclusions

Complete evaluation of the above-presented results needs comparison with similar values gained from some reliable measurements taken on a real engine. Unfortunately, at the time of preparing this paper the Authors had no digital records of the relevant data from tests of the SO-3 engine, where – apart from and in sync with actual values of the rotational speed of the spool (n) – also values of some other parameters would be recorded.

Variable scatter of differences between results of calculations carried out with both the versions of the observer is a real peculiarity of these differences. The scatter ranges depend in some particular way on the rotational speed of the spool.

Percentage values of these differences remain satisfactory low. Therefore, also the simplified version of the observer may take the part of a virtual sensor intended to measure difficult-to-measure parameters of the engine operation. After some modification and optimisation of program codes, both versions of the observer may be operative in the real-time mode.

5. References

[1] Pawlak, W. I., *Nonlinear observer in control system of a turbine jet engine,* The Archive of Mechanical Engineering. Polish Academy of Science Committee of Machine Design, Vol. L, 2003,3, Warsaw.

[2] Pawlak, W. I. et al., *Pomiar widma cyklicznych obciążeń jednowirnikowego jednoprzepływowego turbinowego silnika odrzutowego w eksploatacji wspomagany komputerowa symulacja parametrów jego pracy w stanach nieustalonych, Cz. I i II,* Sprawozdanie z realizacji Projektu Badawczego Nr 9T12D 007 17, Instytut Lotnictwa, Warszawa 2001.

[3] Pawlak, W. I., Wiklik, K., Morawski, J. M., *Synteza i Badanie Układów Sterowania Lotniczych Silników Turbinowych Metodami Symulacji Komputerowej,* Biblioteka Naukowa Instytutu Lotnictwa, Warszawa 1996.

[4] Pawlak, W. I., *A Non-linear observer in the warning system indicating faulty modes of operation of a turbine jet engine,* The Archive of Mechanical Engineering. Polish Academy of Science, Committee of Machine Design, Vol. LII, 2005, 2, Warsaw.

[5] Pawlak, W. I., *Monitorowanie osiągów silników K-15 na samolocie I-22 IRYDA,* Polskie Towarzystwo Mechaniki Teoretycznej i Stosowanej, Mechanika w Lotnictwie „ML-VIII", Warszawa 1998.

[6] Pawlak, W. I., *Non-linear observer of single-rotor single-flow jet turbine engine during operation,* Journal of KONES Internal combustion Engines, Vol.12, No. 1-2, European Science Society of Powertrain and Transport Publication, Warsaw 2005.

[7] Pawlak, W. I., *Problemy monitorowania niskocyklowych obciążeń termicznych lotniczego silnika turbinowego,* V Krajowa Konferencja "Diagnostyka Techniczna Urządzeń i Systemów DIAG'2003", September 13-17, Ustroń 2003.

[8] Pawlak, W. I., *Zastosowania Nieliniowych Obserwatorów Parametrów Pracy Turbinowego Silnika Odrzutowego,* 27th International Science Conference on Combustion Engines KONES' 2001, Conference Proceedings, Jastrzębia Góra, Poland, September 9-12, 2001.

MODELLING THE EMISSION OF NOXIOUS COMPOUNDS OF MAIN ENGINE EXHAUST GASES IN THE GULF OF GDAŃSK REGION

Leszek Piaseczny

Gdansk University of Technology
ul. Narutowicza 11/12, 80-950 Gdańsk, Poland
tel.: +48 58
e-mail: piaseczny@ptnss.pl

Tomasz Kniaziewicz

Naval Academy
ul. Śmidowicza 69, 81-103 Gdynia, Poland
tel.: +48 58 6262851
e-mail: tkniaziewicz@wp.pl

Abstract

The development of marine diesel engines has so far been directed towards raising their power, reducing fuel consumption, burning fuels of the lowest possible quality and the extension of operation time. The rising pro-ecologic pressure has caused atmosphere pollution by exhaust gases of marine engines to be one of the main problems of environment protection of recent years. The Gulf of Gdansk area, just like sea ports or coastal regions, is vulnerable to the effect of noxious compounds contained in vessel exhaust gases, besides those coming from industrial plants, power plants or vehicles. This concerns vessels both in ports and in the roads. In order to determine the share of vessels in environment pollution and counteract the harmful effects of toxic compounds in marine engine exhaust gases, it is necessary to know the emission values of these compounds from particular vessels, which is possible with the knowledge of their movement parameters, concentration values of particular compounds for these parameters and the atmospheric conditions.

The report presents conditions concerning the modelling of noxious compounds emission in the Gulf of Gdańsk region.

1. Introduction

The emergence of regulations concerning the level of toxic compounds emission [1,2,3,4,5,6,7], made both engine manufacturers and shipowners undertake actions aimed at its reduction. Shipowners' activity in this scope is practically enforced by the requirements of local regulations concerning state coastal waters and ports. There is also the opinion that the MARPOL regulations in force will cover not only newly-built engines, but also those currently remaining in operation.

These changes are expected to affect the process of operation and ecologic supervision of marine engines. Apart from technical modification of marine engines and the construction of additional plants aimed at fulfilling the requirements of toxicity standards for exhaust gases, this will bring about the necessity of introducing new methods determining directly or indirectly the toxic compounds emission level in exhaust gases [8].

The above circumstances make it necessary to identify the effect of particular conditions of the engine work on the emission level of toxic compounds in exhaust gases. Whereas the effect of constructional and operational factors on engine work indexes is known and taken account of, their effect on emission indexes for toxic compounds is less known, at least with respect to marine engines. Such a state of things makes us undertake an analysis of this effect.

The Gulf of Gdańsk area (Fig.1), similarly to sea ports or coastal regions, is vulnerable to the effect of noxious compounds in vessels' exhaust gases, besides pollution coming from industrial and power plants or vehicles. This concerns vessels both in ports and in the roads. It should be pointed out that in spite of the small number of vessels in relation to, e.g., city traffic vehicles, emission values of noxious compounds from a marine engine are many times higher.

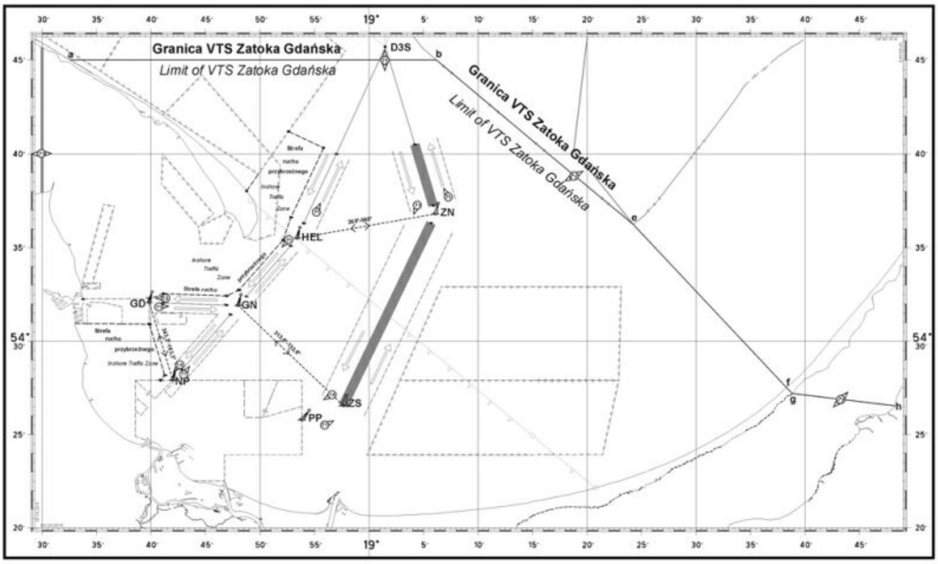

Fig.1. Chart of Gulf of Gdańsk region with marked vessel traffic routes [9]

The problem of air pollution in ports and approaches to ports is insomuch important, as the ports are in the area of large cities, and their limited area causes high concentration of vessels in a small space. Widely conceived operational conditions do not remain without significance, either. The following can be counted among the latter: the method of engine utilization, frequency and abruptness of non-stationary states, transitional processes characterised by higher emission of toxic compounds than when sailing in open areas with constant engine load, and the correctness and frequency of starting the engine. Of course, the toxicity of exhaust gases is no less affected by operational materials applied, that is kinds of fuel and oil.

2. The effect of vessel movement resistance and external conditions on the engine's load

The amount of noxious compounds emitted in the exhaust gases of a marine engine depends on values describing the condition of the engine's work, like torque M_o, rotational speed n, thermal state of the engine J, technical state of the engine Z (parameters of charge exchange system, state of TPC system, technical state and correctness of injection apparatus), conditions of surroundings G (e.g. temperature of surroundings, pressure, air humidity) and changing resistance of the vessel O (vessel resistance in shallow waters, vessel resistance during movement in a canal, air resistance and wave effect). It can thus be written down that the emission of the n^{th} noxious compound in exhaust gases e_n , will have the following form:

$$e_n = f\,(M_o, n, J, Z, G, O) \tag{1}$$

The intensity of emission E being a function of time $m_t(t)$ from a particular source in relation to time t can be written down as follows:

$$E(t) = \frac{dm_t(t)}{dt} \tag{2}$$

where m_t – mass of a given noxious compound.

Road emission [10] is defined as emission derivative, being a function of the road $m_s(s)$ from a source like a vessel, in relation to road s covered by her

$$b_s = \frac{dm_s(s)}{ds} \tag{3}$$

On the basis of equation 3 it can be written down that emission on road S will be equal to

$$m_s(S) = \int_0^S b_s(s)ds \tag{4}$$

and in time T

$$m_t(T) = \int_0^T b_t(t)v(t)dt \tag{5}$$

where v(t) vessel speed.
Road emission can be written down as the functional of value courses describing the combustion engine work state i.e. of torque M_o, rotational speed n and the vectors describing the thermal state of the engine **J**(t), conditions of the surroundings **G**(t) and the changing vessel resistances **O**(t)

$$b_t = \wp[\,M_o(t), n(t), \mathbf{J}(t), \mathbf{G}(t), \mathbf{O}(t)] \tag{6}$$

where $\wp$ – operator transforming torque, rotational speed and the vectors of the engine's thermal state, movement resistance and conditions of the surroundings into average road emission from a vessel.

The power necessary for sailing on vessel with speed v_s can be presented by means of equation:

$$P_o = \frac{V}{L}\frac{x}{\lambda}\sqrt{\psi}\,\frac{v_s^3}{C_p} = f\left(\frac{v_s^3}{C_p}\right) \tag{7}$$

where:

V – volume of the vessel's underwater part [m^3],
L – vessel length on the waterline [m],
v_s – vessel speed [w],
x – coefficient dependent on the number of shafts, taking into account the effect of protruding parts,
λ – length correction factor calculated from the formula $\lambda = 0.7 + 0.3\ L/100$,
ψ – fineness ratio of the hull:

$$\psi = \frac{B}{L}\delta$$

B – vessel width [m],
δ – block coefficient of the hull,
C_p – pressure resistance coefficient.

It should be remembered at the same time that engine power P is also affected by conditions of the surroundings different from exemplary ones, which is why it is necessary to correct the power value given by the engine manufacturer [11]. In the case of a four-stroke engine effective power P_e equals [12]:

$$P_e \cong P_{eo}[k - 0.7(1 - k)(\eta_m^{-1} - 1)] \tag{8}$$

where:

P_e – effective power for real external conditions [kW],
P_{eo} – effective power for normal external conditions [kW],
η_m – mechanical efficiency of the engine,
k – coefficient taking into account a change of external conditions

$$k = \left(\frac{p_1 - a\varphi_1 p_{s1}}{p_0 - a\varphi_0 p_{s0}}\right)^m \left(\frac{T_0}{T_1}\right)^n \left(\frac{T_{c0}}{T_{c1}}\right)^q$$

where:

p_o, p – barometric pressure of air sucked in, in normal and measurement conditions [hPa],
p_{so}, p_s – vapour pressure in air sucked in, in normal and measurement conditions [hPa],
φ_o, φ – relative humidity of the air in conditions as above [%],
T_o, T – air temperature in conditions as above [K],
T_{co}, T_c – cooling water temperature at the inlet of the supercharging air cooler in conditions as above [K].
Coefficient *a* , index exponents *m,n* and *q* depend on engine type and are given in the standard [12].

The effects of external conditions on the vessel's propulsion system and its functional interrelations have been presented in Fig. 2 [13].

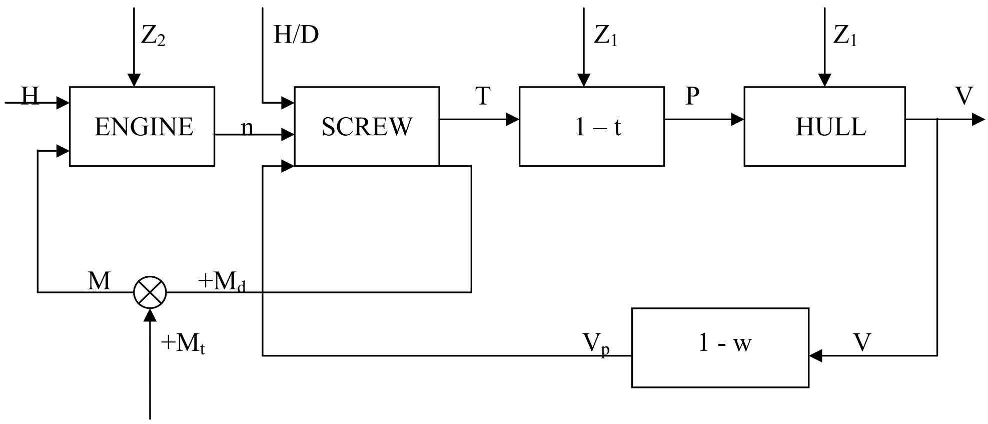

Fig.2. Effect of external conditions on the vessel's propulsion system [13]

The setting of injection pump h and load torque M are input values to the main engine. Pitch coefficient H/D, rotational speed n and forward speed V_p are input values to the screw. Screw torque M_d, increased by friction moment on the shafting (bearings and gears) M_t puts the engine under load. Effective pressure of the screw P=T(1-t) (t – suction coefficient) causes the hull to move and in stationary states determines its speed V. The forward speed of the screw V_p depends on hull speed V_p=V(1-w) (w – wake fraction). Disturbances Z_1 change the hull's resistance characteristic, of suction coefficient t and wake fraction w, and therefore also of the screw's forward speed and engine load. Disturbances Z_2 affect the system's work by changing the engine characteristic. They result from the change of temperature, pressure and relative humidity of the surrounding air, changed calorific value of fuel and the engine's technical condition. Thus, the course of the working process depends on controllable values like the setting of injection pump and screw pitch (in the case of adjustable screws) and a number of uncontrollable values, described as external conditions or disturbances Z_1 and Z_2. Disturbances Z_1 (draft, trim, state of hull surface, state of the sea, wind speed and direction, under-keel clearance etc.) do not effect a change in the engine's characteristic, but they do change the nature of its load.

It follows from this that with current methods of controlling propulsion systems it is practically impossible to accurately program and determine the engine's working point in real conditions, also when doing research on the toxicity of exhaust gases.

3. Possibilities of predicting work conditions of marine engines

Information identifying the vessel and determining her movement parameters can be obtained from VTS system (Vessel Traffic Service), which provides the operator with data in the following categories [14]:

a) hydrometeorological situation in the region,
b) status of navigational marking,
c) vessel positions, movement and intentions,
d) contact with the rescue centre,
e) possible other data indispensable for maintaining order and traffic safety in the responsibility area.

As can be seen, information categories mentioned in positions a) and c) are directly useful for estimating the effect of vessel traffic on air pollution with noxious compounds from exhaust gases. The information can be supplemented with information from an independent identification system - AIS. Information from these systems is combined in Maritime Safety Information Exchange System (SWIBŻ), which makes it possible to filter it according to numerous parameters (e.g. the vessel's name and data). The system has its merits and demerits. Its biggest demerit (from the point of view of the present writers' needs) is the necessity of gathering information of positional character, correlated in time, weather conditions and the vessel's type, engine and load, and the necessity of taking into consideration the loading state, speed and weather conditions. In work [14] at least partial elimination of these faults is suggested, as the system of automatic identification of ships (AIS) can be used more widely.

AIS system is a system of data transmission by radio waves. The data can be divided into three categories:

1) constant information,
2) information on travel,
3) variable information.

The first two categories are of alphanumeric character and are entered by the installer or operator. Variable information is taken from navigational apparatus cooperating with AIS. Information transmitted by AIS can be divided into static (MMSI number, name and call sign, IMO number, length and width, type, location of antenna in relation to hull geometry) and dynamic, determined in the normal course by external devices (vessel position and its accuracy index, UTC time of position determination, track angle over the bottom, speed over the bottom, ship's course, navigational status, angular velocity when making a turn). A separate group of information is constituted by information pertaining to travel (vessel's draft, dangerous cargo, port of destination and ETA, voyage plan).

It follows from the description of AIS system functions that it is viable to make use of the system data for determining models of vessel movement and the attendant models of emission of noxious compounds contained in exhaust gases.

4. Possibilities of modelling noxious compounds emission from main engine exhaust gases in the region of the Gulf of Gdańsk

On the majority of vessels the changes in values of engine load take place in accordance with the screw characteristic. The real screw characteristic of power of a main engine cooperating with a propulsion screw with given geometry (*H/D = const)* in particular external conditions of the vessel's movement *(WZ = const)* is described by the dependence

$$P_e = k_2 \cdot n^m \ [W] \tag{9}$$

where:

$m \sim 3$ for displacement hulls,
$m = 1.8 \div 2.2$ for half-slide hulls,
$m = 1.6 \div 1.8$ for slide hulls.

Relative screw characteristic of power for displacement hulls, averaged for normal operational conditions, is described by the polynomial:

$$P_{e\bullet} = -0.015 + 0.285 \cdot n_\bullet - 0.794 \cdot n_\bullet^2 + 1.523 \cdot n_\bullet^3 \tag{10}$$

where:

$P_{e\bullet} = P_e/P_{e(n)}$
$n_\bullet = n/n_n$

For each marine engine of the main propulsion it is possible to determine the screw characteristics of concentrations or emission of particular noxious compounds in exhaust gases. Within the framework of research conducted at the Naval Academy at Gdynia there were determined toxicity characteristics and quality models describing concentration values of particular compounds as function of the engine's speed [15]

Fig. 3 presents the screw characteristic of torque and the concentrations of nitrogen oxides in the exhaust gases of Sulzer engine type 6AL20/24, and an equation describing the value of nitrogen oxides c_{NOx} concentration as function of the engine's speed.

Determining this type of characteristics for a larger number of engines of the same type or kind would permit, after suitable statistic treatment, the preparation of universal characteristics and models for a given group of engines.

At present, due to lack of universal models, it is possible to determine approximate emission on the basis of average emission for a particular kind of engine. The value of such emission can be calculated on the basis of equations:

$$e_{in} = P_e \cdot \bar{e}_{in} \cdot r \ \ [g/(kW \cdot h)] \qquad or \qquad e_{in} = B_e \cdot t \cdot \bar{e}_{in} \cdot r \ \ [kg/t_{pal}] \tag{11}$$

where:

e_{in} – emission value of the n[th] compound,
P_e – effective power for real external conditions [kW],
B_e – fuel consumption per hour [t/h],
t – mean time of the vessel's stay in the researched region [h],
r – coefficient taking into account the effect of external conditions on additional resistance (vessel resistance in shallow waters, air resistance, wave-caused resistance),
$\bar{e}_{in}$ – value of average emission of the n[th] compound for the kind of engine (based on MAN-B&W and Wartsila catalogues):

medium-speed engines:

- $\bar{e}_{NOx}$ =13.8 g/(kW·h) or 59 kg/t_{pal}
- $\bar{e}_{CO}$ – 1.8 g/(kW·h) or 8 kg/t_{pal}
- $\bar{e}_{HC}$ – 0.6 g/(kW·h or 2.7 kg/t_{pal}
- $\bar{e}_{CO2}$ – 3250 kg/t_{pal}

slow-speed engines:

- $\bar{e}_{NOx}$ – 18 g/(kW·h) or 84 kg/t_{pal}
- $\bar{e}_{CO}$ – 2 g/(kW·h) or 9 kg/t_{pal}
- $\bar{e}_{HC}$ – 0.6 g/(kW·h) or 2.5 kg/t_{pal}
- $\bar{e}_{CO2}$ – 3150 kg/t_{pal}

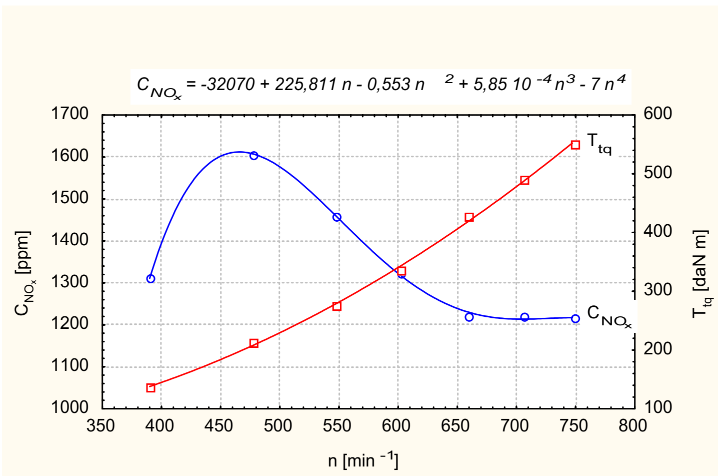

Fig. 3. Screw characteristic of torque and nitrogen oxide concentration in the exhaust gases of Sulzer type 6AL20/24 engine

5. Conclusions

1. With known value of the vessel's speed, and the type and characteristic of the engine, it is possible to determine engine power, and consequently to calculate unit emission of particular noxious compounds in the exhaust gases of marine engine.
2. Determining this type of characteristics for a larger number of engines of the same type or kind would permit, after suitable statistic treatment, the preparation of universal characteristics and models for a given group of engines.
3. Among parameters disturbing the accurate determination of emission of particular compounds (due to lack of information or their changeability) there can be counted the effect

of surface roughness of the hull (unevenness of hull plates and their joints, unevenness of paint layers, and unevenness caused by hull corrosion and overgrowing), technical condition of the engine, fuel apparatus in particular, and atmospheric conditions (especially wind direction and force).

4. In case of lack of the above data, it is possible to determine the approximate emission of noxious compounds on the basis of average emission values.

References

[1] Dietrich, W.R., *Experience with the Germany Clean Air Act of stationary internal-combustion engines*, MTZ 49/1988.

[2] Emission Standards Reference Guide for Heavy-Duty and Nonroad Engines. EPA 420-F-97-014, September 1997.

[3] Euromot Working Group Euromot Proposal on Exhaust Emission Standards for Marine the Prevention of Pollution from Ships (MARPOL 73/78), Annex VI "Regulations for the Prevention of Air Pollution From Ships" - London 26.09.1997

[4] International Maritime Organization - Protocol of 1997 to the International Convention for the Prevention of Pollution from Ships (MARPOL 73/78), AneksVI "Regulation for the Prevention of Air Pollution From Ships" – London 26.09.1997.

[5] Leigh-Jones, C., *Worldwide Developments in Exhaust Emission Legislation for Marine Sources*, Ricardo Consulting Engineers Ltd, West Sussex, 18 April 1994.

[6] The Marine Engineering Society in Japan: Recent trends in the control of emissions from ships, Martch 1996.

[7] Ustawa o zapobieganiu zanieczyszczaniu morza przez statki. Dziennik Ustaw RP Nr 47, Warszawa 09 maja 1995.

[8] Vollenweider, J., *Exhaust Emission Control of Sulzer Marine Diesel Engines*, Marine Engine Symposium, Szczecin, Gdynia/Gdańsk, czerwiec 1994.

[9] www.umgdy.gov.pl

[10] Chłopek, Z., *Modelowanie procesów emisji spalin w warunkach eksploatacji trakcyjnych silników spalinowych*, PN Politechniki Warszawskiej , Mechanika, z.173, Warszawa 1999

[11] Wojnowski, W., *Okrętowe siłownie spalinowe, cz. III Projektowanie siłowni okrętowych*, Wydawnictwo Politechniki Gdańskiej, Gdańsk 1992

[12] Norma ISO 3406/I-1975/E

[13] Berger, T., *Zastosowanie systemów diagnostycznych w użytkowaniu urządzeń okrętowych*., Zeszyty Naukowe AMW Nr 4/88, Gdynia 1988.

[14] Felski, A., *Implementation of AIS in air pollution investigations*, Materials of European Navigation Conference Global Navigation Satellite Systems. Geneva 2007.

[15] Kniaziewicz, T., Piaseczny, L., Merkisz, J., *Charakterystyki śrubowe stężeń NO_x, CO, HC w spalinach silnika SULZER typu 6AL20/24*, Czasopismo Techniczne MECHANIKA, zeszyt 6, str. 333-340, Politechnika Krakowska 2004

MATHEMATICAL MODELS OF MECHANICAL PROPERTIES OF VESSEL SCREW PROPELLERS

Leszek Piaseczny

Naval Academy
ul. Śmidowicza 69, 81- 103 Gdynia 3, Poland
tel: +58 626 26 03
Gdańsk University of Technology
ul. Narutowicza 11/13 80-952 Gdańsk
tel.kom.: 0501 753 261
e-mail: piaseczny@ptnss.pl

Krzysztof Rogowski

Navy Training Centre at Ustka
Lędowo, 76-270 Ustka, Poland
tel.: 512 325 123
e-mail: hiparion_1@wp.pl

Abstract

During repairing screw propellers by welding and plastic deformation it is indispensable to know their material features and strength properties relative to the propeller part subject to repair. The authors have conducted statistical and empirical research aimed at determining those features depending on the propeller's chemical composition and blade thickness. These dependencies are presented in the form of mathematical models useful both cognitively and utilitarian-wise.

Keywords: *ship propeller, mechanical properties, regression equations, copper alloys*

Damage of screw propellers (fractures, fissure of blades) occurs above all on vessels propelled by combustion engines and is caused by unfavourable overlapping of the ship's vibrations, screw propeller and propulsion engine (Fig.1). Besides, fissures, bends and nicks of the blade rubbing edges may occur when the screw propeller strikes against floating beams or ice floes. When the screw propeller works close to the area's bottom, it is worn by the erosion of sand raised from the bottom. Screw propellers are also worn by fatigue corrosion and cavitational erosion. Depending on the kind and extent of damage, location on the propeller and the possibilities of welding or hot straightening, screw propellers are repaired or replaced.

Fig. 1. Broken blade of a screw propeller [2]

There have arisen highly resistant multicomponent copper alloys for screw propellers, among which there can be distinguished manganese brass (Cu1-category alloys), aluminium brass (Cu2-category alloys), aluminium-nickel bronze (Cu3-category alloys) and manganese-aluminium bronze (Cu4-category alloys).

At present, in each category several kinds of copper alloys screw propellers are produced, and in the case of Cu3 category, even dozens of them, appearing under various trade names. Such a large number of copper alloys produced is the cause why before the screw propeller is repaired the exact chemical composition of the propeller material is not known (frequently the chemical composition of propeller material is protected by patent and constitutes an industrial secret), neither the mechanical properties of the screw propeller are known, in particular the blades with variable thickness of the cylindrical section on the propeller radius; whereas such information is indispensable for selecting suitable parameters and proper repair technology for the screw propeller.

Whereas the chemical composition of the propeller material can be roughly determined without destroying the screw propeller, it is more difficult to determine the mechanical properties of the propeller in places repaired. Taking samples from the propeller blade for determining mechanical properties is out of the question.

The mechanical properties of screw propellers given in technical documentation (certificate) are determined by testing separately cast ingots of 25 mm diameter. The results of this examination are only approximate, and are not the real mechanical properties of the blades of the screw propeller cast, and these can be determined only by taking samples from the screw propeller blade places we are interested in.

The knowledge of real mechanical properties, in particular the plastic properties of propeller blades in the area of repair by hot straightening or welding, permits to select suitable repair parameters (copper alloys of categories Cu1, Cu2, Cu3 and Cu4 have different heating temperatures for the repair of screw propeller blade by hot straightening, as well as welding – Tables 1 and 2), facilitates performing the repair, permits the decrease of welding deformation and stress and to avoid possible fissures in the weld and in the SWC of the welded joint.

Tab. 1. Recommended welding materials and temperatures of thermal treatment at welding

Alloy category	Welding materials	Minimal preheating temperature [°C]	Maximal temperature between runs[°C]	Temperature of relief annealing [°C]
Cu1	Aluminium bronze [1] Manganese bronze	150	300	350-500
Cu2	Aluminium bronze Nickel-manganese bronze	150	300	350-550
Cu3	Aluminium bronze Nickel-aluminium bronze [2] Manganese-aluminium bronze	50	250	450-500
Cu4	Manganese-aluminium bronze	100	300	450-600

Remarks:
1) Nickel-aluminium and manganese-aluminium bronze can be applied.
2) Relief annealing is not required if nickel-aluminium bronze is applied as welding material.

Tab. 2. Temperatures of straightening screw propeller blades made of copper alloys [3]

Alloy category	Temperature of hot straightening [°C]
Cu1	500-800
Cu 2	500-800
Cu3	700-900
Cu4	700-850

In connection with this, the idea was conceived that the mechanical properties of the screw propeller in relevant places should be determined from the chemical composition of the propeller material.

Fragmentary research conducted in the laboratories of screw propeller manufacturers, e.g. the firm LIPS in Holland (a known producer of screw propellers), showed that the properties of screw propeller alloys spread over the propeller blade radius.

This stimulated an attempt to collect measurement data of copper alloys for screw propellers (Table 3) and subjecting them to statistical analysis which showed that the nature of changes in mechanical properties with increased thickness of the screw propeller cast is best described by regression equation, WZ_WM = a+b·lg(W).

Tab. 3. Mechanical properties dependent on the thickness of cast sections of screw propellers made of copper alloys [4]

No.	Mean section thickness [mm]	Copper alloy	Number of casts	Mean values					Source
				R_m [N/mm^2]	$R_{0.2}$ [N/mm^2]	A_5 [%]	HB	Grain diameter [mm]	
1.	25	CuAl9.5Mn1.5Ni5Fe4.5	33	679	262	22.3	163	-	[5]
2.	45		4	636	252	18.3	160	-	
3.	67.5		3	613	241	18.9	160	-	
4.	92.5		4	589	230	19.3	149	-	
5.	155		3	582	210	20.7	136	-	
6.	265		12	503	201	14.0	129	-	
7.	300		5	511	199	15.0	128	-	
8.	340		12	487	196	13.8	131	-	
9.	370		17	496	197	15.0	128	-	
10.	400		8	478	195	15.6	126	-	
11.	435		16	489	189	15.9	129	-	
12.	30	CuAl9Fe4Mn1.5Ni2	3	620	-	20.0	-	0.15	[6]
13.	175		3	580	-	22.5	-	0.30	
14.	30	CuMn8Al6Fe2Ni2	3	700	-	22.0	-	0.05	[6]
15.	175		3	627	-	22.0	-	0.12	
16.	30 [1)]	CuMn13Al8Zn8Fe2.5Ni2	3	650	-	19.0	-	0.04	[6]
17.	175 [1)]		3	610	-	21.0	-	0.08	
18.	30 [2)]		3	674	-	17.6	-	-	
19.	250	CuAl9.5Mn1.5Ni5Fe4.5	11	551	207	18.0	-	-	[5]
20.	90		11	582	230	17.3	-	-	

1) determined on separately cast samples
2) determined on propeller of 4.5 m diameter

rRm=-0,94 ; rA5=-0,77 ; rHB=-0,94 ;
rR0,2=-0,95; rDz=0,49

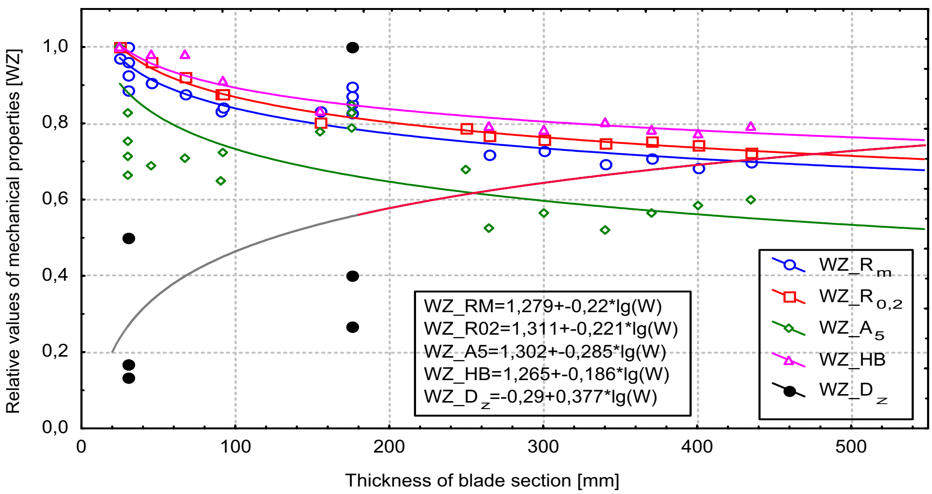

Fig. 2. Dependence of cast properties on the thickness of screw propeller section
$WZ\_R_m=R_m/679$; $WZ\_R_{0.2}=R_{0.2}/262$; $WZ\_A_5=A_5/22.3$; $WZ\_HB=HB/163$; $WZ\_D_z=D_z/0.30$ [4]

The graphic distribution of measurement points in the coordinate system (relative value – blade thickness, Fig.2) and the lines obtained by way of multiple regression analysis describe fairly well the location of mean result values and suggest that when preparing statistically the measurement data in a common coordinate system – thickness, regression lines can be described by the following equations:

$$WZ(R_m, R_{0,2}, A_5, HB, D_z) = a + b\lg(W)$$

where:

WZ – relative value of properties,
W – propeller blade thickness [mm],
a - absolute term,
b - coefficient,
D_z - grain diameter.

Regression lines designated in a common coordinate system show that the changes in the properties of screw propeller cast occur mainly with increased blade thickness in the range from 25 mm to 175 mm and are close to the course of increase in grain diameter D_z; with further screw propeller blade increase, on the other hand, the changes are not very large. This permits the recognition that the deterioration of mechanical properties along with increased thickness of screw propeller blade is due to accompanying grain diameter increase of the copper alloy from which the propeller was cast.

In order to obtain regression equations, data about mechanical properties and chemical composition of copper alloys from various research centres were collected and compared according to categories. The data concerned screw propellers made by various manufacturers, in various conditions of casting. The casts within the framework of the category had different designations, different chemical compositions and different mechanical properties. Differences in the content of main alloy components in particular categories of copper alloys for screw propellers are presented in Table 4. They are generally in agreement with content differences of components in alloys given by Classification Societies.

Tab. 4. Differences in the content of main alloy components in particular categories of copper alloys for screw propellers

COPPER ALLOYS OF CATEGORY Cu1						
Difference between main alloy components [%]						
Cu	Zn	Al	Mn	Ni	Fe	Sn
58±4.0	37.5±2.5	1.75±1.25	2.25±1.75	0.5±0.5	1.5±1.0	0.75±0.75
COPPER ALLOYS OF CATEGORY Cu2						
Difference between main alloy components [%]						
Cu	Zn	Al	Mn	Ni	Fe	Sn
59±9.0	35.5±2.5	3.03±2.55	2.5±1.5	4.25±3.75	2.75±2.25	0.77±0.72
COPPER ALLOYS OF CATEGORY Cu3						
Difference between main alloy components [%]						
Cu	Zn	Al	Mn	Ni	Fe	Sn
81.80±4.8	0.62±0.37	9.0±2.0	3.25±2.75	2.92±2.67	4.0±2.0	0.2±0.15
COPPER ALLOYS OF CATEGORY Cu4						
Difference between main alloy components [%]						
Cu	Zn	Al	Mn	Ni	Fe	Sn
73.0±10.5	4.35±3.85	7.5±1.5	13.5±6.5	2.0±1.0	4.5±2.5	0.55±0.45

The following regression equations were assumed for preparing statistical data:

- for copper alloys category Cu1:

$$R_m = a_1 \cdot c_{Zn} + b_1 \cdot c_{Al} + c_1 \cdot c_{Mn} + d_1 \cdot c_{Ni} + e_1 \cdot c_{Fe} + f_1 \cdot c_{Sn} + g_1 ; \quad [\%],$$
$$A_5 = a_2 \cdot c_{Zn} + b_2 \cdot c_{Al} + c_2 \cdot c_{Mn} + d_2 \cdot c_{Ni} + e_2 \cdot c_{Fe} + f_2 \cdot c_{Sn} + g_2 ; \quad [\%],$$

- for copper alloys category Cu2:

$$R_m = a_1 \cdot c_{Zn} + b_1 \cdot c_{Al} + c_1 \cdot c_{Mn} + d_1 \cdot c_{Ni} + e_1 \cdot c_{Fe} + f_1 \cdot c_{Sn} + g_1 ; \quad [\%],$$
$$A_5 = a_2 \cdot c_{Zn} + b_2 \cdot c_{Al} + c_2 \cdot c_{Mn} + d_2 \cdot c_{Ni} + e_2 \cdot c_{Fe} + f_2 \cdot c_{Sn} + g_2 ; \quad [\%],$$

- for copper alloys category Cu3 without Zn and Sn:

$$R_m = a_1 \cdot c_{Al} + b_1 \cdot c_{Mn} + c_1 \cdot c_{Ni} + d_1 \cdot c_{Fe} + e_1 ; \quad [\%],$$
$$A_5 = a_2 \cdot c_{Al} + b_2 \cdot c_{Mn} + c_2 \cdot c_{Ni} + d_2 \cdot c_{Fe} + e_2 ; \quad [\%],$$

- for copper alloys category Cu4 without Zn and Sn:

$$R_m = a_1 \cdot c_{Al} + b_1 \cdot c_{Mn} + c_1 \cdot c_{Ni} + d_1 \cdot c_{Fe} + e_1 ; \quad [\%],$$
$$A_5 = a_2 \cdot c_{Al} + b_2 \cdot c_{Mn} + c_2 \cdot c_{Ni} + d_2 \cdot c_{Fe} + e_2 ; \quad [\%],$$

- for copper alloys category Cu4 with Zn, but without Sn:

$$R_m = a_1 \cdot c_{Zn} + b_1 \cdot c_{Al} + c_1 \cdot c_{Mn} + d_1 \cdot c_{Ni} + e_1 \cdot c_{Fe} + f_1 ; \quad [\%],$$
$$A_5 = a_2 \cdot c_{Zn} + b_2 \cdot c_{Al} + c_2 \cdot c_{Mn} + d_2 \cdot c_{Ni} + e_2 \cdot c_{Fe} + f_2 ; \quad [\%].$$

as a result of which the following model parameters have been obtained (Table 5):

Tab. 5. Regression equations of the model

No.	Copper alloy	Regression equations for particular categories of copper alloys for screw propellers with model parameters
1.	Cu 1	$R_m = -6.931 \cdot c_{Zn} + 61.241 \cdot c_{Al} - 18.926 \cdot c_{Mn} - 32.660 \cdot c_{Ni} - 101.284 \cdot c_{Fe} - 90.363 \cdot c_{Sn} + 907.069$ $A_5 = -0.067 \cdot c_{Zn} + 3.093 \cdot c_{Al} - 3.636 \cdot c_{Mn} - 1.170 \cdot c_{Ni} - 2.043 \cdot c_{Fe} - 5.375 \cdot c_{Sn} + 34.312$
2.	Cu 2	$R_m = 4.595 \cdot c_{Zn} + 43.680 \cdot c_{Al} + 2.154 \cdot c_{Mn} - 10.632 \cdot c_{Ni} - 21.809 \cdot c_{Fe} - 103.980 \cdot c_{Sn} + 442.035$ $A_5 = 0.090 \cdot c_{Zn} - 1.265 \cdot c_{Al} + 0.298 \cdot c_{Mn} + 0.983 \cdot c_{Ni} + 1.521 \cdot c_{Fe} + 12.339 \cdot c_{Sn} + 8.233$
3.	Cu 3 (without Zn and Sn)	$R_m = -63.538 \cdot c_{Al} + 17.021 \cdot c_{Mn} + 12.697 \cdot c_{Ni} + 42.621 \cdot c_{Fe} + 978.803$ $A_5 = -7.277 \cdot c_{Al} + 2.704 \cdot c_{Mn} - 0.977 \cdot c_{Ni} + 4.010 \cdot c_{Fe} + 71.940$
4.	Cu 4 (without Zn and Sn)	$R_m = 2.352 \cdot c_{Al} + 15.837 \cdot c_{Mn} - 27.970 \cdot c_{Ni} - 37.395 \cdot c_{Fe} + 631.727$ $A_5 = -1.331 \cdot c_{Al} + 0.308 \cdot c_{Mn} - 9.205 \cdot c_{Ni} + 17.545 \cdot c_{Fe} - 0.163$
5.	Cu 4 (with Zn but without Sn)	$R_m = -1.612 \cdot c_{Zn} - 2.804 \cdot c_{Al} + 1.383 \cdot c_{Mn} + 14.214 \cdot c_{Ni} - 8.111 \cdot c_{Fe} + 704.306$ $A_5 = -0.037 \cdot c_{Zn} - 1.296 \cdot c_{Al} - 0.444 \cdot c_{Mn} + 1.639 \cdot c_{Ni} + 0.608 \cdot c_{Fe} + 31.704$

In spite of certain differences in the contents of the main alloy components (Table 4), essential regression equations have been obtained for most cases. Correlation coefficients and the results of Fisher test for checking the essentiality of regression calculated for dependent variables R_m and A_5 have been presented in Table 6.

Tab. 6. Assessment of regression equations

Copper alloy	Dependent variables	Correlation coefficient	Value of Fisher test	Assessment of regression
Cu1	R_m A_5	0.937 0.909	5.989 3.982	essential essential
Cu2	R_m A_5	0.966 0.906	16.247 5.376	essential essential
Cu3 (without Zn and Sn)	R_m A_5	0.836 0.631	12.179 3.483	essential essential
Cu4 (without Zn and Sn)	R_m A_5	0.870 0.933	7.780 16.903	essential essential
Cu4 (with Zn but without Sn)	R_m A_5	0.806 0.997	0.370 32.597	non-essential incidental

Correlation coefficients indicate which of the mechanical properties correlate better with the chemical composition of copper alloy for screw propellers, and which ones worse. The fact that R_m correlates better (Table 6) with the chemical composition than A_5 results from the measurement technique of results. The determination of value A_5 depends on the accuracy of comparing both parts of the culled sample.

As shown by Table 6, only regression equations for alloys of category Cu4 with the addition of zinc proved to be non-essential for the value R_m, and possibly incidental for the value A_5. This was probably decided by the overly large discrepancy of zinc content in those alloys ranging from 3.0% to 8.2%, whereas in alloys of other categories the content of particular components is kept within narrower bounds.

It can be stated on the basis of results obtained that the matching of the model is satisfactory and that the prognostic value of the model high and statistically.

Conclusions

In result of statistical calculations conducted, the following conclusions can be drawn:

1. Regression equations of mechanical properties and chemical composition of marine screw propeller casts made of Cu1, Cu2, Cu3 and Cu4 alloys may be essential and permit the modelling the mechanical properties of the propeller with an accuracy sufficient for repair technology.
2. There has been formulated a new, original shape of regression equations of mechanical properties and chemical composition values of screw propeller casts made of copper alloys of categories Cu1, Cu2, Cu3 and Cu4. There are no such equations in the world's literature. Similar equations are prepared, on the other hand, for highly alloyed steel resistant to corrosion and oxidation in high temperatures, as informed by Prof. F.B. Pickering in his work "*Physical Metallurgy and the Design of Steels*", London 1994.
3. Vessel repair technologies have been given a method of modelling the mechanical properties of screw propeller in the blade section being repaired, which will facilitate the preparation of an effective technology (without shrinkage cracks) of repairing the screw propeller by welding or hot straightening of blades.

References

[1] Scarabello, J. M. et al., *Contribution a l'etude du systeme trenaire Cu-Al-Mn. Détermination de la coupe Cu- Mn-Al_6 limitée au domaine riche en cuivre*, Revue de metallurgie 1982, Vol. 79, No 12, pp. 695 - 708.

[2] Marine News, *New propeller blades in double – quick time*, 2005, N^{o}2, pp. 36÷37.

[3] PRS, Przepisy, Publikacja nr 7/P, *Naprawy śrub napędowych ze stopów miedzi*, Gdańsk 2002.

[4] Piaseczny, L., Rogowski, K., *Zmiana właściwości mechanicznych na promieniu (0.25 – 1)R odlewu okrętowej śruby napędowej*, Zeszyty Naukowe Akademii Marynarki Wojennej, Rok XLIV Nr 3 (154)2003.

[5] Wenschot, P., *The Properties of Ni-Al bronze sand cast ship propellers in relation to section thickness*, Naval Engineers Journal, September 1986, pp. 58 - 69.

[6] Ruddeck, P., Koch, W., *Cumanal - ein neuer Werkstoff fur hochbeanspruchte Schiffspropeller*, Seewirtschaft 1972, H. 3, ss. 196 – 199, H. 4, ss. 269 - 272.

[7] *Rogowski, K., Modelowanie właściwości mechanicznych pędników śrubowych dla doboru technologii ich napraw,* Rozprawa doktorska, AMW, Gdynia 2006.

THE DETERMINATION OF THE DISPERSE PHASE REFINEMENT ON WATER IN FUEL EMULSIONS WITH THE USE OF THIN-LAYER EMULSION IMAGES USING A MICROSCOPE AND A MALVERN MASTERSIZER 2000 DEVICE

Przemysław Rajewski

Maritime University of Szczecin
Wały Chrobrego 1/2, 70-500 Szczecin, Poland
tel.: +48 91 4809542
e-mail: rajp@am.szczecin.pl

Abstract

The paper includes a proposal of methods for testing and evaluation quality and stability of water in fuel emulsion used in combustion tests on marine engine in MAN laboratory test bed. Attempts to satisfy the requirements set forth in Annex VI of the Marpol Convention and Resolution 33EU concerning, among other issues, the reduction of NO_x emission in exhaust gases from marine engines and boilers have resulted in further research on burning of fuel-water emulsions , a fuel considered to reduce the amount of NO_x. The research, within the scope of a project financed by the EU, is performed by the MAN company employing an engine in a test bed of the laboratory in Copenhagen. One of the elements in the research is to indicate a device for making emulsion, such as a static homogenizer developed at the Institute of Technical Marine Power Plant Operation, Maritime University of Szczecin. To obtain reliable results, it was necessary to design the methodology for the examination of emulsion quality. That was basically the objective of the research herein described.

Keywords: *marine fuel, water in fuel emulsion, the examination of emulsion quality*

1. Introduction

Aiming at reducing noxious components of exhausts from ship engines and boilers led to a series of investigations of fuel-water emulsion, i.e. its applications as a fuel reducing NO_x emission. There are two basic theories accounting for the effect of water on the process of water in fuel emulsion combustion in slow speed engines:

- microexplosion theory.
- theory of catalytic role water in fuel emulsion in self-ignition and residual fuel combustion [1].

Dooher, Gondberg, Lippmen, Wraight found from experimental research that for steam contained in a water droplet to undergo micro-explosion, it has to be stronger than fuel surface tension, and the time of water droplet expansion has to be less than fuel expansion time. When this time is longer, steam can penetrate through the droplet surface without its blow-out [1].

The droplet expansion time is described by this equation:

$$\tau_{roz} = \frac{1}{\sqrt{29\Pi}} \cdot \left(\frac{\rho}{\delta}\right)^{\frac{1}{2}} \cdot r_o^{\frac{3}{2}}$$

where:

δ - surface tension [N/m];
ρ - density [kg/m^3]:
r_o - droplet radius [m];

Calculations were made to determine the maximum size of a water droplet in a fuel droplet that causes micro-explosion. This size is 20 μm. The research also implies that emulsions rich in water will burn correctly if smaller diameters of disperse phase particles (water) in fuel are obtained.

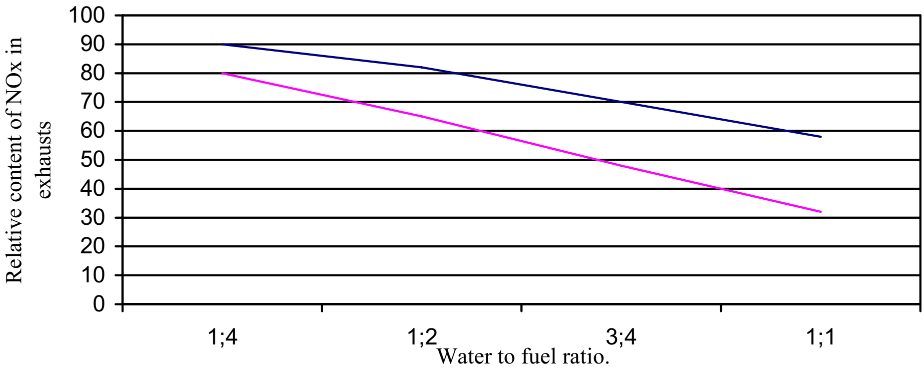

Fig. 1. Effect of water content in a fuel-water emulsion on the amount of NOx in internal combustion engine exhaust gases [2]

Certain research work had been done by this author before joining the research team in Copenhagen where the combustion of fuel-water emulsion was examined in slow speed engines by the MAN company. At the Institute of Technical Marine Power Plant Operation research was done to unequivocally define the emulsion 'quality', understood as the degree of dispersion of water in fuel after homogenization and as the durability of the prepared emulsion, understood as a period in which disperse phase droplets do not increase due to coagulation. The most useful for the burning of emulsion in internal combustion engines are water-in-fuel emulsions, i.e. emulsions in which fuel makes up the liquid phase while water is the disperse phase with most of droplet diameters ranging from 0.5 to 2μ. It was assumed that stability is the time when emulsion maintains its properties making it suitable as a substitute fuel. This time for emulsions made from various fuels is defined experimentally [3]. Because of this, it is important to unequivocally determine the size structure of water droplets (disperse phase) in a fuel-water emulsion used in comparative analysis. To this end an attempt was made to develop a method of evaluating the sizes of the disperse phase (water droplets) of fuel-water emulsion based on microscope images assuring stable conditions for observations of examined emulsions, that is a steady thickness of the observed emulsion layer and stable measurement temperature independent of the time of observation.

2. Microscopic examination of the water in fuel emulsion

Experience from previous tests [4] showed the need for the elimination of convection movements in the examined emulsion caused by heat from illumination of the preparation from the bottom when samples are observed in the transmitted light. Stable observation conditions were obtained using a base plate with a cooled chamber of own design shown on fig.2. Residual fuel with kinematic viscosity of 380 mm^2/s (cSt) was used as the base for producing emulsion. After heating the fuel in an electrical furnace to the temperature of 50-

60°C, it was filtered in a vacuum filter in order to eliminate solid contaminants that might cause coagulation of water into larger droplets. Then, by employing a laboratory homogenizer emulsion specimens were prepared containing 10%, 30%, and 50% of water. Emulsion samples were produced in the homogenizer at the homogenization time of 30 seconds.

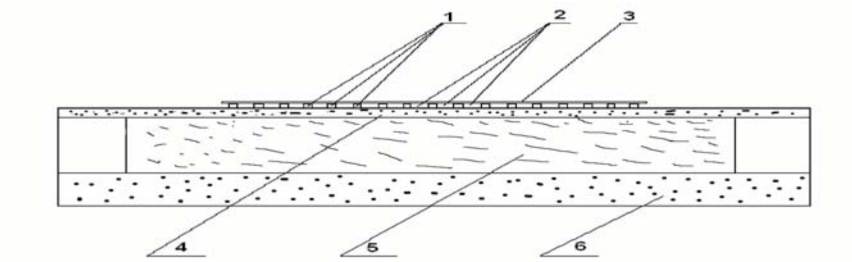

Fig. 2. The design of a base plate with a cooled chamber: 1- distance wires fixing the sample thickness(depending on the plate used, their thickness was, respectively, 0.1 and 0.05 mm); 2- specimen; 3- microscopic cover glass; 4- base glass; 5- chamber cooled by liquid (distilled degassed water at ambient temperature); 6- chambers bottom plate

The equipment used for the research included an Olympus BX50 test bed, a PC computer and Multiscan software, an advanced system of imaging and image analysis created by Computer Scanning Systems.

Emulsion samples were examined on microscopic plates of three types:

- glass Petri dish, where the specimen is put under a microscopic cover glass.
- polycarbonate plate with a cooling chamber allowing to maintain constant temperature of the examined specimen. The design of the base plate assured a steady distance of 0.01 mm between the cover glass and the base plate.
- Polycarbonate plate with a cooling chamber allowing to maintain constant temperature of the examined samples, with a steady distance of 0.05 mm between the cover glass and the base plate with specimen.

The condition of emulsion was observed:

- Immediately after it had been made,
- Three minutes after homogenization,
- Six minutes after homogenization,
- 15- 20 minutes after homogenization of the emulsion.

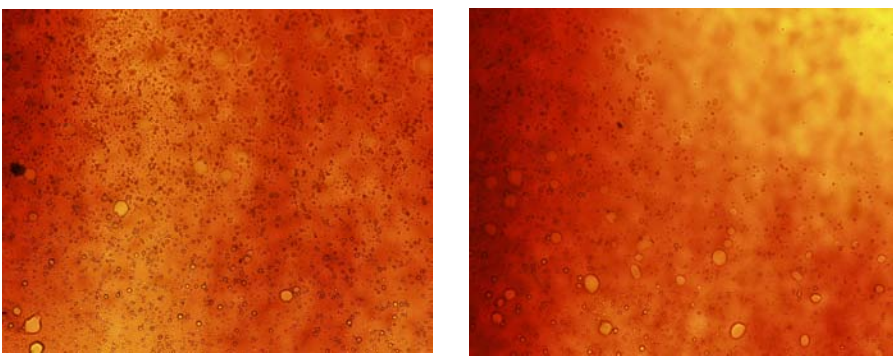

Fig.3. Examples of images of the emulsion made from fuel containing 10% of water, immediately after its homogenization. The measurement performed on a plate with a 'cooling chamber' with distance wire diameter 0.01mm

The created sample was observed with a microscope at 40X magnification. The image was digitally recorded by a camera fitted in the microscope tube. Four photographs were taken at randomly chosen places of each sample. The next step was counting the number of water droplets in the emulsion. After counting the droplets and grouping them in certain size ranges using Multiscan software, the results were gathered in a final report.

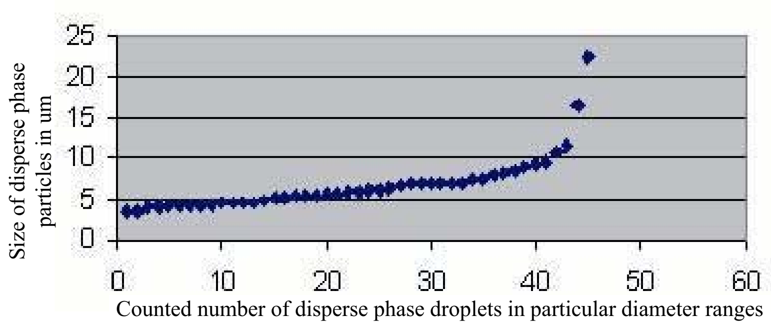

Fig.4. Number of disperse phase particles in emulsion containing 30% water immediately after homogenization, determined on the basis of observed particles

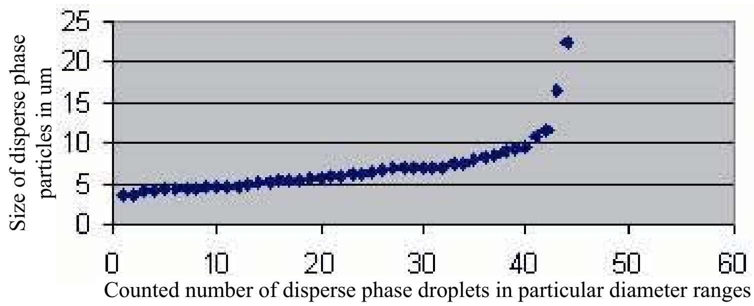

Fig.5 . Number of disperse phase particles in emulsion containing 30% water six minutes after homogenization, determined on the basis of observed particles

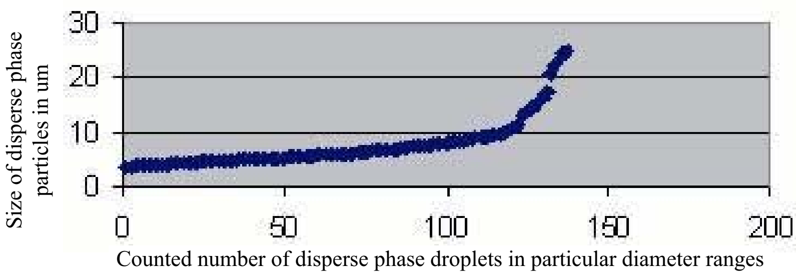

Fig.6 . Number of disperse phase particles in emulsion containing 30% water 20 minutes after homogenization, determined on the basis of observed particles

The application of distance wires and springing push-buttons on cover glasses made it possible to observe emulsion of constant layer thickness, thin enough to obtain an image in transmitted light. Attempts to observe the sample on a plate with the cooling chamber with "distance wire" diameter of 0.05 mm did not yield proper results as the amount of light passing through the examined sample is not sufficient. Consequently, microscopic observation is not possible, nor are measurements of water droplet sizes in the emulsion. The research results have shown that recurrent results can be obtained by placing droplets of fuel-water emulsion on polycarbonate plates with a cooling chamber. Plates of the same design made of glass caused coagulation, thus the size of water droplets increased significantly when in contact with the base or cover glass. The phenomenon was observed as early as three minutes after placing the emulsion on the plate. It was sufficient to cool the chamber for microscopic observation with a stream of water at a constant temperature of 25^0C provided for by an ultrathermostat.

3. Examination of the water in fuel emulsion with the use of a MALVERN Mastersizer 2000 device

A more accurate distribution of the disperse phase droplet diameters in the produced emulsion was obtained by examining fuel-water emulsion based on residual fuel The research aimed at developing methods of measuring the distribution of water droplet size in an emulsion produced on the basis of residual fuel, considered as a supplementary measurement to microscopic observations. Droplet diameter measurements were performed in a MALVERN Mastersizer 2000 device operating on the principle of laser light diffraction measurements. As residual fuel is practically non-transparent (light can pass through a very thin fuel layer), and examinations using this device require the specimen obscuration ranging from 10 to 20%, measurements can be performed only when the fuel or emulsion is properly diluted in a special thinner.

Experience gained from previous research shows that the best thinner for this purpose is n-heptane. Residual fuels, apart from very different physical and chemical properties, also have varied optical properties. Therefore, for measurements to be carried out, it was necessary to dissolve residual fuel of the examined specimen to 0.4 ml in 1000 ml of n-heptane so that the required obscuration could be obtained. Any under fuel under examination has to have such a concentration that the initial obscuration reached by subsequent approximations does not exceed 11 -12%. The determination of water droplet size distribution in an emulsion is considered as a relative measurement in reference to residual fuel containing a large amount of asphaltene particles and solid and liquid contaminants in a size range from nanometers to about 100 μm. This leads to a conclusion that almost all water droplet diameters will fall into the same size range as ashaltene and contaminant particles. The Mastersize device is not capable of identifying which particles (or droplets) it has to deal with; whether these are spheres or irregular particles, whether they are transparent or perhaps absorb light completely; or what is the refraction coefficient of particles and that of the liquid. The device works according to a model of particle distribution assumed by the operator, in which the above parameters have to be strictly defined. So now the basic difficulty of the planned measurement can be seen: in n-heptane there will be both spherical particles (water) and irregular ones (the remaining particles), transparent and non-transparent and those with very different refraction coefficients. It was assumed that first diameter distribution measurement will be executed for a specimen of residual fuel, then another measurement of emulsion specimen containing the same amount of fuel as the reference sample. The difference in measurements should give the examined distribution of water droplet diameter in the emulsion. As water is the medium of our interest, not asphaltenes, both measurements should be performed for the water droplet model. The examinations brought unexpected results, that is diameter distributions divided into three groups of diameter sizes for both fuel and emulsion. This was most probably due to the fact that the computer treated asphaltene particles as water particles. An attempt to determine the difference in results in order to define the distribution of water particles gave no results, because the differences in the diagram were partly positive and partly negative. It was assumed that this explains the behaviour of water droplets in the emulsion which attract polar particles of resins and asphaltenes. Therefore, from the optical point of view a water droplet in the residual fuel-based emulsion should be treated as an asphaltene particle. The computer program of the measuring device makes it possible to calculate the results according to a new model without repeating the examination. Presented below are examples of the results obtained from files counted by Malvern2000 device.

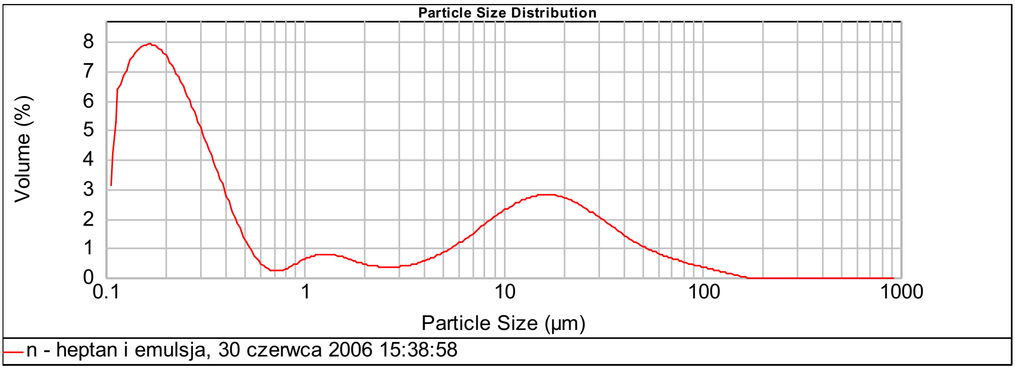

Fig. 7. Emulsion observed as water droplets

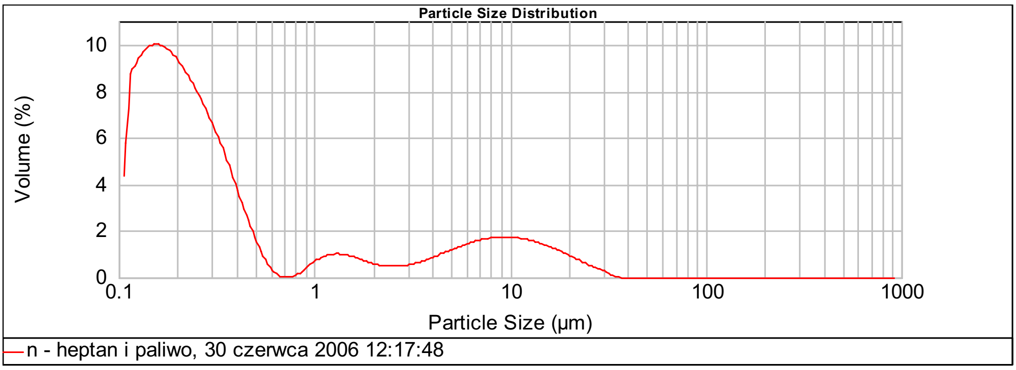

Fig. 8. The background fuel

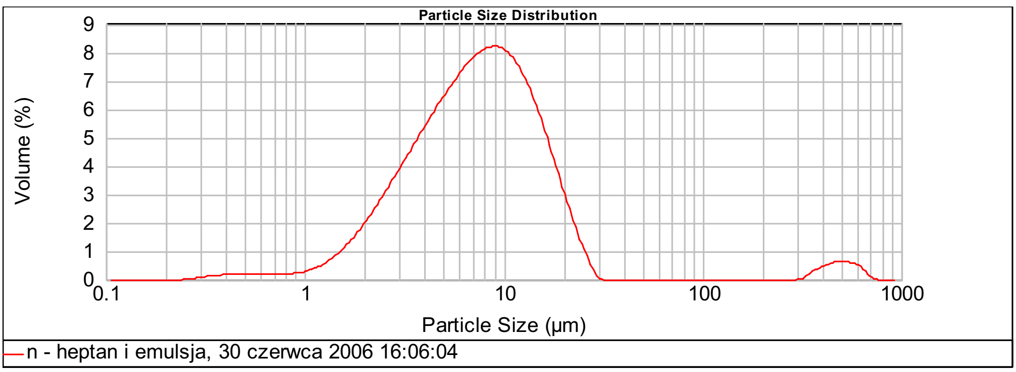

Fig.9. Emulsion observed as asphaltenes after taking away the background

The distribution for residual fuel is a model one, whilst that for the emulsion is somewhat ‘too small’. The reason for this was the presence of various particles in the solution that were not additive in the measuring device program. The use of base fuel solution as the background turned out to solve the problem. The above methodology of measuring the emulsion of water in residual fuel should be verified by microscopic examination. However, it should be done for the value of refraction coefficient for water droplets covered with resins and asphaltenes and for their value of light absorption coefficient, not for the procedures developed. The values of the coefficients used during the examinations described are only approximate, but very probable.

4. Conclusion

The executed tests resulted in a method allowing to obtain reliable information on the refinement of the disperse phase (water droplets) in fuel-water emulsions and the distribution of water droplet size in the emulsion, which allows to observe and record changes in emulsions to be used in the research. In this way the comparative analysis for various types of emulsion will be burdened with smaller errors.

References

[1] Kozak,E., Piotrowski,L., Hulanicki, S., *Emulsje paliwowo-wodne- jako paliwa zastępcze,* Materiały na IV Sympozjum Paliw Płynnych i Produktów Smarnych w Gospodarce Morskiej, Kołobrzeg 14-16 XII 1983.

[2] Piotrowski, I., Witkowski, K., *Okrętowe silniki spalinowe,* Wydanie IIIa, poprawione i uzupełnione, TRADEMAR Gdynia 1996- 2003.

[3] Wiewióra, A., Zapaśnik, T., *Celowość zastosowania emulsji paliwowo– wodnych do zasilania kotłów FAKOP- 0080,* Wyższa Szkoła Morska w Szczecinie. Szczecin 1986.

[4] Rajewski, P., Klaus, O., *Utilization of petroleum based residues on modern marine power plant,* PROBLEMS OF MECHANICS, International scientific journal No4(25)/2006, 73-78, Tbilisi 2006.

MAKING USE OF STARTING THE ENGINE TO DETERMINE THE MOMENT OF INERTIA OF A SHIP PROPULSION SYSTEM

Jan Rosłanowski, PhD in Engineering

Maritime Academy in Gdynia
Faculty of Marine Engineering
Department of Marine Materials and Repair Technology
Morska St. 81-87, 81-225 Gdynia
e-mail: rosa@am.gdynia.pl

Abstract

The article presents the method of determining the moment of inertia of a ship propulsion system while starting the engine which is based on torque and rotational speed measurements . The ship propulsion system in which the measurements were taken consisted of a slow – speed propulsion engine , shafting and fixed pitch propeller . The measurements mentioned above allow determination of a dynamics equation of a ship propulsion system which served the basis for determination of the moment of inertia . The specified method of defining the moment of inertia of a propulsion system is applicable to measurements in transient motion of the engine . This method is distinguished by simplicity of calculations and possibility of defining the moment of inertia of a propeller together with the water accompanying and requires taking measurements in transient motion of a ship .

1. Introduction

The course of starting torque of a ship propulsion engine recorded in time by means of a torque meter on a shaft can be used to determine dynamics of a propulsion system. Starting of the engine occurs after the crankshaft attains starting velocity. This requires supply of sufficient amount of energy via running gear from outer sources which will balance resistance losses of a starting process . For starting ship propulsion engines a pneumatic running gear is commonly used. In these devices air compression is used as a source of energy which while acting directly on a piston produces torque turning the crankshaft of the engine, so-called a starting torque equal to the anti-torque sum. A starting torque of the engine should attain acceleration and crankshaft velocity high enough to ensure the temperature in the cylinder capable to cause fuel self-ignition. In order to provide appropriate conditions for starting the engine, starting air is delivered to the cylinders in which the pistons are in starting position. Starting air admission lasts approximately 90 ÷ 100 º (degrees of crankshaft revolution) from 1 ÷ 100 º (degrees of crankshaft revolution) after TDC to 90 ÷ 100 º (degrees of crankshaft revolution) after TDC at power stroke [3;4].

2. The course of starting a ship propulsion engine

The course of starting process of a two–stroke slow-slow speed propulsion engine which drives directly a fixed pitch propeller at re-steering ahead is shown in fig. 1 and astern is shown in fig. 2.

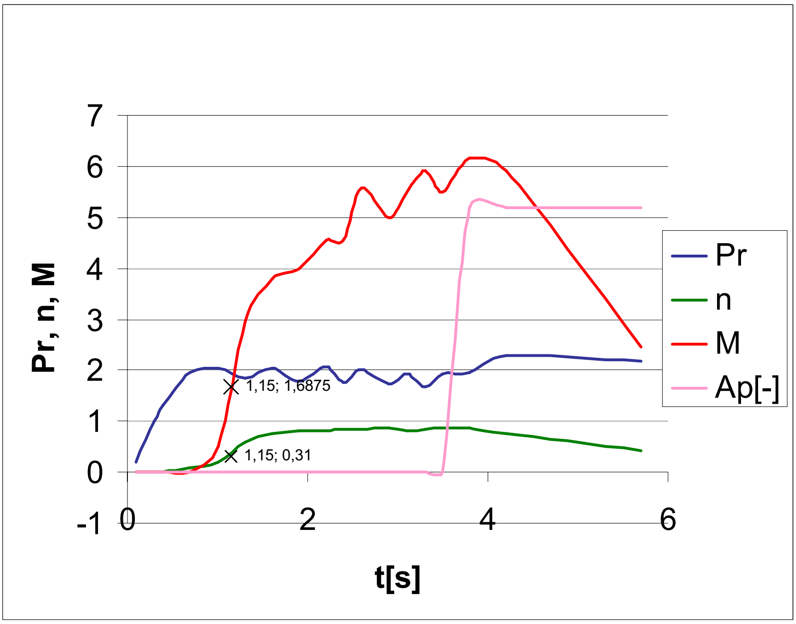

Fig. 1. The ahead course of starting a ship propulsion engine

Explanation:- Pr – pressure of starting air in [MPa], n – engine speed in [1/s], M – turning moment in [10^4Nm] Ap – setting fuel in [-]

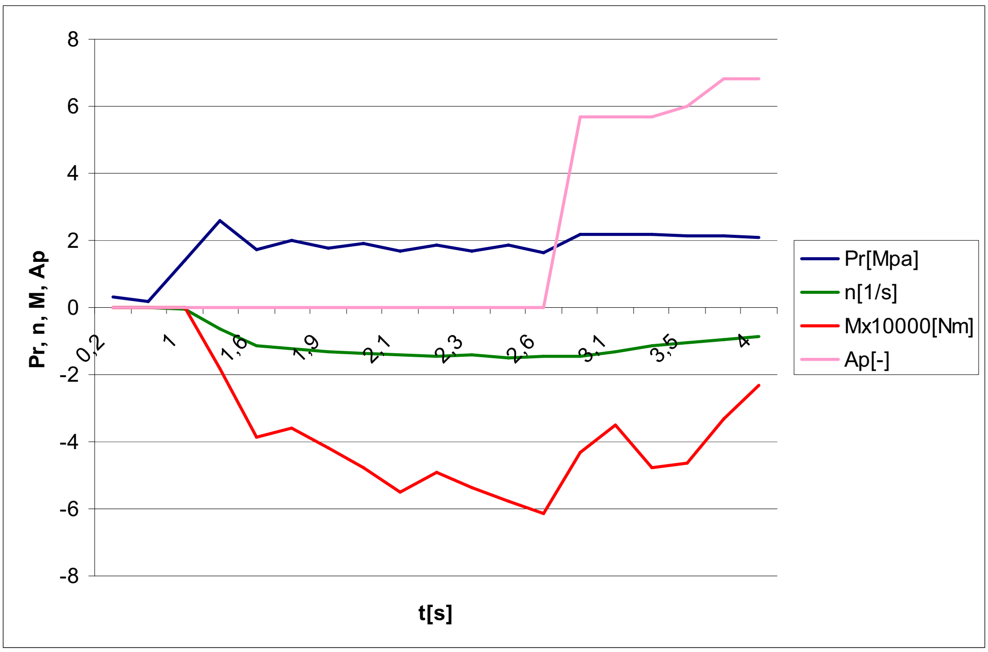

Fig. 2. The astern course of starting a ship propulsion engine

Explanation:- Pr – pressure of starting air in [MPa], n – engine speed in [1/s], M – turning moment in [10^4Nm], Ap – setting fuel in [-]

The process is as follows:- After directing the starting air onto the engine the pressure increases in pipelines which deliver the air to the starting valves. The steering air directed adequately by an air distributor opens the starting valves on the cylinders in which the pistons are in starting position. Compressed air while moving the cylinder expands by approx. 0.03 MPa at the first stage of starting and by approx. 0.02 MPa at the final stage of a starting process. When the piston is approaching BDC a starting air distributor makes a starting valve close. Speeding air stream is rapidly stopped and its kinetic energy is converted to potential energy of the pressure. As a result of such a starting process the diagram of a pressure course in time Pr(t) obtains characteristic sawtooth shape (fig. 1). The number of peaks in the diagram indicates how many starting valves opened at the time of starting. The diagram allows as well the readout of the time of starting air valve opening . This time will be a rotational speed function of a crankshaft. At the beginning of starting when a rotational speed is rather low it amounts to approx. 0.2 ÷ 0.25 sec. When rotational speed of a crankshaft reaches the value of starting speed a starting air admission to the engine closes . The diagram shows clearly almost immediate increase in pressure by approx. 0.03 ÷ 0.04 MPa caused by converting kinematic energy of air stream to potential energy of pressure. In this case the increase in pressure is much higher than for one starting valve because the whole air stream is subject to stop. Simultaneously with the air inflow stop the fuel linkage is shifted to the position corresponding to a fuel starting dose. The way of starting the engine with compressed air and the quantity of a fuel ignition dose affect the course of pressure alteration in the cylinder beginning from the first ignitions until the engine steady running is attained . In general the starting fuel dose amounts to from 30 to 50 % of a nominal dose [2]. The time of starting air effect at the time of starting the engine came to 1.6 sec.

3. The method of determining the moment of inertia of a ship propulsion system based on starting the main engine

The moment of inertia should be big enough to cause such an angular acceleration of a crankshaft which during the first rotation sets its angular velocity conditioning self-ignition of the injected fuel and its stable burning at the further phase of starting [2;3].

This is expressed by the following equation:

$$M(t)=M_r=M_I+M_T+M_S \qquad \textbf{(1)}$$

where:-

$M_I = I \cdot \dfrac{d\omega}{dt}$ - the moment of inertia of moving mass of the engine , propeller shaft , propeller and the mass of the water whirling behind the propeller in [Nm] ;

I – polar moment of inertia of reduced masses on the axis of a crankshaft involved in rotating movement in [Nm s²] ;
- angular acceleration of a crankshaft at starting in [rad/s²];

$M_T = (0{,}01 + 0{,}02 \cdot \dfrac{n}{n_{nom}}) \cdot M_{nom}$ - the moment of friction forces of a propulsion system in [Nm];

n – engine speed in [1/s] ;
n_{nom} – nominal engine speed in [1/s] ;
M_{nom} – nominal moment of inertia of a propulsion engine in [Nm];

$M_S = k_M \cdot \rho \cdot D^5 \cdot n^2$ - hydrodynamic moment demanded by a propeller in [Nm] ;
k_M – non-dimensional coefficient of the moment in [-] ;

ρ – density of sea water in $\left[\frac{N \cdot s^2}{m^4}\right]$;

D – diameter of propeller circle field in [m] ;
n– rotational speed of a propeller in [1/s] ;
$M(t)=M_r$ – measured starting torque in [Nm] .

The equation (1) can be converted to the form:

$$I = \frac{M(t) - M_S - M_T}{2\Pi \cdot \frac{d\omega}{dt}} \tag{2}$$

where: -
- designations as in the formula (1)

The formula (2) makes sense only in transient states i.e. $\frac{d\omega}{dt}$ when is different from zero. This condition is met well in the state of starting the propulsion engine, where the rotational speed and the torque on the propeller shaft increase from zero up to big values in a short time. By measuring the courses of rotational speed and the torque on the propeller shaft at the time of starting the engine they can be defined mathematically in a time function. Their form is the likeliest to be found in the time function where the ship propulsion system is treated as an inertia object of the second order [1]. In this case the input signal is the starting air pressure and the output signals are the rotational speed and the torque on the propeller shaft. The response of such an object to a step function as it is starting the propulsion engine by means of air can be presented in the form:

$$y(t) = k \cdot \left(1 - \frac{1}{1-b} \cdot e^{\frac{-t}{T_1}} + \frac{b}{1-b} \cdot e^{\frac{-t}{b \cdot T_2}}\right) \tag{3}$$

where : -

y(t) - response of the object to a step function;
k - gain coefficient of the object signals;

$b = \frac{T_1}{T_2} > 1$ - coefficient defining the ratio of the two time constants T_1 and T_2;

T_1 , T_2 - time constants of the inertia object of the second order ;
t – the time of the signal occurrence in [s].

By registering the courses of the rotational speed and the torque on the shaft while starting the propulsion engine we can calculate all the components of the equation right side (2), thus calculate the moment of inertia I. The courses of the rotational speed and the torque on the propeller shaft at the initial moment of starting can be approximated by straight lines. Then in this time interval [t_1; t_2] the derivative $\frac{d\omega}{dt}$ can be replaced with the increase $\frac{\Delta\omega}{\Delta t}$; which simplifies considerably calculations of the proposed method. By choosing from this time interval the instant t_0 on the basis of the formula (2) we will receive:-

$$I = \frac{M(t_o) - M_S \cdot [n(t_o)] - M_T \cdot [n(t_o)]}{2\Pi \cdot \dfrac{n(t_2) - n(t_1)}{t_2 - t_1}} \qquad \textbf{(4)}$$

where:-

$t_1 < t_o < t_2$ - chosen time instant in [s];
- other designations as in the formula (2).

By substitution of the expressions defined in the equation (1) to the formula (4) we will receive the final form which allows the calculation of the moment of inertia of the part of the propulsion system from the place where measurements of the torque and the rotational speed were taken up to the propeller with the accompanying water .

$$I = \frac{M(t_O) - k_M \rho D^5 n^2(t_O) - \left[a + b \cdot \dfrac{n(t_O)}{n_n} \right] \cdot M_n}{2\Pi \cdot \dfrac{n(t_2) - n(t_1)}{t_2 - t_1}} \qquad \textbf{(5)}$$

where:-

- designations as in the formulas (1) and (2) .

All the values which appear in the equation (5) can be determined on the basis of a propulsion system documentation and the measurements taken on a ship. The coefficient of the moment k_m can be determined from the hydrodynamic characteristic of a propeller e.g. from Dankwardt diagrams when knowing the advance coefficient.

The specified method of determining the moment of inertia of a part of a ship propulsion system was illustrated on the example of a direct drive. A propulsion engine at nominal revolutions n_n = 135 rev/min = 2.25 rev/sec attained the torque of Mnom = 291800 [Nm]. It drove the propeller screw of a diameter D = 4.55 [m]. At starting the speed ship was low which allowed determination of a moment coefficient from the hydrodynamic characteristic equal to:-

$$k_M(I_p)=k_M(0)=0{,}0311$$

From the measurements of the courses of the rotational speed and the torque on the shaft at the initial instant t_O=1,15[s] of starting the following values were received:-

$M(t_O)$=16875[Nm]
$n(t_O)$=0,31[1/s]

the courses of these values at starting are shown in fig. (1). On the basis of numerical data according to the formula (5) the moment of inertia of the part of the propulsion system which was equal to:-

$$I = 8855{,}8 [Nms^2]$$

The value of the moment of inertia of an appointed part of the propulsion system was compared with the value of this part which was received on the basis of a documentation of torsional vibration calculations. Assuming 25 % of water fraction the moment of inertia in torsional vibration calculations was equal to:

$$I=8253{,}1 [Nms^2]$$

The comparison of the values above points to satisfying accuracy of the method proposed.

4. Summary

The more the values of the function derivative of the rotational speed after time $\left(\frac{d\omega}{dt}\right)$ will differ from zero, the more the moment of inertia of a propulsion system determined by the proposed method will be close to a real one.

The moment of inertia depends on the engine design and the way of the power transmission onto the screw i.e. the quantities of rotational masses and the instant angular acceleration of the crankshaft.

The proposed method of determining the moment of inertia has its advantages and drawbacks. The advantages are following: simple calculations and the possibility of determining the moment of inertia of a propeller together with the accompanying water. The drawbacks of the proposed method involve its restriction to existing propulsion systems and the necessity of taking measurements.

References

[1] Górniak, J., Bogdański, A., *Compression – Ignition and Gas Compressors Control*, WNT Warszawa 1972.

[2] Mysłowski, J., *Starting of Compression –Ignition Car Engines*, WNT Warszawa 1996.

[3] Piotrowski, I., Witkowski, K., *Exploitation of Marine Combustion Engines*, Gdynia Maritime University Publ. 2002.

[4] Włodarski, J.K., *Operatinal states of Marine Combustion Engines*, Gdynia Maritime University 1998.

IDENTIFICATION OF MODELS FOR MULTICRITERIAL OPTIMIZATION OF SAILING VESSEL DRIVING SYSTEMS

Krzysztof Rudzki, Wiesław Tarełko

Gdynia Maritime University
ul. Morska 81-83, 81-225 Gdynia, Poland
tel.: +48 58 6109451, fax: +48 58 3472430
e-mail: rudz@am.gdynia.pl, tar@am.gdynia.pl

Abstract

This paper deals with models of driving system of sailing vessels developed by applying methods of regression analysis and artificial neural networks. In particularly, a general form, identification process, and comparison of these models are presented.

Keywords: *driving system, sailing vessel, optimization, fuel consumption*

1. Introduction

In 1902, the largest, fastest sailing ship the world had ever seen was launched. The legendary Preussen dominated the seas, only to be gone in a few short years. Neither before nor since has the world seen such a magnificent sailing ship. Until today... Inspired by the legendary Tall Ship, Preussen, the new Royal Clipper has the proud distinction of being the largest and only five-masted sailing ship built since her predecessor was launched at the ending of the last century. With her complement of 42 sails, Royal Clipper is a splendid sight to behold. You might think she was an apparition from the grand age of sail, but Royal Clipper is as new as tomorrow. She boasts state-of-the-art navigation systems and all the comforts of today.

We can observe the tendency of increasing such a type of grandiose vessels year after year. In order to assure the passengers' safety, the sailing vessels have to be equipped with engines enabling sailing in any wind conditions. As a rule, such vessels are equipped with adjustable propellers. In order to assure the operating effectiveness, the sailing vessels have to have the reasonable operating costs. But most important factors influencing these costs are expenses connected with engine fuel consumption. We can state that this consumption depends mainly on the following factors:

- the sailing conditions,
- the adjustable propeller speed and pitch.

The first group of factors is out of our control, whereas the adjustable propeller speed and pitch can be controlled by the ship operator. In order to control the engine fuel consumption, we should build an appropriate optimization model enabling selection of optimal settings of the adjustable propeller speed and pitch for various sailing conditions. This, in turn, requires to develop models combining the operating effectiveness of sailing vessels with the mentioned parameters.

In the subject bibliography, for example in [1], [2], [3], [4] and [5], we can find many models of driving system developed for the trade vessels. These models combine the vessel effectiveness with the engine rotation speed and propeller pitch. To combine all factors influencing the vessel effectiveness, methods of regression analysis are applied in these models. As a rule, relations

applied in these models have the form of nonlinear multiple regressions determined for only for three sailing conditions: light, variable and heavy.
In the case of sailing vessels, such an approach is unsatisfactory due to their sensitivity to changes of sailing conditions. It results from the following factors:

- as a rule, sailing vessel engines are auxiliary having a low margin of power,
- tall masts and rigs cause for increasing of air resistance which, in turn, depends on strength and direction of wind,
- hull shapes are sensitive to sea wave influences,
- sometimes a sea navigation is supported by sails.

Due to these factors, applying of classical methods for modeling of the sailing vessel driving system could not provide the expected effects. Therefore, we should develop models, which will take additionally into account:

- the changeability of sailing conditions in a wider range,
- the possibility of a sea navigation supported by sails.

Such models will be applied in the computer-aided system supporting the sailing vessel operator in a decision-making process concerning selection of the most suitable sailing parameters.
This paper deals with some issues connected with identification of models, which could be used for the optimization purpose of sailing vessel driving systems.

2. Concept of optimization model

In the sea navigation of sailing vessels can appear the variety of navigation situations depending on: sea and weather conditions, a time designated to reach the desired target, etc. In generally we could specify the following situations:

- sailing with the maximum speed in order to be just in time in the planned navigational point,
- sailing with the minimum fuel consumption in order to save the operating expenses,
- fast and cheap sailing to the planned navigational point.

In the last situation, we should find the compromise solutions. In order to do it, we should develop a method allowing for the optimal setting up of driving system parameters that is the propeller rotation speed and pitch. These settings, in turn, should assure the desirable values of parameters determining the cheapness and quickness of sailing to the planned navigational point.
Such a method can be developed based on the multicriterial optimization model of sailing vessel driving systems. It, in turn, requires to solve a few partial tasks as follows:

- formulation of the multicriterial optimization objective function together with determining its partial (criteria) functions and constraints,
- choose of the dependent and independent variables of the partial functions,
- selection of the method for identification of models setting up the partial functions,
- development of optimization algorithm (including selection of a method for finding of compromise solutions and computer representation).

In our approach, we have taken into account the following form of the multicriterial optimization objective function:

$$F_{obj} = w_1 \cdot F_{c1} + w_2 \cdot F_{c2} \ , \tag{1}$$

where:

F_{obj} - an objective function of the multicriterial optimization,

w_i - weights determining of the partial function importance; ($w_1 + w_2 = 1$),

F_{ci} - partial (criteria) functions of the multicriterial optimization.

As the partial functions, which should characterize the sailing cheapness and quickness, we have taken in mind relations combining the propeller rotation speed and pitch, and the sailing conditions with the both the engine fuel consumption or the vessel speed. In general description, we can express these functions as follows:

$$B = f(n_p, h_p, X_{sc}), \tag{2}$$

and

$$v = f(n_p, h_p, X_{sc}), \tag{3}$$

where:

B - an engine fuel consumption,
v - a vessel speed,
n_p - a propeller rotation speed,
h_p - a propeller pitch,
X_{sc} - sailing conditions.

A schematic diagram presenting of application of such relations in the optimization model is shown in Figure 1. In this Figure, the partial functions used to the optimization are distinguished by thick lines.

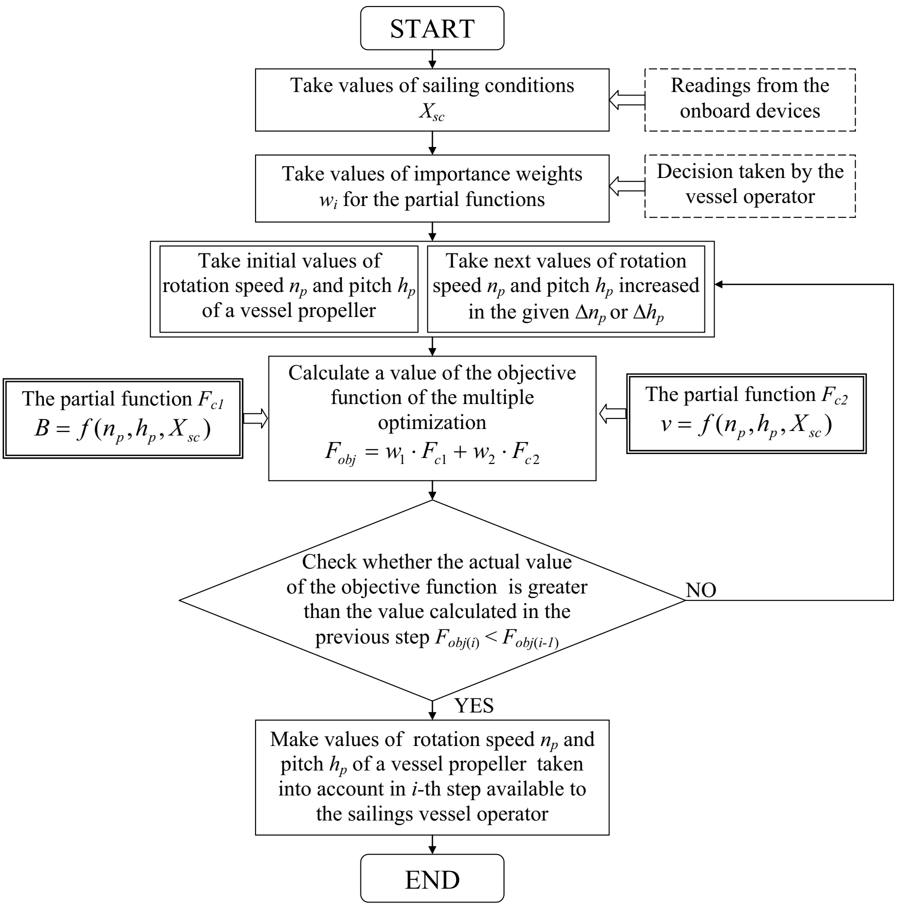

Fig. 1. The simplified schematic diagram of the optimization algorithm

In the further parts of this paper, we consider only modeling issues, which could assist in determining of the distinguished functions.

3. Modeling of driving system

3.1. General form of models

From a mathematical point of view, determination of these relations combining the propeller rotation speed and pitch, and navigational conditions with the engine fuel consumption or the vessel speed is a problem of approximation of multiple functions. This problem we can formulate as follows: for a given set of multiple function values $X_i = [x_1, x_2, ..., x_n]$ and their corresponding value y_i, where $i = 1, 2, ..., m$, we should determine a function combining a variable y called the dependent variable (a model output) and a vector of variables X called the independent variables (model inputs):

$$y = f(X) + \varepsilon \tag{4}$$

where:

y - a dependent variable,
X - independent variables,
ε - a value of an error term.

In the developed models, as dependent variables Y we selected parameters of determining the sailing cheapness and quickness that is the engine fuel consumption and the vessel speed respectively.
The independent variables X in these models are:

- factors characterizing sailing conditions (the wind direction and strength, state of the sea, etc.),
- parameters determining a work of sailing vessel driving system (the engine rotation speed and the propeller pitch).

The last parameters set up the decision-making variables being in disposal of the sailing vessel operator.
Disturbances ε of a model are caused by many factors for example: rig arrangements in relation to a wind direction, sea wave frequencies, mistakes made during readings from measurement devices, etc.
A schematic diagram of these models is presented in Figure 2.

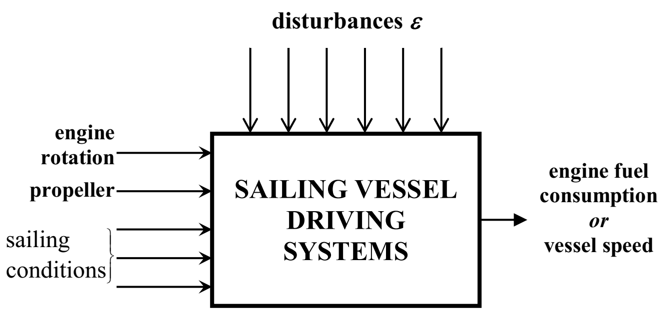

Fig. 2. A schematic diagram of sailing vessel driving system

3.2. Model variables and their acquisition

In the developed models, we have taken into account only such factors which could be read, estimated or calculated by vessel operators (a master or officers in watch) without any problems by readings their values from the onboard measuring devices.

As dependent variables, we select criteria which determining the sailing cheapness and quickness (spending of material and time resources) and can be used in the developed optimization model, namely:

- a specific fuel consumption B [dm^3/min], calculated as difference between indications of fuel gauges installed in the engine inlet and the outlet from injectors,
- a vessel speed v [knots], reading form the GPS receiver.

As the independent decision-making variables which can be controlled by a master or officers in watch, we take into account the following factors:

- an engine rotation speed n [rpm] , reading form the engine tachometer,
- settings of a propeller pitch H [scale intervals] reading form a scale of the propeller pitch lever.

The remaining independent variables are factors characterizing sailing conditions as follows:

- a wind speed v_w [m/s], reading from the anemometer,
- a wind direction K_w [^{o}], reading from the anemometer,
- a state of the sea s_m, [degree], carried out by the indirect estimation according to the Beaufort's scale,
- a tide speed v_p [m/s], calculated on a base of nautical charts and annual tide tables,
- a tide direction K_p [^{o}], calculated on a base of the nautical charts and annual tide tables,
- a vessel compass course KK [^{o}], reading from the magnetic compass,
- a vessel true course (with respect to the sea bottom) KDD [^{o}], reading form the GPS receiver.

In order to collect the appropriate set of data enabling to develop our models we carried out the special experiment on board of the sailing vessel 'POGORIA' during her regular voyages. Our observations were completed in various weather conditions, on variety geographical regions, and for different engine rotation speeds and settings of a propeller pitch. We obtained more than 800 observations, where about 50 percent of them concerned voyages without supporting of sails.

During our experiment we assumed that:

- voyages are realized with stable courses according to the smallest way to the intended point,
- wind and tide directions are orientated perpendicularly to the vessel symmetry axis (it takes into consideration increasing or decreasing dependent variables according to changes of the wind and tide directions - 0^0 perpendicularly to vessel boards, 90^0 from a bow, and -90^0 from a stern).

To solve the identification task for the considered models, we applied methods of regression analysis and artificial neural networks. For a testing purpose of neural networks we separated 37 observations (about 10% data) from the data set.

4. Identification of models

4.1. Regression models

To receive equations of regression models, we have applied methods of:

- the multiple linear regression in the form:

$$\hat{y} = a_0 + a_1 \cdot n + a_2 \cdot H + a_3 \cdot v_w + a_4 \cdot K_w + a_5 \cdot s_m + a_6 \cdot v_p + a_7 \cdot K_p \,, \tag{5}$$

- the multiple regression in the quadratic polynomial form:

$$\hat{y} = b_0 + b_1 \cdot n + b_2 \cdot n^2 + b_3 \cdot H + b_4 \cdot H^2 + b_5 \cdot v_w^2 + b_6 \cdot K_w + b_7 \cdot s_m + b_8 \cdot v_p + b_9 \cdot K_p , \quad (6)$$

– the multiple regression in the quadratic polynomial form limited to the decision-making variables:

$$\hat{y} = c_0 + c_1 \cdot n + c_2 \cdot n^2 + c_3 \cdot H + c_4 \cdot H^2 + c_5 \cdot n \cdot H , \quad (7)$$

The form of the multiple nonlinear regressions we have considered on a base of existing solutions, which can be found in the domain bibliography. All calculations we carried out by using the appropriate modules of STATISTICA programs.
Equations of multiple linear regressions combining the specific fuel consumption B and vessel speed v with the independent variables taken into account received the forms respectively:

$$\begin{aligned}\hat{B} = &-(7{,}43\mathrm{E}+01) + (5{,}67\mathrm{E}-02) \cdot n + (1{,}86\mathrm{E}+00) \cdot H + (1{,}24\mathrm{E}-01) \cdot v_w + (3{,}05\mathrm{E}-02) \cdot K_w + \\ &+ (2{,}21\mathrm{E}+00) \cdot s_m - (4{,}04\mathrm{E}+00) \cdot v_p + (6{,}45\mathrm{E}-02) \cdot K_p\end{aligned} \quad (8)$$

and

$$\begin{aligned}\hat{v} = &(2{,}62\mathrm{E}-01) + (2{,}48\mathrm{E}-03) \cdot n + (2{,}74\mathrm{E}-01) \cdot H - (3{,}67\mathrm{E}-02) \cdot v_w + (2{,}33\mathrm{E}-03) \cdot K_w + \\ &- (4{,}23\mathrm{E}-01) \cdot s_m - (3{,}99\mathrm{E}-01) \cdot v_p - (1{,}47\mathrm{E}-02) \cdot K_p\end{aligned} \quad (9)$$

For the presented models, we obtained values for the multiple determination coefficient R^2 equal 0,751 and 0,442 accordingly. It means that only 44% of the dependent variable variability is 'explained' by the multiple regression equation in the second model.
In a case of the multiple nonlinear regressions, their equations received the forms respectively:

$$\begin{aligned}\hat{B} = &(1{,}53\mathrm{E}+02) - (2{,}25\mathrm{E}-01) \cdot n + (1{,}09\mathrm{E}-04) \cdot n^2 - (5{,}32\mathrm{E}+00) \cdot H + (2{,}76\mathrm{E}-01) \cdot H^2 + \\ &+ (5{,}63\mathrm{E}-03) \cdot {v_w}^2 + (3{,}15\mathrm{E}-02) \cdot K_w + (2{,}41\mathrm{E}+00) \cdot s_m - (4{,}00\mathrm{E}+00) \cdot v_p + 5(,41\mathrm{E}-02) \cdot K_p\end{aligned} \quad (10)$$

and

$$\begin{aligned}\hat{v} = &-(7{,}47\mathrm{E}+00) + (1{,}44\mathrm{E}-02) \cdot n - (4{,}52\mathrm{E}-06) \cdot n^2 + (2{,}26\mathrm{E}-01) \cdot H + (1{,}71\mathrm{E}-03) \cdot H^2 + \\ &- (1{,}41\mathrm{E}-03) \cdot {v_w}^2 + (3{,}33\mathrm{E}-03) \cdot K_w - (3{,}65\mathrm{E}-01) \cdot s_m - (4{,}32\mathrm{E}-01) \cdot v_p - (1{,}43\mathrm{E}-02) \cdot K_p\end{aligned} \quad (11)$$

For these models, we obtained values of the multiple determination coefficient R^2 equal 0,813 and 0,443 accordingly. It means that only 44% of this dependent variable variability is 'explained' by the multiple nonlinear regression equation in the second model.
In order to check the legitimacy of our assumption taking in mind the sailing conditions, we carried out calculations for the multiple regression limited only to the decision-making variables because of its using in the classical approach presented in [[3]], [[4]] and [[5]]. We received the following equations respectively:

$$\begin{aligned}\hat{B} = &(1{,}26\mathrm{E}+02) - (1{,}16\mathrm{E}-01) \cdot n + (1{,}00\mathrm{E}-04) \cdot n^2 - (6{,}92\mathrm{E}+00) \cdot H + \\ &+ (5{,}83\mathrm{E}-01) \cdot H^2 + +(5{,}90\mathrm{E}-03) \cdot H \cdot n\end{aligned} \quad (12)$$

and

$$\begin{aligned}\hat{v} = &-(3{,}35\mathrm{E}+00) + (2{,}07\mathrm{E}-02) \cdot n - (1{,}00\mathrm{E}-06) \cdot n^2 - (9{,}11\mathrm{E}-01) \cdot H + \\ &+ (2{,}21\mathrm{E}-03) \cdot H^2 + 4{,}70\mathrm{E}-04 \cdot H \cdot n\end{aligned} \quad (13)$$

In these cases, we obtained values of the multiple determination coefficient R^2 equal 0,651 and 0,203 accordingly. Such low values of this coefficient confirmed the legitimacy of our assumption taking the sailing conditions into consideration.

Nevertheless, analysis of values of the multiple determination coefficient R^2 calculated for the best forms of multiple regressions shows that the models based on such methods are not suitable for the considered optimization purpose due to not enough explanation of the dependent variable variability.

4.2. Neural network models

To develop neural network models, we applied two independent nets. They represented the same dependences like in a case of regression models. In both models, we used a neural network structure including two hidden layers (Fig. 3). The output layer has one neuron representing a model output (the vessel speed *v* or the specific fuel consumption *B*), whereas the input layer has seven neurons representing model inputs (all independent variables introduced in order). During a teaching process of the neural networks we changed a number of neurons comprised in the hidden layer and their activation function in order to obtain more desirable results.

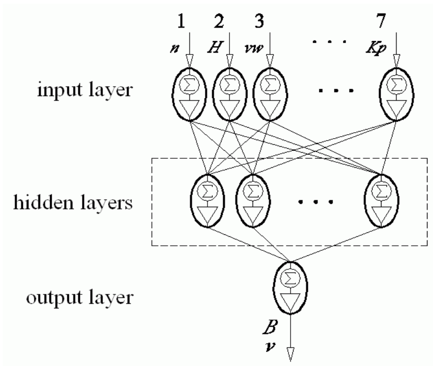

Fig. 3. Two-layer neural network

Values of a teaching set subjected to linear normalization in a range from 0,1 to 0,9. In this teaching process, we applied the backpropagation method. All calculations have been carried out by using the appropriate modules of MATLAB programs.

As it was mentioned, from the data set we separated 37 observations (about 10% data) for a testing purpose of neural networks. The highest differences between values obtained from both the testing set and the primary set were equal 15 % for the specific fuel consumption *B* and 11% for the vessel speed *v* respectively**.** Comparison of both networks is presented in Figure 4.

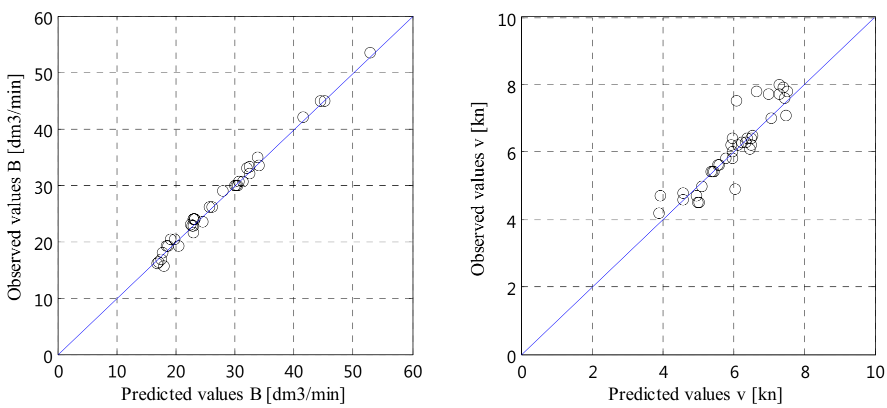

Fig. 4. Comparison of the primary and testing networks

5. Comparison of models and conclusion

In the first step we try to assess differences expressed as percentage between the observed and estimated values of the dependent variable. The estimated values of specific fuel consumption *B* outnumbered the observed values more than 10% in 22 cases for the multiple linear regression and 21 cases for the multiple nonlinear regression. We obtained the same results for the second model where the dependent variable is a vessel speed *v*. In a case of neural network models, we noticed that the estimated values outnumbered the observed values more than 10% in 2 cases for the first model and 7 cases for the second one. Analysis of these results allowed us to state that the greatest differences appeared in atypical operating situations, for example in heavy wind conditions with large settings of a propeller pitch.

In the second step we carried out comparison of the considered model by using index estimating of variances between the observed and estimated values of the dependent variable frequently termed as the standard error of estimate [6]:

$$\hat{\sigma}_\varepsilon = \sqrt{\frac{\sum (y_i - \hat{y}_i)^2}{n-2}} \ , \tag{14}$$

where:

$\hat{\sigma}_\varepsilon$ - the standard error of estimate,

y_i - the observed value of the dependent variable,

$\hat{y}_i$ - the estimated value of the dependent variable,

n - a number of observations.

The standard error of estimate allows to compare all used methods because of its universality. Results of such comparison are presented in Table 1.

Tab. 1. The standard error of estimated models.

Method	Specific fuel consumption B_h [dm^3/min]	Vessel speed v [knots]
Multiple linear regression	15,00	1,39
Multiple nonlinear regression	14,74	1,38
Multiple nonlinear regression limited to decision-making variables	23,78	1,20
Neural networks	1,08	0,74

Analysis of Table 1 shows that the most suitable models of the sailing vessel driving system are models based on neural networks. However, these models can not be presented in the analytical forms, even so they will be taken into consideration in the future optimization procedure enabling selection of optimal settings of sailing vessel operating parameters for various sailing conditions.

References

[1] Górski, Z., *Metody doboru nastaw elementów głównego układu napędowego statków ze śrubą nastawną w aspekcie efektywności eksploatacji siłowni*, Praca doktorska, Akademia Morska w Gdyni, 2003.

[2] Chachulski, K., *Numeryczna metoda doboru optymalnych nastaw silnika spalinowego w okrętowym układzie napędowym*, Dział Wydawnictw WSM Szczecin, 1987.

[3] Chachulski, K., *Podstawy napędu okrętowego,* Wydawnictwo Morskie, Gdańsk 1988.
[4] Brandowski, A., *Wyznaczanie optymalnych parametrów pracy okrętowego układu napędowego ze śrubą nastawną i silnikiem spalinowym wysokoprężnym za pomocą metod numerycznych*, Praca doktorska, Politechnika Gdańska, Wydział Budowy Okrętów, Gdańsk 1967.
[5] Cwilewicz, R, Sroka, K., *The problem of fuel minimization during the crossing of a ship between two ports,* Scien.J. of Merchant Marine Academy Gdynia 1990, 3, s. 52-64.
[6] Van Matre, J.G., Gillbreath, G.H., *Statistics for Business and Economics,* 3rd Ed. BPI. Homewood. 1997.

TESTING THE RESISTANCE OF PISTON ENGINE OILS AGAINST MECHANICAL DEGRADATION

Ph. D. Eng. Jarosław Sarnecki

Ph. D. Eng. Jerzy Zieliński

Air Force Institute of Technology, Warsaw, Poland

1. Introduction

Piston engine oils contain viscosity improvers, often called viscosity modifiers, that include polymer compounds improving viscosity-temperature characteristics of oils. Oil-soluble polymers with high molecular weight are commonly used as viscosity modifiers.

Long polymer chains of viscosity improvers during lubrication of kinematic pairs (i.e. piston-cylinder) or high velocity flow through gaps (pumps, oil tubings and hoses) are machanically degraded (polymer chains are teared), which results in drop of kinematic viscosity.

Rhelogical properties (viscosity parameters) for engine oils are presented in Table 1.

Table 1 Engine oils viscosity classification (SAE J 300)

SAE viscosity grade	Low temperature viscosity (starting) - mPas, in temperature, ^{0}C max.	Low temperature viscosity - pumping, mPas, in temperature, ^{0}C max.	Kinematic viscosity in temperature 100^{0}C, mm^2/s		HT/HS viscosity w temperature 150^{0}C, mPas, min.
			min.	max.	
0W	6200 in -35	60000 in -40	3.8	-	-
5W	6600 in -30	60000 in -35	3.8	-	-
10W	7000 in -25	60000 in -30	4.1	-	-
15W	7000 in -20	60000 in -25	5.6	-	-
20W	9500 in -15	60000 in -20	5.6	-	-
25W	13000 in -10	60000 in -15	9.3	-	-
20	-	-	5.6	<9.3	2.6
30	-	-	9.3	<12.5	2.9
40	-	-	12.5	<16.3	2.9 (for 0W-40, 5W-40 and 10W-40)
40	-	-	12.5	<16.3	3.7 (for 15W-40, 20W-40, 25W-40 and 40)
50	-	-	16.3	<21.9	3.7
60	-	-	21.9	<26.1	3.7

It is assumed, that engine oil kinematic viscosity change as a result of mechanical degradation can not lead to change of oil viscosity grade according to SAE J 300, i.e. SAE 40 engine oil viscosity in 100^{0}C after polymer additive shear should be not less than 12.5 mm^2/s.

2. Research methodology

Following three methods are commonly used to evaluate mechanical degradation of oils:

- testing with „pump-injector" rig (method applied in research described below);
- testing with „pump-gap" rig (method commonly used in the United States);
- testing with ultrasonic apparatus (method cancelled, used for jet engines oils).

Dla olejów silnikowych w badaniu z wykorzystaniem aparatu „pompa wtryskiwacz" (patrz fot. 1) wykonuje się 30 cykli ścinania a następnie wykonuje się badanie lepkości kinematycznej w temperaturze 100^0C (patrz fot. 2).

For engine oils, during pump-injector rig test (fig. 1) 30 shear cycles must be carried out, and then kinematic viscosity in 100°C is measured.

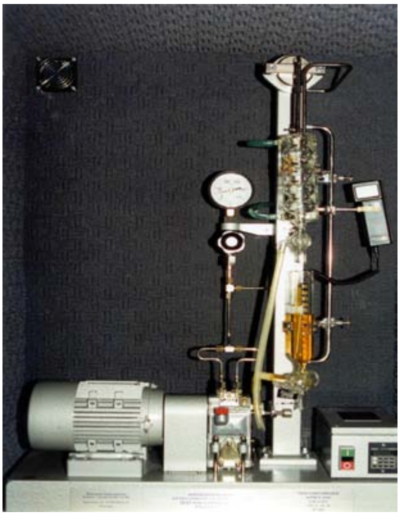

Fot. 1 Pump-injector rig

Fot. 2 Baths for kinematic viscosity measurements

3. Tests performed

Most of engine oils resistance against mechanical degradation testing results are positive – oil viscosity grade is not changing after 30 shear cycles. Although in case of more shear cycles applied on-going mechanical degradation is observed – oil viscosity is decreasing.

During testing of various oils, the resistance against mechanical degradation was evaluated with „pump-injector" rig, with up to 250 shear cycles, and kinematic viscosity measurements were carried out after specific number of shear cycles. Tests results are presented in Table 2.

Table 2. Tests results for different oils

Oil name/ID	Kinematic viscosity in 100^oC, mm^2/s. After specific number of shear cycles						
	0	30	50	100	150	200	250
Mineral oil SAE 50	18,0	17,6	17,5	17,5	17,4	17,4	17,4
Mineral oil SAE 20W-50	16,6	15,3	14,4	13,8	13,4	13,4	13,3
Mineral oil SAE 15W-40	14,0	12,5	12,0	11,9	11,7	11,7	11,6
Semi-syntetic oil SAE 10W-40	14,6	12,8	12,6	12,5	12,1	12,0	11,9
Syntetic oil SAE 5W-40	13,4	13,3	13,3	13,2	13,2	13,2	13,2
Syntetic oil SAE 0W-40	12,7	12,5	12,5	12,4	12,2	12,2	12,2

Obtained results are presented graphically on Fig. 1 and 2. For SAE 50 oil with no viscosity improver positive result was obtained, but for multi-season oil SAE 20W-50 viscosity after 250 shear cycles was below limit in SAE J 300 classification. Similar results were obtained for majority of SAE 40 oils.

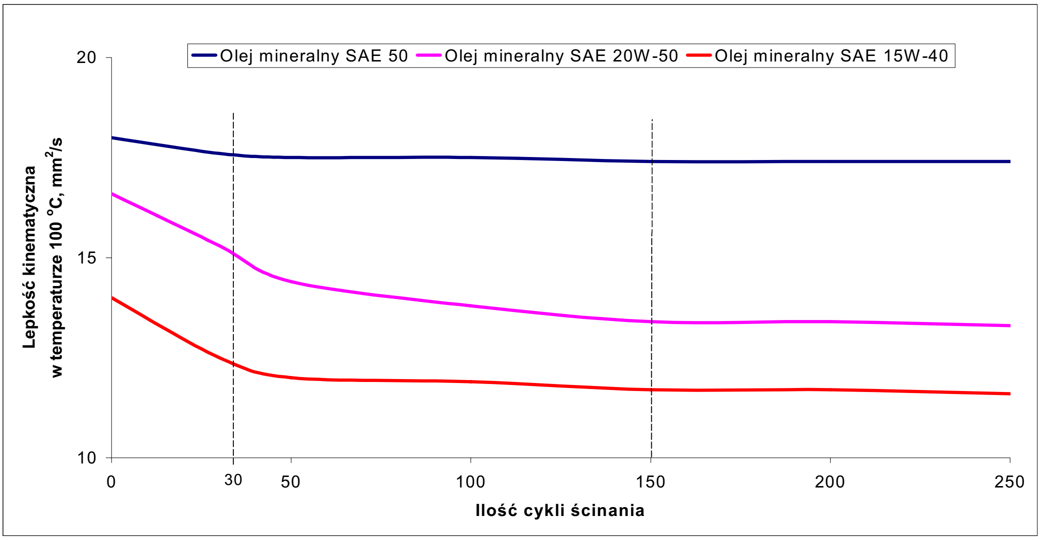

Fig. 1. Shear resistance for selected mineral oils used in piston engines

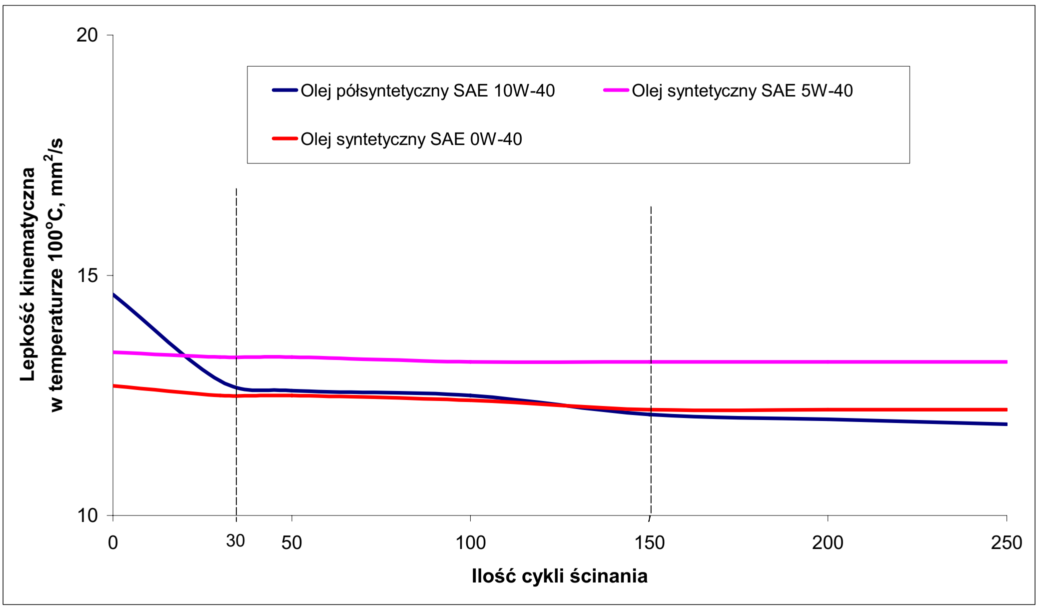

Fig. 2. Shear resistance for selected semi-syntetic and syntetic oils used in piston engines

4. Summary

Obtained results are the basis for consideration of possible changes to methodology of piston engine oils mechanical degradation resistance testing and implementation of i.e. 150 shear cycles.

Presented methodology may be also used during preparation of new technologies for engine oils (removing of unstable viscosity improvers) and for quality verification for piston engine oils.

Literature

[1] Briant, J., Denis, J., Parc, G., *Rheological Properties of Lubricants*, Institut Francais du Petrole, Edition Technip 1989.

[2] Zieliński, J., *Modyfikacja właściwości reologicznych olejów do silników tłokowych*, Rozprawa doktorska, ITWL 2002.

[3] Wilkowski, W., Łagowska, K., Kolczyński J., *Badanie odporności na degradację mechaniczną olejów do silników wojskowych pojazdów mechanicznych*, SILWOJ 2001.

[4] SAE Fuels & Lubricants Standard Manual, HS-23 Edition 2004

THE MEASUREMENT OF LOSSES GENERATED IN KINEMATIC NODES OF ENGINE RUN AT TEST STAND

Wojciech Serdecki

Institute of Combustion Engines and Transport
Poznań University of Technology
3, Piotrowo St., 60-965 Poznań
tel.+48 665 2243, fax: +48 6652204
e-mail: wojciech.serdecki@put.poznan.pl

Piotr Krzymień

Institute of Combustion Engines and Transport
Poznań University of Technology
3, Piotrowo St., 60-965 Poznań
tel.+48665 2239, fax: +48 6652204
e-mail: piotr.krzymien@put.poznan.pl

Abstract

Reduction in losses accompanying the operation of IC engine requires previous identification of their sources and estimation of their value. Reduction in friction losses that is the most important component of the resistance to motion is particularly substantial. In following study the authors presented the best known methods of friction losses estimation pointing out their advantages and shortcomings. In authors' opinion the method of balance of torques generated during engine run is the most accurate one. The basic source of error in this method is an additional torque due to the torsional vibrations. Finally, torsional vibrations calculations concerning the VWR5 TDI diesel have been presented as an example.

Keywords: *combustion engine, friction losses, mentioned methods, torsional vibrations*

1. Introduction

Energy generated during fuel combustion in engine cylinder is higher than that transmitted to the receiver of a part indispensable for overcome the resistance in kinematic nodes and necessary for driving the auxiliaries. Difference between the indicated mean effective pressure (p_i) and the brake mean effective pressure (p_e) is so called resistance to motion mean pressure (p_m) and can be expressed in following formula:

$$p_m = p_i - p_e , \tag{1}$$

or expressed by the relation of relevant torques (or power):

$$M_m = M_i - M_e, \quad N_m = N_i - N_e, \tag{2}$$

where:

M_i, N_i – indicated torque and power,
M_e, N_e – effective torque and power,
M_m, N_m – torque and power due to the resistance to motion.

The concept of mechanical efficiency η_m is used in order to define a relative loss of energy necessary for overcoming engine natural resistance, at the same time proving the correct collaboration and quality of lubrication of engine moving parts. It can be expressed as follows:

$$\eta_m = \frac{N_e}{N_i} = \frac{N_e}{N_e + N_m}. \tag{3}$$

The total power of resistance to motion denoted as N_m contains losses that could be divided into five basic groups.

$$N_m = N_t + N_w + N_p + N_k + N_d. \tag{4}$$

Friction losses (N_t) are generated in engine kinematic nodes, above all in piston-cylinder assembly, main and crank bearings, and camshaft bearings. As tests show, they contribute for about 75% of all losses generated during engine run. Their increase proves worsening the conditions of collaboration in kinematic pairs due to wear of mating surfaces, insufficient lubrication, aging of lubricating oil and so on.

Charge exchange losses (N_w) caused by negative pressure acting on the piston during aspiration stroke as well as overpressure during exhaust stroke, what corresponds to the hydraulic resistance in inlet and outlet systems. The hydraulic resistance depends on construction of manifolds, condition of air filter and muffler.

Auxiliaries drive (N_p) requires power for driving such systems as fuel system, lubricating system or cooling system. Necessary energy is in most cases taken from the crankshaft.

Ventilation losses (N_k) include effect of surroundings on engine moving parts, i.e. all what is connected with pumping gases by pistons in crank case as well as air drag of connecting rod, flying wheel and attached elements.

Blower or compressor drive (N_d) present first of all in two stroke engines and engines mechanically supercharged (compressor driven by the crankshaft).

It is obvious that friction losses have the most considerable share in total resistance to motion. In order to determine these losses different methods are applied, but only few of them are suitable for determination of their variations within the entire cycle. A precise recognition of friction losses changes, in particular those relative to the run of individual engine subassemblies allows to point out necessary modifications in their construction and conditions of operation.

That is why the authors have analyzed the so far utilized methods of their determination, evaluating their suitability for planned tests.

2. Methods of friction losses measurement

There are computational and experimental methods of friction losses (expressed by forces, moments or power of friction) determination. In the case of computational ones the friction losses generated in engine individual subassemblies are determined using appropriate models of phenomena and processes, and eventually summarized. Accomplished results are as correct as precise are mathematical models and input data.

The experimental methods consist in the measurement of friction losses, carried out on running engine or a physical model of selected subassembly. The examples of application of both methods to particular engine kinematic nodes one can find in [3].

Methods utilizing the direct measurement of quantities needed for calculation of the resistance to motion (e.g. using formula 2) as well as those using indirect measurement of selected engine performance data and its dynamic properties can be classified as the experimental methods.

The method utilizing parallel engine indicating (p_i) and the measurement of break mean effective pressure (p_e) can be classified as the most accurate method of direct determination of friction losses. Instantaneous value of cylinder pressure are measured during engine indication and eventually the value of indicated mean effective pressure and indicated torque are determined. For a measurement of effective power the test stand brake or torque meter fixed to the drive shaft can be utilized. This method can be applied to the one or multi cylinder engines but for the latter case differentiation of phenomena in individual cylinders might affect the accuracy of the method (higher accuracy could be attained indicating cylinders individually).

Method of:

– engine motoring,
– combustion switch off in consecutive cylinders,
– run off,
– load characteristics,

can be classified as the indirect methods.

The method of engine motoring consists in the forcing of engine shaft rotation with the external drive. An electrical motor which during other measurements can serve as combustion engine brake is a part of the test stand. When carrying out the measurements, the torque needed for crankshaft drive with a given rotational speed is being determined. The value of torque can be found through the measurement of energy consumed by the motor or measuring the moment of reaction acting on a swinging brake housing. Results obtained using this method are considered as inaccurate due to the lack of combustion. These changes affect to the considerable measure the collaboration between the mating elements and finally the value of resistance to motion.

However, use of other, earlier mentioned methods is restricted with various limitations and brings about considerable errors. For example, the method of switching off cylinders can be applied to multi cylinder engines and friction losses found concern fireless cylinder. The run off method requires in turn a precise knowledge on the dynamic properties of engine and its subassemblies.

3. Measurement of coupling torque between engine and power receiver

A number of measurements within a single engine cycle is necessary in order to define an instantaneous value of losses on a running engine using the method of indicated and load moment direct measurement. The measurement of pressure variations in engine cylinder require the use of typical electronic measurement system. On the other hand, an accurate measurement of load moment is quite a problem [1]. Most of the test stands equipped with electrical brakes allow a precise measurement of braking moment or power, but the result is the average one and the measurement of momentary value is impossible. However, the measurement of an instantaneous value of torque is possible using the modern torquemeters. The principle of their operation consists in a measurement of changes in a chosen physical quantity, relative to a selected section of coupling shaft (a part of torquemeter) as stress (using tensometer measuring system, see Fig. 1) or angle of torsion (Fig. 2). The angle of shaft torsion is proportional to the value of torque M (also called the coupling torque) as in Eq. (5):

$$M = \frac{G \cdot I \cdot \varphi}{l} , \tag{5}$$

where:

l – distance between terminal cross sections,
φ – angle of torsion of shaft measuring section,
G – modulus of rigidity,
I – moment of inertia.

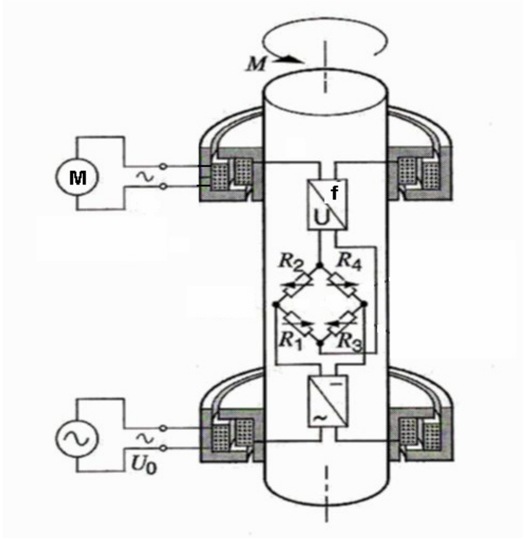

Fig. 1. Tensometric torquemeter with contactless, transformer signal transmission: M – torque, U_0 – supply voltage, $R_1 \div R_4$ – tensometers [4]

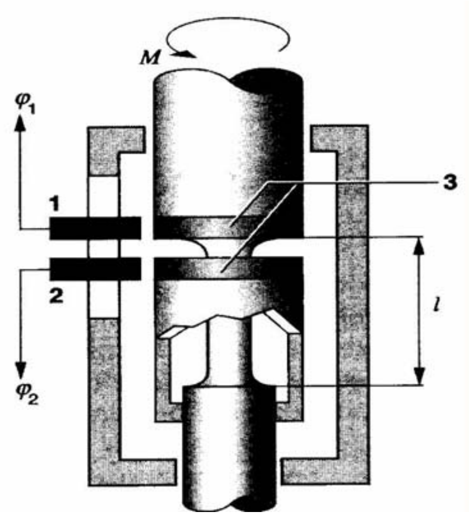

Fig. 2. Torquemeter; 1, 2 – angle (or angular velocity) transducers, 3 – twisted shaft section of the l length [4]

In both torquemeters presented in Fig. 1 and 2 the signal of measured value is transmitted contactless from rotating shaft to measuring system what improves measurement precision and limits distortions like sparkling characteristic for typical system of transmission.

Instead of torquemeter one can use measuring system containing sensors of angle or angular speed. Anyhow they work, the most important parameter is the number of impulses per one revolution because it decides about precision of measurement. In most cases there are inductive sensors which cooperate with toothed wheel (connected to the flying wheel for instance or separate). So called encoders, i.e. photoelectrical sensors of shaft angle producing great number of impulses per revolution are used.

Impulse from sensor is computer processed, which allows to obtain information on momentary value of displacement, angular velocity and acceleration of selected points of coupling shaft. Phase shift between impulses is a base for determination of instantaneous value of torque.

Application of high class torquemeter connected to the system of signal recording and analysis allows for precise analysis of torque momentary value. Besides of information on indicated and load torque, the registered signal contains also information on torques of other kind and on distortions as well (see Fig. 3). There could be different causes of these distortions and they could result from phenomena typical for combustion engine as well as distortions of electrical origin.

The latter can be easily eliminated or minimized using screening of measuring system. It is far more difficult to define sources and courses of distorting torques. One of the sources of significant distorting torque are the torsional vibrations produced by changing gas and inertia forces that cyclically act on the crankshaft. This additional torque adds to the torques substantial for the analysis and limits or even makes impossible their precise evaluation (it should be noted that the torque relative to the torsional vibrations can be used as valuable diagnostic parameters conveying information on engine technical condition). Because of that its elimination is necessary using, for instance, a filter in transmission and processing route.

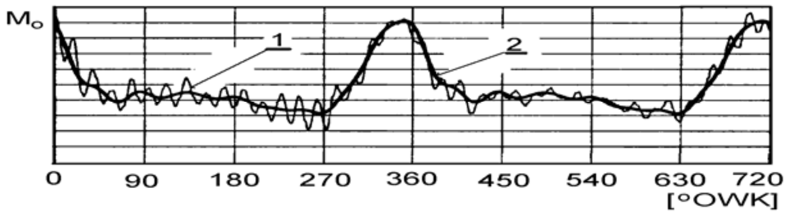

Fig. 3. Exemplary course of torque recorded for a single rotation of engine crankshaft; 1 – actual course of recorded torque, 2 – filtered course of torque signal [2]

However, application of filter requires previous definition of vibration parameters like frequency and amplitude. They can be estimated computationally but verification is possible only in a test stand.

4. Crankshaft torsional vibrations

Presented further results have been achieved in a course of analytical calculations of torsional vibrations using DELPHI computer program. A modern, five cylinder diesel of the R5 TDI type (AXD code) has been adopted as an exemplary test object (its basic technical data are shown in Table 1).

Tab. 1. Basic technical data of the R5 TDI engine [5]

Parameter	Data
Engine swept volume, cm^3	2460
Cylinder diameter, mm	81
Stroke, mm	95,5
Compression ratio	18,5
Cylinder number	5 (in line)
Cooling	water
Torque, Nm	320/2000
Power, kW	96/3500
Firing order	1 – 2 –4 –5 – 3

Taking into consideration the goal of investigation, i.e. determination of additional torque from torsional vibration, a computer program has been written which allows to find such quantities like vibration frequencies of different order, deflection amplitudes of equivalent masses (relative and actual) and courses of additional torques relative to cyclic forces resulting from engine operation. An earlier input of certain characteristic data was necessary such as those measurable (dimensions of piston-crankshaft assembly, for example) or those estimated (like damping coefficients of crankshaft sections).

Since the engine selected for exemplary calculations is a multi cylinder one its equivalent system has been assumed as the multi mass one. There are formulas obtainable in literature which can be used for calculation of system natural frequency of less than three masses. When larger number of masses is to be taken into consideration the universal formula of mechanics, known also as Lagrange formula should be applied (like in the presented program). This formula has following form:

$$\frac{d}{dt}\left(\frac{\partial E}{\partial \dot{q}_i}\right)-\frac{\partial}{\partial q_i}\left(E-V\right)+\frac{\partial D_t}{\partial \dot{q}_i}+\frac{\partial D_h}{\partial \dot{q}_i}=M_i\left(t\right), \tag{6}$$

where:

E – kinetic energy of vibrating system,
V – potential energy of the system,
q_i – general coordinate,
D_t – losses due to hysteresis,
D_h – losses due to friction.

Angular deflection β of individual equivalent mass has been assumed as general coordinate. Motion of each mass should satisfy the Lagrange formula.

At the initial stage of calculations the crankshaft (Fig. 4) and cooperating elements have been replaced with the equivalent torsional system.

Fig. 4 . A view of R5 TDI engine crankshaft

When defining the characteristic properties of equivalent shaft a principle has been assumed that shaft stiffness should be the same as that of real shaft and even along the whole structure. Masses of shaft parts (cranks, counterweights, damper) as well as masses of elements connected (piston, connecting rod) were replaced with rings of the same inertias mounted at relevant positions. The most important data of equivalent system have been summarized in Table 2.

Tab. 2. Classification of polar inertias and equivalent stiffness of the R5 TDI engine

Cyl. No	Symbol	Moment of inertia kg m^2	Equivalent length m	Remarks
1	Θ_1	0.010	0.150	Moment of inertia can vary when engine runs
2	Θ_2	0.010	0.150	
3	Θ_3	0.010	0.150	
4	Θ_4	0.010	0.150	
5	Θ_5	0.010	0.105	
6	Θ_6	0.36		Flywheel set

Input data used gave the following natural frequencies:

ω_1 = 2474 rad/s,
ω_2 = 6850 rad/s,
ω_3 = 10643 rad/s,
ω_4 = 13449 rad/s

of the first, second, third and fourth order, respectively. Relative angular deflections corresponding to these frequencies are summarized in Table 3 and presented in Fig. 5.

Tab. 3. Classification of relative amplitudes of equivalent system masses

Mass No	1st order	2nd order	3rd order	4th order
1	1.000	1.000	1.000	1.000
2	0.899	0.226	-0.866	-1.981
3	0.707	-0.722	-1.115	0.943
4	0.444	-1.112	0.718	1.035
5	0.136	-0.642	1.211	-1.979
6	- 0.088	0.034	-0.026	0.026

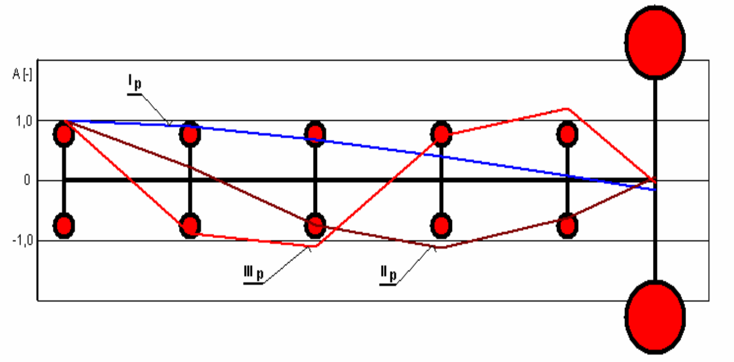

Fig. 5. Relative angular deflection of equivalent system masses; I p, II p, III p – consecutive vibration order

Only the knowledge of equivalent system parameters facilitates achievement of the main goal, i.e. calculation of additional torques from torsional vibrations. The course of coupling torque M_s calculated for the section of crankshaft close to the flywheel has been presented in Fig. 6.

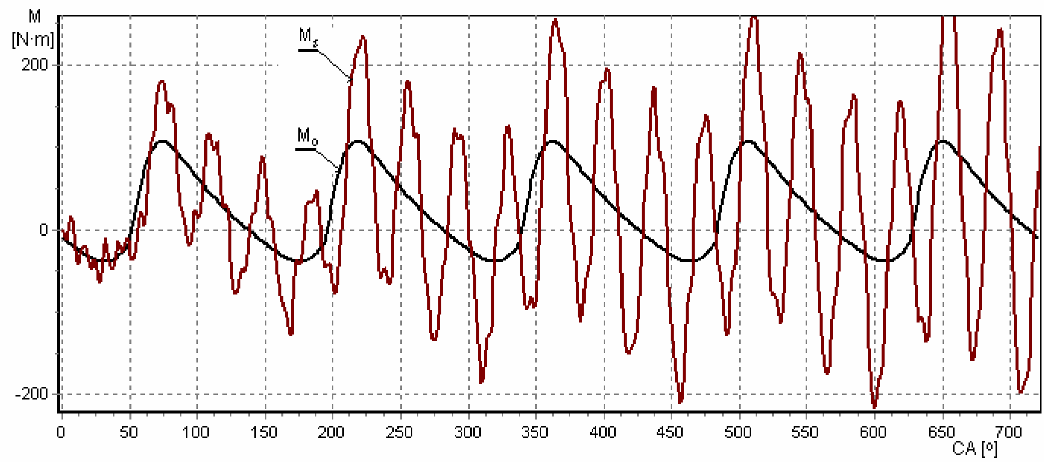

Fig. 6. Calculated courses of torque M_o and coupling torque M_s determined at the flywheel

Despite of cyclic change in value of forcing moment M_o the course of coupling torque M_s is of complex character, and its amplitude differs for each cylinder.The basic reason for such course of M_s is engine operation at speeds close to the resonanse frequencies of individual orders. Theoretic explanation of these phenomena is extremely difficult and will be the subject of eventual paper.

References

[1] Iskra, A., *Problems with determination of friction torque fluctuations at the cumbustion engin work cycle,* Journal of KONES Internal Combustion Engines 2004, vol.11, No. 1-2, pp.65-71, Warsaw 2004.

[2] Iskra, A., *Transformacja wyników pomiaru momentu sprzęgającego silnik z odbiornikiem mocy do momentu rzeczywistego*, Transformation of the Engine-to-receiver Coupling Torque Measurement Results to the Actual Value of Torque, Pomiary Automatyka Kontrola. 5/2005, pp. 41-45, 2006, Warszawa.

[3] Serdecki, W., *Badania współpracy elementów układu tłokowo-cylindrowego silnika spalinowego*, Wydawnictwo Politechniki Poznańskiej, Poznań 2002.

[4] Informator techniczny Bosch, *Czujniki w pojazdach samochodowych*, WKiŁ, Warszawa 2002.

[5] Materiały informacyjne firmy Volkswagen.

SELECTED PROBLEMS OF MODELLING THE WORKING OF CONTAINER INJECTION SYSTEMS OF COMMON RAIL TYPE

Mirosław Walkowski

Naval Academy, Institute of Vessel Construction and Operation
81 – 103 Gdynia, ul. Śmidowicza 69
tel.: +48 (58) 6262653, 6262665
email: mwal@interia.eu

Abstract

In the work an attempt was made to replace the conventional system of controlling the dose and angle of advance of fuel injection by an electronically controlled system, which was implemented by attaching a fuel container to the conventional high-pressure fuel system, and an electronically controlled, electro-hydraulic fuel-dosage valve.

It was assumed that by controlling the current impulse of the electro-hydraulic valve it would be possible to model the dose of fuel injected into the combustion chamber and to control injection time.

The kinematics of the valve slide has been presented taking account of fuel parameters, hydrodynamic phenomena and axial leakage occurring during valve overdrive.

Keywords: *Common rail, electro-hydraulic valve electronically controlling the fuel dose*

1. Introduction

In conventional and distributional injection pumps, as well as in pump injectors, the combining of the fuel stamping and dosing process with angular location of the shaft or cam ring brings in undesirable changes in the course of fuel injection parameters, with the change of rotational speed of the pump shaft.

Widening of the combustion engine's optimal work range became possible due to an electronic control system, which enables controlling the course of basic parameters of fuel dosage and injection in the whole work range of the engine, in various conditions of the surroundings, also taking into account fuel properties.

The replacement of a conventional control system (by fuel dose and injection angle of advance) with an electronically controlled system was implemented in that the conventional high-pressure fuel system was supplemented with a fuel tank and an electronically controllable electro-hydraulic fuel dosage valve.

This work presents the course of kinematic parameters (shift and speed) of the control valve slide and a calculation fragment from the second phase of the slider movement, i.e. when the slide is shifted upwards up to the moment when the upper piston of the slide exposes the bore chamber in the cylinder at the outlet orifice to the injector.

2. Diagram of a CR JCB – 1 laboratory engine feeding system

A diagram of a fuel system with attached fuel tank and electronically controllable electro-hydraulic fuel-dosage valve has been presented in Fig. 1. A similar feeding system has been applied in Sulzer RT – flex60C engine. By controlling the current impulse of the electro-hydraulic valve it becomes possible to freely model the size of the fuel dose flowing into the combustion chamber in the engine cylinder and to control injection time.

Below is a diagram of a Common Rail (CR) feeding system of a one-cylinder research engine (JSB), which will replace the conventional fuel system.

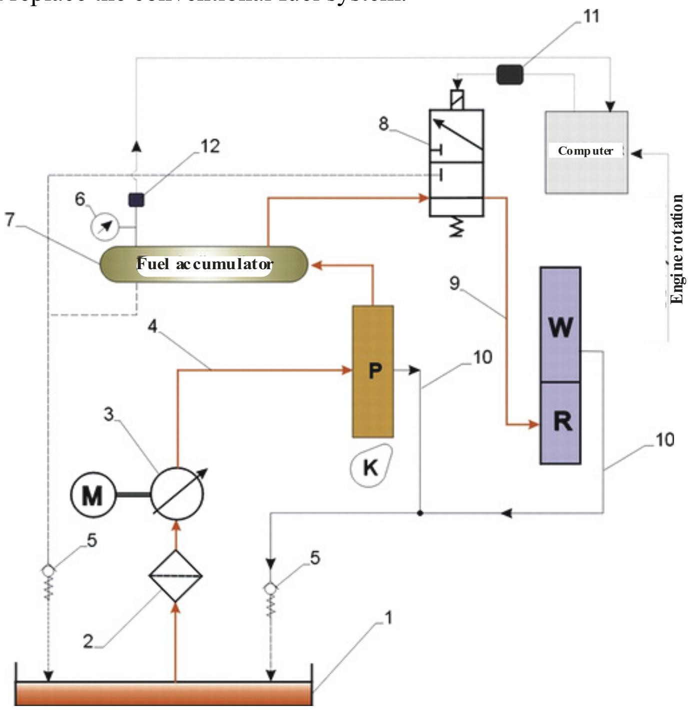

Fig. 1. Diagram of CR injection system of a JSB engine: 1 – fuel tank; 2 – filter; 3 – pump; 4 – low-pressure fuel conduit; 5 – overflow valve; 6 – manometer; 7 – high-pressure fuel tank; 8 – electro-hydraulic valve electronically controlling the fuel dose; 9 – high-pressure fuel conduit; 10 – low-pressure (overflow) fuel conduit; 11 – signal amplifier; 12 – pressure sensor; K – cam; P – high-pressure fuel pump; R – sprayer; W – injector

2.1. Fuel-injection controlling valve

A fuel-injection controlling valve was singled out in the feeding system, designed on the base of JSB engine work parameters and on the required unit of fuel dose, control parameters and the injection angle of advance.

Below there is a figure of the injection-control valve.

The work of the electro-hydraulic valve was divided into nine characteristic phases of the control slide movements [6]: in the first phase the slide is in the bottom position; then it is shifted upwards up to the moment when the upper piston of the slide exposes the bore chamber in the cylinder at the outlet orifice to the injector; the next phase is further movement upwards with two open channels: the overflow channel and the channel delivering fuel to the sprayer; the control slide continues its upward movement – the upper piston is above the bore chamber edge at the orifice supplying fuel to the injector, the overflow orifice being closed. In the fifth movement phase the control slide leans against the upper fender (maximum piston travel); 6^{th} phase – the control slide moves downwards to the moment when the overflow orifice is opened; the next phase is the slide moving downwards with open channels, the overflow channel and the one supplying fuel to the injector; in the eighth phase the movement of the control slide is downwards and the fuel is pumped to the overflow channel; in the final ninth phase, the control slide rests on the lower fender.

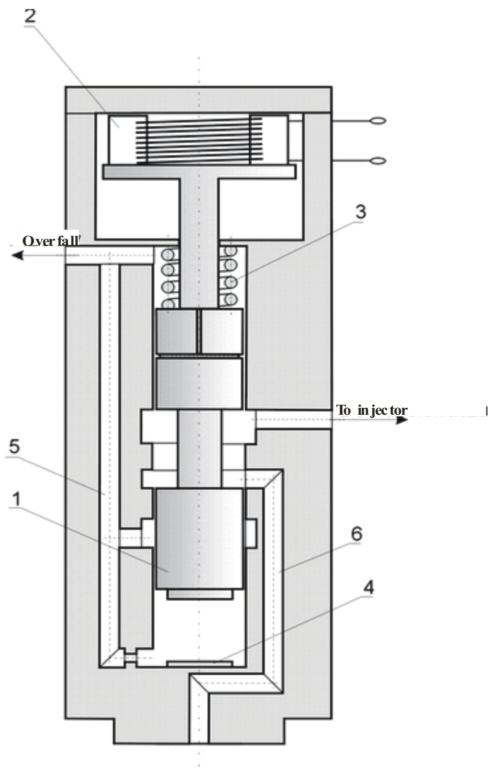

Fig. 2. Electro-hydraulic valve electronically controlling the fuel dose:
1– control slide, 2–coil, 3–rebound spring, 4–fender, 5– overflow channel, 6– main fuel channel

3. Dampened slide movement of the electromagnetic valve

In calculating operation parameters of the electromagnetic valve the following simplified assumptions were made: fuel is a compressible fluid, with longitudinal modulus of elasticity E and is subject to Hooke's law; what was omitted were the elastic deformations of the fuel injection conduit caused by its pressure changes; fuel flow in the high-pressure conduit was treated as an isothermic one-dimension flow (flow characteristic parameters change along the conduit axis, but are constant in cross section); friction effect was taken account of with the assumption that losses caused by its effect during stationary and non-stationary flow are equal (in dependencies describing fuel flow in the conduit they are expressed by the hydraulic resistance coefficient); omitted were the undulatory phenomena in the injection system; when calculating the mean flow speed of fuel in the fuel conduit the time required for opening and closing the injector valve was omitted; injection pressure change does not affect fuel density (ρ= const.).

When analysing the slide movement of the electromagnetic valve the following were taken account of [5, 6]:

- Energy losses when the fuel flows through constant and variable valve section areas;
- Hydraulic losses between pistons and the control valve cylinder;
- Hydrodynamic forces in successive phases of the valve slide movement;
- Viscous resistance forces in extreme positions of the control valve [5];
- Spring resistance force (including its initial tension);
- Inertial force from the return spring mass, electromagnet armature mass, control slide mass (including fuel shifted with the slide).

4. Selected problems of modelling the work of an electro-hydraulic control valve

This work presents the course of kinematic parameters (shift and speed) of the control valve slide and a calculation fragment from the second phase of the slider movement, (i.e. when the slide is shifted upwards up to the moment when the upper piston of the slide exposes the bore chamber in the cylinder at the outlet orifice to the injector) and the share of axial leaks in particular phases of the slide movement, and also the effect of hydrodynamic forces of the flowing fuel on the slide movement.

4.1. Hydrodynamic force in successive phases of the valve slide movement

The designation of hydrodynamic force variable in time and dependent on the position of the hydrodynamic force slide $\mathbf{F_h}$ [4, 6].

$$AB(t)=\sqrt{s_p^2+e_p^2(t)}=e_p(t)\sqrt{1+\frac{s_p^2}{e_p^2(t)}}\ ;$$

$$CD(t)=\sqrt{s_w^2+e_w^2(t)}=e_w(t)\sqrt{1+\frac{s_w^2}{e_w^2(t)}}\ ;$$

$$A_{AB}(t)=\pi D_c AB(t); \qquad A_{CD}(t)=\pi D_c CD(t);$$

$$\cos\Theta_p(t)=\frac{s_p}{AB(t)}\ ; \qquad \cos\Theta_w(t)=\frac{s_w}{CD(t)}\ ;$$

$$F_{hp}(t)=A_{AB}\Delta P_{1,5}(t)\cos\Theta_p(t); \qquad F_{hw}(t)=A_{CD}\Delta P_{1,8}(t)\cos\Theta_w(t);$$

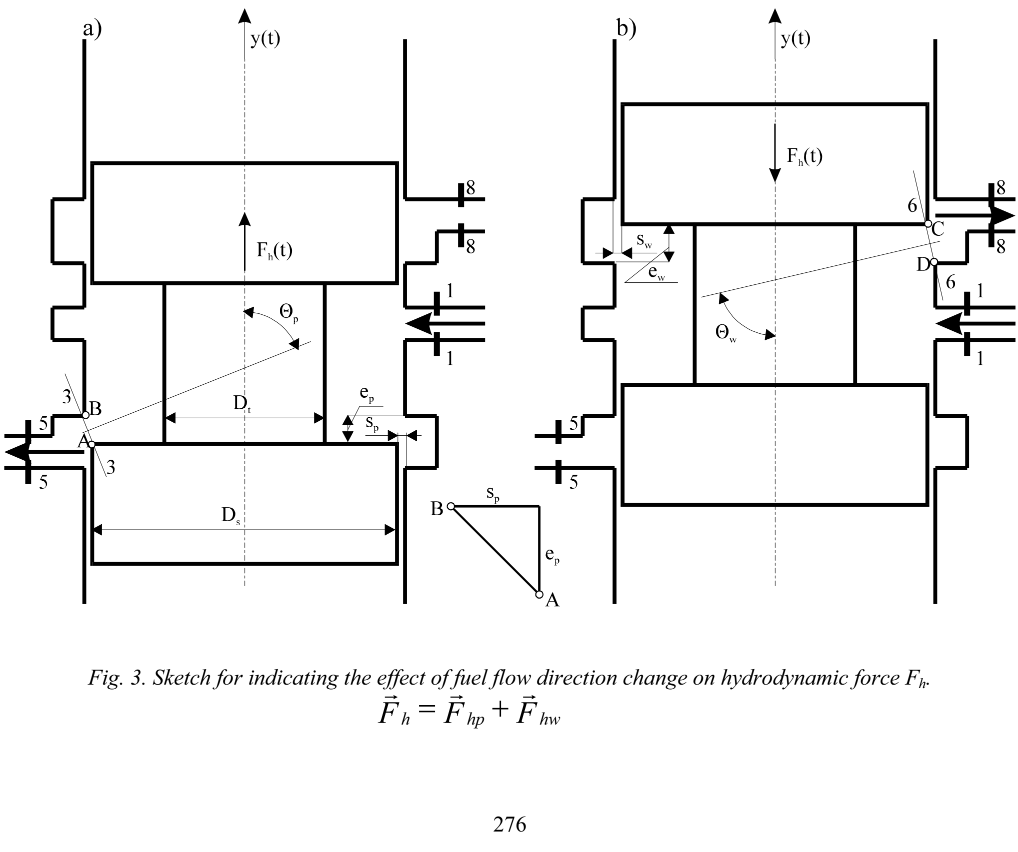

Fig. 3. Sketch for indicating the effect of fuel flow direction change on hydrodynamic force F_h.

$$\vec{F}_h=\vec{F}_{hp}+\vec{F}_{hw}$$

AB(t), CD(t) - distance between the control slide edge from the edge of cylinder bore chamber of the control valve (Fig. 9.), m,
e_p, e_w - respectively: $e_p = b_p - y(t)$; $e_w = b_w - y(t)$; (Fig. 3), m,
s_p, s_w - size of slot between control slide and valve cylinder, m,
Θ_p, Θ_w - inclination stream of fuel stream in relation to slide axis, [^{o}],
$F_{hp}(t)$, $F_{hw}(t)$ - hydrodynamic forces: when flowing through overflow orifice or when flowing through orifice supplying fuel to the injector, N,
F_h - resultant hydrodynamic force, N,
B_p, b_w - bore chamber height, m.

Flow losses resulting from axial leaks in annular gaps

The gap between piston and cylinder was assumed to be concentric.
$s_0 = (D_2 - D_1) / 2$ – gap between cylinder and piston,
$D = (D_1 + D_2) /2$ **–** mean gap diameter with the assumption that $\mathbf{s_0 \ll D}$**,**
μ - dynamic viscosity coefficient, [kg/m·s],
ν - kinematic viscosity coefficient, [m^2/s], $\nu = \mu / \rho$.

The expense through the gap with piston immobile in relation to the cylinder:

$$Q = \frac{\Delta p\, s_0^3 \pi D}{12\mu l} = \frac{\Delta p\, s_0^3 \pi D}{12\nu\rho l}$$

For a piston moving in relation to the cylinder with constant speed $\mathbf{v_0}$, the flow expense through the gap will be equal to

$$Q = \left[\frac{\Delta p\, s_0^3}{12\mu l} \pm \frac{v_0 s}{2}\right]\pi D = \left[\frac{\Delta p\, s_0^3}{12\nu\rho l} \pm \frac{v_0 s}{2}\right]\pi D$$

sign **„ + ”** – corresponds to the state when the piston is moving towards higher pressure,
sign **„ - ”** – corresponds to the movement of the piston towards lower pressures.

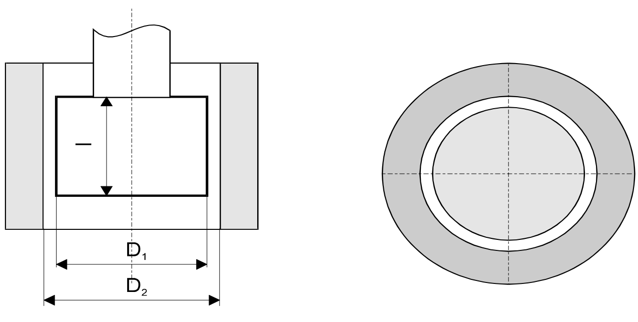

Fig. 4. Concentric annular gap

5. Kinematic equations of control valve slide

In the selection of equations of the 2nd phase of the control valve slide movement the limitation was made to general kinematic dependencies, the limitation resulting from general framework assumed for this study. The recording of equations given does not infringe on the principles of model adequacy for the object analysed, although its more detailed solutions are possible too.

Shifts, speeds and accelerations of the slide caused by forces in the valve (excluding rebounds from movement limiters) are described by the dependencies [6]:

2nd phase; $t_1 \leq t < t_4$,

$$y(t) = Y\left[1 - e^{h_i(t-t_1)}\cos\lambda_i(t-t_1)\right],$$
$$\dot{y}(t) = Y\,\lambda_i\,e^{-h_i(t-t_1)}\sin\lambda_i(t-t_1),$$
$$\ddot{y}(t) = Y\lambda_i^2 e^{-h_i(t-t_1)}\left[\cos\lambda_i(t-t_1) - \frac{h_i}{\lambda_i}\sin\lambda_i(t-t_1)\right]$$

Substitutions:

$$h_i(t) = \frac{c_z(t)}{2m_z}, \qquad h_j(t) = \frac{c_z(t)}{2m_z}$$

$$\lambda_i(t) = \left[\frac{k_z}{m_z} - h_i^2(t)\right]^{0.5} = \frac{\pi}{2T_{14}}, \quad \lambda_j(t) = \left[\frac{k_z}{m_z} - h_j^2(t)\right]^{0.5} = \frac{\pi}{2T_{69}},$$

$c_z(t)$ – coefficient of viscous dampening for respective time intervals, [Ns/m],
k_z – coefficient of spring stiffness, [N/m],
$\lambda_i(t),\lambda_j(t)$ – angular frequency of the slide and the armature in respective time intervals, [s^{-1}].

The angular frequency of free vibration of the slide and the armature are equal to:

when: $0 < t < t_4$ $\qquad \omega_i = \left[\lambda_i^2(t) + h_i^2(t)\right]^{0.5}$,

when: $t_6 < t < t_9$, $\qquad \omega_j = \left[\lambda_j^2(t) + h_j^2(t)\right]^{0.5}$.

Exciting force frequency of valve slide movement

$$f_i = 2\pi n_i, \qquad f_i = 2\pi n_w.$$

ni , nw – frequencies of electric impulse and fuel injection.

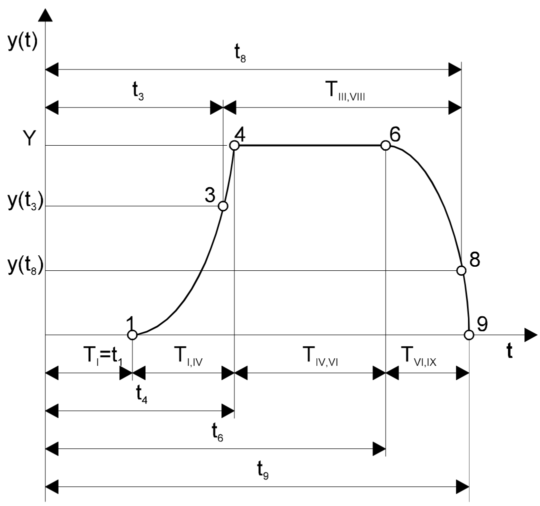

Fig. 5. Diagram for describing the course of slide movement of a viscously dampened valve [8]

Fig. 6 presents the time courses of the electro-hydraulic valve slide shift and speed.

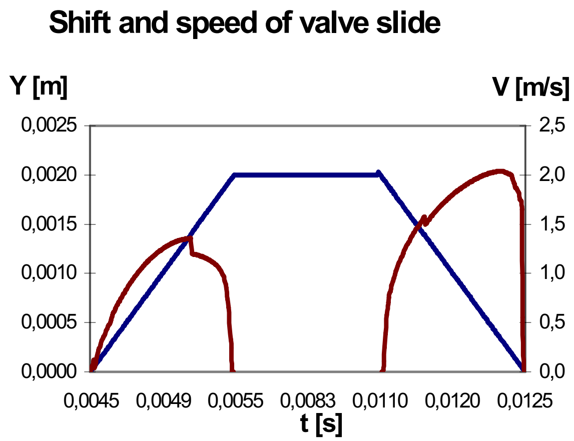

Fig.6. Electro-hydraulic valve slide movement and speed courses

After making initial assumptions, determining valve work parameters and introducing input data, there were determined the kinematic parameters of slide movement, i.e. the time course of slide movement, the change of its speed and acceleration at a single overdrive caused by forces active in the valve.

The graph in Fig. 4 presents the time course of the slide movement, with visible main movement phases:

Preparation for starting the slide, $y = 0$, $t = 0$,

Starting the slide, $y = 0$ whereas $t = t_1$,

Slide movement under the effect of electromagnet force, $0<y<Y$, $t_1<t<t_4$,

Stopping and holding down the slide at the upper fender, $y = y_4 = Y$, $t_4 \leq t \leq t_6$

Return movement of the slide under the effect of spring forces, $t_6<t<t_9$, $0<y<Y$,

Holding down the slide at the lower fender, $t>t_9$, $y = 0$.

6. Résumé

Adapting particular elements of the electronic control system, that is, an electronically controlled fuel-dosing valve and fuel tank into the conventional high-pressure injection system of a JSB engine, it is possible to obtain a completely controllable injection process.

The results obtained, that is the calculation of slide movement kinematics of the valve controlling the fuel dosage, constitute very important information enabling to analyse the particular movement phases of the valve slide and to shape fuel injection course during the engine's work cycle.

When controlling the current impulse it is possible to control the fuel dose size, and also to model multiple injection, characteristic for electronically controlled injection systems.

Simulation calculations were conducted based on theoretic and empirical dependencies without verification and research on a real valve model, which is why they should be treated as estimation results.

In order to verify the model assumed experimental research should be conducted on a real valve and the results obtained should be used for correcting the assumed calculation model.

References

[1] *Elektroniczne sterowanie silników wysokoprężnych. Układ wtryskowy Common Rail*, WKŁ, Warszawa 2000.

[2] *Elektroniczne sterowanie silników wysokoprężnych. Układy wtryskowe UIP/UPS*, WKŁ, Warszawa 2000.

[3] Gałąska, M., Kaczmarczyk, J., Maruszkiewicz, J., *Hydromechanika stosowana*, Wojskowa Akademia Techniczna im. J. Dąbrowskiego, Warszawa 1972.

[4] Guillon, M., *Teoria i obliczanie układów hydraulicznych*, WNT Warszawa.

[5] Landau, L. D., Lifszyc, E. M., *Hydrodynamika*. PWN Warszawa 1994.

[6] Ochocki, W., *Numerycznie sterowane systemy wtrysku paliwa silników wysokoprężnych,* Wydawnictwo Poznańskiego Towarzystwa Przyjaciół Nauk, Poznań 1994.

[7] Sobieszczański, M., *Modelowanie procesów zasilania w silnikach spalinowych*, WKŁ Warszawa 2000.

[8] *Zasobnikowe układy wtryskowe Common Rail*, BOSCH. WKŁ Warszawa 2005.

[9] Zbierski, K., *Układy wtryskowe Common Rail*, MiW Łódź 2001.

STOCHASTIC CONTRIBUTIONS ON THE PRESSURE IN SLIDE BEARING GAPS AFTER IMPULSE

Krzysztof Wierzcholski

Gdansk University of Technology
ul. Narutowicza 11/12, 80-950 Gdańsk, Poland
tel. +48 58 348612
e-mail: wierzch@pg.gda.pl

Abstract

This paper concerns the derivation of the stochastic modified Reynolds equations describing the hydrodynamic pressure for non-Newtonian, viscoelastic, lubricant inside the curvilinear orthogonal (spherical, conical, cylindrical, parabolic) slide bearing. Non- isothermal, unsteady and random flow conditions and thermal deformations of the bearing and its bearing sleeve are taken into account. This problem finds application in ship power plants, electric locomotive designing, and precision engineering. In particular case are determined pressure and capacity distributions in spherical bearing.

Keywords: *time depended stochastic hydrodynamic theory, bearing surfaces with curvilinear sections*

1. Introduction and basic equations

This paper presents the general analysis of the influence of unsteady non isothermal flow of, visco-elastic oil in magnetic field on the pressure, within deformed curvilinear bearing gaps between two rotational surfaces in random conditions (see Fig.1).

The flow analysis of the viscoelastic lubricant, will be performed by means of the Helmholtz Equation and the equations of continuity, motion and energy Ref.[1],[2],[3]:

$$\nabla^2 \boldsymbol{H} = \mu\mu_e\, \partial^2 \boldsymbol{H}/\partial t^2, \tag{1}$$

$$div(\rho \boldsymbol{v})=0, \tag{2}$$

$$Div\boldsymbol{S}+\mu(\boldsymbol{N}\nabla)\boldsymbol{H}=\rho d\boldsymbol{v}/dt, \tag{3}$$

$$div(\kappa\, gradT)+div(\boldsymbol{vS})-\boldsymbol{v}Div\boldsymbol{S}-\mu T\Xi d\boldsymbol{H}/dt=\rho dc_v T/dt, \tag{4}$$

where:

v - lubricant velocity vector,
T - temperature of lubricant,
N - magnetization vector of lubricant,
H - magnetic intensity vector,
Ξ - first derivative of the magnetization vector with respect to the temperature,
c_v - specific heat,
μ,μ_e - magnetic and electric permeability coefficient of lubricant,
S - stress tensor in the lubricant,

∇ - Del vector,
κ - thermal conductivity coefficient of the lubricant.

The magnetic susceptibility coefficient of the lubricant has constant scalar value. The relationship between the stress tensor $\mathbf{S}\equiv||\tau_{ij}||$ and the strain Rivlin-Ericksen tensor $\mathbf{A_1}$, $\mathbf{A_2}$ in the lubricant is as follows [3]:

$$\boldsymbol{S}=-p\boldsymbol{I}+\eta\,\boldsymbol{A_1}+\alpha\boldsymbol{A_1}\boldsymbol{A_1}+\beta\boldsymbol{A_2}, \tag{5}$$

where:

$\mathbf{I}=||\delta_{ij}||$ - unit tensor,
δ_{ij} - Kronecker delta.

Symbols α and β denote empirical coefficients of lubricant, which describes viscoelastic properties of the fluid in Pas^2 units. Lubricant dynamic viscosity depends on magnetic induction and temperature, i.e. $\eta=\eta(H,T)$.

The stationary equation of motion and heat equation for the elastic bearing sleeve have the following form:

$$Div\boldsymbol{S}^*+\mu^*(\boldsymbol{N}^*\nabla)\boldsymbol{H}^*=\rho^*\partial^2u/\partial t^2+(\xi/T_o)gradT^*, \tag{6}$$

$$\mathrm{div}(\kappa^*\mathrm{grad}T^*)=(c_v\,\rho)^*\partial T^*/\partial\, t+\xi\,\partial(\mathrm{div}u)\partial\, t, \tag{7}$$

where:

$$\xi\equiv 3K\times(\alpha_T)^*T_o,$$

K - bulk modulus,
T_o - value of characteristic temperature,
$\boldsymbol{N}^*$ - magnetization intensity,
$\boldsymbol{H}^*$ - vector of magnetic intensity vector in elastic body,
μ^* - magnetic permeability coefficient of hyper-elastic body.

The following symbols: ρ^*, $(c_v)^*$, κ^*, $(\alpha_T)^*$ denote: density, specific heat, thermal conductivity, linear expansion coefficient for elastic body material respectively. We take into account the Duhamel-Neumann relations between the components τ^*_{ij} of the stress tensor S^* in the elastic body and the components ε_{ij} of the strain tensor [1]. Moreover we consider strain-displacement dependencies [2] for $u_{\alpha 1}$, $u_{\alpha 2}$, $u_{\alpha 3}$ - components of displacement vector u of elastic body. The characteristic dimensional height of elastic layer ε_s is about thousand times smaller than radius of body curvature and other quantities occurring in the friction region. The total dimensional gap height has the following form:

$$\varepsilon_T=\varepsilon_p+u_{\alpha 2}+u_{\alpha 2B}, \tag{8}$$

where:

ε_p - primary height of the gap,
$u_{\alpha 2}$ - dimensional temperature and pressure displacement in gap height direction of the external elastic layer surface being in contact with the lubricant,
$u_{\alpha 2B}$ - dimensional magnetic displacement in gap height direction of the external elastic layer surface being in contact with the lubricant.

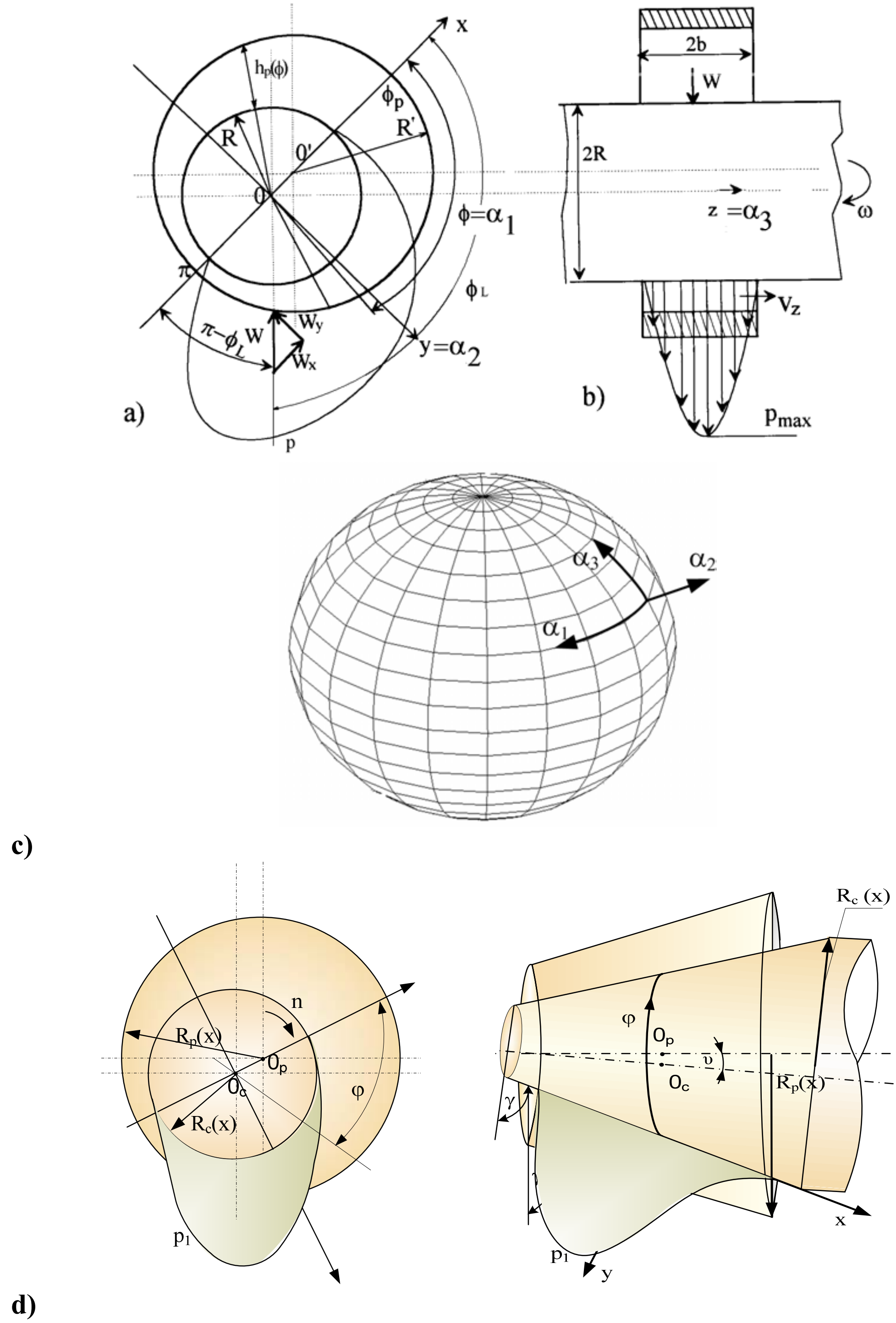

Fig. 1. Slide bearing geometries: a) cylindrical surface, b) cylindrical bearing gap, c) spherical surface, d) conical surface, where $x=\alpha_3$, $y=\alpha_2$, $\phi=\alpha_1$

The system of Eqs.(1), (2), (3), (4), (6), (7) has the following unknowns: $v_{\alpha 1}$, $v_{\alpha 2}$, $v_{\alpha 3}$ – three dimensional components of lubricant velocity vector in three curvilinear, orthogonal dimensional α_{1d}, α_{2d}, α_{3d} directions, p - hydrodynamic dimensional pressure, T - dimensional temperature in lubricant, T^* - dimensional temperature in the superficial layer of the sleeve body and $u_{\alpha 1}$, $u_{\alpha 2}$, $u_{\alpha 3}$ three components displacements of displacement vector $\boldsymbol{u}$ in elastic body. Symbol α_{1d} indicates circumferential direction in each coordinate system for example φ in cylindrical or spherical bearings. Symbol α_{2d} indicates gap height direction for example r in cylindrical or spherical bearings. Symbol α_{3d} indicates longitudinal direction in each coordinate system for example z in cylindrical and ϑ in spherical ones. Hence in cylindrical and spherical coordinates we have: $(v_{\alpha 1}, v_{\alpha 2}, v_{\alpha 3})=(v_{\phi}, v_r, v_z)$, $(v_{\alpha}, v_{\alpha 2}, v_{\alpha 3})=(v_{\phi}, v_r, v_{\vartheta})$.

2. Estimation of hydrodynamic equations

In order to simplify the boundary conditions for lubricant flow equations, we introduce following dimensionless components of velocity vector in the circumferential, radial and longitudinal directions v_1, v_2, v_3 respectively. And, the dimensionless components of magnetic induction vector, magnetization vector, magnetic intensity vector, have here the following form: B_1, B_2, B_3; N_1, N_2, N_3; H_1, H_2, H_3, respectively and they depend on the dimensionless variables α_1 and α_3. Dimensionless components of displacement vector in the dimensionless variables $(\alpha_1, \alpha_2, \alpha_3)$ have the form u_1, u_2, u_3. Symbols T_1, p_1, t_1, η_1, κ_1, h_{p1} denote dimensionless temperature, dimensionless pressure, time, dimensionless viscosity, dimensionless thermal conductivity coefficient and dimensionless gap height, respectively. Between dimensional and dimensionless quantities we have following relationship [1], [3]:

$$p=p_o p_1,\ v_{\alpha 1}=Uv_1,\ v_{\alpha 2}=\psi U v_2,\ v_{\alpha 3}=Wv_3,\ T=T_o+BrT_oT_1,\ \eta=\eta_o\eta_1,\ \kappa=\kappa_o\kappa_1,\ \varepsilon_p=\varepsilon\varepsilon_{p1},\ u_{\alpha 2}=\varepsilon u_2, \tag{9}$$

$$\alpha_{2d}=R(1+\psi\alpha_2),\ \ \alpha_{3d}=R^*\alpha_3,\ \alpha_{1d}=R\alpha_1. \tag{10}$$

We denote: R - radius of the curvature in α_1 direction, R^* - radius of the curvature in α_3 direction or length of the bearing of cylindrical bearing, $U=\omega R$ surface linear dimension velocity in α_1 direction, $W=U/L_1$ - surface linear dimension velocity in α_3 direction, $L_1=R^*/R$, ε - average dimensional gap height, ω - angular journal velocity, $B_o=\mu H_o$, $p_o=\omega\eta_o/\psi^2$, $\psi\equiv\varepsilon/R$. Other dimensional characteristic values are distinguished by symbol (o) in lower index namely: η_o, κ_o, ρ_o, H_o, T_o, N_o, t_o. We determine the quantities: dimensionless radial clearance, dimensionless length, Magnetic, Brinkman, Reynolds, Strouhal, and two Deborah Numbers, in the following form, respectively:

$$\begin{gathered}\psi\equiv\frac{\varepsilon}{R}\cong 10^{-3},\ L_1\equiv\frac{R^*}{R},\ R_f\equiv\frac{N_oB_o}{p_o},\ Br\equiv\frac{U^2\eta_o}{\kappa_oT_o},\\ Re\equiv\frac{U\varepsilon\rho_o}{\eta_o},\ Str\equiv\frac{R}{Ut_o},\ D_\alpha\equiv\frac{\alpha U}{\eta_oR},\ D_\beta\equiv\frac{\beta U}{\eta_oR},\end{gathered} \tag{11}$$

where:

$0\le D_\alpha\le 1$, $0\le D_\beta\le 1$, $0\le Q_{Br}\equiv BrT_o\delta_T\le 1$,
δ_T - dimensional coefficient which describes the influence of temperature on oil viscosity.

3. Boundary conditions with random effects

The lubricant flow in bearing gap is generated by the rotation of a cylindrical spherical, conical, or parabolic journal. Bearing sleeve is motionless. Hence the boundary conditions for the lubricant velocity components have the form:

$$v_1=h_1 \quad for \quad \alpha_2=0, \quad v_1=0 \quad for \quad \alpha_2=\varepsilon_{T1},$$

$$v_2=0 \quad for \quad \alpha_2=0, \quad v_2=0 \quad for \quad \alpha_2=\varepsilon_{T1}, \tag{12}$$

$$v_3=0 \quad \text{for} \quad \alpha_2=0, \quad v_3=0 \quad \text{for} \quad \alpha_2=\varepsilon_{T1},$$

where

$\varepsilon_{T1} \equiv \varepsilon_{p1} + u_{or1} + u_{o2B}$,
h_1 - Lame coefficient.

In cylindrical and spherical coordinates the dimensionless oil velocity components (v_1,v_2,v_3) have the dimensional form: $(v_{\alpha 1},v_{\alpha 2},v_{\alpha 3})=(v_\phi,v_r,v_z)$, $(v_{\alpha 1},v_{\alpha 2},v_{\alpha 3})=(v_\phi,v_r,v_\vartheta)$. Hence the first dimensionless condition (12.1) in cylindrical $(h_1=1)$ and spherical $(h_1=\sin\vartheta)$ coordinates has the following dimensional forms: $v_\phi=\omega R$ *for* $\alpha_{2d}=0$, $v_\phi=0$ for $\alpha_{2d}=\varepsilon_T$ and $v_\phi=\omega R\sin\vartheta$ for $\alpha_{2d}=0$, $v_\phi=0$ for $\alpha_{2d}=\varepsilon_T$. Symbol R denotes radius of cylindrical of spherical journal and symbol ω denotes angular velocity of cylindrical journal and spherical journal in circumferential direction.
Dimensionless temperature distribution along the bearing gap has the constant dimensionless value $f_{c1}=1$ on the journal surface and on the sleeve surface it changes into the form $f_{p1}(\alpha_1,\alpha_3)$. Hence:

$$T_1(\alpha_1,\alpha_2,\alpha_3)=1 \quad \text{for} \quad \alpha_2=0,$$
$$T_1(\alpha_1,\alpha_2,\alpha_3)= f_{p1}(\alpha_1,\alpha_3) \quad \text{for} \quad \alpha_2=\varepsilon_{T1}. \tag{13}$$

Heat flux is transferred from the journal (rotational bearing surface) into the lubricant, hence we obtain boundary condition in the following form:

$$\frac{\partial T_1}{\partial \alpha_2} = -q_{c1} \quad for \quad \alpha_2 = 0. \tag{14}$$

For free heat exchange between the journal and lubricant and by virtue of Newton-Fourier law, then the dimensionless heat flux obtains the following form:

$$q_{c1} \equiv \frac{\zeta\varepsilon}{\kappa_o}\Delta f_1, \tag{15}$$

where:

ζ - heat transfer coefficient,
Δf_1 - dimensionless difference of temperature between journal temperature and ambient oil temperature.

By using the optimal function f of probability density distribution for the stochastic gap changes caused by the roughness, then the mean value of total film thickness $E(\varepsilon_{T1})$ and mean the value of pressure function $E(p_{10})$ are presented by virtue of the expectancy operator in the following form:

$$E(*)=\int_{-\infty}^{+\infty}(*)\times f(\delta_1)d\delta_1,\quad \sigma_1=\frac{c_1}{\sqrt{13}}=0{,}375,$$

$$f(\delta_1)\equiv\begin{cases}\left(1-\dfrac{\delta_1^2}{c_1^2}\right)^5 & for\ -c_1\le\delta_1\le+c_1,\\ 0 & for\ \ |\delta_1|>c_1,\end{cases}\tag{16}$$

where symbol $c_1=1{,}353515$ denotes the half total range of random variable of the thin layer thickness for normal hip joint. Symbol $\sigma_1=0{,}37539$ denotes the dimensionless standard deviation.

4. Particular solution of non-isothermal problem

Now we consider a particular case of the system of equations (1)-(4) in curvilinear coordinates for steady flow, various viscosity $\eta_1(\alpha_1,\alpha_2,\alpha_3)$, constant thermal conductivity coefficient $\kappa_1=1$, and Newtonian flow without magnetic effects, where centrifugal forces and convection forces are neglected and $(0<Re\psi Str<<1,\ 0<D_\beta Str<<1,\ 0<Re\psi<<1,\ 0<Gz<<1)$.

The particular dimensionless solution of the energy equation (4) under boundary conditions (12), (13), (14) has the following form:

$$T_1(\alpha_1,\alpha_2,\alpha_3)=1-q_{c1}\alpha_2-\int_0^{\alpha_2}\int_0^{\alpha_2}\eta_1\left[\left(\frac{\partial v_1}{\partial\alpha_2}\right)^2+\frac{1}{L_1^2}\left(\frac{\partial v_3}{\partial\alpha_2}\right)^2\right]d\alpha_2 d\alpha_2,\tag{17}$$

$0\le\alpha_1\le2\pi\theta_1$, $0\le\theta_1\le1$, $b_{m1}\le\alpha_3\le b_{s1}$, $0\le\alpha_2\le\varepsilon_{T1}\equiv\varepsilon_{p1}+u_{o2}+u_{o2B}$, $s\equiv\alpha_2/\varepsilon_{T1}$, $\varepsilon_{T1}=\varepsilon_{T1}(\alpha_1,\alpha_3)$, η_1 - const.

Dimensionless temperature on the internal sleeve surface has the following form:

$$f_{p1}(\alpha_1,\alpha_3)=T_1(\alpha_1,\alpha_2=\varepsilon_{T1},\alpha_3)=1-q_{c1}\varepsilon_{T1}-\int_0^{\varepsilon_{T1}}\int_0^{\alpha_2}\eta_1\left[\left(\frac{\partial v_1}{\partial\alpha_2}\right)^2+\frac{1}{L_1^2}\left(\frac{\partial v_3}{\partial\alpha_2}\right)^2\right]d\alpha_2 d\alpha_2\tag{18}$$

where:

$0\le\alpha_1\le2\pi\theta_1$, $0\le\theta_1\le1$, $b_{m1}\le\alpha_3\le b_{s1}$.

For the rotational journal we have $h_1=h_1(\alpha_3)$, $h_3=h_3(\alpha_3)$. Solutions of the partial differential equations (3) under the boundary conditions (12) have the following form [4], [5]:

$$v_1(\alpha_1,\alpha_2,\alpha_3)=\frac{1}{h_1}\frac{\partial p_1}{\partial\alpha_1}A_\eta+(1-A_s)h_1,\tag{19}$$

$$v_3(\alpha_1,\alpha_2,\alpha_3)=\frac{1}{h_3}\frac{\partial p_1}{\partial\alpha_3}A_\eta,\tag{20}$$

$$A_s \equiv \frac{\int\limits_0^{\alpha_2} \frac{1}{\eta_1} d\alpha_2}{\int\limits_0^{\varepsilon_{T1}} \frac{1}{\eta_1} d\alpha_2}, \quad A_\eta \equiv \int\limits_0^{\alpha_2} \frac{\alpha_2}{\eta_1} d\alpha_2 - A_s \int\limits_0^{\varepsilon_{T1}} \frac{\alpha_2}{\eta_1} d\alpha_2, \tag{21}$$

where:

$0 \le \alpha_1 \le 2\pi\theta_1$, $0 \le \theta_1 \le 1$, $b_{m1} \le \alpha_3 \le b_{s1}$, $0 \le \alpha_2 \le \varepsilon_{T1} \equiv \varepsilon_{p1} + u_{or1} + u_{o2B}$, $\varepsilon_{T1} = \varepsilon_{T1}(\alpha_1, \alpha_3)$, $\eta_1(\alpha_1, \alpha_2, \alpha_3)$.

Solutions of the continuity equations (15) under the boundary conditions (12.2) $v_2=0$ for $\alpha_2=0$ has the following form:

$$v_2(\alpha_1, \alpha_2, \alpha_3) = -\int\limits_0^{\alpha_2} \frac{1}{h_1} \frac{\partial v_1}{\partial \alpha_1} d\alpha_2 - \frac{1}{L_1^2} \int\limits_0^{\alpha_2} \frac{1}{h_1 h_3} \frac{\partial (h_1 v_3)}{\partial \alpha_3} d\alpha_2 .$$

(22)

We put the solutions (19), (20) in solution (22) and we take expected value of the both sides of the equation using the expectancy operator E. If we impose second boundary condition (12.2) for radial component of lubricant velocity i.e. $v_2=0$ for $\alpha_2=\varepsilon_{T1}$ then it is easy to see that the pressure function p_1 in the curvilinear coordinates (α_1, α_2, α_3) satisfies the following modified stochastic Reynolds equation:

$$\frac{1}{h_1} \frac{\partial}{\partial \alpha_1} \left[\frac{\partial p_1}{\partial \alpha_1} E\left(\int\limits_0^{\varepsilon_{T1}} A_\eta \right) d\alpha_2 \right] + \frac{1}{L_1^2} \frac{1}{h_3} \frac{\partial}{\partial \alpha_3} \left[\frac{h_1}{h_3} \frac{\partial p_1}{\partial \alpha_3} E\left(\int\limits_0^{\varepsilon_{T1}} A_\eta \right) d\alpha_2 \right] = h_1 \frac{\partial}{\partial \alpha_1} \left[E\left(\int\limits_0^{\varepsilon_{T1}} A_s \right) d\alpha_2 - E(\varepsilon_{T1}) \right]. \tag{23}$$

If oil dynamic viscosity is constant in gap height direction i.e. $\eta_1(\alpha_1, \alpha_3)$, then:

$$A_s = \frac{\alpha_2}{\varepsilon_{T1}} \equiv s, \quad \int\limits_0^{\varepsilon_{T1}} A_\eta d\alpha_2 = -\frac{\varepsilon_{T1}^3}{12\eta_1}, \quad \int\limits_0^{\varepsilon_{T1}} A_s d\alpha_2 - \varepsilon_{T1} = -\frac{1}{2}\varepsilon_{T1}. \tag{24}$$

Hence the stochastic Reynolds equation (23) tends to the following form:

$$\frac{1}{h_1} \frac{\partial}{\partial \alpha_1} \left[\frac{E(\varepsilon_{T1}^3)}{\eta_1} \frac{\partial p_1}{\partial \alpha_1} \right] + \frac{1}{L_1^2} \frac{1}{h_3} \frac{\partial}{\partial \alpha_3} \left[\frac{h_1}{h_3} \frac{E(\varepsilon_{T1}^3)}{\eta_1} \frac{\partial p_1}{\partial \alpha_3} \right] = 6 h_1 \frac{\partial E(\varepsilon_{T1})}{\partial \alpha_1} . \tag{25}$$

For cylindrical bearing we have $\alpha_1=\phi$, $\alpha_2=r_1$, $\alpha_3=z_1$ and dimensionless Lame coefficients are as follows $h_1=h_3=1$, where $L_1=b/R$, b - bearing length, R - radius of the journal. In this case the stochastic Reynolds equation (23) has the form:

$$\frac{\partial}{\partial \phi} \left[\frac{E(\varepsilon_{T1}^3)}{\eta_1} \frac{\partial E(p_1)}{\partial \phi} \right] + \frac{1}{L_1^2} \frac{\partial}{\partial z_1} \left[\frac{E(\varepsilon_{T1}^3)}{\eta_1} \frac{\partial E(p_1)}{\partial z_1} \right] = 6 \frac{\partial E(\varepsilon_{T1})}{\partial \phi}, \tag{26}$$

where:

$p_1(\varphi, z_1)$, $0 \le \varphi \le 2\pi$, $-1 \le z_1 \le 1$, $\varepsilon_{T1} = \varepsilon_{T1}(\varphi_1, z_1)$.

For the spherical bearing we have $\alpha_1=\phi$, $\alpha_2=r_1$, $\alpha_3=\vartheta_1$ and dimensionless Lame coefficients are as follows: $h_1=sin\vartheta_1$, $h_3=1$, $L_1=1$. In this case the dimensionless pressure function p_1 in the spherical coordinates (φ, ϑ_1) satisfies the modified Reynolds equation (25) in the form:

$$\frac{1}{sin\vartheta_1}\frac{\partial}{\partial\phi}\left[\frac{E(\varepsilon_{T1}^3)}{\eta_1}\frac{\partial E(p_1)}{\partial\phi}\right]+\frac{\partial}{\partial\vartheta_1}\left[\frac{E(\varepsilon_{T1}^3)}{\eta_1}\frac{\partial E(p_1)}{\partial\vartheta_1}sin\vartheta_1\right]=6\frac{\partial E(\varepsilon_{T1})}{\partial\phi}sin\vartheta_1, \tag{27}$$

where:

$$0\leq\phi<2\pi\theta_1,\ 0\leq\theta_1<1,\ \pi/8\leq\vartheta_1\leq\pi/2.$$

For the conical bearing we have $\alpha_1=\phi$, $\alpha_2=y_1$, $\alpha_3=x_1$ and dimensionless Lame coefficients are as follows: $h_1=x_1cos\alpha$, $h_3=1$, $L_1=b_c/R$, where α - angle between conical surface and the plane of cross section of the journal, b_c - the length of the cone generating line, R - radius of the journal. In this case the dimensionless pressure function p_1 in the conical coordinates (φ, y_1, x_1) satisfies the modified Reynolds equation (25) in the form:

$$\frac{1}{x_1}\frac{\partial}{\partial\phi}\left[\frac{E(\varepsilon_{T1}^3)}{\eta_1}\frac{\partial E(p_1)}{\partial\phi}\right]+\frac{cos^2\alpha}{L_1^2}\frac{\partial}{\partial x_1}\left[\frac{x_1E(\varepsilon_{T1}^3)}{\eta_1}\frac{\partial E(p_1)}{\partial x_1}\right]=6\frac{\partial E(\varepsilon_{T1})}{\partial\phi}x_1cos^2\alpha, \tag{28}$$

where:

$$0\leq\phi<2\pi\theta_1,\ 0\leq\theta_1<1,\ 0\leq x_1\leq 1,\ x_1=x/b_c.$$

In parabolic bearing we have the non monotone generating line of the journal in length direction. For the conical bearing we have: $\alpha_1=\phi, \alpha_2=y_1$, $\alpha_3=\chi_1$ and dimensionless Lame coefficients are as follows:

$$h_1=cos^2(\Lambda_1\chi_1),\quad h_3=\sqrt{1+4\Lambda_1^2 sin^2(\Lambda_1\chi_1)}\ cos(\Lambda_1\chi_1),\quad \Lambda_1\equiv\frac{1}{L_1}\sqrt{\frac{R-a}{R}}, L_1\equiv\frac{b_p}{R}, \tag{29}$$

where:

R - the largest radius of the parabolic journal,
a - the smallest radius of the parabolic journal,
$2b_p$ - the bearing length.

In this case the dimensionless pressure function p_1 in the conical coordinates (φ, y_1, χ_1) satisfies the modified Reynolds equation (25) in the following form:

$$\frac{\partial}{\partial\phi}\left[\frac{E(\varepsilon_{T1}^3)}{\eta_1}\frac{\partial E(p_1)}{\partial\phi}\right]+\frac{cos(\Lambda_1\chi_1)}{L_1^2\sqrt{1+4\Lambda_1^2 sin^2(\Lambda_1\chi_1)}}\frac{\partial}{\partial x_1}\left[\frac{cos(\Lambda_1\chi_1)}{\sqrt{1+4\Lambda_1^2 sin^2(\Lambda_1\chi_1)}}\frac{E(\varepsilon_{T1}^3)}{\eta_1}\frac{\partial E(p_1)}{\partial\chi_1}\right]=$$

$$=6\frac{\partial E(\varepsilon_{T1})}{\partial\phi}cos^4(\Lambda_1\chi_1),\quad |\chi_1|\leq\frac{1}{2\Lambda_1}arccos\sqrt{\frac{a}{R}}, \tag{30}$$

where:

$$0\leq\phi<2\pi\theta_1,\ 0\leq\theta_1<1, \chi_1=\alpha_3/R.$$

The dimensionless gap height ε_{T1} depends on the variable α_1 and α_3 and consists of two parts:

$$\varepsilon_{T1}=\varepsilon_{T1s}(\alpha_1\alpha_3)+\delta_1(\alpha_1\alpha_3,\xi), \tag{31}$$

where ε_{T1s} denotes the total dimensionless nominal smooth part of the geometry of thin fluid layer. This part of gap height contains dimensionless corrections of gap height caused by the hyper elastic deformations. Symbol δ_1 denotes the dimensionless random part of changes of gap height resulting from the vibrations, unsteady loading and surface roughness and asperities measured from the nominal mean level. Symbol ξ describes the random variable, which characterizes the roughness arrangement.

Using the probability function (31), then after calculations we obtain:

$$\begin{aligned} E(\varepsilon_{T1}) &= \int_{-c_1}^{+c_1} (\varepsilon_{T1s}+\delta_1) f(\delta_1) d\delta_1 = \varepsilon_{T1s}, \\ E(\varepsilon_{T1}^3) &= \int_{-c_1}^{+c_1} (\varepsilon_{T1s}+\delta_1)^3 f(\delta_1) d\delta_1 = \varepsilon_{T1s}^3 + 3\sigma_1^2 \varepsilon_{T1s}. \end{aligned} \tag{32}$$

5. Conclusions

The main achievements of this paper are the hydrodynamic pressure derivations for slide bearing journals in arbitrary curvilinear orthogonal coordinates and in particular case for cylindrical, spherical, conical, parabolic bearings with random conditions during the lubrication.

Acknowledgement:
The present research is financially supported within the frame of the TOK–FP6, MTKD-CT-2004-517226.

References

[1] Wierzcholski, K., *Analytical simulations of deformations for journal bearing gap*, Proc. of Third Inter. Congress on Thermal Stresses, Vol. 1, pp. 391-394, Cracow 1999.

[2] Wierzcholski, K., *Non Isothermal Lubrication for Viscoelastic Ferromagnetic Oils*, Proc. of Thermal Stresses, Fourth Inter. Congress on Thermal Stresses, pp. 613-616, Osaka 2001.

[3] Wierzcholski, K., *Ferromagnetic Turbulent Lubrication for Thermoelasticity Deformations of Bearing Gap*, Proc. of Thermal Stresses, The Fifth Inter. Congress on Thermal Stresses, WA4-3, pp. WA4-3-1– WA4-3-4, Blacksburg, Virginia USA 2003.

[4] Wierzcholski, K., The *Method of Solving of the System of non-Linear Differential Equations for non-Isothermic Laminar non-Newtonian Flow in the Thin Layer Between Two Certain Surfaces*, (in Polish), Scientific Papers of the Institute of Machine Design and Operation Studies and Research - *The boundary integral equation method in fluid mechanics*, Technical University of Wrocław, Nr 59, Ser. Nr 26, pp. 134 -144, Wrocław 1993.

[5] Wierzcholski, K., *Contribution to the analytical solutions of non linear basic equations for ferrolubricant flow in a film between two non rotational surfaces*, 7-th International Symposium on System Modelling Control, Polish Cybernetical Society, Vol. 2, pp. 286-291, Zakopane 1993.

PRESSURE AND CAPACITY DISTRIBUTIONS IN DEFORMABLE SPHERICAL SLIDE BEARING GAPS

K. Wierzcholski, A. Miszczak

Department of Basic Engineering, Maritime University of Gdynia
ul. Morska 83, 81-225 Gdynia, Poland
tel. +48 58 6901348, fax: +48 58 6901399
e-mail: wierzch@am.gdynia.pl; miszczak@am.gdynia.pl

Abstract

This paper presents the pressure and capacity distributions in a thin layer of non-Newtonian, viscoelastic, lubricant inside the slide spherical bearing. Non-isothermal, unsteady and random flow conditions and thermal deformations of the bearing surfaces are taken into account. This problem finds application in ship power plants, electric locomotive designing, and precision engineering.

Keywords: *time depended hydrodynamic pressure, capacity distributions in spherical bearings*

1. General assumptions

This paper presents the general analysis of the pressure and capacity distributions for unsteady non isothermal flow of visco-elastic oil within the gap between two rotational spherical deformed bearing surfaces in random conditions (see Fig.1).

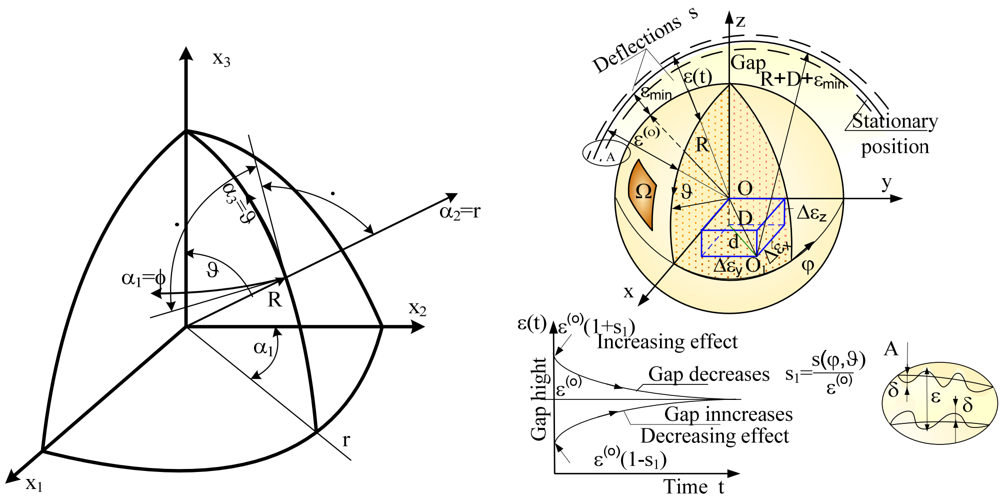

Fig.1. Spherical geometry on the spherical journal

We take into account following assumptions:

- unsteady asymmetrical oil flow in spherical bearing gap,
- spherical bearing gap changes in circumferential and meridional directions,
- hyper-elastic and random deformations of bearing surfaces.

The time- dependent, gap- height with impulsive perturbations has the following form [1]:

$$\varepsilon_{T1} = \varepsilon_{T1s}(\phi,\vartheta_1,t_1) + \varepsilon_{33}(t_1) = \varepsilon_{T1s}(\phi,\vartheta_1)\,[1+s_1 \exp(-t_o t_1 \omega_o)] + \varepsilon_{33} = \varepsilon_{T1s}(\phi,\vartheta_1,t_1) + p(t)/E_{33} =$$
$$= \varepsilon_{T1s}(\phi,\vartheta_1,t_1) + Ca\, p_{10}(t_1), \tag{1}$$

where

ε_{33} – dimensionless corrections caused by the hypo-elastic deformations in the gap-height directions,
$Ca=p_o/E_{33}$ – Cauchy number,
p_o – characteristic value of hydrodynamic pressure.

The time- independent part of value of gap- height for smooth bearing surfaces without deformations has the dimensional form: $\varepsilon_o\, \varepsilon_{T1s}(\phi,\vartheta_1)$.
If we take into account the unsteady effects in impulsive motion, then from the stochastic Reynolds equation presenting in spherical coordinates in papers [1], [2], [3], [4] it follows:

$$\frac{1}{\sin\vartheta_1}\frac{\partial}{\partial\phi}\left[\frac{E(\varepsilon_{T1}^3)}{\eta_1}\frac{\partial E(p_1)}{\partial\phi}\right] + \frac{\partial}{\partial\vartheta_1}\left[\frac{E(\varepsilon_{T1}^3)}{\eta_1}\frac{\partial E(p_1)}{\partial\vartheta_1}\sin\vartheta_1\right] =$$
$$= 6\frac{\partial E(\varepsilon_{T1})}{\partial\phi}\sin\vartheta_1 + 12 Str\frac{\partial E(\varepsilon_{T1})}{\partial t_1}\sin\vartheta_1, \tag{2}$$

In numerical calculations we use the real values of Young modulus and Poisson's ratio of bearing soft material. We obtain from that the total Young modulus of bearing soft material in perpendicular direction to the sliding surface, has the value $E_{33}=0,1\ GPa$.

During the impulsive motion the dimensionless pressure p_1 in the lubrication region Ω: $\{0<\phi<\pi,\ \pi/8\le\vartheta_1\le\pi/2\}$ is determined by virtue of the modified Reynolds equations (2). The gap height (1), is taken into account.

2. Numerical calculations

The numerical calculations are performed in Matlab 7.2 by means of the finite differences method. In the calculations we assume: the radius of spherical journal R=0.025 *m*, angular velocity of the impulsive perturbations of bearing sleeve $\omega_o=15\ s^{-1}$, characteristic dimensional time $t_o=0.00001\ s$. To obtain real values of time we must multiply the dimensionless values t_1 by the characteristic time value $t_o=0.00001\ s$. For example $t_1=100000$ denotes one second after impulse.

We assume the following eccentricities of spherical journal: $\Delta\varepsilon_x=4.0\ \mu m$, $\Delta\varepsilon_y=0.5\ \mu m$, $\Delta\varepsilon_z=3\ \mu m$ and the characteristic gap-height value $\varepsilon_o=10\ \mu m$. Moreover we assume the following quantities: the dynamic viscosity of oil $\eta_o=0.030\ Pas$, pseudo-viscosity coefficient $\beta=0.0000002\ Pas^2$, density of the lubricant $\rho=890\ kg/m^3$, angular velocity of spherical journal $\omega=157\ s^{-1}$. The average minimum gap- height ε_{min} changes within the time interval $0.00001\ s\le t\le 10\ s$ and attains values from 6.1 μm to 10.1 μm; the average relative radial clearance amounts to $\psi\equiv\varepsilon_o/R=0.0004$.

Under the above assumptions we obtain the characteristic dimensional value of pressure $p_o=29.452431\ MPa$, Cauchy Number Ca=0.295, Strouhal Number Str=636.6 and additionally: $Re\cdot\psi\cdot Str=0.297$, $De\cdot Str=0.667$. In this case we have $0\le\beta/\eta_o t<1$. For the dimensionless time values: $t_1=1$, $t_1=10000$, $t_1=1\ 000\ 000$, i.e. for the dimensional time values: t=0.00001 *s*; t=0.1 *s*; t=10.0 *s*, respectively, the dimensionless pressure distributions are presented in Fig. 2 (for $s_1=+1/4$), in Fig.3 (for $s_1=-1/4$) without hypo-elastic deformations of bearing soft material (the left column of Fig. 1, and Fig. 3 for Ca=0.00) and with hypo-elastic deformations of bearing soft material (the right column of Fig. 1, and Fig. 2 for Ca=0.295).

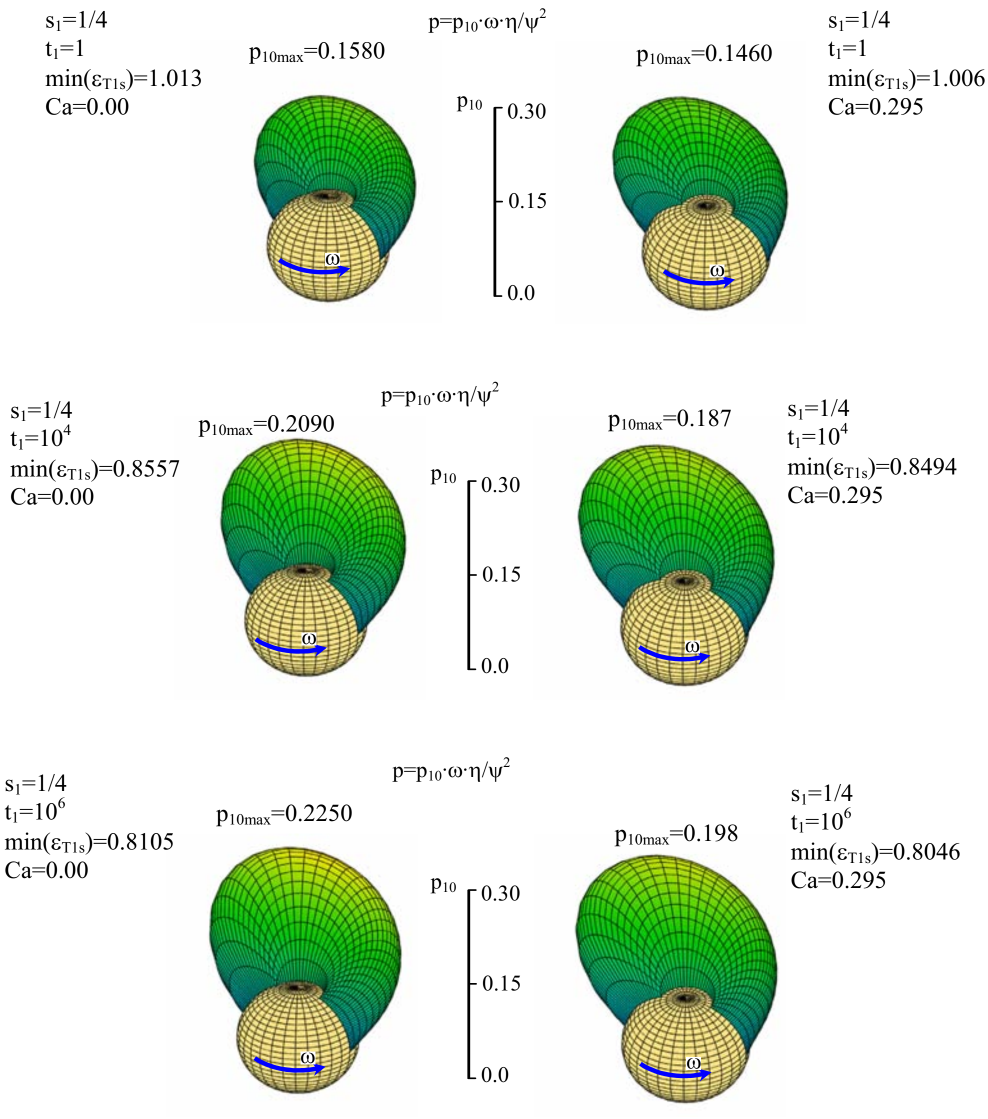

Fig. 2. Dimensionless hydrodynamic pressure distributions inside the gap of spherical bearing without bearing soft material deformations (the left column of figures for Ca=0.00) and with hypo-elastic soft material deformations (the right column of figures for Ca=0.295) in the region Ω: $0\le\varphi\le\pi$, $\pi R/8\le\vartheta\le\pi R/2$, for the dimensionless time values: $t_1=1$ (i.e. t=0.00001 s), $t_1=1\ 0\ 000$ (i.e. t=0.1 s), and $t_1=1\ 000\ 000$ (i.e. t=10 s) after the moment of the impulse causing first an increase and then a decrease of the gap height ($s_1=+1/4$).
The results were obtained for the following data:
$R=0.025$ m; $\eta_o=0.030$ Pas; $\rho=890$ kg/m^3; $p_o=29.452$ MPa, $\varepsilon_o=10$ μm; $\Delta\varepsilon_x=4$ μm; $\Delta\varepsilon_y=0.5$ μm; $\Delta\varepsilon_z=3$ μm; $\psi\equiv\varepsilon_o/R\approx0.0004$; $\omega=157$ s^{-1}; $\omega_o=15$ s^{-1}; Str=636.6; Re·ψ·Str=0.297; De·Str=0.667

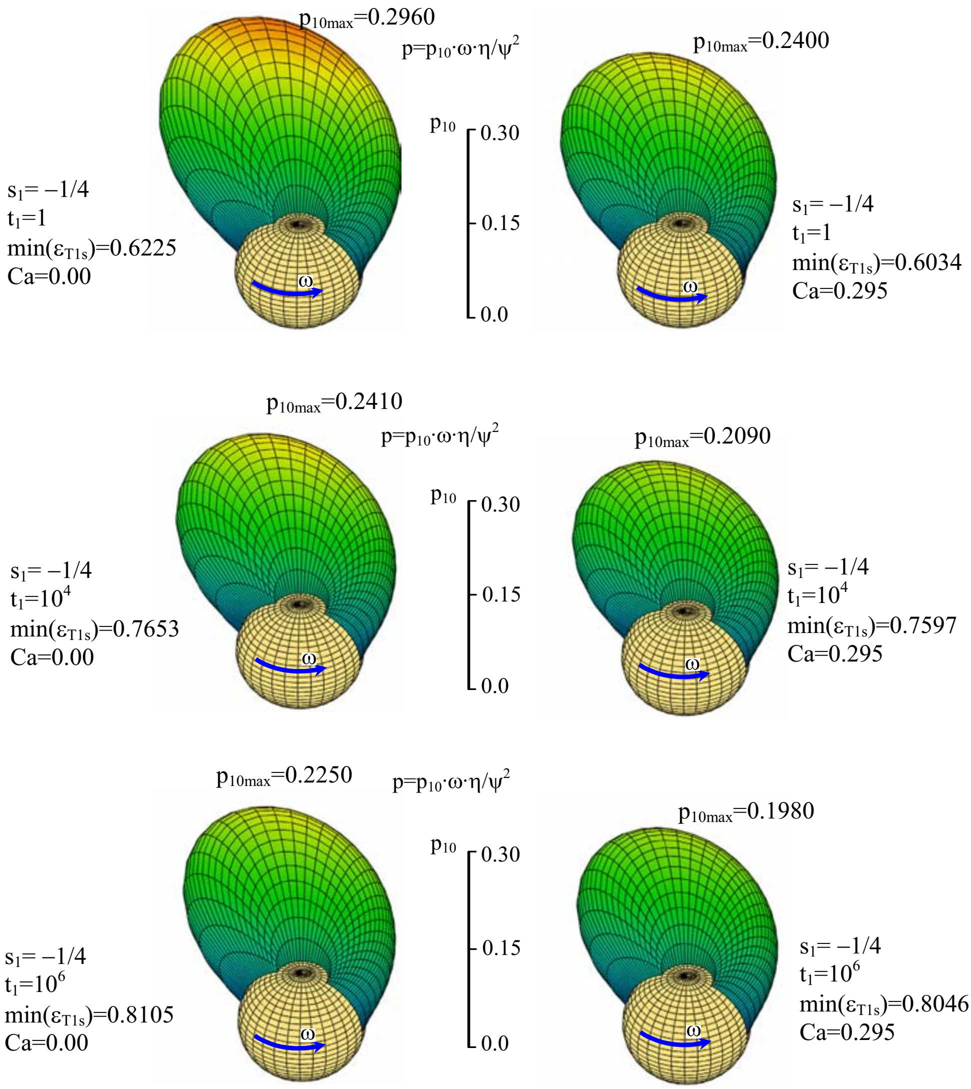

Fig. 3. Dimensionless hydrodynamic pressure distributions inside the gap of spherical bearing without bearing soft material deformations (the left column of figures for Ca=0.00) and with hypo-elastic soft material deformations (the right column of figures for Ca=0.295) in the region Ω: $0\le\varphi\le\pi$, $\pi R/8\le\vartheta\le\pi R/2$, for the dimensionless time values: $t_1=1$ (i.e. t=0.00001 s), $t_1=1\ 0\ 000$ (i.e. t=0.1 s), and $t_1=1\ 000\ 000$ (i.e. t=10 s) after the moment of the impulse causing first an decrease and then a increase of the gap height, for $s_1= -1/4$.
The results were obtained for the following data:
$R=0.025$ m; $\eta_o=0.030$ Pas; $\rho=890$ kg/m^3; $p_o=29.452$ MPa, $\varepsilon_o=10$ μm; $\Delta\varepsilon_x=4$ μm; $\Delta\varepsilon_y=0.5$ μm; $\Delta\varepsilon_z=3$ μm; $\psi\equiv\varepsilon_o/R\approx0.0004$; $\omega=157$ s^{-1}; $\omega_o=15$ s^{-1}; Str=636.6; Re·ψ·Str=0.297; De·Str=0.667

To obtain dimensional values of pressure we must multiply the dimensionless values indicated in Fig. 2, 3 by the factor $p_o=\omega\eta/\psi^2$.

The case of Ca=0.295 presents the influence of soft material deformations on the pressure values. The pressure values for Ca=0.295 are obtained in 6 steps. We assume the dimensionless pressure values p_{10}~$p_{10(1)}$ obtained from Eq. (2) for Ca=0.00 i.e. values of the pressure without influences of bearing soft material deformations, to be the first step of the pressure calculations. The dimensionless values $p_{10(1)}$ are multiplied by the non- zero Cauchy Number Ca and hence we obtain the dimensionless gap-height in the form: ε_{T1s}+Ca $p_{10(1)}$. For this dimensionless gap- height, from Eq. (2) we obtain the dimensionless pressure values p_{10}~$p_{10(2)}$ as the next step of the pressure calculations. The dimensionless values $p_{10(2)}$ are multiplied by the non-zero Cauchy Number Ca and hence we obtain the dimensionless gap-height in the form: ε_{T1s} +Ca $p_{10(2)}$. For this gap-height, from Eq. (2) we obtain the dimensionless pressure values p_{10}~$p_{10(3)}$ as the third step of the pressure calculations. The obtained series describing the dimensionless pressure values is convergent to the dimensionless boundary value of the pressure p_{10}. The dimensionless pressure value $p_{10(6)}$ obtained in sixth step of calculations can be found in the neighborhood of the dimensionless value of pressure p_{10}, where we have the inequality:

$$\frac{\left|p_{10(5)} - p_{10(6)}\right|}{\left|p_{10(6)}\right|} \leq 0.1\%$$

Fig. 4 presents the dimensional capacity distributions versus dimensional time in seconds in logarithmic scale (Fig. 4a) and in decimal gradation (Fig. 4b).

The numerical values of capacity are calculated for the following dimensionless times: t_1=1, t_1=10, t_1=50, t_1=100, t_1=500, t_1=1 000, t_1=2 000, t_1=4 000, t_1=6 000, t_1=8 000, t_1=10 000, t_1=20 000, t_1=40 000, t_1=60 000, t_1=80 000, t_1=100 000, t_1=1 000 000 i.e. for the dimensional times: t=0.00001 *s*; t=0.0001 *s*; t=0.0005 *s*; t=0.001 *s*; t=0.005 *s*; t=0.01 *s*; t=0.02 *s*; t=0.04 *s*; t=0.06 *s*; t=0.08 *s*; t=0.1 *s*; t=1.0 *s*; t=10.0 *s*, respectively. The first two curves depicted in the upper part of Fig. 3a and Fig. 3b, show the dimensional capacity values obtained without taking into account soft material deformations for Ca=0.00. The first two curves in the lower part of Fig. 3a and Fig. 3b, show the dimensional capacity values obtained for bearing soft material deformations with Ca=0.295. The upper curve of each two curves in Fig.3a and Fig. 3b denotes the dimensional capacities obtained for s_1=–1/4. The lower curve of each two curves in these figures denotes the dimensional capacities obtained for s_1=+1/4.

If the gap height increases (s_1>0) due to the impulse, then in the time after impulse the gap-height decreases and the pressure increases. In a sufficiently long time after impulse the gap-height and pressure attains the time- independent values of gap height and pressure, respectively.

If the gap height decreases (s_1<0) due to the impulse, then in the time after impulse the gap height increases and the pressure decreases. In a sufficiently long time after impulse the gap height and pressure attains the time- independent values of gap height and pressure, respectively.

If the time distant after the impulse moment is long enough, i.e. for $t_1\rightarrow\infty$, then the pressure distributions for the increasing (s_1>0) and decreasing (s_1<0) effects of gap height changes caused by the bearing surface roughness, tend to identical pressure distributions. This limit of pressure distribution can be also obtained from the pseudo-classical Reynolds equation (2).

Pressures in joint gap attain identical distributions only when in both cases: s_1>0, s_1<0 the gap height gains the same but not durable damages in a sufficiently long time after impulse.

From the terms multiplied by the Cauchy number Ca in the formula (1) it follows that we can obtain durable and not identical deformations of joint gap height if the number Ca attains not the same values for s_1>0, s_1<0 in an enough long time after impulse moment.

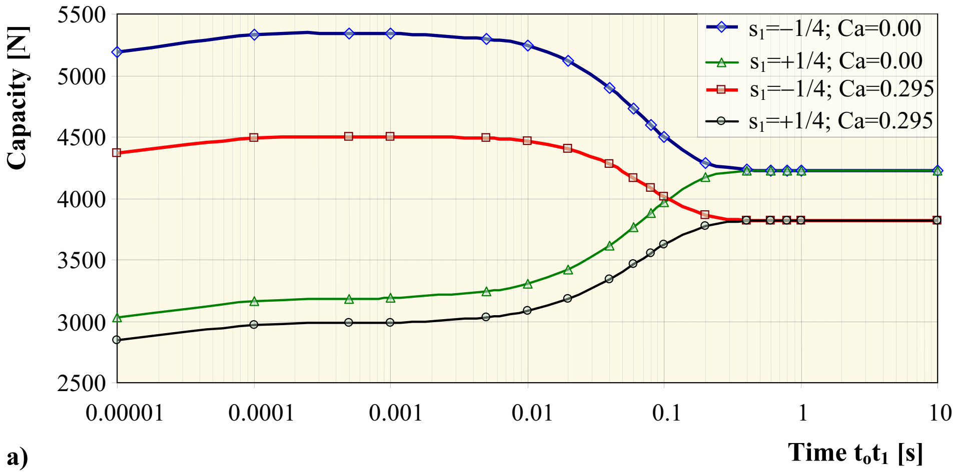

a)

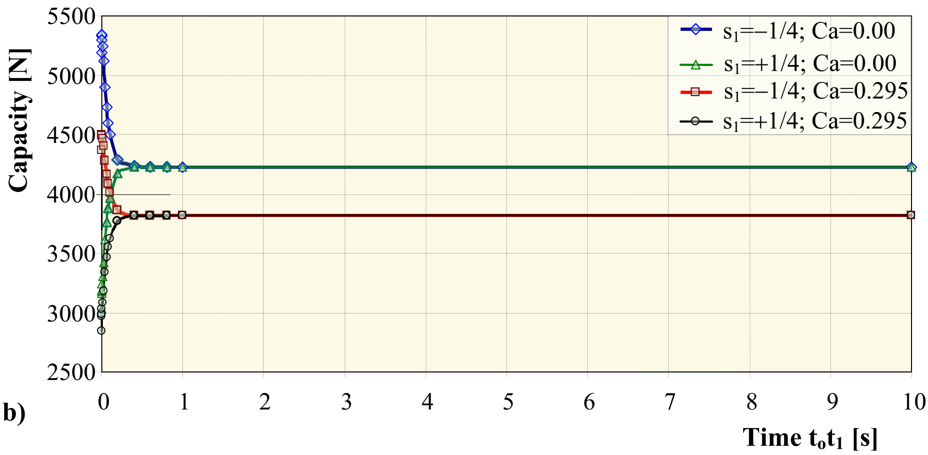

b)

Fig. 4. Dimensional capacity distributions inside the gap of human spherical hip joint, in the region Ω: $0\le\varphi\le\pi$, $\pi R/8\le\vartheta\le\pi R/2$ versus dimensional time values from 0.00001 s to 10 s after impulse, expressed in logarithmic scale (Fig. 3a), and in decimal time scale (Fig. 3b).
The results were obtained for the following data: R=0.025 m; η_o=0.030 Pas; ρ=890 kg/m^3; ε_o=10 μm; $\Delta\varepsilon_x$=4 μm; $\Delta\varepsilon_y$=0.5 μm; $\Delta\varepsilon_z$=3 μm; $\psi\equiv\varepsilon_o/R\approx0.0004$; ω=157 s^{-1}; ω_o=15 s^{-1}; Str=636.6; Re$\cdot\psi\cdot$Str=0.297; De$\cdot$Str=0.667

3. Conclusions

◇ If bearing soft material deformations are neglected and the stroke increases (decreases) the bearing gap height, then the gap decreases (increases), i.e. it returns to its initial shape in the time interval from 0.00001 *s* to the 10.0 *s*. For this case the pressure distributions are presented in the left column of Fig. 2 (Fig.3). In two above cases, a hundred seconds after injury the pressure attains the same values (see the lower figure in the left column of Fig. 1 and Fig. 3).

◇ If bearing soft material deformations are taken into account and the stroke increases (decreases) the bearing gap height, then the gap decreases (increases), i.e. it returns to its initial shape but with the same bearing soft material deformations in the time interval from 0.00001 *s* to the 10 *s*.

For this case the pressure distributions are presented in the right column of Fig. 2 (Fig. 3). In two above cases, a hundred seconds after injury the pressure attains the same values (see the lower figure in the right column of Fig. 2 (Fig. 3).

◇ The pressure distributions in the right column of figures of Fig. 2 and Fig. 3 are of much smaller values than those of the pressure distributions in the left column of figures of Fig. 2 and Fig. 3. From this fact it follows that the pressure distributions obtained without bearing soft material deformations are of greater values than those of the pressure distributions in spherical bearing with soft material deformations in every moment after injury within the time interval from 0.00001 *s* to 10 *s*.

◇ The spherical bearing capacity with bearing soft material deformations taken into account is much smaller than that obtained for not deformable bearing surface.

◇ The greatest changes in the capacity of spherical bearing are attained within the time interval from 0.01 *s* to 0.3 *s* after injury. In the time interval from 0.00001 *s* to the 0.01 *s* after injury, the capacities are not changed, irrespective of whether the gap height increases or decreases due to the stroke.

References

[1] Wierzcholski, K., *Stochastic contributions on the pressure in slide bearing gaps after impulse,* Diesel & Gas Turbine Proceedings 2007, V International Scientific–Technical Conference, Gdańsk-Stokholm-Tumba, in print.

[2] Wierzcholski, K., *Analytical simulations of deformations for journal bearing gap*, Proc. of Third Inter. Congress on Thermal Stresses, Vol. 1, pp. 391-394, Cracow 1999.

[3] Wierzcholski, K., *Non Isothermal Lubrication for Viscoelastic Ferromagnetic Oils*, Proc. of Thermal Stresses, Fourth Inter. Congress on Thermal Stresses, pp. 613-616, Osaka 2001.

[4] Wierzcholski, K., The *Method of Solving of the System of non-Linear Differential Equations for non-Isothermic Laminar non-Newtonian Flow in the Thin Layer Between Two Certain Surfaces*, (in Polish), Scientific Papers of the Institute of Machine Design and Operation Studies and Research - *The boundary integral equation method in fluid mechanics*, Technical University of Wrocław, Nr 59, Ser. Nr 26, pp. 134-144, Wrocław 1993.

THE EFFECT OF TEMPERATURE ON THE PROPERTIES OF FUEL-WATER EMULSION APPLIED FOR FEEDING MARINE COMBUSTION ENGINES

Ryszard Zadrąg

Naval University of Gdynia
Mechanical-Electric Faculty
ul. Śmidowicza 69; 81-103 Gdynia
tel. +48 58 626 28 29
e-mail: zadra_g@wp.pl

Abstract

Delivering water to cylinders is a means of restricting the emergence of nitrogen oxides in the combustion process in SI engines. In consequence of feeding the engine with fuel-water emulsion with simultaneous decrease of nitrogen oxides in the exhaust gases, there occur changes in the concentrations of: carbon oxide, hydrocarbons, solid particles, and also changes in the basic indexes of engine work. The values of these changes depend in large degree on the assumed method of producing emulsion. Depending on the method applied there exists a definite set of control parameters characteristic for each method, whose values of particular parameters determine the properties of emulsion produced. One of these parameters is the temperature of, essential insomuch as it can be controlled in a simple way.

The work presents the results of research on the effect of temperature of fuel-water emulsion produced in a helicoidal agitator on its properties, essential from the point of view of NO_x emission load in the exhaust gases.

Keywords: *marine diesel engine, emission of toxic compounds, fuel-water emulsion*

1. Introduction

One of the factors determining the further development of combustion engines, marine ones included, are the ever sharpened criteria of toxic compounds emission. A way of ensuring fulfilment of the ever more strict requirements is the constant improvement of the combustion process in the whole range of the engine's work, not excluding non-stationary states and the transitory states connected with them.

An ever more frequently applied method of actively influencing the combustion process is supplying water to the cylinders, aimed at decreasing the maximum values of combustion temperature in the cylinder. A method of supplying water to the cylinders is the injection of fuel-water emulsion by a standard but more efficient injector [3,9].

In the author's opinion, the application of fuel-water emulsion ensures the largest effect of NO_x emission, with simultaneous complete control of combustion process in the cylinder. This is due to the fact, among other things, that the injected water contained in the emulsion is supplied directly to the flame zone in the cylinder, i.e. the area where the nitrogen oxides are directly produced [1,9].

The selection of composition and methods of producing fuel-water emulsion remains an essential topic. In the case of selecting the composition of fuel-water emulsion for a particular engine (with definite features of utilization process), what becomes essential is such selection of emulsion that with the required toxic compounds emission level the engine's operational parameters should possibly be affected as little as possible [4,5,6,7].

An equally important problem is obtaining significant emulsion stability, which is small by nature. Attempts are made to improve this condition by applying various methods of its production. Depending on the method applied there is a set of control parameters characteristic for each method, determining the properties of emulsion produced [4,5]. The physical state of emulsion already produced is not without significance either, among which temperature is a very essential factor, conditioning the degree of emulsion comminution, but simultaneously affecting the unfavourable process of secondary emulsion.

2. Properties of fuel-water emulsion

As mentioned before, fuel-water emulsion is characterised by small stability, which is a result of considerable differences in the chemical construction of water and hydrocarbons. Oil-related fuels, propulsion fuels included, evince limited ability to mix with water. The solubility of water in fuels of this type depends mainly on their fractional composition (particularly the content of aromatic hydrocarbons) and temperature. It is assumed that the amount of water dissolved in hydrocarbons of $20^{o}C$ temperature does not exceed 582 ppm. With the increase of temperature there increases the solubility of water in hydrocarbons, particularly aromatic ones. After passing the solubility threshold, when the diameter of water droplets reaches the value of 0.1 μm, fuel-water emulsion forms a typical two-phase system. From the balance of various influences in both phases there results the value of free energy of phase distribution surface, that is interfacial tension. The surface tension of fractions and kerosene products depends on their molar mass, hydrocarbon composition and the presence of surface-active compounds.

The formation of water emulsion in kerosene fuel consists in the comminution of water with total area A_1 to small droplets with area A_2, i.e. $A_2 > A_1$ [8]. Thus, the increment of total area of dispersed phase is equal to

$$\Delta A = A_2 - A_1 \tag{1}$$

Assuming that the value of interfacial tension coefficient in the system remains constant, the thermodynamic condition of emulsion formation can be written down as

$$\Delta G^{tw} = \sigma_{HW} \cdot \Delta A - T \cdot \Delta S \tag{2}$$

where:

ΔG^{tw} – change of thermodynamic potential of emulsion formation,
σ_{HW} – interfacial tension coefficient at the water – hydrocarbon phase boundary,
ΔS – change of system entropy.

As the increment of interfacial surface and the value of interfacial tension and entropy change are positive values, and also

$$\sigma_{HW} \cdot \Delta A > -T \cdot \Delta S, \tag{3}$$

so

$$\Delta G^{tw} > 0 \tag{4}$$

This signifies that emulsion formation does not occur spontaneously, but requires energy supply from outside the system.

In the presence of certain surface-active compounds (emulsifiers), interfacial tension is reduced. An emulsifier in the two-phase system decreases the energy required for water comminution, initiates the formation of a boundary layer around the new water droplets and eventually increases the stability (durability) of emulsion.

Emulsifying water in the fuel takes place in two stages: comminution of water droplets and emulsion stabilisation. In general, water comminution takes place by deformation of the droplets to unstable cylinders with such size that they disintegrate spontaneously. The stabilisation of emulsion takes place in result of formation on water droplet surface of an adsorptive-solvate layer by a surface-active compound (surfactant).

In the descriptions of patents and specialist literature a very large number of surfactants are mentioned, which are suggested as water emulsifiers in propulsion oil. This signifies lack of uniform recipes for additives efficiently influencing the formation and stabilisation of the system. It should also be underlined that engine propulsion oils are similar as to composition and properties, independently of location and method of production. Emulsifiers evince rather low effectiveness, which is testified by the amounts added to obtain fairly stable emulsions (for example 2 – 3 % for emulsion with 10 % water content). Even larger amounts of surfactants are added for the formation of microemulsion (0.5 to 2 parts for each part of water added to the fuel).

To sum up, with regard to combustion in the cylinder the most important features of fuel-water emulsion are viscosity, dispersion degree and stability.

Viscosity affects energetic inputs attendant on mixing and transporting emulsified fuel, first of all the quality of emulsion dispersion in the engine's combustion chamber. Emulsion viscosity depends mainly on water content, the system's dispersion degree, temperature and the properties of the emulsifier. Water content up to 20 % of total emulsion volume slightly exceeds viscosity of the emulsion in relation to fuel viscosity. With water content of 40 % and more viscosity rapidly increases up to the gel stage and subsequently the system's inversion.

From stability point of view, combustion in particular, dispersion degree and homogeneity of water emulsion in the fuel are very important. The maximal diameter of water particles should not exceed the droplet diameter of emulsion sprayed. Water dispersion degree depends then on the spraying quality of emulsion in the cylinder. On this condition the droplets of emulsion sprayed consist of water surrounded by a layer of hydrocarbons and emulsifier. It is assumed that the diameter of water droplets should not exceed 10 μm, and their main part should be contained in the range of 2 – 3 μm. If the emulsion contains water droplets larger than the diameter of droplets formed in result of spraying by the injector, there comes direct contact in the cylinder of water with the combustion chamber walls, and consequently to deterioration of combustion conditions.

One of emulsion stability aspects is its resistance to low and high temperatures. Emulsions with high water contact are particularly sensitive. Exceeding the limit values of temperature causes inversion of phases or the disintegration of emulsion into separate components of fuel and water.

The emulsion's high resistance to the effects of heightened temperature is enhanced by high fuel viscosity and high degree of water dispersion. Resistance to the effects of lowered temperature is obtained by the addition of small amounts of aliphatic alcohols.

As mentioned before, the formation of emulsions does not take place spontaneously, but requires energy supply from outside the system. The most effective means of emulsifying water in fuels for engines with self-ignition is introducing it beneath the surface of propulsion oil. For the production of emulsion rotational devices are used: disc dispersants, mixers, ultrasonic, cavitational, injector devices, helicoidal agitators etc.

In the case of helicoidal agitator the properties of obtained fuel-water emulsion depend on the agitators setting parameters [10]. These are: rotational speed of the rotor, slot height in the agitator and efficiency understood as total stream of fuel and water mass flowing through the agitator.

3. Research on the effect of temperature of fuel-water emulsion production on its properties

The purpose of the experiment was to find the dependence of the effect of input values, i.e. rotational speed of the rotor – E and the fuel-water emulsion temperature – T on changes in output parameters. Elements of the output values set are: number of droplets, size of droplets (understood as their diameter) and dispersion degree.

During the experiment emulsion was produced described with complete plan 3^3, and subsequently microscopic photographs were taken of samples taken during the experiment. Analysis of particular photographs made it possible to obtain a set of water droplets, for which set its amount was determined and a division was made into populations of droplets with various diameters into classes. A comparison of results has been presented in Table 1.

Tab. 1. Comparison of water droplet amounts in particular classes

Number of measurement system	Amount of water droplets in emulsion in particular classes							
	P1	P2	P3	P4	P5	P6	P7	P8
	(…-0.2> [μm]	(0.2 - 0.4> [μm]	(0.4 - 0.6> [μm]	(0.6 - 0.8> [μm]	(0.8 - 1.0> [μm]	(1.0 - 1.2> [μm]	(1.2 - 1.4> [μm]	(1.4-…> [μm]
1	17	11	12	5	0	0	0	0
2	11	8	10	3	6	6	4	0
3	41	10	7	7	5	1	1	7
4	34	13	16	9	3	1	2	2
5	6	18	7	4	3	3	1	1
6	49	22	6	5	3	1	1	13
7	68	57	46	24	7	0	0	0
8	66	36	12	18	24	2	0	0
9	54	26	7	4	2	0	0	18
10	36	21	10	10	4	12	6	5
11	40	38	7	7	2	4	6	6
12	38	24	7	4	2	0	6	10
13	48	27	21	14	7	6	4	3
14	57	49	27	14	12	2	1	2
15	64	44	6	10	4	2	1	14
16	56	41	16	9	3	3	7	12
17	74	37	32	24	14	6	3	1
18	31	27	8	8	9	10	16	17
19	42	28	18	7	6	1	0	0
20	66	58	17	9	4	4	5	7
21	86	61	21	7	3	1	1	9
22	44	67	46	42	12	3	4	6
23	98	44	21	12	8	7	1	0
24	71	51	6	4	2	0	2	9
25	69	46	44	21	11	3	3	4
26	48	40	12	4	6	6	6	8
27	61	14	7	3	1	2	1	15

In connection with the large amount of information contained in the microscopic photographs, decomposition of the research object was performed by creating two models, each research model being characterised by one output value (Fig. 1, 2).

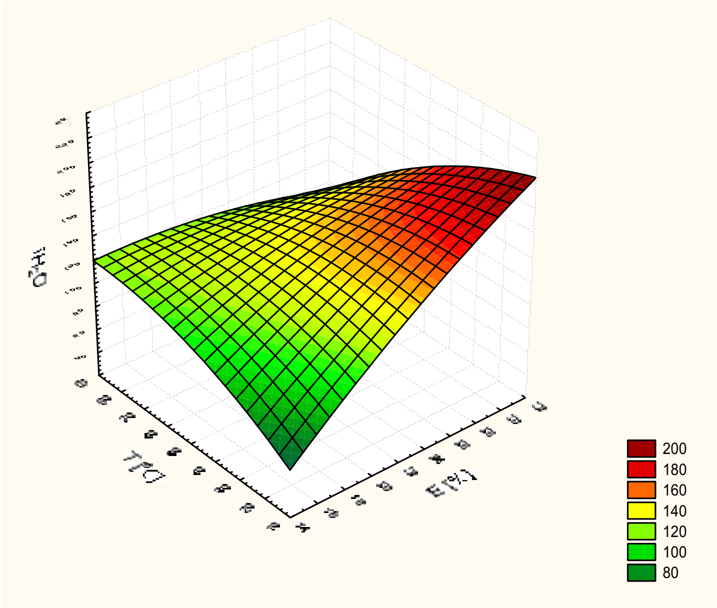

Fig. 1. Dependence between percentage concentration of emulsion, emulsion temperature and the amount of water droplets in area researched, where T- temperature [°C], E- emulsion concentration [%], iH_2O – amount of water droplets in the researched area

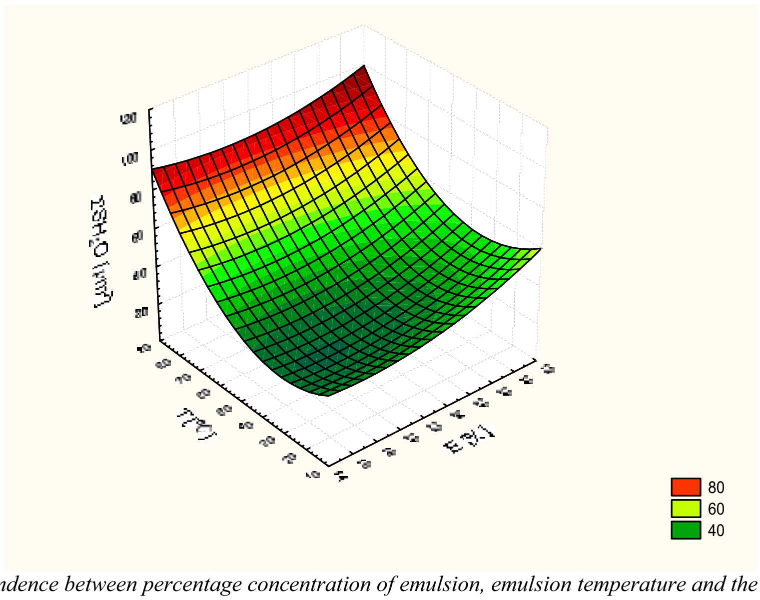

Fig. 2. Dependence between percentage concentration of emulsion, emulsion temperature and the sum of water droplet surfaces in area researched, where T- temperature [°C], E- emulsion concentration [%], ΣSH_2O – summary area of water droplets on researched surface [μm^2]

The first of suggested models presents the dependence of input parameters (rotational speed of agitator rotor – n, percentage concentration of emulsion – E, emulsion temperature – T) for the total amount of water droplets in the photograph (iH_2O) (Fig. 1). The second model, on the other hand, presents relations between input parameters and the sum of areas of all water droplets ($\Sigma S\ H_2O$) (Fig. 2).

During analysis of the experimental material collected, secondary emulsion formation was found in samples of measurement systems of the experiment plan described by the highest temperature. This process manifests itself by the increment of water droplet diameter in the emulsion. Therefore it was determined to examine this problem additionally by making a third model, which presents the relations between input parameters and the sum of droplet areas for classes P5-P8 (Table 1) in the control area.

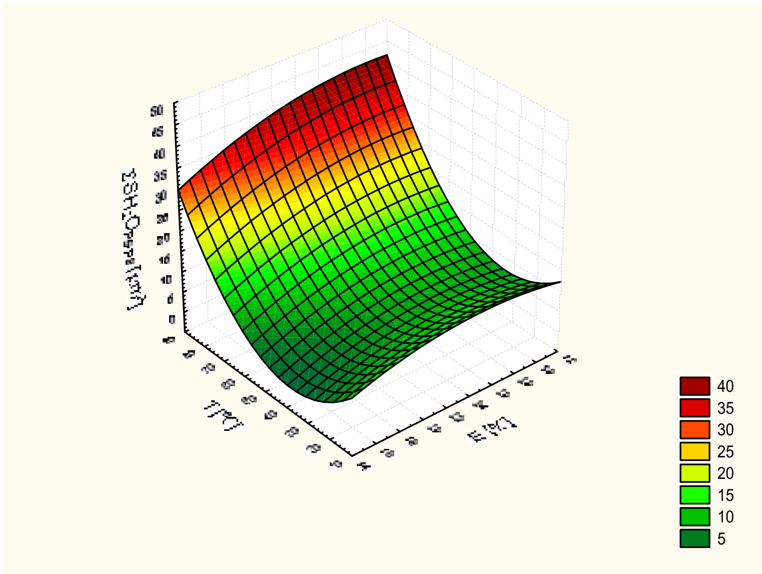

Fig. 3. Dependence between emulsion concentration, its temperature and the sum of droplet areas Σ H_2O classes P5-P8, where: T- temperature, E- emulsion concentration, ΣS H_2O $_{P5\text{-}P8}$ – sum of water droplet areas classes P5-P8 [μm.^{2}] acc. to Table 1

Analysis of Figures 1, 2 and 3 confirmed, in accordance with expectations, a significant effect of the temperature of fuel-water emulsion formation on its parameters. Thus, the temperature of fuel-water emulsion directly translates both into water droplets amount and the area occupied by those droplets. The character of changes in the physical properties of fuel-water emulsion is basically similar. Initially, with the increase of temperature the amount of droplets with medium size decreases, and then the amount of droplets with diameter larger than 0.8 μm increases. The most dynamic changes in this process are observed for temperature of 80°C.

This phenomenon is accurately presented in Fig. 4. As can be seen, the amount of droplets increases for classes P1, P2, P6, P7, P8. This proves the merging of droplets with medium size into large drops, as the temperature increases. The phenomenon of secondary emulsion is by all accounts unfavourable, as it decreases the dispersion of water droplets and affects emulsion stability by lowering it. It may also negatively affect the durability of fuel apparatus, and in an extreme case the flushing of oil film off cylinder surface. Yet it is supposed that by proper selection of the means of decreasing surface tension (in this case called Rocanol) this unfavourable phenomenon can be decreased. Undoubtedly, this problem may well constitute a separate research task.

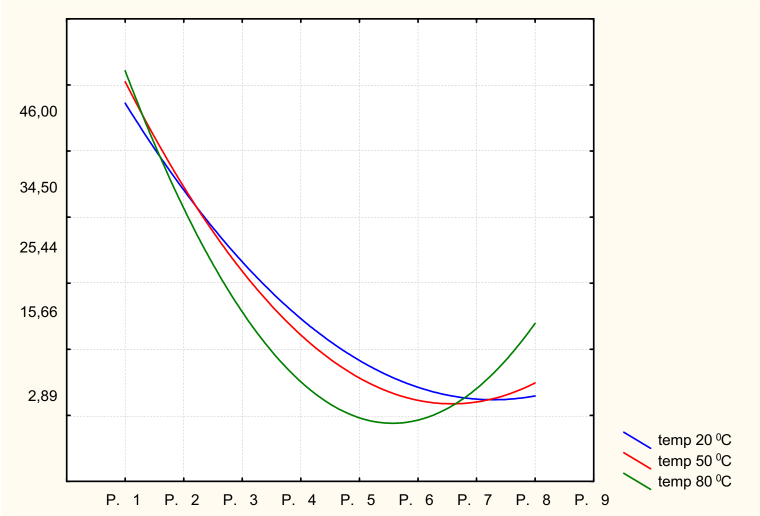

Fig. 4. Amount of droplets of particular class in emulsion depending on its temperature, where: P1-P9 classes of droplet size in accordance with Table 1

Analysing the process of secondary emulsion formation it was observed that the rotational speed of the helicoidal agitator rotor slightly affected this unfavourable phenomenon (Fig. 5).

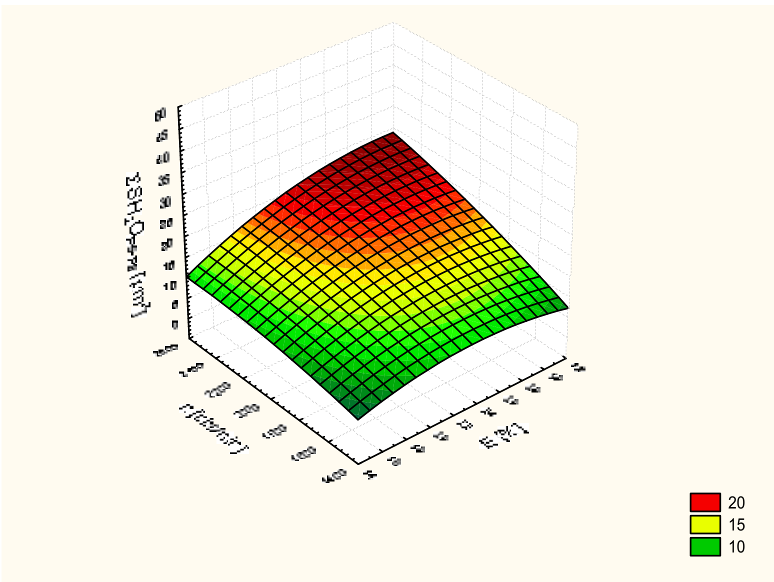

Fig. 5. Dependence between rotational speed of the agitator rotor – n [rpm] and emulsion concentration – E [%] and the sum of droplet areas ΣS $H_2O_{P5\text{-}P8}$ of classes P5-P8 in the area researched [μm.[2]]

Among the agitator setting parameters the rotational speed of the rotor is the decisive factor for water droplet dispersion; meanwhile, the formation of secondary emulsion increases with the increase of emulsion concentration for temperatures above 50°C. Therefore it is not advisable to apply large rotational speeds for the rotor, unlike in the case of emulsion temperatures about 20°C.

4. Résumé

The subject matter presented above does not fully exhaust the subject; it is just an attempt to describe it. An analysis of the effect of temperature of fuel-water emulsion formation – one of the parameters controlling the process of emulsion formation in a helicoidal agitator – on emulsion properties, confirmed the existence of such a parameter set that directly affects its physical properties. They obviously affect the processes in the engine cylinder.

In result of the experiment conducted it was found that with the increase of temperature there increases the amount of droplets of population classes 1, 2, 6, 7, 8 and the area occupied by them. This testifies to the merging of medium-size droplets into large drops with the increase of temperature, which is unfavourable as it decreases emulsion stability.

Further research work on the application of fuel-water emulsion for feeding piston combustion engines should first of all be directed toward its stability. This stability depends mainly on the content of additives decreasing the surface tension of combined liquids. The proper selection of emulsifiers would have an essential effect on maintaining emulsion dispersion, which would directly influence the repeatability of combustion processes in the piston engine cylinder.

References

[1] Chomiak, J., *Performance Analysis of a Steam Injected Diesel (STID) Engine,* Marine Science and Technology for Sustainability – ENSUS 2000, CQD Journal, Newcastle 2000.

[2] Dłuska, E., Hubacz, R., Wroński S., *Simple and multiple water fuel emulsions preparation in helical flow,* Conference Proceedings of the Fourth Mediterranean Combustion Symposium, Lisbon 2005.

[3] Paro, D., *The Smokeless Engines, Marine News nr 1 – 2000,* Wartsila NSD Corporation.

[4] Piaseczny, L., Zadrąg, R., *Wpływ zasilania emulsją paliwo-wodną na dymienie okrętowego silnika spalinowego,* Journal of KONES Internal Combustion Engines, Warszawa – Bielsko-Biała 2003.

[5] Piaseczny, L., Zadrąg, R., *Wpływ zasilania emulsją paliwowo-wodną na toksyczność okrętowego silnika spalinowego,* Zeszyty Naukowe Politechniki Gdańskiej 598 BUDOWNICTWO OKRĘTOWE Nr 65, Gdańsk 2004.

[6] Piaseczny, L., Zadrąg, R., *Parametry energetyczne silnika okrętowego Sulzer typu 6AL20/24 zasilanego emulsją paliwowo-wodną,* XXVI Sympozjum Siłowni Okrętowych Symso 2005, Zeszyty Naukowe AMW, nr 162K/2, Gdynia 2005.

[7] Piaseczny, L., Zadrąg R., *Researches of Influence of Water Delivery to Cylinder on Parameters of Combustion Process and Toxicity of CI Engine.* Silniki Spalinowe, No 2/2005 (121), s. 34-38.

[8] Scherman, F., *Emulsji*. Izd. Chimija, Moskwa 1972.

[9] Velji, A., Remmels, W., Schmidt, R. M., *Water to reduce NOx emissions in diesel engines, a basic study,* CIMAC, Interlaken 1995.

[10] Wroński, S., Dłuska, E., Hubacz, R., Ciach, T., *Sposób wytwarzania emulsji,* Patent P.375688